DISSERTATION

zur

Erlangung des Doktorgrades (Dr. rer. nat.)

an der

Mathematisch-Naturwissenschaftlichen Fakultät

der

Rheinischen Friedrich-Wilhelms-Universität Bonn

MITOCHONDRIAL REGULATION THROUGH THIOL-SWITCHING IN PLANTS

vorgelegt von

Thomas Jürgen Uwe Nietzel

geboren in Henstedt-Ulzburg

Bonn, Juni 2017

THIS THESIS HAS BEEN CARRIED OUT IN THE LAB OF:

Dr. Markus Schwarzländer
Plant Energy Biology
Institut für Nutzpflanzenwissenschaften und Ressourcenschutz
Universität Bonn
Friedrich-Ebert-Allee 144
D-53113 Bonn

FIRST EXAMINER: Prof. Dr. Andreas Meyer
Chemical Signalling
Institut für Nutzpflanzenwissenschaften und Ressourcenschutz
Universität Bonn
Friedrich-Ebert-Allee 144
D-53113 Bonn

SECOND EXAMINER: Prof. Dr. Volker Knoop
Molekulare Evolution
Institut für Zelluläre & Molekulare Botanik
Universität Bonn
Kirschallee 1
D-53115 Bonn

TAG DER PROMOTION: 08.09.2017

TABLE OF CONTENTS

SUMMARY 6

1. INTRODUCTION 7

1.1 Early seed germination – transition from quiescence to activity 7

1.1.1 Seed dormancy, seed ageing and their influencing factors 7

1.1.2 Onset of respiration in germinating seeds 9

1.2 Metabolic regulation enables efficient germination 11

1.2.1 Plant hormones facilitating long-term germination control 11

1.2.2 Redox regulation of protein cysteines in germinating seeds may enable dynamic metabolic fine-tuning 11

1.3 Thiol redox switches of proteins and their identification 12

1.3.1 Proteine-cysteine modifications and their characteristics 12

1.3.2 Redox regulation of Cys-proteins in a physiological context 13

1.3.3 Proteomic identification of redox-regulated proteins 15

1.3.3.1 Thioredoxin-/ and glutaredoxin-trapping approaches 15

1.3.3.2 Approaches for thiol labelling and labelling of sulfenylated proteins 16

1.3.3.3 Thiol labelling with (tandem-)mass-tags 18

1.3.3.4 Differential thiol labelling to determine the redox state of individual Cys-peptides 20

1.4 Hydrogen peroxide sensing *in planta* 20

1.4.1 Hydrogen peroxide-mediated signalling in plants 20

1.4.2 Dynamic sensing of hydrogen peroxide in plants with genetically encoded probes 21

1.4.3 The hydrogen peroxide probe roGFP2-Orp1 22

1.5 Objectives 23

1.5.1 To assess dynamics in energy metabolism during early seed imbibition 23

1.5.2 To elucidate the involvement of the mitochondrial thiol redox machinery in germination 23

1.5.3 To identify *in situ* target proteins of the mitochondrial redox machinery 24

1.5.4 To establish monitoring of hydrogen peroxide dynamics *in planta* with the genetically encoded probe roGFP2-Orp1 24

2. RESULTS 25

2.1 Physiological changes in Arabidopsis seeds in response to imbibition 25

2.1.1 Considerable oxygen consumption rates occur immediately at imbibition 25

2.1.2 Fluorescent protein biosensors allow for monitoring physiological changes at seed imbibition 26

2.1.3 Fluorescent protein-based ATP sensing allows ATP monitoring in intact seeds 28

2.1.4 Fluorescence sensing of NADH / NAD^+-redox status in seeds remains technically inconclusive 30

2.1.5 Measurement of TCA cycle intermediates pinpoints a transient rise of citrate at imbibition 33

2.1.6 Glutathione is efficiently reduced in response to imbibition 34

2.2 Germination performance of Arabidopsis seeds with impaired redox machinery 41

2.2.1 Fresh seeds of different redox mutants are only slightly affected in the germination vigour 41

2.2.2 Aged seeds of different redox mutants show significantly lowered germination vigour 44

2.3 Measuring the redox changes of individual mitochondrial cysteine-peptides at restart of metabolism 46

2.3.1 Metabolic restart in mitochondria through substrate feeding 46

2.3.2 Identifying endogenous redox switches of mitochondrial matrix proteins 50

2.3.2.1 Starting metabolic activity in mitochondria can trigger global, yet differential, reduction of proteins 50

2.3.2.2 Redox-switching of Cys-peptides may serve as an indicator of their subcellular (fine) localisation 56

2.3.2.3 The most highly redox-shifted peptides belong to proteins of the mitochondrial thiol redox machinery 58

2.3.2.4 Multiple redox-switched Cys-peptides identified for unique proteins at key-positions of the mitochondrial metabolism 60

2.3.2.5 Multiple non-redox-switched Cys-peptides identified for non-mitochondrial proteins 65

2.4 Physiological alterations of early seed germination in Arabidopsis redox mutants 66

2.4.1 Mutants impaired in the redox machinery show lowered respiratory efficiency 66

2.4.2 The adenosine nucleotide energy charge is not affected in the redox mutants 67

2.4.3 TCA cycle associated intermediates dynamics are altered in in imbibed seeds of the redox mutants 68

2.4.4 The amino acid fingerprint is altered in seeds of the redox mutants 69

2.5 Identification of differentially redox-switched peptides in the mutants of the redox machinery 71

2.5.1 Investigating mutants of the mitochondrial thioredoxin system to elucidate redox switches involved in germination efficiency....71

2.5.1.1 Mitochondrial redox machinery is also kick-started in mutants of the thioredoxin-linked redox machinery....71

2.5.1.2 Identification of individual Cys-peptides with altered Cys-oxidation state in mutants impaired in the mitochondrial thioredoxin system....75

2.5.2 Investigating mutants of the mitochondrial glutathione-linked system to elucidate redox switches involved in germination efficiency....80

2.5.2.1 Mitochondrial glutathione redox state is partially reestablished in a mutant impaired in the mitochondrial glutathione reductase....80

2.5.2.2 Identification of individual Cys-peptides with altered Cys redox state in mitochondria lacking GLUTATHIONE REDUCTASE 2....83

2.6 *In vitro* characterisation of the hydrogen peroxide sensor roGFP2-Orp1....86

2.6.1 Expression and purification of roGFP2-Orp1 protein....86

2.6.2 Optical characteristics of roGFP2-Orp1 protein....87

2.6.3 pH sensitivity of roGFP2-Orp1 protein....89

2.6.4 Hydrogen peroxide oxidises roGFP2-Orp1 effectively and reversible *in vitro*...90

2.6.5 Reduction of roGFP2-Orp1 by reconstituted redox machineries....91

2.7 Characterisation of the roGFP2-Orp1 protein sensor *in planta* 92

2.7.1 Arabidopsis sensor lines for cytosolic and nuclear expression of the roGFP2-Orp1 sensor....92

2.7.2 Arabidopsis lines for expression of the roGFP2-Orp1 sensor in the mitochondrial matrix....93

2.7.3 RoGFP2-Orp1 responds to external applied oxidative stress in living Arabidopsis tissues....94

2.7.4 Response of mitochondrial roGFP2-Orp1 to the redox cycling agent menadione....95

2.7.5 Mutants with impaired redox homeostasis investigated with roGFP2-Orp1....96

2.7.6 Cytosolic roGFP2-Orp1 redox homeostasis in seeds in response to imbibition....98

3. DISCUSSION....99

3.1 Rapid restart of the energy metabolism in imbibed seeds requires a refined concept of mitochondria in early germination....99

3.2 The role of the cellular redox machinery on germination....101

3.3 Thiol-switched mitochondrial proteins at the global level....103

3.4 Thiol-switched proteins involved in primary metabolism....106

3.5 Differentially thiol-switched proteins in mutants of the thiol redox systems 109

3.6 Monitoring of hydrogen peroxide with the probe roGFP2-Orp1....110

4. MATERIAL & METHODS....112

4.1 Technical equipment and consumables 112
4.1.1 Laboratory equipment 112
4.1.2 Consumables 113
4.1.3 Enzymes 113
4.1.4 Specific chemicals, antibodies, materials and commercial kits 113
4.1.5 Software 113
4.1.6 Online resources and databases 114
4.2 Plant methods 114
4.2.1 Plant material 114
4.2.2 Stable transformation of Arabidopsis by `floral dip` 115
4.2.3 Harvesting of Arabidopsis seeds and long-term storage 115
4.2.4 Surface sterilisation of Arabidopsis seeds and *in vitro* cultivation 115
4.2.5 Estimation of the germination efficiency of Arabidopsis seeds 115
4.2.6 Plant growth on soil for seed propagation 116
4.2.7 Hydroponic culture of Arabidopsis seedlings 116
4.2.8 Imbibition of seeds 116
4.3 Bacteriological methods 117
4.3.1 Bacterial strains 117
4.3.2 Bacterial growth 117
4.3.3 Glycerol stocks 117
4.3.4 Preparation of competent cells and transformation of bacteria 117
4.3.5 Plasmid isolation from *E. coli* cultures 118
4.3.6 Recombinant protein expression and affinity-based purification 118
4.4 Protein methods and biochemical assays 119
4.4.1 Isolation of coupled and functional mitochondria 119
4.4.2 Mitochondrial substrate supplementation assay 120
4.4.3 Respiration assay of isolated mitochondria 121
4.4.4 Extraction of seed proteins with conserved redox state 121
4.4.5 Labelling of the endogenous redox state with iodoTMT 121
4.4.6 Trypsination of precipitated proteins 123
4.4.7 Immunoprecipitation of iodoTMT-labelled peptides 123
4.4.8 Sample clean-up for mass spectrometry 124
4.4.9 Mass spectrometry-based identification of peptides and quantification of TMT reporter ion intensity with subsequent data analysis 124
4.4.10 Determination of protein concentration 126
4.4.11 SDS-PAGE and Coomassie-staining 126
4.4.12 Determination of the total thiol concentration in seeds 126

4.4.13 Determination of organic acids in seeds 127
4.5 DNA methods 128
4.5.1 Oligonucleotides 128
4.5.2 Plasmids 128
4.5.3 DNA gel electrophoresis and DNA purification 130
4.5.4 Quantification of DNA content 130
4.5.5 DNA sequencing 130
4.5.6 GATEWAY® cloning strategies 130
4.6 Imaging methods (microscopy methods & platereader assays) 131
4.6.1 Seed respiration assay 131
4.6.2 Platereader-based emission and excitation scans of Arabidopsis seeds 131
4.6.3 Emission and excitation scans of purified roGFP2-Orp1 in a spectro-fluorometer 132
4.6.4 Platereader-based dynamic monitoring of fluorescent biosensors 132
4.6.5 CLSM-based monitoring of fluorescent biosensors (in isolated embryos or in Arabidopsis seedlings) 133
4.6.6 Screen for fluorescent, transgenic plants 134
4.6.7 Documentation of different germination stages 134
4.7 Cooperation partners 134
5. REFERENCES 135
FIGURES & TABLES 147
ABBREVIATIONS 151
PUBLICATIONS 154
GENERAL STATEMENT 155
ACKNOWLEDGEMENT 156

SUMMARY

The seed represents a key stage in the lifecycle of *spermatophytes* (seed plants). Dry seeds can overcome unfavourable conditions, such as drought, heat or cold, by maintaining their metabolism in a quiescent state. Yet, the reactivation of the metabolism is an important prerequisite for germination to provide energy and organic compounds, and is initiated by imbibition with water. How exactly the restart of metabolism occurs and how it is regulated to drive germination while operating in a resource efficient manner is insufficiently understood. Since *de novo* gene expression is energy demanding and starts comparably late in germination, posttranslational protein modifications have been implicated as a key regulatory mechanism in quiescence release.

In this work the reestablishment and the regulation of the (respiratory) energy metabolism was investigated. A methodology was developed to monitor rearrangements of energy and redox metabolism in seeds live and with subcellular specificity and very early at imbibition. That was possible by optimising and employing different genetically encoded fluorescent probes, including a probe for monitoring hydrogen peroxide (roGFP2-Orp1), targeted to the mitochondrial matrix and the cytosol in seeds of *Arabidopsis thaliana*. Rapid rebooting of ATP homeostasis and thiol redox systems within the first hour of imbibition was observed and independently confirmed by established analytical methods. To generate a framework of redox regulation of mitochondrial proteins during this restart, a model system of isolated, functional mitochondria was established. Monitoring of the glutathione redox potential dynamics by roGFP2-Grx1 in the matrix showed that the addition of specific substrates led to a sharp activation of the matrix thiol redox systems, similar to what had been observed in imbibed seeds. Cysteine residues of proteins underwent specific reduction mediated by the endogenous thiol redox machinery of the mitochondrial matrix, while the thermodynamic, kinetic and structural constraints that provide specificity to thiol redox switching *in vivo* were largely maintained. *In situ* targets of the mitochondrial redox machinery were identified and the degree of redox-switching was quantified by iodoacetyl tandem mass tag (iodoTMT)-based thiol redox proteomics. Proteins involved in mitochondrial energy metabolism, such as of different respiratory complexes and the tricarboxylic acid cycle, and of the amino acid metabolism, were identified as targets of redox-switching. To dissect target specificity of the individual redox machineries and their potential impact on the seed physiology during germination, different mutants of the individual mitochondrial redox systems were investigated. Mutants impaired in either the glutathione-/ or thioredoxin-linked redox machineries of the mitochondrial matrix showed lowered germination vigour, especially in aged seeds. Their seeds showed increased respiration rates at imbibition, while the reestablishment of their adenine nucleotide energy charge was not affected, but intermediates of the tricarboxylic acid cycle were altered. Only a small subset of proteins was found to be affected in their thiol redox status in the different mitochondrial redox mutants, as investigated in the isolated mitochondria model by redox proteomics.

Taken together, the observations of this work suggest that redox and energy physiology of seeds are reactivated immediately at imbibition. A global reductive shift of specific protein cysteine residues includes enzymes of the respiratory metabolism, which redox-switching may trigger (de-)activation, allowing fine-tuning of activities at imbibition to optimise germination efficiency.

1. INTRODUCTION

1.1 Early seed germination – transition from quiescence to activity

Plant seeds are our main food source, either consumed directly or to feed livestock. For plants, seeds allow to overcome a major drawback of a sessile lifestyle by facilitating propagation over long distances. Certain seeds can also resist desiccation and freezing and are named *orthodox* seeds, whereas *recalcitrant* seeds are sensitive to these conditions. Orthodox seeds enable the survival of the plant species in temporally hostile environments, such as cold, drought or even bush fires. Orthodox seeds preserve a preformed embryo in a desiccated, quiescent metabolic state, which is rapidly reactivated when the conditions are favourable.

1.1.1 Seed dormancy, seed ageing and their influencing factors

Seed embryos are `complete plants in miniature`, well provided with energy and nutrient reserves to fuel germination until an autotrophic growth state is established. For the plant embryo the decision whether or not to germinate is literally vital: germination during unfavourable growth conditions must be strictly inhibited, which is achieved by quiescence. In addition, also germination during favourable conditions in the end of a growth season has to be prevented, which is typically achieved by seed dormancy. Dormancy is often regarded as an adaptation to different seasonal cycles and blocks the completion of germination during favourable conditions. Seed dormancy can be manifested by diverse mechanisms in different plant species, ranging from robust seed coats preventing radicle penetration to metabolic blocks with unknown molecular mechanisms (BEWLEY 1997; NÉE *ET AL.,* 2017). Depending on the plant species and the underlying type of dormancy, initiation of germination is achieved by distinct mechanisms - in some cases triggered only by extreme ambient conditions, *e.g.* for seeds of some specialised plants of fire-prone environments great heat is required to overcome dormancy (MOREIRA AND PAUSAS 2012). For other seeds dormancy is broken by cold stratification or by resting in quiescence for several months up to several years, also referred to as *after-ripening*. It is assumed that specific oxidation of certain mRNAs and proteins during after-ripening gradually releases dormancy (BAZIN *ET AL.,* 2011). Yet, the ability of (both dormant and non-dormant) orthodox seeds to pass extended periods in a quiescent, desiccated state comes at the price of ageing, which manifests in decreased germination vigour over time (**Figure 1**). A complete mechanistic concept of how seed ageing affects the germination vigour has not been identified, but different biochemical alterations were described for aged seeds, *e.g.* lowered total adenosine pool sizes in sunflower seeds (KIBINZA *ET AL.,* 2006) and lowered total glutathione pool sizes in seeds of different barley accessions (NAGEL *ET AL.,* 2015), of aged sunflower seeds (TORRES *ET AL.,* 1997) and of tomato seeds (DE VOS *ET AL.,* 1994). The glutathione redox potential (E_{GSH}) was less negative in extracts of aged seeds depending on storage temperature and air moisture content and was correlated with germination vigour (NAGEL *ET AL.,* 2015 and **Figure 1**). Furthermore, the peroxidation of lipids was shown to negatively affect seed longevity of Arabidopsis seeds (SATTLER *ET AL.,* 2004) and seed proteins were carbonylated during ageing (JOB *ET AL.,* 2005; RAJJOU *ET AL.,* 2008). This has raised the hypothesis that oxidation of diverse cellular components may be involved in decreasing seed longevity while breaking seed dormancy (ARC *ET AL.,* 2011 and **Figure 1**).

Although the molecular mechanisms of seed ageing are not fully understood, progression of ageing is determined by plant-intrinsic factors such as species and initial seed quality, as well as environmental factors such as humidity and temperature (WALTERS 1998; NAGEL *ET AL.,* 2015). When favourable factors coincide, ageing can be slowed down remarkably, resulting in seeds with their intact embryos remaining vital and competent to undergo germination over decades, centuries or even millennia. A date palm seed germinating after 2,000 years has set a record (SALLON *ET AL.,* 2008), but the underlying principle holds true for most seeds. Seed bank initiatives worldwide make use of this knowledge to preserve biodiversity and crop germplasm for the future. High germination vigour is typically achieved by storage at low temperatures, low air moisture and a low oxygen content of the ambient atmosphere. Hypoxic conditions diminish detrimental effects of seed ageing and prevent germination of seeds of several plant species.

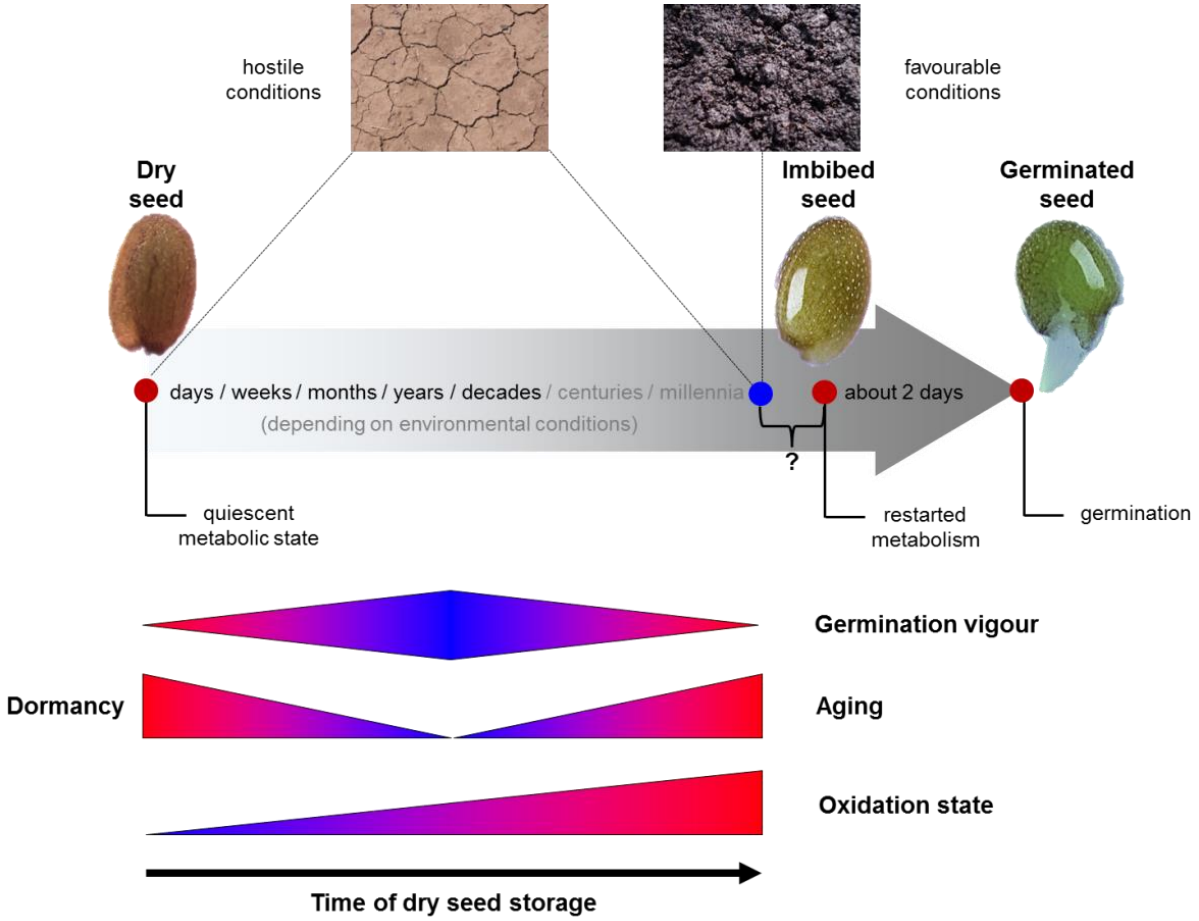

Figure 1: Restart of metabolism from quiescence in response to imbibition in orthodox seeds. Desiccated seeds, here illustrated for *Arabidopsis thaliana*, are in a quiescent metabolic state to maintain their resources and their germination vigour when environment is unfavourable for germination and subsequent growth. Germination after quiescence for many years has been reported, but depends on species and the environmental conditions. Seed viability decreases gradually over time while dormancy is broken. Glutathione pool and different proteins were shown to be oxidised during quiescence. When imbibed with water, metabolism is restarted after an unknown time finally triggering germination within about two days. Figure elements modified from NÉE *ET AL.,* 2017.

1.1.2 Onset of respiration in germinating seeds

The necessity of water and oxygen for successful germination of many orthodox seeds was already observed more than a century ago and comprehensively demonstrated by a simple experimental setup (**Figure 2**). These observations imply that respiration is essential to fuel the embryo with energy to allow growth and development eventually leading to germination and subsequent establishment of an autotrophic plant. However, seeds of several plant species manage to germinate also under hypoxic conditions *e.g.* rice in flooded paddies (MAGNESCHI AND PERATA 2009). This is achieved by the substitution of respiration by alternative metabolic pathways during germination of submerged seeds. Lactate and ethanol fermentation were shown to provide the energy for seed germination after submergence, which enables initial seedling growth to reach normoxic regions (RAYMOND *ET AL.,* 1985). A species-dependent accumulation of lactate and ethanol in submerged seeds was described and different plant species varied drastically in their adenosine energy charge as indicated by their ATP/ADP/AMP ratios after submergence. This reflects the adaptation of certain plant species at the metabolic level to hypoxic conditions during germination. Non-adapted plants fail to maintain a high energetic state in submerged seeds, which finally prevents germination. It was observed that there is a general tendency for starchy seeds to cope better with hypoxic conditions than oily or protein-rich seeds (RAYMOND *ET AL.,* 1985). This was explained by a fast and resources-efficient availability of sugars after starch breakdown, which can fuel glycolysis directly. In contrast, the breakdown of lipids and proteins results mainly in metabolic intermediates, which have to be further metabolised in mitochondria in the presence of oxygen. Oxygen is also a direct substrate for β-oxidation of fatty acids in plant peroxisomes, which may add to the germination sensitivity of oily seeds under hypoxic conditions.

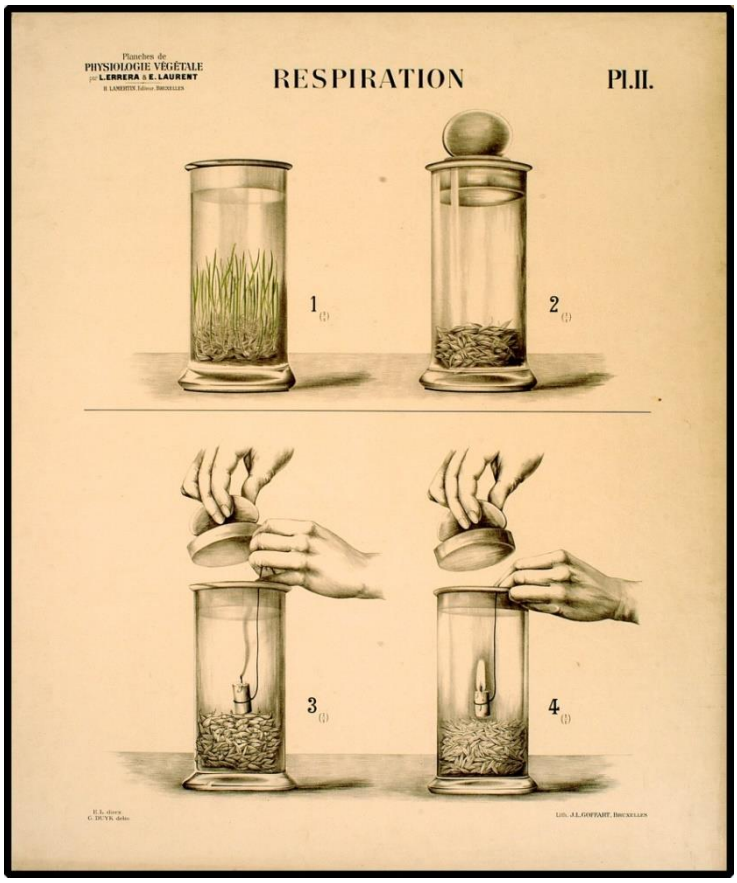

Figure 2: Oxygen-dependency of wheat seeds during germination. Germination of most desiccated seeds is dependent of oxygen availability, as already observed in the 19th century. Dry wheat seeds with unlimited oxygen supply germinate when imbibed with water (1), while imbibed seeds with limited oxygen supply (2), as achieved by sealing the glass cylinder, do not germinate. Consumption of oxygen in response to imbibition was shown by a flame of a candle, which dies down in a glass cylinder filled with imbibed seeds (3), while it keeps burning in a glass cylinder with dry seeds (4). Lithography from ERRERA AND LAURENT, 1897, Planches de physiologie végétale.

Although there are species-dependent differences in the need for oxygen to complete germination, desiccated seeds have in common that they rely on rehydration to boot their metabolism to high rates to fuel the cellular processes that underpin germination with energy. In nature, availability of water, which enables successful germination, can change within minutes as a consequence of rainfall. The metabolic activation of the embryo must be rapid to allow for initiation of plant growth and development. Efficient and fast germination constitutes an important fitness trait that is decisive for plant performance through optimal use of narrow meteorological windows or for the competition for limited resources with other plants. Rapid, reliable and synchronous germination are also important agronomical characteristics with major impact on crop yield. Inefficiency of metabolic controls in seeds can be detrimental for the individual embryo and in an agricultural context, pre-harvest sprouting can lead to significant yield losses (GUBLER *ET AL.,* 2005). Despite the importance of this transition for the plant, the picture of the underlying mechanistic events, controlling and driving germination, remains incomplete.

1.2 Metabolic regulation enables efficient germination

1.2.1 Plant hormones facilitating long-term germination control

The switch from quiescence to restarted metabolism in imbibed seeds requires metabolic regulation to enable resources-efficient and fast germination. The fundamental roles of the plant hormones abscisic acid (ABA) and gibberellins (GA) for control of dormancy, the quiescence release and for the completion of germination were identified over 50 years ago (KALLIO AND PIIROINEN 1959; SONDHEIMER *ET AL.,* 1968). In recent years also crosstalk with other plant hormones, such as ethylene, was described (LINKIES AND LEUBNER-METZGER 2012). The balance between these plant hormones facilitates a controlled dormancy release. In many plant species ABA maintains seed dormancy, while GA and ethylene promote germination, *e.g.* by weakening of the micropylar endosperm to allow penetration by the growing radicle. While plant hormones mainly act on gene-expression allowing for long-term metabolic adjustments, posttranslational regulation of metabolic enzymes allows for immediate and direct fine-tuning of enzyme activities, and metabolic fluxes, in turn, to cope with the rapidly fluctuating metabolic needs of the reactivated embryo. Water uptake during imbibition is fast, requiring rapid control mechanisms. Specific remodelling of several posttranslational protein modifications (PTM) were observed in maturating and germinating seeds (reviewed in ARC *ET AL.,* 2011).

1.2.2 Redox regulation of protein cysteines in germinating seeds may enable dynamic metabolic fine-tuning

Active and precise regulation of the metabolism is essential for the efficient utilisation of limited storage compounds, such as starch, lipids and proteins. A thioredoxin-dependent reduction of the main storage proteins in response to imbibition was described under *in vitro* and *in vivo* conditions (*e.g.* KOBREHEL *ET AL.,* 1992; LOZANO *ET AL.,* 1996; YANO *ET AL.,* 2001; MARX *ET AL.,* 2003; ALKHALFIOUI *ET AL.,* 2007), with direct impact on the storage protein solubility and accessibility (WONG *ET AL.,* 2004). This suggests a contribution of the thioredoxin-linked redox machinery to the mobilisation of storage proteins during germination. However, the thioredoxin-mediated reduction in response to imbibition is not restricted to the main storage proteins, but was also observed for several other thioredoxin-linked proteins (ALKHALFIOUI *ET AL.,* 2007; BYKOVA *ET AL.,* 2011 a; BYKOVA *ET AL.,* 2011 b). As such, the overall reduction of thioredoxin-linked proteins during seed imbibition may be considered a conserved phenomenon, although specific proteins, such as protein disulfide isomerases and glutathione S-transferases, are oxidised during imbibition (ALKHALFIOUI *ET AL.,* 2007), which may reflect the reestablishment of the typical redox states, which can also be oxidised, *e.g.* in the endoplasmic reticulum (ER). However, an in-depth understanding of the redox-switched proteins and potentially redox-regulated metabolic pathways has been lacking. Further, the exact timing of restarting the thioredoxin-linked redox machinery in seeds in response to imbibition has remained unclear. Yet, already in 1943, the fast appearance of reduced glutathione during the first hours of germination was reported as a characteristic of spermatophytes (HOPKINS AND MORGAN 1943). The rapid reduction of the glutathione pool is not based on increased glutathione biosynthesis but was shown to be dependent on glutathione reductase (GR) activity (KRANNER AND GRILL 1993; TOMMASI *ET AL.,* 2001). Taken together these observations suggest an important regulatory function of the establishment of a reduced glutathione pool and a reduced thioredoxin-linked redox machinery during germination, *e.g.* for the mobilisation of storage proteins. Both, the

thioredoxin-/ and the glutathione-dependent redox machineries are able to modulate enzyme activities in plants via modification of specific cysteine thiols (*e.g.* WOLOSIUK AND BUCHANAN 1977; MICHELET *ET AL.,* 2005). While cysteines account for about 2 % of the total cellular amino acid (AA) content, making it the least abundant amino acid, it is one of the most conserved amino acids in proteins, emphasising its crucial role for diverse protein functions (MAILLOUX *ET AL.,* 2014). Different to many other chemically plausible oxidative protein modifications, such as carbonylation, thiol-modifications are mostly reversible, enzymatically controlled and selective *in vivo*. Thiol chemistry further allows a diverse chemical array of modifications providing the basis for tuneable systems by multiple switching steps (NIETZEL *ET AL.,* 2017). This can be attributed to the unique chemical properties of the cysteine-thiol group, which can exist in several oxidation states. Therefore diverse protein thiol modifications are highlighted in the following sections to discuss their fundamental roles in regulating enzyme activities and their potential role in seed germination.

1.3 Thiol redox switches of proteins and their identification

(modified sections of 1.3 were published in NIETZEL *ET AL.,* 2017)

1.3.1 Proteine-cysteine modifications and their characteristics

Cysteines have to be accessible to interact with the endogenous redox machineries, allowing for diverse redox modifications. Cysteine residues buried in the protein scaffold often fulfil structural functions. The modification of cysteine thiols depends on both, the cellular conditions as well as the individual characteristics of each thiol. The reactivity of a cysteine residue strongly depends on its ability to deprotonate to the more reactive thiolate anion (**Figure 3 a**), while the thiol form is comparatively unreactive. Deprotonation to the reactive thiolate strongly depends on the pH of the surrounding microenvironment, but also substantially on the pK_a of each individual cysteine residue. The pK_a of a cysteine residue can be decreased by neighbouring, positively charged amino acids, while negatively charged amino acids can increase the pK_a. As such the reactivity of individual cysteine residue can differ markedly, which enables specificity of thiol-based enzyme regulation.

Hydrogen peroxide is considered the most physiologically relevant reactive oxygen species (ROS), based on its reactivity combined with relatively long half-life, and triggers cysteine modifications. Hydrogen peroxide is produced under physiological conditions, is not charged and is capable of passing membranes, *e.g.* via aquaporins, making it a good candidate to act as a signal transmitter (BIENERT *ET AL.,* 2007). The nucleophilic thiolate anion of a cysteine attacks hydrogen peroxide, forming a sulfenic acid (-SOH). Sulfenic acid groups are mostly deprotonated ($-SO^-$) under physiological conditions, making them highly reactive to a variety of modifications (**Figure 3 a**). When sulfenic acids undergo further oxidation, they generate sulfinic acids ($-SO_2H$) and finally sulfonic acids ($-SO_3H$). Both modifications are typically non-reversible (**Figure 3 b**). Yet, sulfinic acids of 2-Cys-peroxiredoxins were shown to be reduced by sulfiredoxins in yeast (BITEAU *ET AL.,* 2003) and humans (WOO *ET AL.,* 2005), and sulfiredoxins were also identified in Arabidopsis (IGLESIAS-BAENA *ET AL.,* 2010). If sulfinic acid formation contributes to redox regulation of enzyme functions or is a result of (mostly) irreversible protein damage remains under discussion (MAILLOUX *ET AL.,* 2014). Glutathionylation of sulfenic acids is often considered a mechanism to prevent the (irreversible) overoxidation to sulfinic or sulfonic acids. Glutathionylation is assumed to regulate enzyme functions also in plants (DIXON *ET AL.,* 2005; MICHELET *ET AL.,* 2005), with *e.g.* the glycine decarboxylase complex as a prominent example (HOFFMANN *ET*

AL., 2013). Glutathionylation can be either initiated enzymatically by glutaredoxins (Grx) and glutathione S-transferases or non-enzymatically. At very high oxidised glutathione (GSSG) concentration, which are generally not considered physiological in the cytosol and the mitochondrion (MAILLOUX *ET AL.,* 2014), thiolate anions can directly react with GSSG in a thiol disulfide exchange reaction to produce reduced glutathione (GSH) and a glutathionylated cysteine residue. Glutathionylation of sulfenic acids occurs also at oxidised glutathione pools. Non-enzymatic glutathionylation of proteins is generally considered non-specific (MAILLOUX *ET AL.,* 2014). Mediated by glutaredoxins and glutathione S-transferases, (de-)glutathionylation of proteins occurs also specifically under physiological conditions and is achieved by disulfide exchange reactions between glutaredoxins and its target proteins. Furthermore, cysteine residues can react with other cysteines resulting in disulfide bridges (S-S), either with cysteines of the same protein or even forming intermolecular disulfide bridges with other proteins. For instance, in the dark the chloroplastidic protein 12 (CP12) can bind to enzymes of the Calvin-Benson-cycle, namely the glyceraldehyde-3-phosphate dehydrogenase and the phosphoribulokinase, via intermolecular disulfide bridges (WEDEL *ET AL.,* 1997), which results in the formation of an inactive protein complex, which can be reversibly dissociated in the light to activate the Calvin-Benson-cycle.

1.3.2 Redox regulation of Cys-proteins in a physiological context

Whether or not an individual protein thiol is modified under *in vivo* conditions requires specific assessment. The actual redox state of a protein thiol *in vivo* is set by its midpoint potential, the endogenous thermodynamics of the cell compartment and the kinetic properties including steric constraints. For many enzymes activity changes of the purified protein in response to treatment with an oxidant (such as hydrogen peroxide, dipyridyl disulfide (DPS) or diamide), or a reductant (such as dithiothreitol (DTT), tris(2-carboxyethyl)phosphine (TCEP), or reconstituted thioredoxin or glutathione systems) have justified a classical *in vitro* definition of redox regulation. Those assays have frequently been combined with site-directed mutagenesis of specific cysteine residues to determine the contribution from specific thiols. Such assays have been powerful tools to demonstrate thiol-switching and redox regulation of individual proteins *in vitro*. However, *in vitro* thiol-switching is not sufficient, and potentially not even necessary, for redox regulation to occur *in vivo* (**Figure 3 c**). The specific cellular conditions set by the endogenous thermodynamics, kinetics and structural organisation are of particular significance for thiol redox regulation and can be harder to reconstitute *in vitro* than those for other PTMs, such as phosphorylation or acetylation. The interplay of thermodynamics, kinetic and organisational factors is likely to have a stabilising effect on the redox state of most protein thiols *in vivo*. It further implies that only a subset of the protein thiols that are operational *in vitro* are also active thiol-switches *in vivo*, while others may be missing *in vitro*. Thiol-switching is hence likely to be rarer and more specific under physiological conditions than can be inferred from reductionist approaches. Even if a thiol can be reduced by the thioredoxin or glutathione system, this does not necessarily imply any regulatory function, but can be part of protein maturation, localisation or maintenance (HERRMANN AND RIEMER 2012). For *bona fide in vivo* redox regulation to occur, a protein thiol needs to be detectable in at least two interconvertible states, and an active switch between those states needs to occur under a physiologically meaningful situation. In addition, the function of the protein needs to be modified by operation of the switch and the switch needs to be separable from the catalytic mechanism of the protein. This makes *in vivo* analysis in the context of the entire functional system, with its thermodynamic, kinetic and organisational constraints, indispensable to decide if a protein is

genuinely redox-regulated. Absence of activity changes in response to thiol-switching, or even thiol-switching itself, *in vitro* does not exclude *bona fide* redox regulation. A switch and/or a change in function *in vivo* may then still be linked to mixed protein-protein interactions, formation of protein complexes or localisation of the protein (*e.g.* HOLSCHER *ET AL.*, 2014; WEDEL *ET AL.*, 1997).

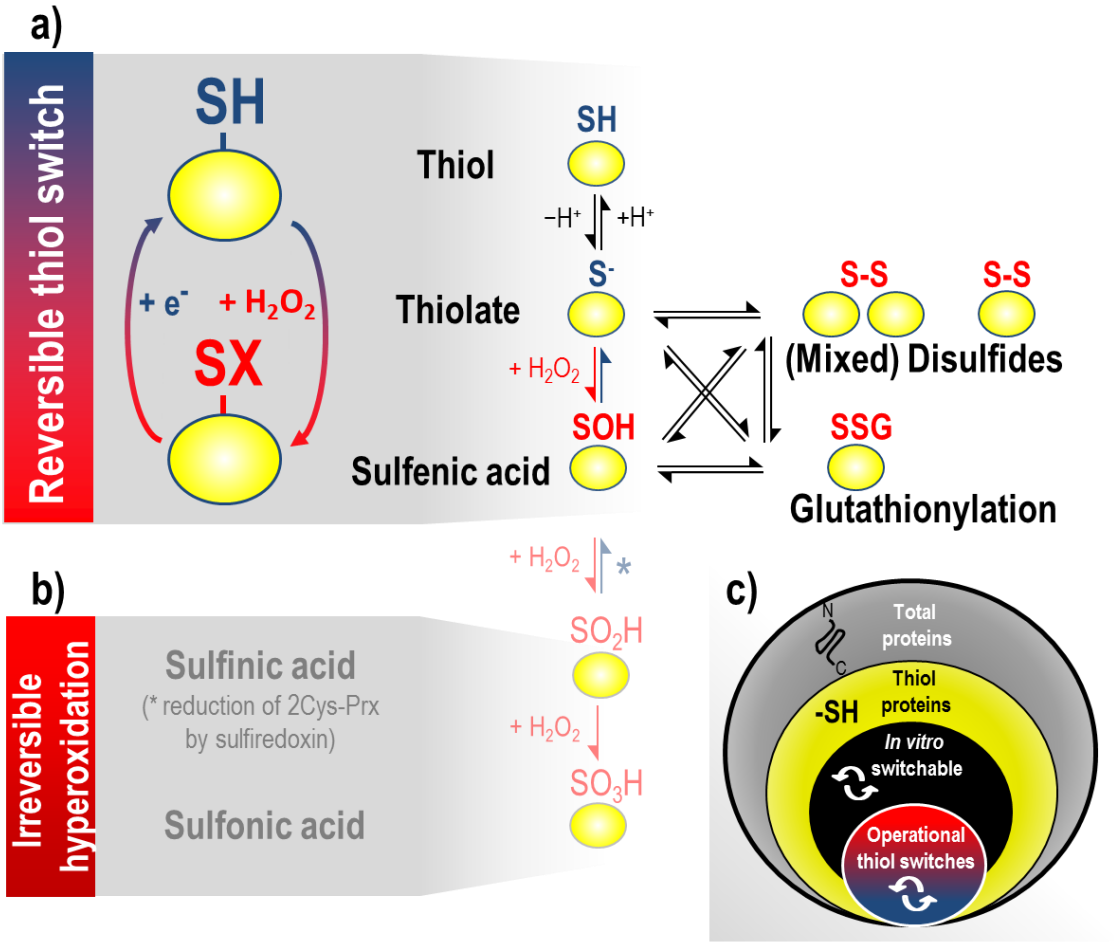

Figure 3: Thiol redox modifications of proteins. Protein thiols can undergo various oxidation reactions; several modifications are reversible a), whereas others are not or only in exceptional cases b), *e.g.* the reduction of sulfinic acid on 2Cys-peroxiredoxins by sulfiredoxins (BITEAU *ET AL.*, 2003; WOO *ET AL.*, 2005). Thiols are deprotonated to give rise to the reactive thiolate anion allowing reversible oxidation to sulfenic acid. Reactive sulfenic acids can be glutathionylated, form inter- or intramolecular disulfide bonds, or can be further oxidised to sulfinic or sulfonic acids, while other thiol redox modifications will not be discussed in detail. Reversible redox modifications can be converted to the thiolate anion by glutaredoxins and thioredoxins. Of all thiol proteins c), a subset of thiols is switchable under *in vitro* conditions; whether or not those thiol-switches are functional under physiological meaningful conditions requires empirical validation *in vivo*. *Vice versa*, not all thiol-switches that are operational *in vivo* are necessarily detectable under *in vitro* conditions. Figure modified from NIETZEL *ET AL.*, 2017.

1.3.3 Proteomic identification of redox-regulated proteins

1.3.3.1 Thioredoxin-/ and glutaredoxin-trapping approaches

State-of-the-art proteomic approaches have opened a new door allowing to make the critical step towards assessing the redox behaviour of protein thiols in their endogenous context. First efforts towards a global identification of thiol protein switches emerged with the realisation that chloroplast thioredoxins alter the activity of specific target enzymes of the Calvin-Benson-cycle and other chloroplastic processes via thiol-switching (WOLOSIUK AND BUCHANAN 1977). By adjusting techniques that were initially developed for the identification of redox-regulated proteins of yeast (VERDOUCQ *ET AL.,* 1999), the first proteome-wide studies on thiol-switched proteins were conducted in plant chloroplasts (MOTOHASHI *ET AL.,* 2001) and were extended to cytosolic proteins (YAMAZAKI *ET AL.,* 2004) and mitochondrial proteins (BALMER *ET AL.,* 2004; MARTI *ET AL.,* 2009; YOSHIDA *ET AL.,* 2013). These commonly applied thioredoxin (Trx) -trapping approaches are based on the mutation of the resolving cysteine of the conserved active-site motif of thioredoxins (CxxC) to serine or alanine (CxxS or CxxA; VERDOUCQ *ET AL.,* 1999). This prevents the release step in the reaction mechanism of thioredoxins with their oxidised targets. A stable heterodisulfide is formed between the attacking cysteine of the thioredoxin active site and the target cysteine of a protein from an extract. The target protein is trapped by the thioredoxin that is itself bound to a column and can be released for identification by washing with a reductant such as DTT (**Figure 4 a**). In a comparable approach, resolving of the heterodisulfide can be slowed down by the mutation of a highly conserved proline in close proximity to the active-site motif (KADOKURA *ET AL.,* 2004). Rouhier and colleagues expanded this technique to use a dithiol glutaredoxin, mutating its CxxC motif (ROUHIER *ET AL.,* 2005), to identify targets in whole cell extracts from poplar. These pioneering works have allowed the discovery of novel potential targets of plant thioredoxins and glutaredoxins, which has been a valuable starting point for further assessment. The power of the available data critically depends on a rigorous interpretation, however. The trapping is usually performed at ambient conditions and oxidised target thiols are a prerequisite for successful trapping, meaning that the thermodynamic environment is oxidatively shifted as compared to *in vivo*, where reductive and oxidative influences result from active metabolism. The irreversible nature of the binding also implies that kinetic competition is minimal, and *in vivo* compartmentalisation is lost in organellar or whole cell protein extracts. Furthermore, it is unclear to what extent the recombinant thioredoxins and glutaredoxins from different cell compartments and species that have been used can recreate the endogenous target specificity. This appears relevant in the light of the recent finding that specificity depends on the surface composition of the entire contact area, rather than just on the active site motif (BERNDT *ET AL.,* 2015). For instance, candidate glutaredoxin targets of mitochondrial origin have been identified in Arabidopsis extracts using a classical dithiol CxxC (mutated to CxxS) glutaredoxin from poplar cytosol (ROUHIER *ET AL.,* 2005). However, no enzymatically active dithiol glutaredoxin is known to reside in the mitochondrial matrix of Arabidopsis (MOSELER *ET AL.,* 2015; STRÖHER *ET AL.,* 2016). This makes it unclear if and how regulation of enzyme activities, as observed for glycine decarboxylase after glutaredoxin addition *in vitro* (HOFFMANN *ET AL.,* 2013), can occur in plant mitochondria *in vivo*. The danger of introducing an unknown number of false positives has been a limitation that has been pointed out in the reports on *in vitro* trapping, and does not take away from the fact that longlists of potential targets carrying a thiol-switch have provided a valuable platform for follow-up work. A sophisticated variant of thioredoxin-trapping has recently been applied by expressing a mitochondrial Trx2 with a mutated resolving cysteine in human cells *in situ*

under the control of the endogenous promotor (ENGELHARD *ET AL.,* 2011). This addresses concerns about the ambient redox potential and preserves the *in vivo* structural organisation of actively respiring mitochondria. Yet, kinetic competition is disabled and, once trapped irreversibly, Trx2 targets accumulate over time, which may still generate false positives, but comes with the technical advantage of increasing sensitivity.

1.3.3.2 Approaches for thiol labelling and labelling of sulfenylated proteins

As an alternative to the thioredoxin-/glutaredoxin-trapping approaches, labelling of redox modified cysteines is commonly applied to identify redox-switched proteins (**Figure 4 b**). Reduced protein thiols can be labelled via thiol-specific compounds linked to a number of different reporter tags (for a detailed recent review see CHOUCHANI *ET AL.,* 2011). Specificity for these reporter tags often comes from iodoacetamide or maleimide groups, covalently modifying reduced cysteine thiols. Both reagents are highly specific for the thiolate anion, although this specificity drops at very high pH values (LEICHERT AND JAKOB 2006). Several reporter tags have been used in combination, including radioisotope labels and fluorescent dyes (YANG *ET AL.,* 2016) and biotin to allow streptavidin-based blot analysis (LEICHERT AND JAKOB 2006) or enrichment steps. Individual thiol-reactive fluorescent probes, such as monobromobimane, have also been used in combination with 2D-PAGE (YANO *ET AL.,* 2001), but cyanine-based fluorescent dyes (*Cy2*, *Cy3* and *Cy5*) offer application in more sophisticated differential gel electrophoresis (DIGE, more specifically redoxDIGE; **Figure 4 b**) approaches allowing sample multiplexing (HURD *ET AL.,* 2007). The relative redox state of a protein can be quantified based on the relative reporter tag intensities in both experimental conditions after gel-based separation; and the identity of the protein can be subsequently determined by mass spectrometry (MS, **Figure 4 b**).

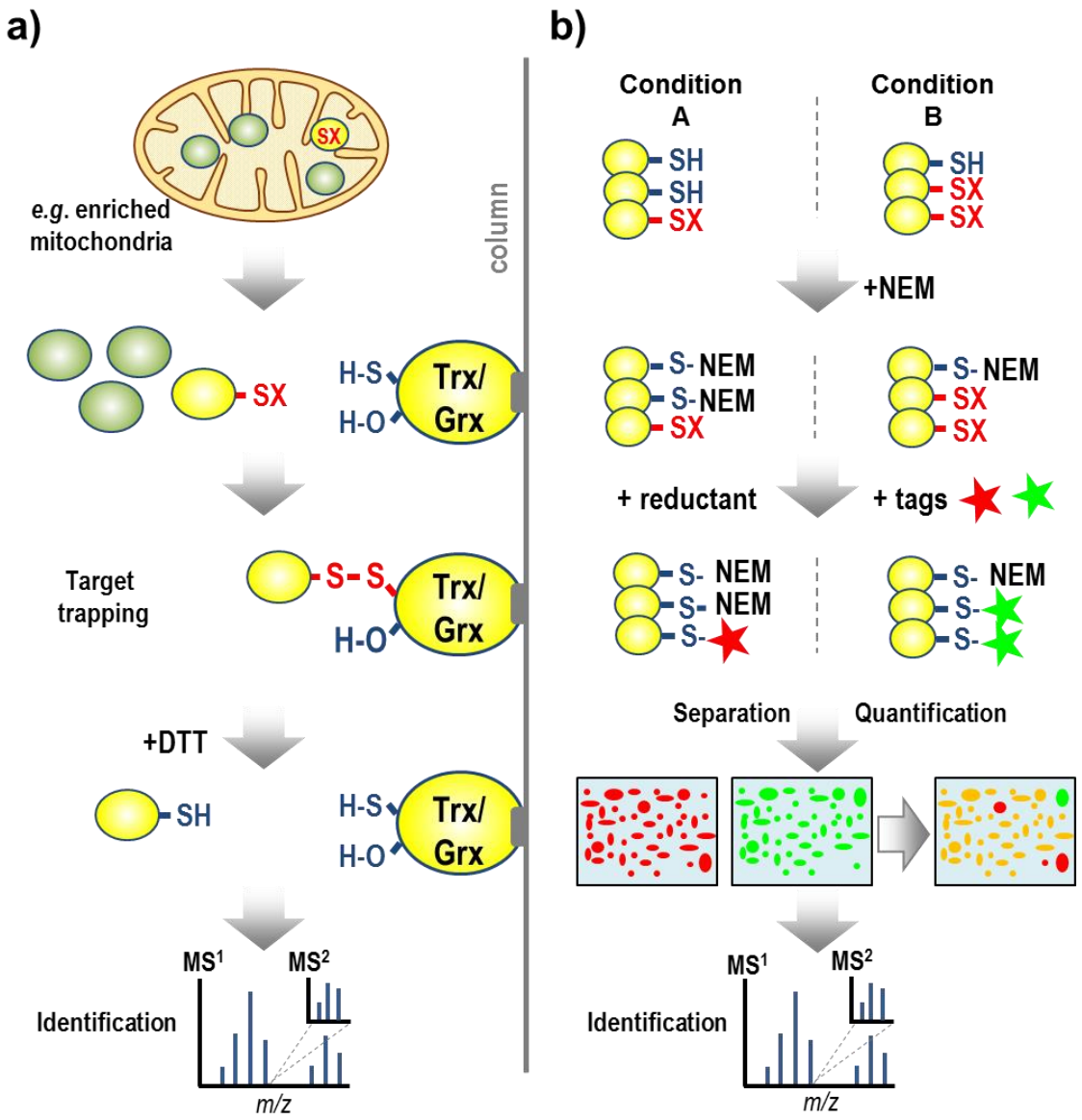

Figure 4: *In vitro* identification of targets of the cellular redox machinery. Commonly used strategies for the global identification of redox active protein thiols. For *in vitro* thioredoxin-/ glutaredoxin-trapping a), protein fractions, *e.g.* of isolated mitochondria, are applied to a column carrying an immobilised, reduced thioredoxin/glutaredoxin variant that lacks the second resolving cysteine. Stable hetero-disulfides are formed with target proteins allowing depletion of non-target proteins, followed by elution of target proteins by reduction, *e.g.* with dithiothreitol (DTT), and their identification by mass spectrometry (MS). For redoxDIGE thiol labelling in b), reduced thiols are blocked with N-ethylmaleimide (NEM) in a first step in both samples, *e.g.* control and treatment. After reduction of the remaining oxidised cysteines, *e.g.* with TCEP, different thiol-specific fluorescent tags allow quantification based on fluorescent ratio of protein spots after separation of the mixed extracts on 2-dimensional gel and identification of protein spots by MS. Figure modified from NIETZEL *ET AL.,* 2017.

While thioredoxin and glutaredoxin-based target-trapping relies on the reactivity to specific oxidised protein cysteines, labelling of protein cysteines by iodoacetamide or maleimide groups depends on the presence of reduced thiol residues. Also labelling of sulfenylated proteins has become available by using 4-(pent-4-yn-1-yl) cyclohexane-1,3-dione (DYn-2) that reacts with sulfenic acids residues as a tag for click chemistry (PAULSEN *ET AL.,* 2012). DYn-2 probes are membrane permeable, allowing direct application within the

native cell environment making them suitable for labelling proteins that are sulfenylated *in vivo*. In a pioneering study in plants, Arabidopsis suspension cells were stressed by external hydrogen peroxide application, followed by DYn-2 labelling (AKTER *ET AL.,* 2015). In a technically orthogonal approach, 97 sulfenylated proteins were recently identified by *in vivo* trapping in the cytosol of Arabidopsis cells using a genetically encoded probe. The probe consists of the C-terminal domain of the yeast activator protein 1-like transcription factor (YAP1) fused to a tandem affinity purification tag (WASZCZAK *ET AL.,* 2014). The ability of Cys^{598} of YAP1 to specifically react with sulfenic acid moieties of target proteins, in combination with the removal of the resolving cysteine, allows tagging of sulfenylated proteins by stable disulfide formation even with capacity for subcellular resolution when targeted to certain organelles. Both tags for labelling of sulfenylated proteins rely on the protein identification by mass spectrometry.

1.3.3.3 Thiol labelling with (tandem-)mass-tags

For the relative quantification of reversible thiol oxidation by mass spectrometry the thiol-specific isotope-coded affinity label set (ICAT, two labels; GYGI *ET AL.,* 1999) or iodoacetyl tandem mass tags (iodoTMT, six labels, **Figure 5 a**; THOMPSON *ET AL.,* 2003) have been used in multiplex labelling experiments. Both tags consist of a thiol-reactive iodoacetyl group, a linker and an affinity group for purification. For the analysis of cysteine-oxidations in proteomes, reduced cysteines in cell lysates are blocked with iodoacetamide or N-ethylmaleimide (NEM) and reversibly oxidised cysteine residues are reduced and labelled with ICAT or iodoTMT. For ICAT, the biotin moiety enables the streptavidin-based enrichment of peptides derived from proteolytically cleaved protein samples (typically using trypsin). IodoTMT-labelled peptides are purified by immunoprecipitation with an antibody directed against the TMT. ICAT-labelled peptides can be distinguished in peptide mass spectra by the 9 Da mass difference between the light and heavy isotope-labelled variant and the comparison of the signal intensities of two different conditions indicates changes in the level of thiol oxidation. An advantage of iodoTMT-labelling is its multiplexing capacity. The six isobaric iodoTMTs, with the same total molecular mass of the complete tags but differences in the distribution of the individual isotopes, release six specific reporter groups with different masses that are detected during MS/MS and are used for quantification (see **Figure 5** for an illustrative explanation). The immunoprecipitation with the anti-TMT-directed antibody resin is not as efficient as with ICAT, which results in higher non-labelled peptide background. This, however, does typically not lead to less peptide identifications with modern, fast scanning tandem mass spectrometers.

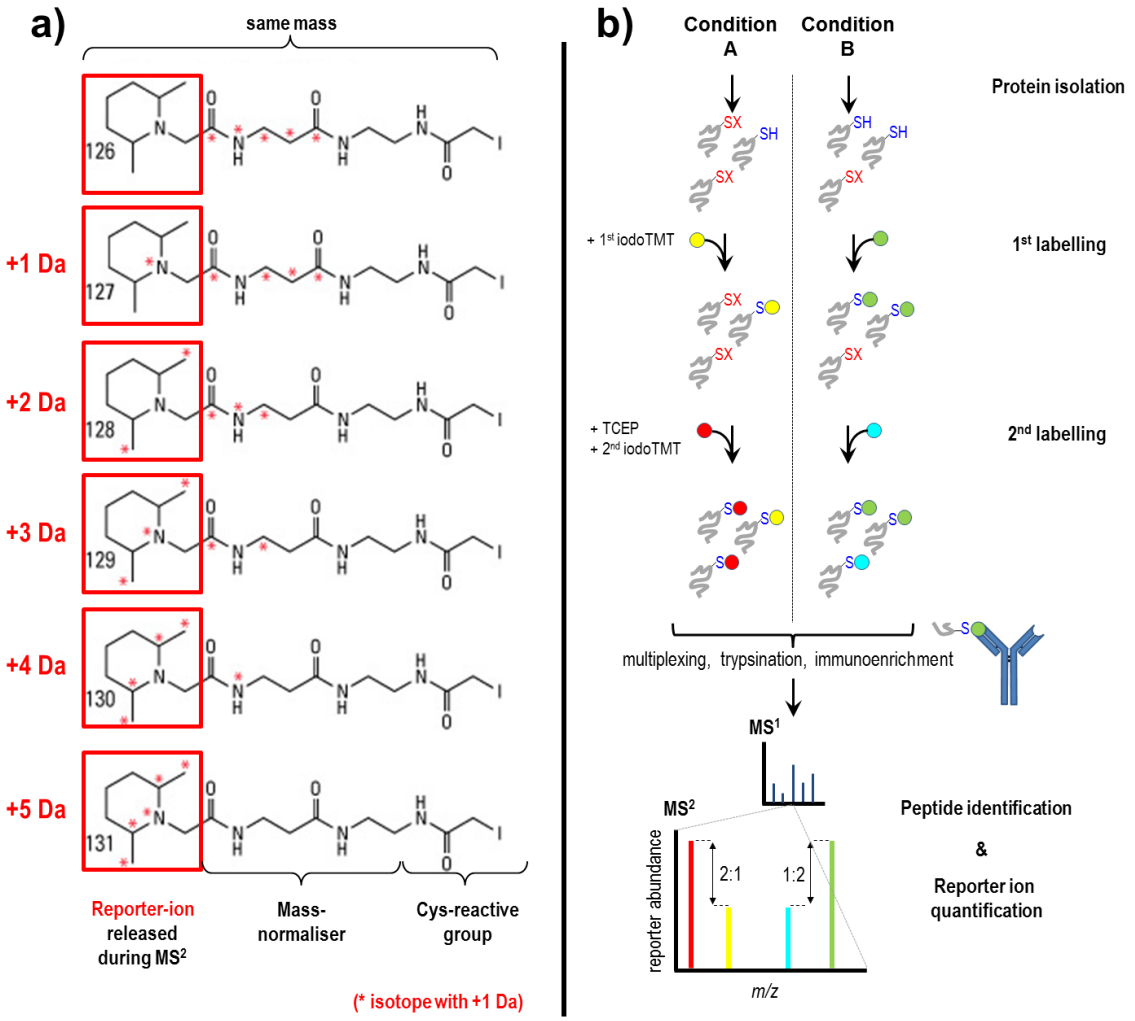

Figure 5: Global analysis of the redox state of individual thiol peptides by differential thiol labelling strategy and iodoacetyl tandem mass tags. In a), structural properties of the six different iodoacetyl tandem mass tags (iodoTMT 126 - 131) and of the specific reporter ions generated during MS/MS fragmentation (red boxes, 126 – 131 Da) are shown (chemical structures of the iodoTMTs obtained from www.thermofisher.com). For estimation of the global protein thiol redox state in b), protein thiols (-SH) were specifically labelled during or after protein extraction with different iodoTMTs (illustrated by yellow and green circles). Excess iodoTMT reagent is depleted, TCEP reduces reversibly oxidised cysteine residues (-SX), which are then labelled with a second iodoTMT (red and blue circles). Labelled proteins are combined and then processed for mass spectrometry including an immunoenrichment step against iodoTMT-labelled peptides; example shows multiplexing of two samples but can be extended to three samples with two different tags each. By fragmentation at MS^2, unique reporter ions of the individual iodoTMT are generated (126-131 Da in size) allowing the calculation of the Cys-peptide redox state based on the relative quantity of the 1st and 2nd TMT. Exemplary hypothetical Cys-peptide population in condition A shows a Cys-oxidation state of 66 %, whereas in condition B the Cys-peptide oxidation state is 33 % resulting in a Δ Cys-reduction of 33 % between both conditions. While for OxICAT-based analysis labelled peptides are quantified by peptide peaks in the MS^1 spectra, iodoTMTs are isobaric, which allows for the generation of unique reporterions for quantification by MS^2 fragmentation.

1.3.3.4 Differential thiol labelling to determine the redox state of individual Cys-peptides

The exclusive analysis of thiol-oxidised peptides by mass spectrometry does not consider changes in protein abundance and does not allow calculation of reduced and oxidised proportions of individual thiol-oxidised peptides. Hence, a direct calculation of the oxidation level is not possible. To this end, differential thiol labelling techniques have been developed, based on the same principles, to identify thiol-switched proteins and quantify the redox state of their switches (**Figure 5 b**). The OxICAT approach makes use of the ICAT reagents (LEICHERT *ET AL.,* 2008): unmodified cysteine residues in protein samples are labelled with one tag to freeze the *in vivo* thiol status. Reversibly oxidised cysteine residues are subsequently reduced with TCEP followed by labelling with the second tag. Measuring the relative abundances of light and heavy labelled peptides allows to determine the oxidation state of individual cysteine residues in proteins. The possibility for the absolute quantification of the thiol redox state with resolution for individual cysteines, commercial accessibility of appropriate reagents and increased sensitivity of state-of-the-art mass spectrometers have been decisive advantages. The OxICAT technique is currently widely used and has made prior redox proteomics methods largely obsolete for routine application. The versatility of the OxICAT technique has been shown in numerous studies of different organisms (BRANDES *ET AL.,* 2011; KNOEFLER *ET AL.,* 2012; LEICHERT *ET AL.,* 2008; MENGER *ET AL.,* 2015). Different to thioredoxin-/ or glutaredoxin-based trapping approaches, the differential labelling strategy of thiol proteins not only allows the identification of potentially redox-regulated thiol proteins, but also pinpoints the exact reactive cysteine and quantifies its percentage of oxidation. By enrichment of all labelled peptides via the biotinylated tags, even low abundant redox-switched proteins can be identified. This combination offers unprecedented depth and detail, the potential of which has only begun to be systematically exploited. OxICAT, however, is based on the light and heavy version of the ICAT reagents, resulting in labelled reduced and oxidised cysteine peptides differing in their molecular masses. With only two different tags available no sample multiplexing can be performed. Here the availability of six different iodoTMT variants, which can be discriminated by the molecular weight of the reporter ion generated during MS/MS fragmentation, can be of advantage (**Figure 5 a**). Up to three different samples can be labelled analogously to OxICAT but allow multiplexing. Also iodoTMTs were already successfully applied in the differential labelling strategy to estimate the global Cys-peptide redox state (CHOUCHANI *ET AL.,* 2016; ARAKI *ET AL.,* 2016).

1.4 Hydrogen peroxide sensing *in planta*

1.4.1 Hydrogen peroxide-mediated signalling in plants

For a protein thiol to undergo redox-switching, by definition it either has to be specifically reduced from an oxidised state or it needs to be oxidised when it is initially in a reduced state (**Figure 3 a)**. In plants, the driving force for the reduction of an oxidised cysteine derives ultimately from water being split during photosynthesis and passing its electrons to the ferredoxin/thioredoxin system. The electrons are used to reduce $NADP^+$ to NADPH, eventually fuelling the cellular redox machineries. On the other hand hydrogen peroxide is considered an important electron sink driving the oxidation of initially reduced protein thiols (*e.g.* NEILL *ET AL.,* 2002). Hydrogen peroxide can either directly oxidise protein thiols or oxidation can be mediated by specialised enzymes, *e.g.* by peroxiredoxins, such as the yeast

oxidant receptor peroxidase-1 (Orp1), which shows a particularly high affinity to react with hydrogen peroxide and mediates the targeted oxidation of the YAP1 transcription factor (DELAUNAY *ET AL.,* 2002). These mediating peroxidases enable specificity of a signal coded by the oxidant hydrogen peroxide formed in the metabolism, *e.g.* in the respiratory chain of mitochondria (MURPHY 2009) or during β-oxidation in the peroxisomes, by the specific oxidation of their target proteins, which in turn triggers a specific response. Hydrogen peroxide signalling in Arabidopsis was shown to be involved in diverse fundamental signalling processes, *e.g.* the formation of root hairs (FOREMAN *ET AL.,* 2003) or pollen tube growth (POTOCKY *ET AL.,* 2007). Also for orthodox seeds hydrogen peroxide has been suggested to be involved in multiple developmental steps, such as embryogenesis, reserve compound accumulation, maturation and initiation of germination (reviewed in BAILLY 2004). While for the desiccated seed it is assumed that hydrogen peroxide is formed non-enzymatically via Maillard reactions, in germinating seeds the β-oxidation of fatty acids in peroxisomes and the restarted mitochondrial respiration are thought to contribute to hydrogen peroxide formation (EL-MAAROUF-BOUTEAU AND BAILLY 2008). The release of seed dormancy and the transition from quiescence to increased metabolic activity have also been associated with hydrogen peroxide generation (*e.g.* SCHOPFER *ET AL.,* 2001; ORACZ *ET AL.,* 2009). However, any mechanistic understanding of the implied hydrogen peroxide-mediated signalling processes is currently lacking.

1.4.2 Dynamic sensing of hydrogen peroxide in plants with genetically encoded probes

To understand at which specific regulatory processes and at which developmental stage hydrogen peroxide signalling is actually involved, the specific detection of hydrogen peroxide *in planta* would help to make the first step towards the identification of these hydrogen peroxide-mediated signalling processes, for which so far only few examples are known in plants (*e.g.* FOREMAN *ET AL.,* 2003). While *in vitro* detection of hydrogen peroxide is well established, mostly by using diverse fluorescent dyes (*e.g*. GOMES *ET AL.,* 2005), *in vivo* measurements of hydrogen peroxide still suffer from major technical confinements. Up to now, mostly dichlorofluorescein (DCF) derivatives are used for the detection of hydrogen peroxide *in vivo*. As a major constraint of these fluorescent dyes, they are lacking specificity for hydrogen peroxide and show significant reactivity to several other reactive oxygen species. The irreversible reaction mechanism prevents a dynamic monitoring of the endogenous hydrogen peroxide levels, but allows sensitive quantification of ROS levels based on signal accumulation over time. A serious disadvantage of DCF derivatives is their potential to produce ROS at exposure to light, which may trigger artificial signal amplification (MARCHESI *ET AL.,* 1999). Because most fluorescent dyes are intensiometric with single excitation and single emission characteristics, the absolute emitted fluorescence intensity detected is directly correlated to the amount of fluorescent dye. Thus, the emission read-out is biased by the uptake efficiency of the tissue or cell for the fluorescent dye. Furthermore, fluorescent dyes cannot be specifically targeted to different subcellular compartments; many fluorescent dyes are also membrane-impermeable excluding intracellular hydrogen peroxide measurements.

Genetically encoded fluorescent probes were designed to overcome several of the key constraints of commonly used fluorescent dyes, such as low specificity for hydrogen peroxide and the lacking possibility to target subcellular compartments. This allows monitoring hydrogen peroxide dynamics directly at its origin of formation in the metabolism.

Although often (mis)used for the detection of hydrogen peroxide, redox sensitive green fluorescent protein 2 fused to human glutaredoxin 1 (Grx1-roGFP2) shows a very low reactivity to hydrogen peroxide when compared with competing endogenous thiols of specialised hydrogen peroxide detoxifying enzymes (SCHWARZLÄNDER *ET AL.,* 2016), but is highly specific for the E_{GSH} (GUTSCHER *ET AL.,* 2008). With Grx1-roGFP2 sensors hydrogen peroxide formation may be monitored indirectly via the oxidation of the cellular glutathione pool; which is assumed to rarely happen under most physiological conditions. To overcome these limitations of E_{GSH}-biosensors to detect hydrogen peroxide, several more specific genetically encoded sensors were engineered (*e.g*. HyPer: BELOUSOV *ET AL.,* 2006; HyPer2: MARKVICHEVA *ET AL.,* 2011; HyPer3: BILAN *ET AL.,* 2013; HyPerRed: ERMAKOVA *ET AL.,* 2014; roGFP2-Orp1: GUTSCHER *ET AL.,* 2009; roGFP2-Tsa2: MORGAN *ET AL.,* 2016). A common characteristic of these fluorescent biosensors is the fusion of a hydrogen peroxide sensitive domain - such as peroxidases to facilitate specificity - to a fluorescent protein allowing dynamic detection via changes in its optical properties (**Figure 6**).

1.4.3 The hydrogen peroxide probe roGFP2-Orp1

Even though the HyPer probe was already characterised in Arabidopsis (COSTA *ET AL.,* 2010) and is widely used for monitoring of hydrogen peroxide in different organisms, its underlying chromophore, a circular permutated yellow fluorescent protein (cpYFP), was found highly pH-sensitive (SCHWARZLÄNDER *ET AL.,* 2011; SCHWARZLÄNDER *ET AL.,* 2014) making the unambiguous interpretation of obtained data complex. Minor changes observed in the HyPer read-out, as described in different organisms (*e.g.* NIETHAMMER *ET AL.,* 2009), may be caused by a slightly altered local pH. In different studies a HyPer probe response was indeed caused by an altered pH and not or only partially by the formation of hydrogen peroxide (ROMA *ET AL.,* 2012; WELLER *ET AL.,* 2014). In contrast, the roGFP2-based sensors for monitoring E_{GSH} were found as pH-inert in a physiological meaningful range (SCHWARZLÄNDER *ET AL.,* 2008), are characterised in detail (*e.g.* DOOLEY *ET AL.,* 2004; HANSON *ET AL.,* 2004) and are therefore reasonable sensing domains for the design of hydrogen peroxide specific probes by the fusion to specific peroxidases with high affinity for hydrogen peroxide, and may offer an increased robustness of the sensor read-out towards physiological pH changes. The probe roGFP2-Orp1 was established for monitoring of hydrogen peroxide dynamics in yeast (GUTSCHER *ET AL.,* 2009), but was also successfully applied to Drosophila (ALBRECHT *ET AL.,* 2011). The probe roGFP2-Orp1 is based on the fusion of the yeast glutathione peroxidase 3, also known as Orp1, to roGFP2 (GUTSCHER *ET AL.,* 2009). Upon encountering hydrogen peroxide, Orp1 forms a sulfenic acid (-SOH) at its cysteine (Cys^{36}, DELAUNAY *ET AL.,* 2002 and **Figure 6**). This sulfenic acid then condenses with Cys^{82} to generate an intramolecular disulfide (S-S). Enhanced by close proximity, the disulfide bridge of the oxidised Orp1 is transferred to the reduced roGFP2 on the basis of conventional thiol-disulfide exchange. Disulfide bridge formation slightly influences the conformation of the β-barrel affecting the optical characteristics of the chromophore. Oxidation of roGFP2 is reversible and can be monitored dynamically by changes in its optical characteristics at sequential excitation at about 405 and 488 nm and single emission at about 511 nm. After the oxidation of the probe by hydrogen peroxide *in vivo*, the oxidised probe is reduced by the cellular redox machinery, which allows a dynamic monitoring of the hydrogen peroxide homeostasis. Yet, the contribution of the individual redox machineries to the *in vivo* reduction of the probe is not known and may be very complex. The reduction of the free roGFP2 specifically depends on the cellular E_{GSH} (*e.g.* DOOLEY *ET AL.,* 2004; HANSON *ET AL.,* 2004), whereas the reduction of the linked Orp1 was characterised as dependent on the

thioredoxin-linked redox machinery (DELAUNAY *ET AL.,* 2002). A functional redox-relay active between the glutathione-linked roGFP2 and the thioredoxin-linked Orp1 may short-circuit both cellular redox machineries, and therefore predictions for the redox machinery responsible for reduction of the probe *in vivo* are particularly hard and ambiguous. Yet, the reduction of the probe by the endogenous redox machineries directly influences its oxidation level and therefore also the probe read-out. The precise estimation of the individual contribution of both redox machineries to the reduction of the probe *in vivo* is essential to discriminate between the impact of the reducing system and the actual formation of hydrogen peroxide.

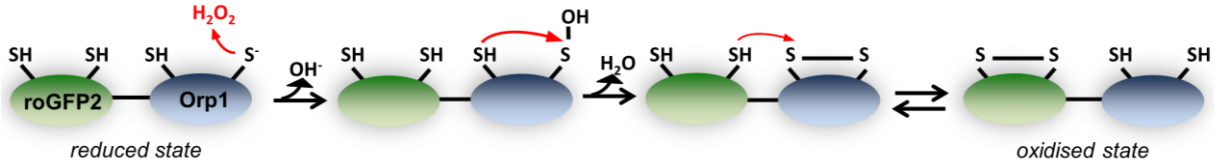

Figure 6: Molecular mechanism of hydrogen peroxide sensing by the genetically encoded probe roGFP2-Orp1. Yeast oxidant receptor peroxidase-1 (Orp1) is fused to the redox-sensitive green fluorescent protein 2 (roGFP2). In presence of hydrogen peroxide, the reactive Cys^{36} of the Orp1 domain forms a sulfenic acid (-SOH), which triggers the formation of an intramolecular disulfide bride (S-S) with Cys^{82}. The disulfide bridge is transferred to roGFP2 by a conventional thiol disulfide exchange. Orp1 acts as specificity domain for hydrogen peroxide whereas roGFP2 acts as a read-out domain. Figure modified from ALBRECHT *ET AL.,* 2011.

1.5 Objectives

1.5.1 To assess dynamics in energy metabolism during early seed imbibition

Detailed insight into the metabolic rearrangements and underlying regulatory processes facilitating the quiescence release of seeds are missing, especially for early phases at imbibition, as so far mostly later phases of germination have been addressed by classical biochemical analysis with low temporal resolution. Different fluorescent biosensors are utilised to characterise the early transition from a quiescent seed to a metabolically restarted plant with resolution for fast metabolic alterations. Targeting of the genetically encoded probes to different subcellular compartments complements the insight obtained by classical biochemical detection methods, which are lacking subcellular resolution. A novel approach for the read-out of genetically encoded probes in intact seeds is applied as an alternative for classical confocal imaging of isolated seed embryos avoiding potential artefacts by seed manipulation.

1.5.2 To elucidate the involvement of the mitochondrial thiol redox machinery in germination

Posttranslational modifications in seeds involved in the quiescence release, *e.g.* redox modifications, are hardly investigated and only poorly understood and thus, the physiological relevance of the cellular redox machinery for the regulation of germination is not known. The impact of the redox machinery on the germination vigour is investigated in fresh and in artificially aged seeds of different mutants impaired in the different redox machineries, as seeds impaired in the mitochondrial thioredoxin-linked redox machinery

show slightly lowered germination efficiency (DALOSO *ET AL.*, 2015). Seeds with impaired redox machineries are also assessed for alterations of different primary metabolites in the dry state and after restarting of the metabolism shortly after imbibition.

1.5.3 To identify in situ *target proteins of the mitochondrial redox machinery*

So far known target proteins of the mitochondrial redox machinery were only obtained from *in vitro* experiments with limited biological significance (*e.g*. BALMER *ET AL.*, 2004). Structural organisation of intact mitochondria was commonly neglected, kinetic competition and thermodynamics set by actively respiring and functional mitochondria were not considered. A novel redox proteomic approach is established in which the physiological conditions of actively respiring and functional mitochondria are reconstituted to identify *in situ* target proteins of the mitochondrial redox machinery. This proteomic approach is then applied to different mutants impaired at different positions of the mitochondrial redox machinery to dissect the contribution of the individual components of the redox machinery to the reduction of target proteins.

1.5.4 To establish monitoring of hydrogen peroxide dynamics in planta *with the genetically encoded probe roGFP2-Orp1*

The *in vivo* monitoring of hydrogen peroxide has got several technical constraints and common fluorescent dyes lack specificity and subcellular resolution, whereas the genetically encoded probe `HyPer` is characterised by strong pH sensitivity. Here, the alternative probe for the detection of hydrogen peroxide, roGFP2-Orp1, is characterised *in vitro* and *in vivo* and the contribution of the cellular redox machinery to the probe read-out was estimated to establish dynamic monitoring of hydrogen peroxide levels in the living plant. This may enable to detect hydrogen peroxide dynamics in different physiological states, *e.g.* during the quiescence release of imbibed seeds.

2. RESULTS

2.1 Physiological changes in Arabidopsis seeds in response to imbibition

2.1.1 Considerable oxygen consumption rates occur immediately at imbibition

Dry, after-ripened *Arabidopsis thaliana* seeds were used to analyse different physiological parameters during early phases of imbibition with water. Oxygen consumption was used as an integrative read-out for flux through mitochondrial respiratory metabolism during early germination.

At imbibition the O_2 concentration started to decrease immediately, as measured by an increase of the fluorescence lifetime of the oxygen sensitive probe MitoXpress®Xtra (**Figure 7 a**; WILL *ET AL.,* 2006). The fluorescence lifetime continuously increased after imbibition. The rate of lifetime increase reached a first local maximum after 25 min of imbibition (**Figure 7 b**). After 125 min the maximal fluorescence life time increase rate was observed, followed by a phase of decreasing lifetime rates. Relative changes in fluorescent lifetime are directly proportional to relative changes in O_2 concentration. This observation suggests an immediate restart of the mitochondrial respiration in response to imbibition. However, conversion of altered fluorescent lifetime of the probe to absolute oxygen concentration requires additional assumptions, and was therefore not carried out.

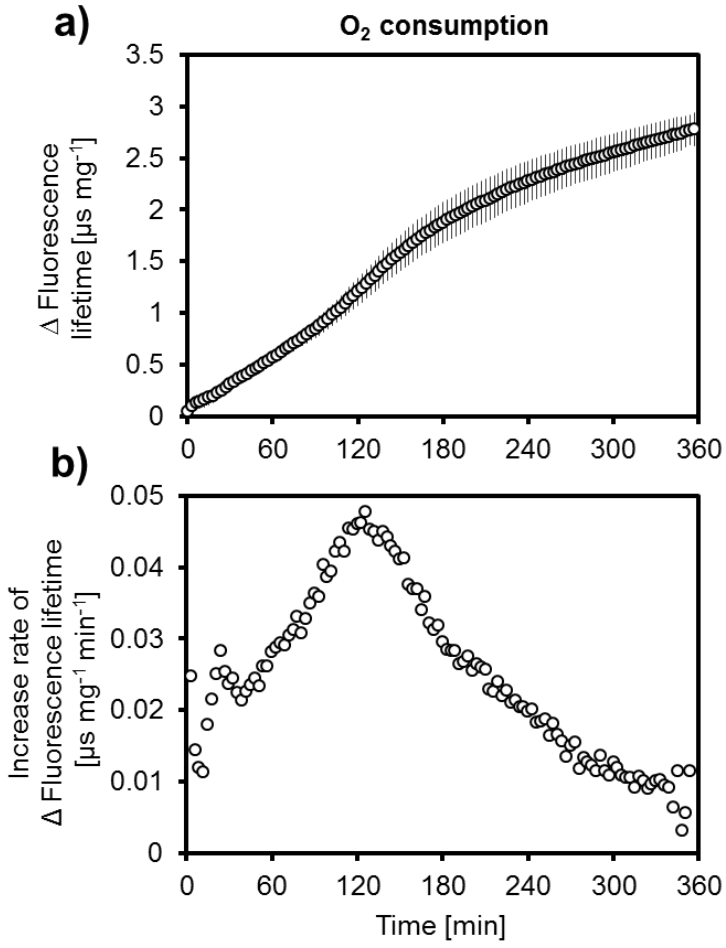

Figure 7: Oxygen consumption of Arabidopsis seeds in response to imbibition. The respiratory activity of *Arabidopsis thaliana* seeds during imbibition was measured using the MitoXpress®Xtra (Luxcel Biosciences) fluorescent probe (presence of oxygen physically quenches fluorescence lifetime) in a platereader assay (according to SECHET *ET AL.,* 2015). Fluorescence lifetime was recorded (excitation: 340 nm; emission: 605 - 705 nm). a) Probe lifetime increase (Δ Fluorescence lifetime) was calculated by subtraction of fluorescence lifetime at timepoint T_0 from the increasing fluorescence lifetime upon oxygen consumption during imbibition (average ±SD, *n* = 5 different seed batches). Δ Fluorescence lifetime was normalised to seed weight. b) Average rate of increase in the Δ fluorescence lifetime as a measure of oxygen consumption rate. Each data point derived from the average of the fluorescence lifetime increase rates in a three minute window. Measurements were performed by the group of Prof. Macherel.

2.1.2 Fluorescent protein biosensors allow for monitoring physiological changes at seed imbibition

The instant onset of oxygen consumption in response to imbibition implies a rapid restart of the mitochondrial energy metabolism. This rapid switch between the largely quiescent metabolism of dry seeds to a considerable metabolic activity in response to imbibition implies flux through the metabolic network with impacts on the size of metabolite pools. To analyse the transition that is triggered by imbibition at more depth, genetically encoded fluorescent biosensors were used to monitor the dynamics of selected metabolic co-factors with subcellular resolution, including cytosolic MgATP concentration (IMAMURA *ET AL.,* 2009), cytosolic NAD redox state (HUNG *ET AL.,* 2011) and glutathione redox potential in the cytosol and the mitochondrial matrix (DOOLEY *ET AL.,* 2004; HANSON *ET AL.,* 2004; GUTSCHER *ET AL.,* 2008). The fluorescent biosensors are commonly monitored by confocal imaging, but high auto-fluorescence of the seed coat and the endosperm is impairing the probe read-out. To detect sufficient light emitted from the fluorescent probes through the surrounding tissues of the plant embryo, the optical slice has to be increased by opening of the pinhole. This makes confocal imaging obsolete, as now emitted light is also detected from other focal planes. However, removal of the seed coat and the endosperm allows imaging of the plant embryo, but manipulation of the seed needs a few minutes and cannot be performed in the dry state. This precludes imaging of the fluorescent probes in dry seeds in the quiescent metabolic state, and also of the early transition that may be triggered by imbibition. Manipulation of the seed may also introduce artefacts, *e.g.* removal of multiple surrounding cell layers may have got an influence on the water uptake efficiency of the embryo and potentially also on the kinetics of the metabolic restart. To follow the rapid dynamics in imbibed seeds with high temporal resolution, and to allow imaging of intact seeds, also in the dry stage, a platereader-based assay was established to analyse the different fluorescent biosensors instead of using conventional confocal imaging (**Figure 8**). Although a platereader-based analysis lacks spatial resolution as confocal imaging facilitates, the fluorescence biosensors were targeted specifically to individual cellular compartments, which gives subcellular specificity to the probe signals. This allows dynamic monitoring of different metabolite pools with subcellular resolution, globally for intact seeds, as the removal of the seed coat and the endosperm is not needed. Platereader-based probe read-out also offers the capacity for high-throughput analysis of seeds during imbibition, and side-by-side comparisons of different fluorescent probes are feasible. In principal various sensors targeted to different subcellular localisations can be used to obtain a detailed overview of the metabolic dynamics triggered by imbibition, but low absolute fluorescence intensities of the sensor in seeds, as often observed for mitochondrial targeted sensor constructs, are the major constraint for platereader-based assays. The high auto-fluorescence *e.g.* of the seed coat and the endosperm, in combination with low probe signals, gives a low signal-to-noise-ratio, which may preclude unambiguous measurements. Fluorescence emission and excitation spectra were performed with a platereader to check for specific and bright sensor signals in seeds in dry and imbibed state (**Figure 9**, **Figure 12**, **Figure 15**).

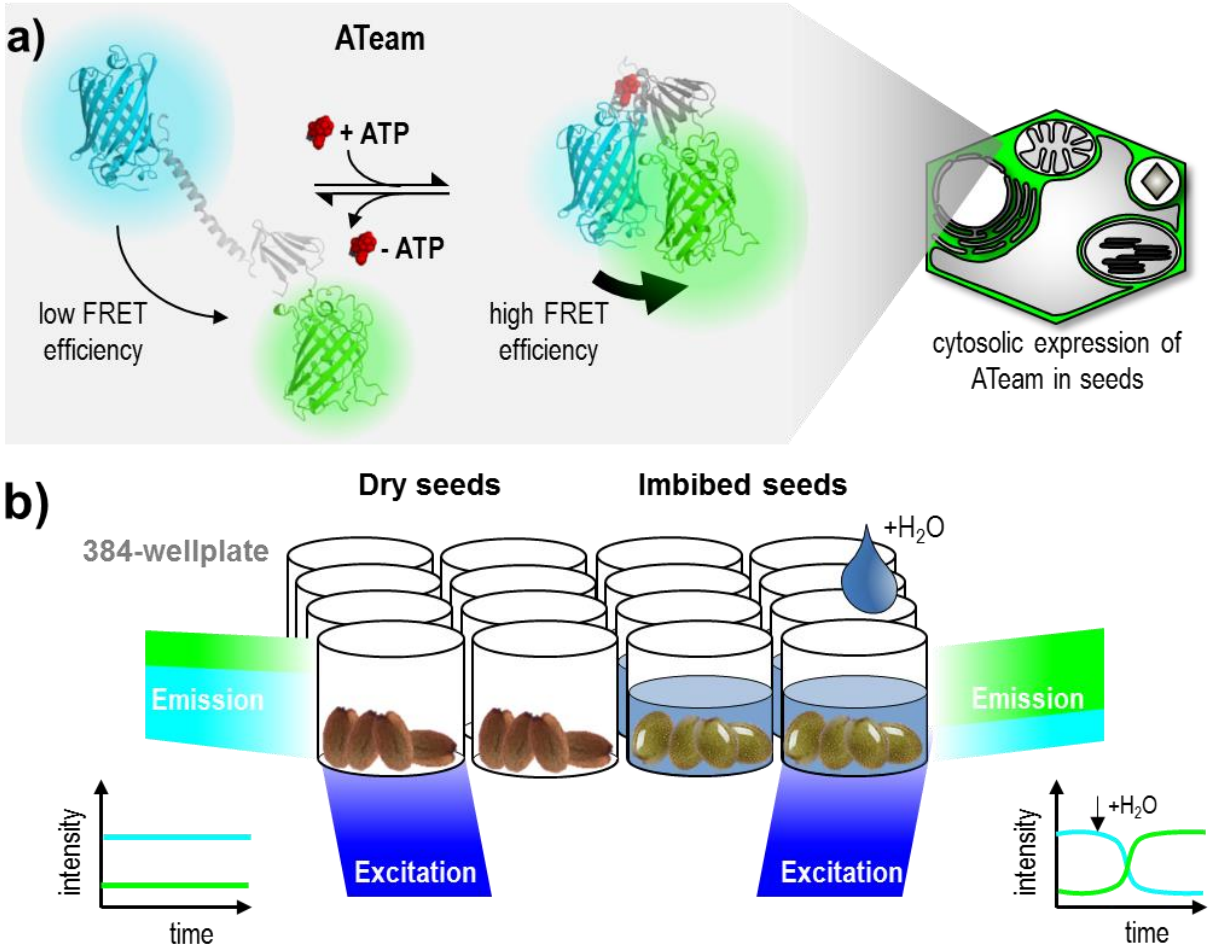

Figure 8: Platereader-based detection of fluorescent biosensors in seeds. Schematic representation of the rationale of monitoring fluorescent protein biosensors in seeds using a 384-well plate format. The specific example of cytosolic MgATP-sensing using the biosensor ATeam 1.03 is illustrated. a) ATeam undergoes a conformational change at MgATP-binding by the ATP-synthase ε-subunit domain, which increases the Förster resonance energy transfer (FRET) efficiency between the cyan-fluorescent-protein (CFP) and circular-permutated-yellow-fluorescent-protein (cpYFP, modified from DE COL *ET AL*., 2017, *in preparation)*. b) FRET of ATeam-fluorescence can be monitored over time in dry and imbibed seeds with high temporal resolution; side-by-side measurements of seeds without sensor expression allows for subtraction of background.

2.1.3 Fluorescent protein-based ATP sensing allows ATP monitoring in intact seeds

To validate the immediate onset of O_2 uptake at seed imbibition, cytosolic adenosine triphosphate (ATP) dynamics were investigated. ATP, as a main product of the oxidative phosphorylation, was used as a further read-out for mitochondrial respiration during early germination. Seeds with cytosolic expression of the MgATP-specific FRET-sensor ATeam 1.03 (IMAMURA *ET AL.*, 2009; DE COL *ET AL.*, 2017, *in preparation*) were assessed for adequate fluorescence intensities and signal-to-noise-ratio by performing platereader-based emission scans. When excited at 435 ± 5 nm, two characteristic peaks were present at 475 nm and 527 nm in the emission spectrum (**Figure 9**) corresponding for the cyan-fluorescent-protein (CFP) and the circular-permutated-yellow-fluorescent-protein (cpYFP) of the FRET-sensor. Both defined peaks were absent in wildtype seeds, whereas auto-fluorescence was detected over the whole spectrum of emitted light. Total intensities of both characteristic peaks changed at imbibition with water for 1 h (**Figure 9 b**), with an overall decrease in absolute signal intensity, also of the auto-fluorescence of wildtype seeds. The 527 nm peak increased relatively to the 475 nm peak. Based on the defined and characteristic fluorescence characteristics of cytosolic ATeam seeds (cyt-ATeam), which are distinct from those of wildtype seeds, the cyt-ATeam sensor line was further used for dynamic measurements of cytosolic MgATP concentration in seeds in response to imbibition.

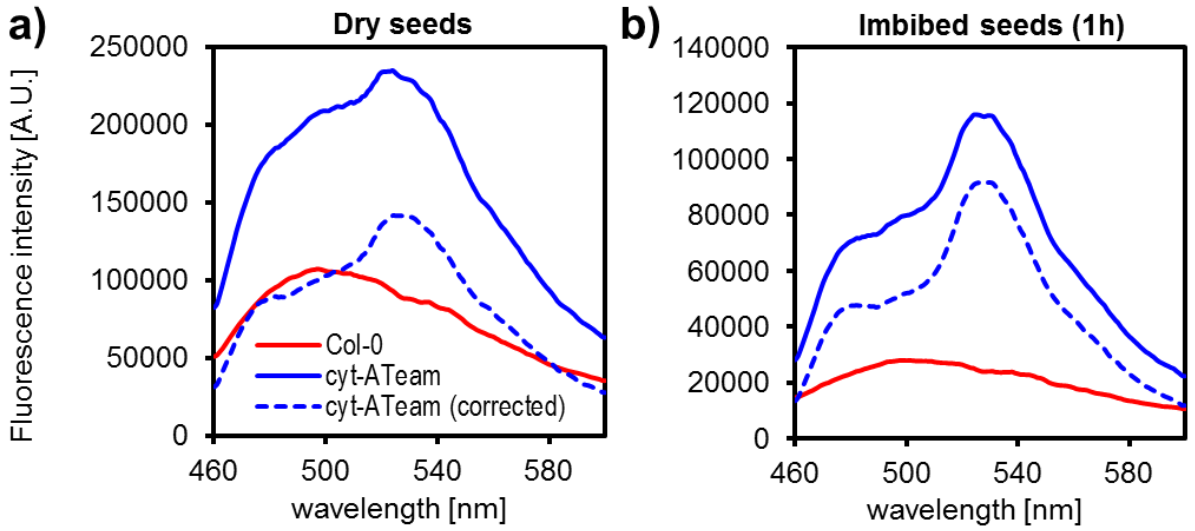

Figure 9: Emission spectra of Arabidopsis seeds expressing cytosolic ATeam. Emission scan was performed for dry seeds a) and after 1 h of imbibition b) with a platereader. Wildtype seeds without sensor (Col-0) were used for background subtraction (corrected emission-spectra as dashed blue lines). Excitation: 435 ± 5 nm; emission in 1 nm steps with 10 nm bandwidth (average fluorescence intensity; *n* = 4 different seed batches).

Time-resolved analysis of the cytosolic targeted ATeam revealed an increase of the corresponding FRET-ratio immediately at imbibition (**Figure 10 a**). Ten minutes after imbibition the FRET-ratio increase slowed down temporally to then speed up again and reached a plateau after 75 min. The FRET-ratio was increased by factor 1.25 at imbibition and half sensor response ($T_{1/2}$) was observed at 34 ± 2 min. In dry seeds the FRET-ratio remained unchanged. To verify the platereader measurements, which are lacking spatial information of the origin of the fluorescence signal, confocal imaging of isolated embryos was performed (**Figure 10 b**). Testa and endosperm were removed to allow imaging of the embryo and to preclude auto-fluorescence contribution of the surrounding tissues. To achieve this,

imbibition of dry seeds on a wet filter paper for 10 min was mandatory, preventing confocal imaging at earlier time-points. Confocal images revealed a high auto-fluorescence of protein storage vacuoles at the employed fluorescence settings. To minimise the impact of auto-fluorescence, regions of interest were selected to nuclear structures, where vacuoles were absent, as part of the data analysis. Nuclear pores are likely to allow efficient equilibration of MgATP between the cytosol and the nucleoplasm implying that measurement of MgATP concentration in the nucleus also reflect the cytosolic MgATP concentration. Measured by confocal laser scanning microscopy (CLSM), the ATeam FRET-ratio of isolated embryos increased by a factor of 2.2 within 90 min of imbibition. The FRET-increase was more pronounced than in the platereader measurements (1.3 x increase) and covered almost to full spectroscopic dynamic range of ATeam as measured *in vitro*. (IMAMURA *ET AL.*, 2009). Overall, confocal microscopy support the initial observations by platereader fluorimetry of a very rapid onset of ATP production. It even suggested a stronger increase of the cytosolic MgATP concentration, as measured by a stronger increase of the FRET-efficiency in response to imbibition. Whether cytosolic MgATP concentration indeed plateaued after 60-90 min or was still increasing further cannot be determined, because sensor has likely reached its maximum response. For an in-depth understanding of the sensor-read-out a calibration of the maximal sensor response *in vivo* would be required, but this also would require additional assumptions. Hence the raw FRET data are presented indicating relative dynamics.

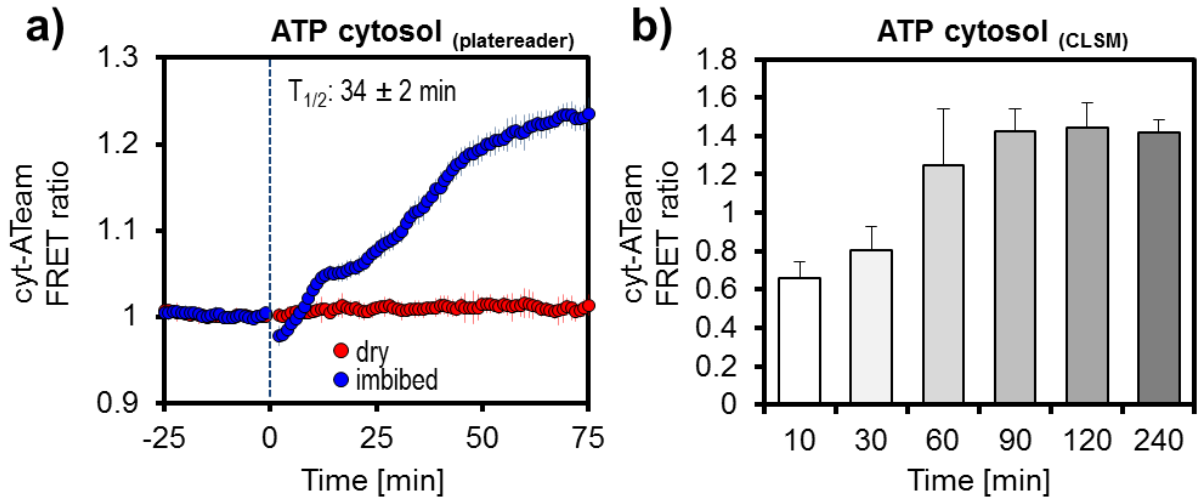

Figure 10: Cytosolic ATeam response in Arabidopsis seeds at imbibition. Cytosolic MgATP concentration in seeds was measured with the fluorescent biosensor ATeam 1.03. Intact seeds were analysed in a platereader a) with high temporal resolution. Excitation: 450 ± 5 nm; emission: 490 ± 10 nm for CFP and 535 ± 10 nm for cpYFP. Wildtype seeds without sensor (Col-0) were used for auto-fluorescence correction. Dashed blue line indicates start of imbibition with water. The normalised FRET-ratio of whole seeds is plotted over time (average ±SD, *n* = 6 different seed batches). $T_{1/2}$ gives time point of half-maximal sensor response. The radicles of isolated embryos were analysed by CLSM b) for high spatial resolution. Testa and endosperm were removed from intact embryos after imbibition for 10 - 240 min to minimise auto-fluorescence of surrounding tissues. Excitation: 458 nm, emission: 475 - 500 nm for the CFP-domain and 525 - 550 nm for the cpYFP-domain. The FRET-ratio of defined nuclei of the radicle is plotted (average +SD, *n* = 8-12 different embryos).

For an orthogonal verification of rapid ATP formation at imbibition and to obtain complementary information about the adenosine energy charge, as defined by the ratios of ATP, adenosine diphosphate (ADP) and adenosine monophosphate (AMP), high-performance liquid chromatography (HPLC) - based measurements of whole seed extracts

were performed (**Figure 11**). To further investigate if the ATP concentration indeed reaches a stable level after 60-90 min of imbibition, samples are also taken after 4 h of imbibition.
In dry seeds total AMP was identified with the highest concentration of 160 pmol mg^{-1}, whereas ADP accounted for 67 pmol mg^{-1} and ATP for 14 pmol mg^{-1}. After 1 h of imbibition AMP concentration decreased to 60 pmol mg^{-1}, ADP concentration decreased to 30 pmol mg^{-1}, whereas ATP increased to a concentration of 89 pmol mg^{-1}. Longer imbibition for 4 h did not significantly change AMP or ADP concentration, and slightly increased the ATP concentration to 105 pmol mg^{-1} seeds. These data suggest that total adenosine pool size was mostly unaffected by imbibition, but energy charge was increased by converting AMP and ADP to ATP already within the first hour of imbibition. This is in agreement with the observations of imbibed seeds expressing the cytosolic ATeam biosensor showing an increase of cytosolic ATP concentration. It further suggests that after 1 h to 4 h of imbibition the ATP concentration is still increasing slightly, but may not be detected with cytosolic ATeam, as it response plateaued already after 60-90 min and then remains constant (**Figure 10 b**). This observation may be either explained by increasing ATP concentration in other cellular compartments than the cytosol, by a saturated ATeam sensor response or by other varying influences on the sensor read-out, such as fluctuating free magnesium concentration affecting the sensor characteristics (DE COL *ET AL*., 2017, *in preparation*).

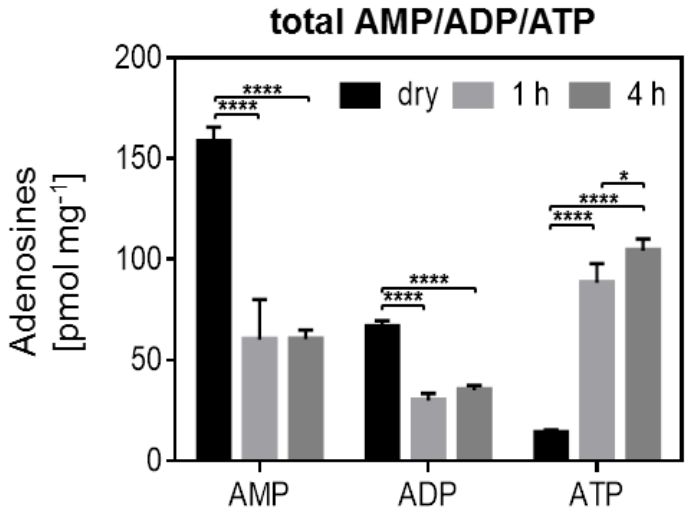

Figure 11: Total adenosine pools in Arabidopsis seed extracts in response to imbibition. AMP, ADP and ATP were measured with HPLC in Arabidopsis whole seed extracts (average +SD; *n* = 4, seeds of two individual plants were pooled; *p<0.05, ****p<0.0001 with two-sided ANOVA and Tukey`s multiple comparison test). Dry seeds were imbibed in water at 25°C for 0 h, 1 h or 4 h before extraction. Measurements were performed by the group of Prof. Hell.

2.1.4 Fluorescence sensing of NADH / NAD^+-redox status in seeds remains technically inconclusive

As an additional read-out for the respiratory activity of imbibed seeds, the redox state of cytosolic nicotinamide adenine dinucleotides (NAD) was analysed with the fluorescent biosensor Peredox-mCherry (HUNG *ET AL.,* 2011). The Peredox-mCherry probe shows an intensiometric response to reduction of NAD^+ by its T-Sapphire fluorophore, whereas the intensity of the fused mCherry remains unchanged and is used to normalise for the absolute protein amount, generating a *pseudo-ratiometric* probe. Seeds with cytosolic expression of Peredox-mCherry (cyt-Peredox-mCherry) were analysed for adequate fluorescence intensities and signal-to-noise-ratios by performing platereader-based emission-scans. Based on the non-FRET sensor concept of Peredox-mCherry, both fluorophores, the mCherry and the T-Sapphire, required separate excitation. In the emission spectra of dry and imbibed seeds, pronounced peaks for the mCherry were present at 610 nm, which were

absent in wildtype seeds (**Figure 12 a** and **c**); auto-fluorescence emission was relatively high between 580 - 670 nm. At seed imbibition, absolute mCherry fluorescence intensity increased. Excitation at 400 nm revealed a high auto-fluorescence contribution to the emission in both, seeds of the wildtype control and of cyt-Peredox-mCherry line, especially in the range of 450 - 500 nm (**Figure 12 b** and **d**). In the characteristic emission range of the T-Sapphire fluorophore at about 515 nm, no pronounced sensor signal was detectable in dry seeds (**Figure 12 b**). After 1 h of imbibition with water cyt-Peredox-mCherry seeds showed a small, but characteristic emission peak at 515 nm (**Figure 12 d**).

The absence of the characteristic peak of T-Sapphire in dry seeds, together with the high auto-fluorescence contribution of wildtype seeds, is resulting in a low signal-to-noise-ratio, which complicates the interpretation of the obtained data. In addition, also the fluorescence intensity of mCherry is significantly changed in response to imbibition, impairing normalisation of the T-Sapphire fluorescence intensity. Thus it is questionable if Peredox-mCherry can be successfully applied to investigate the NAD redox state in seeds during imbibition and obtained data have to be analysed with extreme caution. However, qualitatively the absence of the T-Sapphire peak in the emission of dry seeds and its appearance after 1 h of imbibition suggests a reduction of the NAD pool.

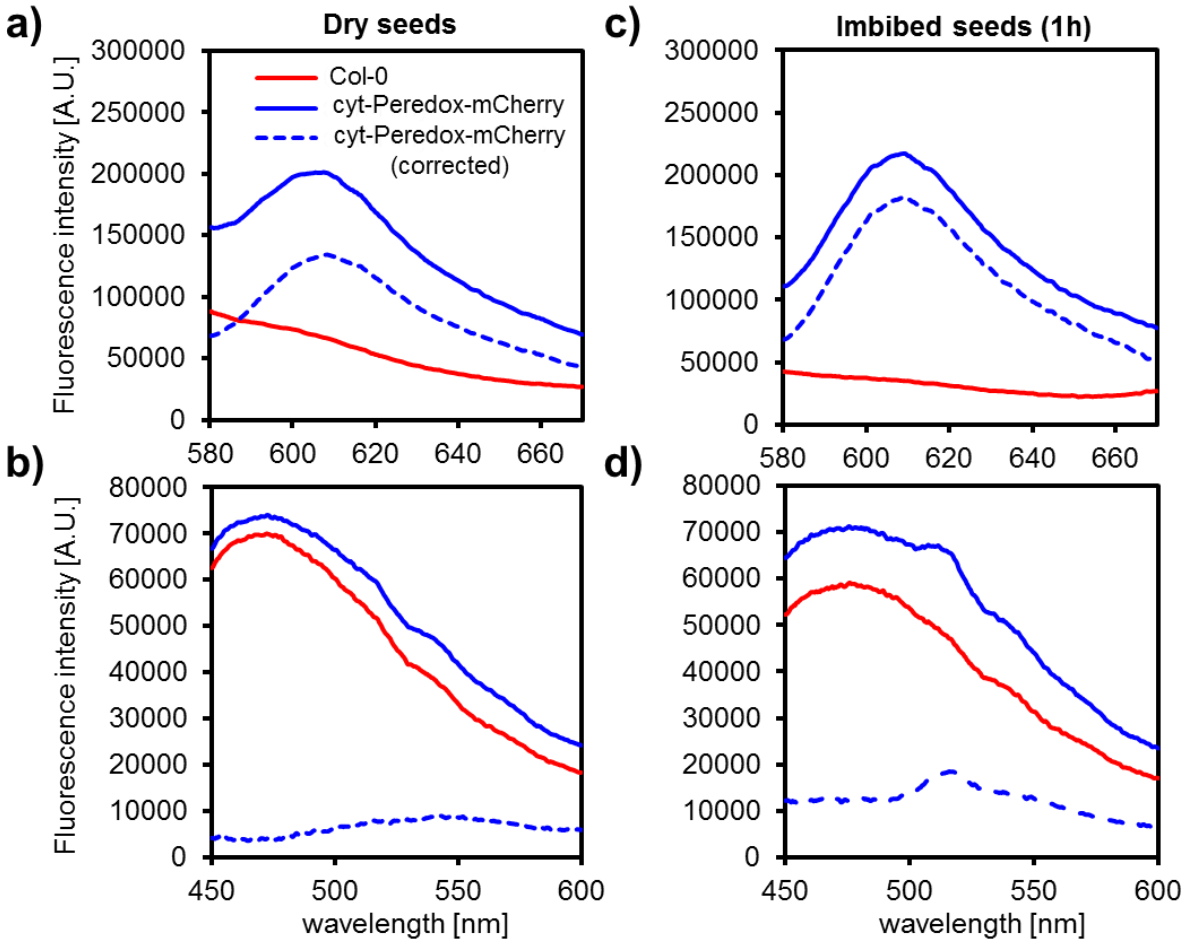

Figure 12: Emission spectra of Arabidopsis seeds expressing Peredox-mCherry in the cytosol. Emission spectra of dry seeds a) and b), and after 1 h of imbibition c) and d) with a platereader. Non-sensor expressing control seeds were used for background subtraction (corrected emission spectra as dashed blue line). Peredox-mCherry emission scan was performed separately for both fluorophores, for the spectral emission regions of T-Sapphire b) and d) and for mCherry a) and c). Excitation a), c): 550 ± 7.5 nm; b), d): 400 ± 10 nm; emission for both fluorophores in 0.5 nm steps and with 15 nm bandwidth (average fluorescence intensity; *n* = 10 different seed batches).

Although the characteristic T-Sapphire signal was absent in dry seeds and the absolute fluorescence intensity of mCherry increased at imbibition, cyt-Peredox-mCherry seeds were used to monitor the cytosolic NAD redox state in dry seeds in response to imbibition. In a time-resolved analysis the T-Sapphire / mCherry-ratio decreased rapidly after a lag-phase of 10 min. The ratio decreased by a factor of two and approached a plateau after 75 min, with half sensor response at 22 ± 1 min (**Figure 13 a**), while the ratio of dry seeds remained unchanged.

In an orthogonal approach NADH concentration of whole seed extracts was analysed by HPLC (**Figure 13 b**). In dry seeds total concentration of NADH was 3.8 pmol mg^{-1} and was not changed after 1 h and 4 h of imbibition. These data imply that total NADH pool size in dry and imbibed seeds is small and shows no significant fluctuations within the first 4 hours of imbibition. However, fluxes through the NAD pool at imbibition cannot be inferred from steady-state-measurements.

If the cytosolic NAD redox state is indeed lowered at imbibition, as implied by the data obtained by the cytosolic T-Sapphire / mCherry-ratio, remains open. The absolute fluorescence intensities of the T-Sapphire domain increased in response to imbibition (**Figure 12 b** and **d**), which rather suggests a reduction than ab oxidation of the NAD redox state, as suggested by the decreased T-Sapphire / mCherry-ratio. This can be explained by the fact that also the fluorescence intensities of the normalisation domain mCherry increased in response to imbibition (**Figure 12 a** and **c**). This has a strong impact on the T-Sapphire / mCherry ratio covering the actual small increase of the fluorescence intensity of T-Sapphire (**Figure 12 d)**. Thus it appears likely that the T-Sapphire / mCherry ratio is dominated by the change of fluorescence intensity of the normalisation domain and is not reflecting a true oxidation of the NAD pool. As such a convincing real-time method for NAD redox sensing in seeds remains to be optimised.

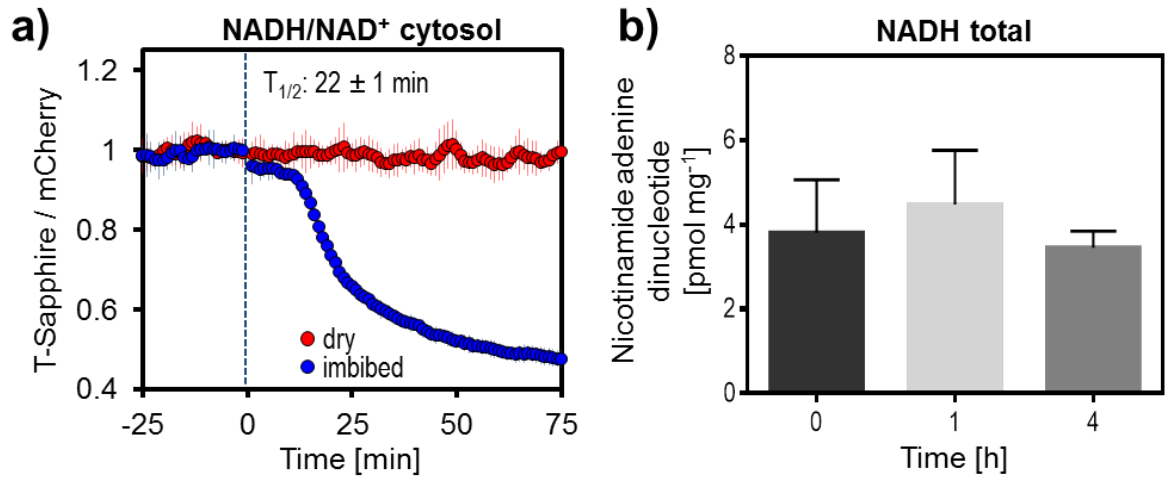

Figure 13: Nicotinamide adenine dinucleotides in Arabidopsis seeds in response to imbibition. Cytosolic NADH/NAD^+ ratio measured with the fluorescent biosensor Peredox-mCherry in intact seeds in a platereader a). Excitation of mCherry: 570 ± 10 nm, T-Sapphire: 400 ± 10 nm; emission of mCherry: 620 ± 15 nm, T-Sapphire: 530 ± 20 nm. Dashed blue line indicates start of imbibition. Non-sensor-expressing control seeds (Col-0) were used for auto-fluorescence correction. The T-Sapphire/mCherry-ratio of intact seeds is plotted over time (average ±SD, *n* = 6 different seed batches). $T_{1/2}$ gives time point of half-maximal sensor response. In b) total NADH concentration in extracts of dry and imbibed seeds as determined by HPLC (average +SD, *n* = 4, seeds of two individual plants were pooled). HPLC measurements in b) were performed by the group of Prof. Hell.

2.1.5 Measurement of TCA cycle intermediates pinpoints a transient rise of citrate at imbibition

Seed respiration commenced rapidly in response to imbibition, as suggested by decreased oxygen concentration (**Figure 7**) and a reestablished energy state of the adenosine pool (**Figure 10** and **Figure 11**). To obtain further insight into the metabolic processes, which may fuel the oxidative phosphorylation during seed imbibition with reductant in form of NAD(P)H, tricarboxylic acid cycle (TCA cycle) intermediates and associated organic acids were quantified with gas chromatography-mass spectrometry (GC-MS) (**Figure 14**).

The content of several free organic acids in seeds changed markedly in response to imbibition. In dry seeds mainly malate was detectable, while a citrate/isocitrate peak was not detected. Pyruvate, lactate, oxalic acid, 2-oxoglutarate (2OG), succinate and fumarate were present in small quantities. The content of pyruvate, oxalic acid, 2OG and fumarate did not change within the first 4 hours of imbibition. The content of malate was transiently increased after 1 h of imbibition. Succinate and lactate content increased after 4 h of imbibition. Most strikingly, the content of citrate/isocitrate increased strongly after 1 h, but fell below the detection limit after 4 h of imbibition. Several organic acids show fluctuations of their absolute quantities already after 1 h of imbibition, suggesting flux through primary metabolism including the TCA cycle. This is in agreement with the observations made for oxygen uptake and ATP dynamics. Together these data support the observations of a rapid restart of energy metabolism in seeds at imbibition. If mitochondrial respiration is directly involved in the observed dynamics of organic acids cannot be concluded unambiguously since measurements in seed extracts lack subcellular resolution and organic acid metabolism can also take place in other compartments. For instance the sharp increase of lactate indicates a contribution by fermentation to energy metabolism. Low steady-state content in pyruvate, oxalic acid, 2OG or fumarate does not exclude significant flux through the metabolite pools. Of particular interest is the strong, transient increase of citrate/isocitrate after 1 h, which may be interpreted as a result of a transient imbalance between flux into (*e.g.* by β-oxidation of fatty acids in peroxisomes) and out of the citrate/isocitrate pool (*e.g.* by mitochondrial respiration).

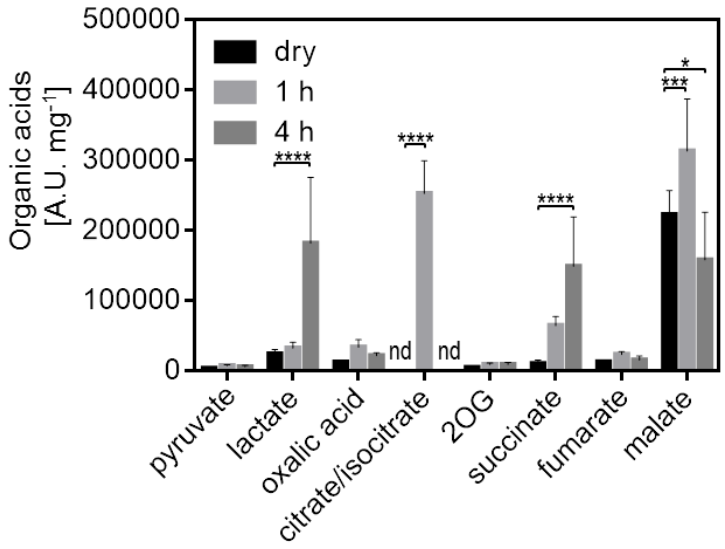

Figure 14: Organic acid content in seeds in response to imbibition. Organic acids of total seed extracts were analysed with GC-MS (average peak intensity +SD, *n* = 4 seeds of two individual plants were pooled, *p<0.05, ***p<0.001, ****p<0.0001; with two-way ANOVA and Bonferroni`s multiple

comparison test). Seeds were either imbibed with water for 1 h, for 4 h or were directly used for extraction in their dry state. Due to their identical molecular masses, signals for citrate/isocitrate are indistinguishable by GC-MS. Measurements were performed by the group of Prof. Hell.

2.1.6 Glutathione is efficiently reduced in response to imbibition

Switching rapidly between metabolic quiescence in dry seeds to considerable metabolic activity of imbibed seeds, changes in the redox state of nicotinamide adenine dinucleotide phosphate (NADP) pools may be expected, given that the reduction of $NADP^+$ is directly coupled to the primary metabolism (MOLLER AND RASMUSSON 1998; NOCTOR *ET AL.,* 2006). During writing this thesis, no fluorescent biosensor was available for monitoring the NADP redox state, and only recently a sensor for monitoring the amount of NADPH was published (TAO *ET AL.,* 2017), but different fluorescent biosensors for the E_{GSH} are well established in plants (MEYER *ET AL.,* 2007; SCHWARZLÄNDER *ET AL.,* 2008). The redox state of the glutathione pool is coupled to the regeneration of NADPH via the NADPH-specific glutathione reductases. As such, monitoring of the E_{GSH} with roGFP2-based probes may provide an indirect means to follow NADP-dynamics, if the glutathione pool is oxidised in the quiescent state, as *e.g.* described for barley seeds (NAGEL *ET AL.,* 2015).
For platereader-based assays (see section *2.1.2*), seeds were checked for adequate sensor expression levels by spectral scans. Seeds expressing either cytosolic Grx1-roGFP2 (cyt-Grx1-roGFP2, **Figure 15 a** and **c**) or mitochondrial matrix roGFP2 (mt-roGFP2, **Figure 15 b** and **d**) showed a characteristic peak in the excitation spectra at about 488 nm in dry and imbibed state, with a better signal-to-noise-ratio in the cyt-Grx1-roGFP2 line. In contrast, the characteristic peak for roGFP2-based sensors at about 405 nm was not resolved in both sensor lines. Wildtype seeds showed high auto-fluorescence when excited at 420-470 nm. The imbibed mitochondrial roGFP2 line showed an additional peak of emitted light when excited at 360-390 nm. In response to imbibition, the 405/488 nm ratio of both sensors was shifted, which suggests changes of the respective redox states of the subcellular glutathione pools. Although spectral curves for both sensor lines show no characteristic peak at about 405 nm, roGFP2-signal can be resolved at 488 nm. This provides a qualitative estimation of dynamic changes in the subcellular E_{GSH} in seeds.

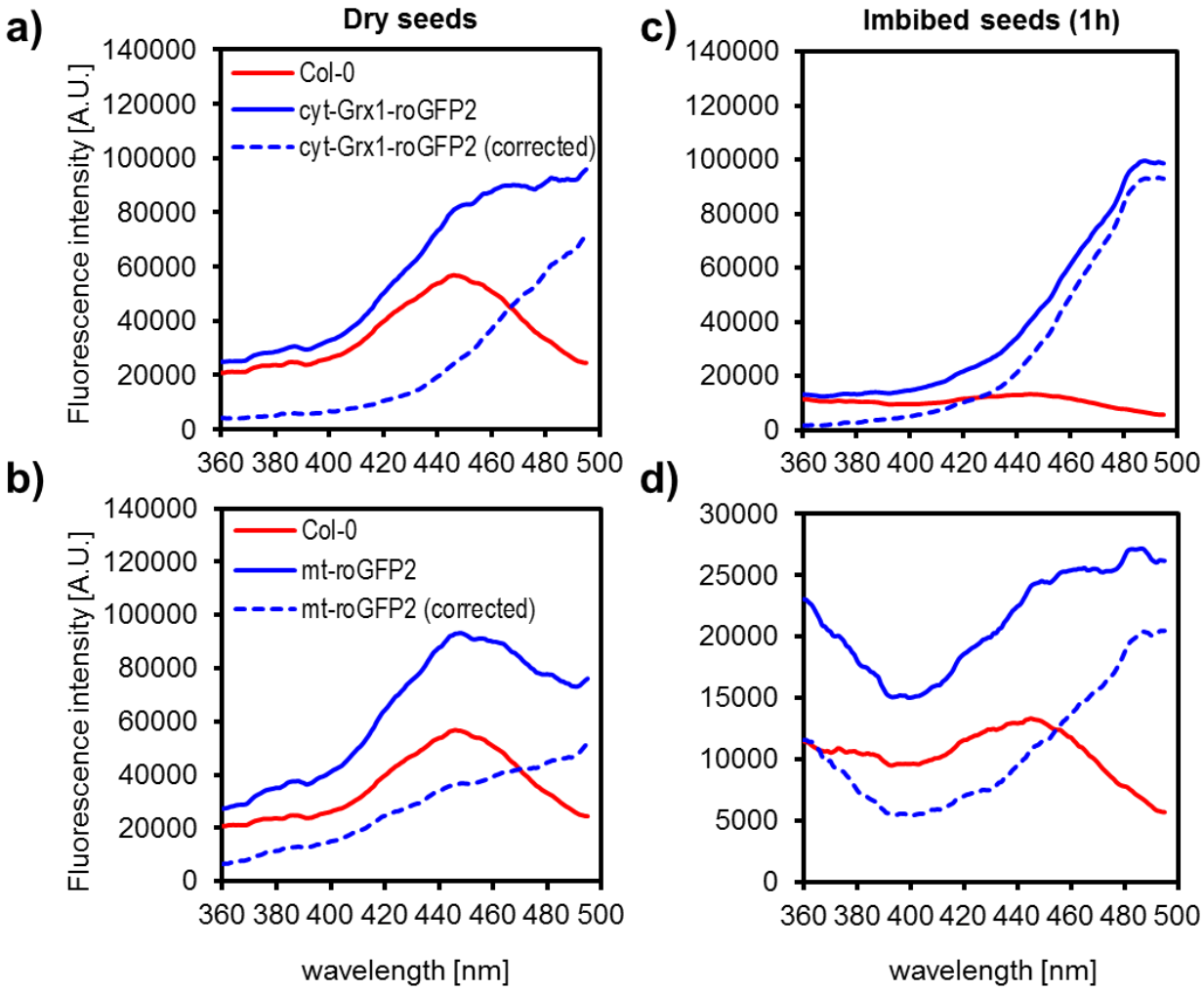

Figure 15: Excitation spectra of Arabidopsis seeds expressing roGFP2-based fluorescent biosensors in the cytosol and the mitochondrial matrix. Excitation spectra of Arabidopsis seeds expressing cytosolic Grx1-roGFP2 a) and c) or mitochondrial roGFP2 b) and d). Spectra were recorded for dry seeds a) and b) and after 1 h imbibition c) and d) with a platereader. Wildtype seeds without sensor expression (Col-0) were used for background subtraction (corrected excitation-spectra as dashed blue line). Emission: 530 ± 20 nm; excitation in 1 nm steps with 5 nm bandwidth (average fluorescence intensity, *n* = 5 different seed batches).

In a platereader-based time-resolved analysis, the cytosolic E_{GSH} specific sensor Grx1-roGFP2 was being reduced following a characteristic biphasic response curve at imbibition with water, as indicated by a decrease of the 400/482 nm ratio (**Figure 16 a**). After a lag-phase of about 10 minutes the reduction of the sensor was initiated, reaching a first plateau after 20-30 min. After 75 min, the ratio reached a second plateau amounting to a 2.3 fold decrease of the 400/482 nm ratio and half sensor response was observed at 36 ± 2 min. The matrix E_{GSH} of seeds was analysed with mitochondrial matrix targeted roGFP2 (**Figure 16 b**). Mitochondrial roGFP2 reduction started to become apparent after a lag-phase of 10 min, reaching a plateau after 75 min with a total decrease of the 400/482 nm ratio by factor 1.6 and half sensor response was observed at 21 ± 8 min. The decrease of the 400/482 nm ratio in both roGFP2-based E_{GSH} sensor lines indicates a rapid reduction of the cytosolic and mitochondrial glutathione redox state in response to imbibition. However, the sensor response was not as high as the theoretical dynamic range of roGFP2-based sensors, especially in the mitochondrial sensor lines, which may be explained by the high

auto-fluorescence of seeds, and goes in line with the observations obtained for a lowered dynamic range of roGFP2-based probes located in the mitochondrial matrix (SCHWARZLÄNDER *ET AL.,* 2008). For monitoring the mitochondrial E_{GSH} free roGFP2 sensor was used, because seeds from mitochondrial roGFP2-Grx1 sensor lines, that were also tested, showed an even lower signal-to-noise-ratio, probably due to low sensor expression. Yet mt-roGFP2-Grx1 expressing seeds can be used for confocal microscopy, which increases the signal-to-noise-ratio by removal of the testa and the endosperm and by setting of regions of interest during data analysis (see section *2.1.3*).

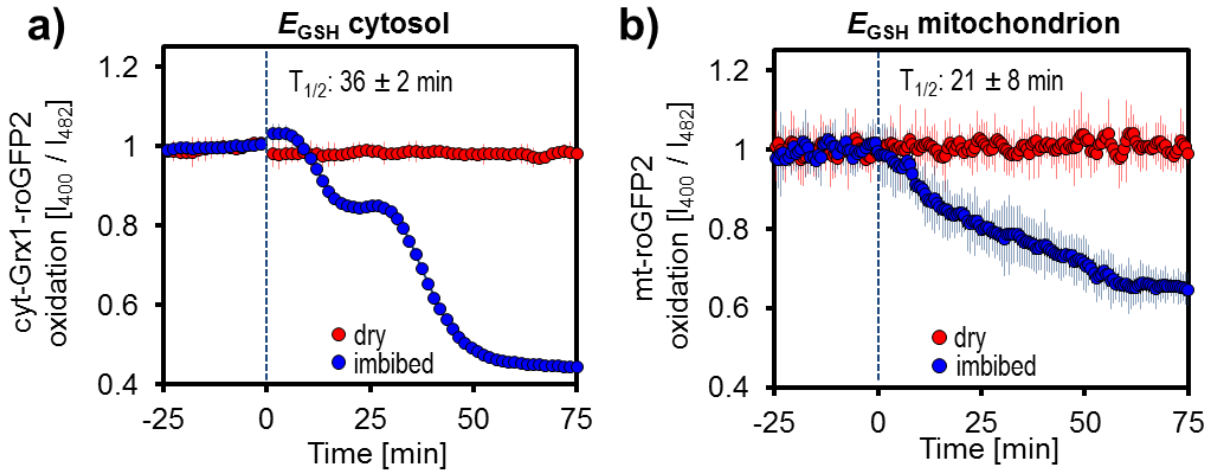

Figure 16: Glutathione redox state estimated with roGFP2-based fluorescent biosensors in Arabidopsis seeds in response to imbibition. Glutathione redox state of Arabidopsis seeds was measured with cytosolic Grx1-roGFP2 a) or mitochondrial matrix roGFP2 b). Wildtype seeds without sensor expression (Col-0) were used for auto-fluorescence correction. Dashed blue lines indicate start of imbibition with water. Seeds excited at 400 ± 5 nm and 482 ± 8 nm, emission at 530 ± 20 nm. The 400/482 nm ratio of whole seeds is plotted over time (average ±SD, *n* = 6 different seed batches). $T_{1/2}$ gives time point of half-maximal sensor response.

To verify the platereader-based measurements of seeds expressing free roGFP2 in the mitochondrial matrix (**Figure 16 b**), confocal imaging of isolated embryos with mitochondrial roGFP2-Grx1 was performed similarly to ATP monitoring (see section 2.1.3). Testa and endosperm were removed to allow imaging of the embryo and to preclude auto-fluorescence contribution of the surrounding tissues. Therefore imbibition of dry seeds on a wet filter paper for 10 min was mandatory, preventing confocal imaging of seeds in the quiescent, dry state. Confocal images showed multiple protein storage vacuoles (PSV) as big roundish structured auto-fluorescence signals per individual cell, which contributed strongly to emission after excitation at 405 nm, but much less if excited at 488 nm (**Figure 17**). Mitochondria could be clearly spatially separated from the bigger auto-fluorescence signals of the PSVs, allowing a subsequent region-of-interest (ROI) analysis to minimise auto-fluorescence artefacts (FRICKER 2016).

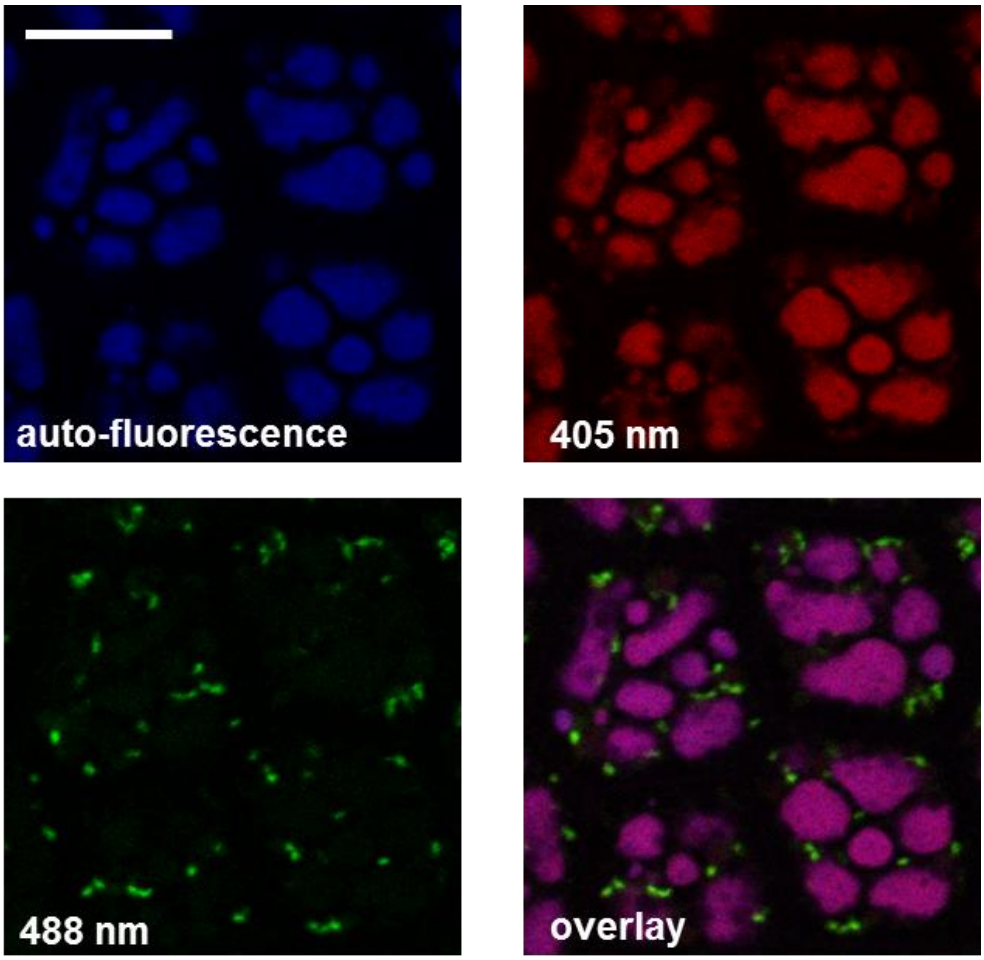

Figure 17: Representative confocal images of Arabidopsis seeds expressing roGFP2-Grx1 in the mitochondrial matrix. Arabidopsis embryos with mitochondrial roGFP2-Grx1 were analysed by CLSM. Cells of the radicle are shown in an exemplary image obtained from seeds imbibed for 1 h. Scale bar = 10 µm. Sequential excitation at 405 and 488 nm, emission at 520 ± 15 nm. Auto-fluorescence is shown at 450 ± 20 nm after excitation at 405 nm. Fluorescence intensities of the individual channels are illustrated in false-colour; overlay shows merge of individual images of the 405 nm, the 488 nm and the auto-fluorescence channel.

The 405/488 nm ratio of the mitochondrial roGFP2-Grx1 decreased by factor 2.2 within 4 h of imbibition, but was already far progressed after 1 h (**Figure 18 a**; high auto-fluorescence of large PSVs in the 405 nm channel is indicated in red in the pseudo-colour-illustration of the 405/488 nm ratio; mitochondrial structures show a decreasing ratio as indicated by green colours for the early imbibition phases and blue colours after 60-240 min). These data confirm the observation of a rapid reduction of the mitochondrial glutathione pool in response to imbibition. It can be hypothesised that the rapid reduction of cysteine residues is a general hallmark of early germination and occurs across several subcellular compartments, which show highly reduced glutathione in active plant tissues (MEYER *ET AL.,* 2007; SCHWARZLÄNDER *ET AL.,* 2008).

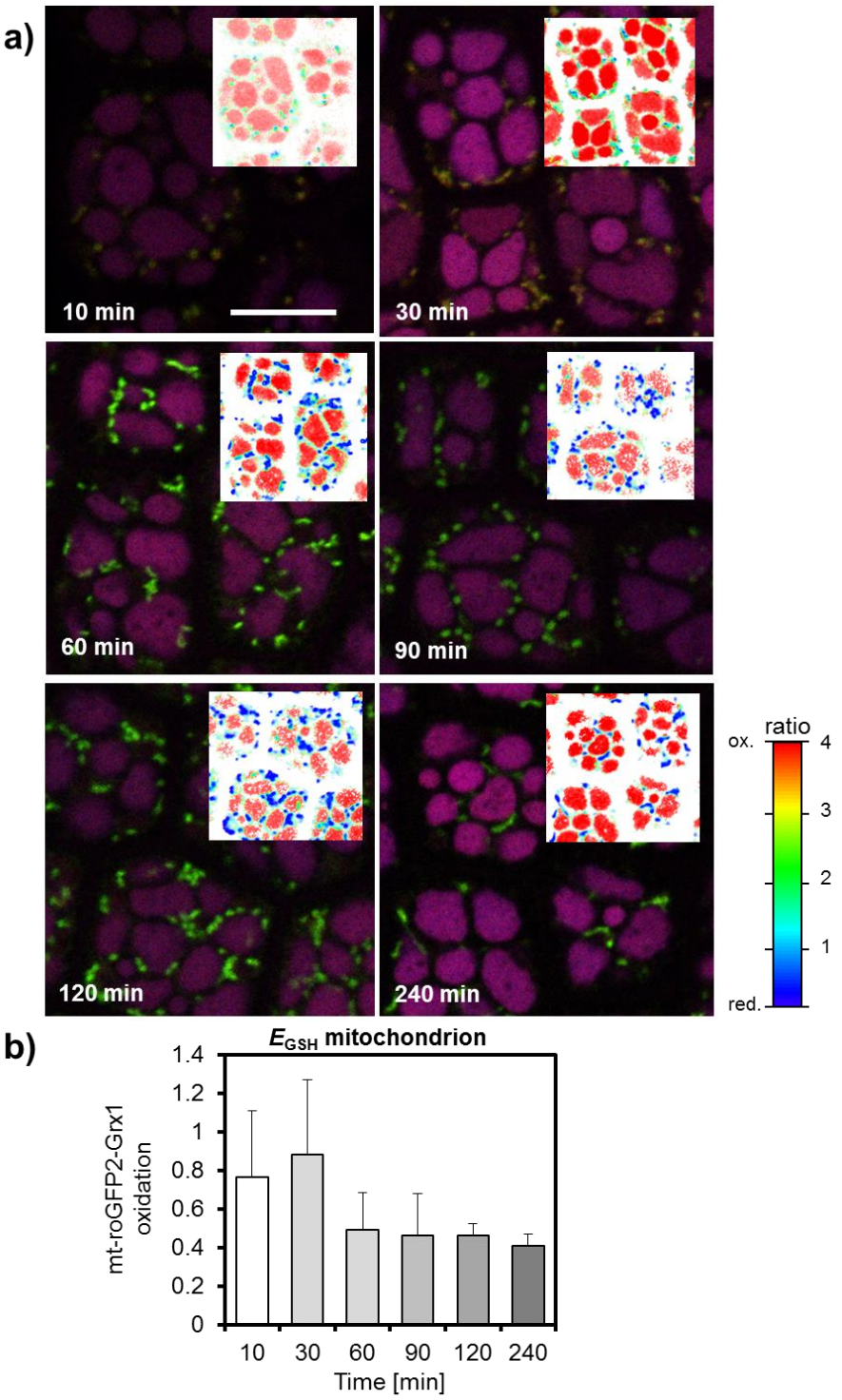

Figure 18: Mitochondrial matrix roGFP2-Grx1 measurement in isolated embryos of imbibed seeds. Matrix E_{GSH} in embryos was measured with mt-roGFP2-Grx1 by CLSM. After imbibition for 10 - 240 min, testa and endosperm were removed. Sequential excitation of isolated embryos with 405 and 488 nm; emission at 520 ± 15 nm. For separation of auto-fluorescence and mitochondrial roGFP2-Grx1 signals, regions of interest (ROI) were manually set on individual mitochondria as part of the data analysis. In a) overlays of representative false colour images of the fluorescence intensities of the 405/488 nm and the auto-fluorescence channel are shown. Scale bar = 10 µm. Images shown as insets are the corresponding pseudo-colour illustrations of the 405/488 nm ratio; oxidised roGFP2-Grx1 sensor is illustrated in red and reduced sensor in blue; large PSVs are artificially represented in red, but were not considered for the quantification. In b) the 405/488 nm ratio is plotted for the ROI-analysis of mitochondria (average +SD, *n* = 400 - 700 individual mitochondria per time-point in 8 - 12 individual embryos).

In addition to the GSH/GSSG ratio, the E_{GSH} is further set by the absolute glutathione concentration, *i.e.* by *de novo* synthesis or degradation of glutathione. To assess the contribution of the glutathione turnover to the reduction of the glutathione pool observed during imbibition (**Figure 16**, **Figure 18**), total glutathione concentration (GSH + GSSG) in whole seed extracts was analysed using HPLC after derivatisation with monobromobimane (mBBr; **Figure 19**). The total glutathione concentration of dry seeds was 1540 ± 160 pmol mg^{-1} and was neither changed after 1 h of imbibition at 1175 ± 195 pmol mg^{-1}, nor after 4 h of imbibition at 1246 ± 108 pmol mg^{-1}.
Furthermore, the concentration of free cysteine was quantified in total extracts of dry and imbibed seeds. The cysteine concentration was 89 ± 20 pmol mg^{-1} in dry seeds (**Figure 20**) and was not changed after imbibition for 1 h (65 ± 14 pmol mg^{-1}) or 4 h (119 ± 23 pmol mg^{-1}). Cysteine was the amino acid detected with the lowest concentration of all proteinogenic amino acids. Neither the other glutathione constituents, glycine and glutamic acid, nor any other amino acid was changed in their concentration at 4 hours of imbibition (**Figure 20**). Only the free alanine concentration was increased in response to imbibition at initially 2810 pmol mg^{-1} in dry seeds and 4512 pmol mg^{-1} after 4 h. Several other amino acids show a consistent, yet non-significant, trend towards an increase in their free concentration within the 4 h. Glutamic acid was identified with the highest concentration of all amino acids at about 7500 pmol mg^{-1}, whereas glycine was identified at about 1000 pmol mg^{-1}.

Figure 19: Total glutathione content of Arabidopsis seeds. The total glutathione content of whole Arabidopsis seed extracts was analysed by HPLC after derivatisation with monobromobimane (average +SD, *n* = 4, seeds of two individual plants were pooled). GSSG was reduced to GSH by addition of DTT prior to the labelling. Seeds were either imbibed with water for 1 h and 4 h or were used for extraction in their dry state. Measurements were performed by the group of Prof. Hell.

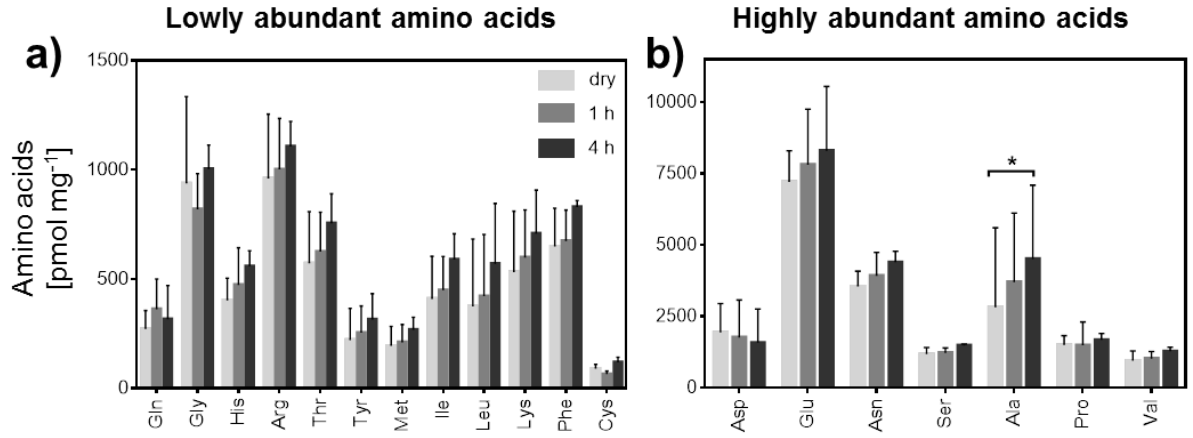

Figure 20: Amino acid concentration in dry and imbibed Arabidopsis seeds. Free amino acids were analysed by HPLC in total seed extracts (average +SD, *n* = 4, seeds of two individual plants were pooled; *p<0.05 with two-way ANOVA and Bonferroni`s multiple comparison test). Seeds were either imbibed in water for 1 h and 4 h or were used for extraction in their dry state. a) Lowly abundant amino acids and b) highly abundant amino acids. Free cysteine was quantified after derivatisation with monobromobimane in a separate extraction and analytics. Measurements were performed by the group of Prof. Hell.

Summarised, these data suggest that the reduction of the glutathione pool is based on the reduction of GSSG by glutathione reductase activity and not due to an increase of the GSH concentration by *de novo* synthesis. The total concentration of glutathione is not changed within 4 h, yet, it will be heavily influenced by the large vacuolar glutathione pool potentially masking smaller changes in the glutathione concentration in the cytosol or the mitochondrial matrix. Here, there is a major drawback of HPLC-based analysis of total seed extracts and resolution for individual compartments is currently impossible to achieve. Based on the chemical reduction of GSSG to 2GSH by the addition of DTT during sample processing for HPLC, no orthogonal information on the redox state of the glutathione pool was obtained, which may provide further information about the suspected glutathione reductase-mediated reduction of GSSG in response to imbibition, as suggested by fluorescent *in vivo* sensing. However, also the absolute concentration of the main building blocks of glutathione, cysteine, glycine and glutamic acid, were not significantly changed in response to imbibition. Although constant steady-state-levels do not exclude significant flux through the amino acid pools and the observed constant amino acid concentration may be explained by tight regulation of their corresponding metabolic pathways, constant cysteine, glycine and glutamic acid pool sizes further support the hypothesis of rapid reduction of the glutathione pool in response to imbibition.

The quantification of the proteinogenic amino acid pools gives further insight into the metabolic rearrangements of imbibed seeds. Based on the observation that just the free alanine concentration varied within the first 4 h, it may be hypothesised that neither the protein biosynthesis machinery shows high activity, nor storage proteins are extensively degraded during this early phase of germination. This is in line with observations obtained for ^{35}S-methionine supplemented seeds at imbibition, showing only little incorporation of the radioactive-labelled methionine into neo-synthesised proteins during the first eight hours of imbibition, but an increase of ^{35}S-methionine incorporation into proteins later during imbibition (GALLAND *ET AL.,* 2014).

2.2 Germination performance of Arabidopsis seeds with impaired redox machinery

2.2.1 Fresh seeds of different redox mutants are only slightly affected in the germination vigour

Glutathione redox homeostasis in the cytosol and the mitochondrial matrix is established rapidly at imbibition, which raises the possibility of an important physiological role in germination. To test this hypothesis, mutants impaired at different positions in the cellular thiol redox machinery were analysed for defects in their germination efficiency. Non-dormant, synchronised seeds, which are obtained by plants grown side-by-side, were analysed for five days after sowing to track germination performance over time (**Figure 21 a** and **b**). Radicle penetration of the endosperm and the testa was used as the criterion for complete germination (**Figure 22**). Seeds were sown on media either with or without 1 % (w/v) sucrose as an additional, external carbon and energy source. Three days after sowing, 95-99 % of all seeds had successfully germinated (**Figure 21 a** and **b**). First successfully germinated seeds were present two days after sowing. Seeds growing on sucrose media showed a slightly decreased germination rate on the second day after sowing. This is consistent with the observed sugar-induced active ABA-signalling in seeds, as ABA is known to manifest dormancy (see section *1.2.1*; DEKKERS *ET AL.,* 2008). Mutants of the mitochondrial thioredoxin-o1 (*trx-o1*) showed a significantly decreased germination rate after two days of sowing on both media compositions (**Figure 21 a** and **b**, **Tab. 1**). In addition, mutants of both glutathione reductases, the cytosolic/peroxisomal GR1 (*gr1*) and the mitochondrial GR2 (GR2 is dually targeted to mitochondria and plastids and *gr2* mutants are lethal, but survival of plants by the complementation of the plastidic GR2 was observed (MARTY *ET AL*., *in preparation*); *gr2-1 epc. 2* mutants with complemented plastidic GR2 are named `*gr2*` for simplicity, see *4.2.1*), showed a slightly reduced germination rate on sucrose media on the same day. Based on the impaired germination performances of individual redox mutants, it cannot be concluded that the observed phenotypes are monitoring differences of the seeds acting during germination, or which were already imprinted during seed filling and seed maturation process. Yet, it can be hypothesised that the effects, which are impaired during germination in the mutants, may be amplified by ageing of seeds, as ageing was shown to gradually increase oxidation in the quiescent seeds (NAGEL *ET AL.,* 2015). Thus the efficient rebooting of the cellular thiol redox systems may be of particular physiological relevance and raises the hypothesis that mutants of the thiol redox machinery are overly affected by ageing.

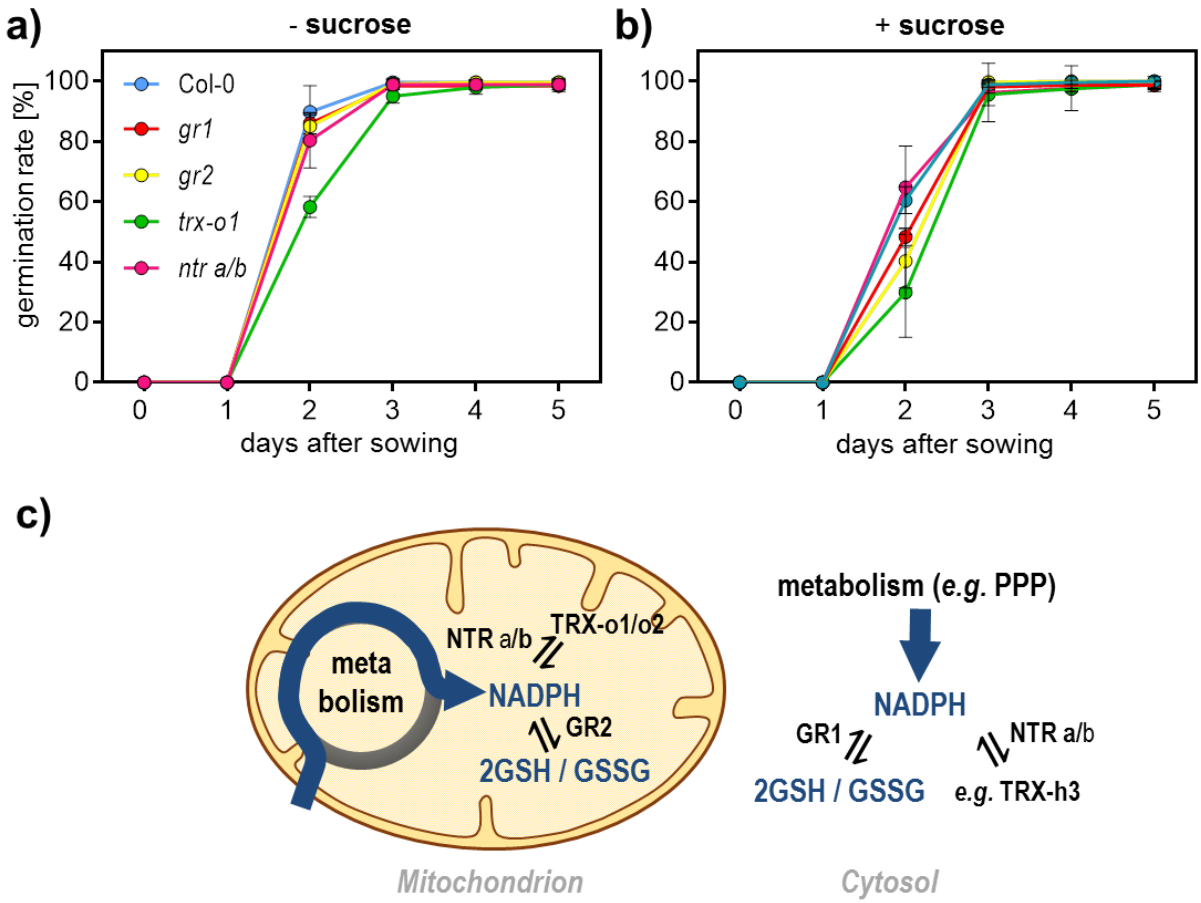

Figure 21: Germination efficiency of Arabidopsis seeds with impaired cytosolic and mitochondrial redox systems. After-ripened, synchronised Arabidopsis seeds were sown on plates (0.5x MS, 10 mM MES, pH 5.8 with KOH, 0.8 % (w/v) phytagel) without sucrose a) or with 1 % (w/v) sucrose b). The average germination percentage for the first five days after sowing is shown for quadruplicate experiments (n = 200 - 250; average ±SD). Statistically different germination rates, evaluated with two-way ANOVA and Tukey`s multiple comparison test, are highlighted in **Tab. 1**. The cytosolic and the mitochondrial redox machineries are coupled to central metabolism via the production of NADPH, *e.g.* by pentose phosphate pathway (PPP) in the cytosol (c). GSSG is reduced by glutathione reductases (cytosol: GR1, mitochondrial matrix: GR2) to 2GSH, NADPH thioredoxin reductases (NTR a/b, both isoforms dual-targeted to cytosol and mitochondria) reduce thioredoxins (TRX-o1 and TRX-o2 in mitochondrion; several different TRXs in the cytosol).

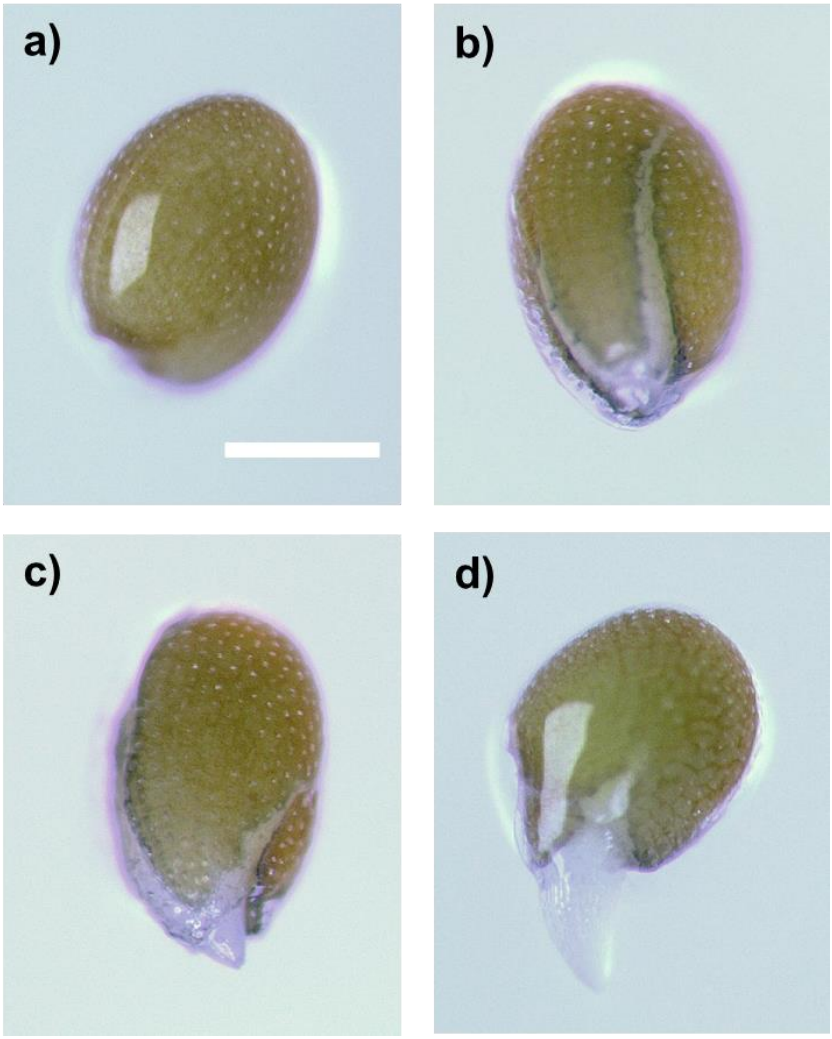

Figure 22: Stages of Arabidopsis seed germination. Representative images of *Arabidopsis thaliana* Col-0 seeds in different germination stages. Seeds were cultivated under long-day conditions for two days without prior stratification (0.5x Murashige-Skook-medium (MS-medium), 10 mM MES, pH 5.8 with KOH, 0.8 % (w/v) phytagel). Incomplete germination stages in a) and b); successful germination stages in c) and d). Scale bar = 250 µm. At imbibition with water dry seeds gain size and round up a), followed by the rupture of the testa b). In late germination phase the radicle penetrates the endosperm c) followed by further elongation d). For estimating the germination rates over time, testa rupture and endosperm penetration of the radicle was used as the criterion of complete germination (HOLDSWORTH *ET AL.,* 2008; WEITBRECHT *ET AL.,* 2011). Seeds solely showing a ruptured testa as in b) were not considered as germinated yet. Germination was tracked using a stereomicroscope.

2.2.2 Aged seeds of different redox mutants show significantly lowered germination vigour

Germination phenotypes of the investigated redox mutants are comparably mild (**Figure 21 a** and **b**), indicating that disruptions of individual components of the redox machinery can be partially compensated in seeds that have been handled under optimal conditions, with only short storage at low temperatures and at low humidity for after-ripening (see section *1.1.1*). Yet, under natural conditions seeds are also exposed to unfavourable conditions, such as heat and high humidity. To investigate the germination performance of mutants under more challenging and potentially more realistic conditions, dry seeds were artificially aged by storage for 0, 5, 12, 19 and 26 days at 37°C and 70-75 % rel. humidity. Seeds were then sown on media either with (**Figure 23 b**) or without 1 % (w/v) sucrose (**Figure 23 a**). With increasing time under ageing-enhancing conditions, germination rates of all seeds were decreased. 26 days of accelerated ageing were sufficient to completely inhibit germination within five days after sowing for all lines. For seeds artificially aged for twelve days, 89 % and 94 % germinated after five days incubation on sucrose-free and sucrose media, respectively. Germination rate on the day two after sowing was decreased strongly. Ageing for five days was already sufficient to lower the germination rates also for the *gr1* and *gr2* mutants on sucrose-free media (**Tab. 1 a** and **b**). Most pronounced differences of the germination rates of all mutants were observed after 19 days of artificial ageing after incubation of seeds for four and five days. Overall, germination efficiency of all redox mutants (*gr1*, *gr2*, *ntr a/b* & *trx-o1*) were considerably stronger affected by ageing than the corresponding wildtype seeds.
These data support the hypothesis that rapid reestablishing of the glutathione redox homeostasis in different cellular compartments at imbibition has an important physiological role in germination. This becomes evident especially for aged seeds, which potentially is an even more realistic scenario, as seeds in nature are also exposed to unfavourable conditions throughout the seasons.

Tab. 1: Statistics for germination assays of aged Arabidopsis seeds. Arabidopsis seeds were artificially aged by storage for 0, 5, 12, 19 and 26 days at 37°C and 75 % relative humidity. Seeds were grown on plates (0.5x MS-medium, 10 mM MES, pH 5.8 with KOH, 0.8 % (w/v) phytagel) either in the absence of sucrose (a) or supplemented with 1 % (w/v) sucrose (b). According to two-way ANOVA and Tukey`s multiple comparison test, p-values for comparisons with germination rates of Col-0 are given. p > 0.05 in grey.

a) - sucrose

days of aging	day 2				day 3				day 4				day 5			
	gr1	*gr2*	*trx-o1*	*ntr a/b*	*gr1*	*gr2*	*trx-o1*	*ntr a/b*	*gr1*	*gr2*	*trx-o1*	*ntr a/b*	*gr1*	*gr2*	*trx-o1*	*ntr a/b*
0	0.8668	0.7713	< 0.0001	0.1024	0.9578	0.9984	0.0526	0.9829	0.9805	> 0.9999	0.9342	0.9924	0.9874	> 0.9999	0.9981	0.9951
5	< 0.0001	0.0311	< 0.0001	0.3669	0.3378	0.5502	0.2596	> 0.9999	0.5264	0.9497	0.7979	> 0.9999	0.8321	0.9998	0.9975	> 0.9999
12	0.1814	0.3642	0.0015	0.0779	< 0.0001	0.9947	< 0.0001	0.0800	0.0054	0.9754	< 0.0001	0.7345	0.4524	0.9840	0.0003	0.9949
19	> 0.9999	> 0.9999	> 0.9999	> 0.9999	< 0.0001	< 0.0001	< 0.0001	< 0.0001	< 0.0001	< 0.0001	< 0.0001	< 0.0001	< 0.0001	< 0.0001	< 0.0001	< 0.0001
26	> 0.9999	> 0.9999	> 0.9999	> 0.9999	> 0.9999	> 0.9999	> 0.9999	> 0.9999	> 0.9999	> 0.9999	0.9992	> 0.9999	0.9996	0.9996	> 0.9999	0.9996

b) + sucrose

days of aging	day 2				day 3				day 4				day 5			
	gr1	*gr2*	*trx-o1*	*ntr a/b*	*gr1*	*gr2*	*trx-o1*	*ntr a/b*	*gr1*	*gr2*	*trx-o1*	*ntr a/b*	*gr1*	*gr2*	*trx-o1*	*ntr a/b*
0	0.0358	< 0.0001	< 0.0001	> 0.9999	0.9983	0.9984	0.6108	0.2045	0.9950	0.9998	0.8768	0.2997	0.9824	> 0.9999	0.9664	0.9415
5	0.0269	0.0147	< 0.0001	0.9995	0.7414	0.9499	0.1210	0.7252	0.9736	0.9997	0.8999	0.9841	0.9907	> 0.9999	> 0.9999	0.9997
12	0.7386	0.2505	0.0274	0.1871	< 0.0001	< 0.0001	< 0.0001	< 0.0001	0.3487	0.1186	< 0.0001	0.1790	0.9744	0.6027	0.2409	0.8563
19	> 0.9999	> 0.9999	> 0.9999	> 0.9999	0.7621	0.1727	0.1727	0.8897	< 0.0001	< 0.0001	< 0.0001	< 0.0001	< 0.0001	< 0.0001	< 0.0001	< 0.0001
26	> 0.9999	> 0.9999	> 0.9999	> 0.9999	0.9998	0.9998	> 0.9999	0.9998	0.9997	0.9997	> 0.9999	0.9997	0.9997	0.9997	> 0.9999	0.9997

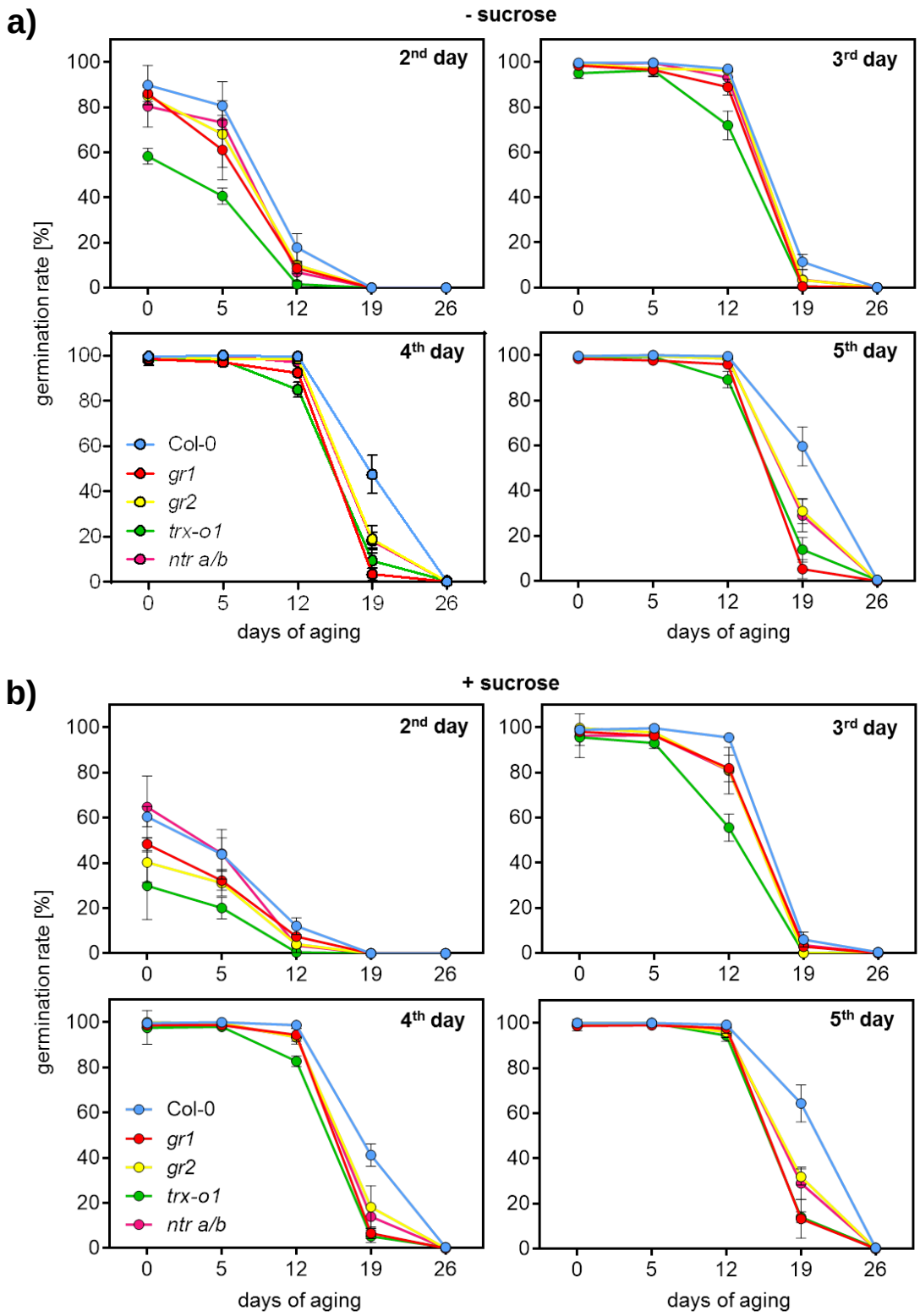

Figure 23: Germination rates of artificially aged Arabidopsis seeds impaired in components of the thiol redox machinery. Arabidopsis seeds were aged by storage for 0, 5, 12, 19 and 26 days at 37°C and 75 % relative humidity. Seeds were incubated on plates (0.5x MS media, 10 mM MES, pH 5.8 with KOH, 0.8 % (w/v) phytagel) without sucrose a) or with 1 % (w/v) sucrose b). Radicle penetration of the testa and the endosperm was used as the criterion of germination (**Figure 22**). Germination rates for days 2-5 after sowing are shown as average of four experiments (average ±SD, *n* = 200-250). Data of fresh seeds of Col-0 are also shown in **Figure 21**. Statistically different germination rates of *gr1*, *gr2*, *trx-o1* and *ntr a/b* as compared to wildtype control (Col-0) seeds are highlighted in **Tab. 1**.

2.3 Measuring the redox changes of individual mitochondrial cysteine-peptides at restart of metabolism

2.3.1 Metabolic restart in mitochondria through substrate feeding

Rapid reduction of the glutathione pools and impairment of germination in thiol redox mutants raises the question, which protein targets undergo redox modifications in early germination. Yet, redox proteomic approaches to identify protein targets in whole seeds are technically challenging, as in Brassicaceae the proportion of different storage proteins in the total seed proteome can easily reach 80 % and more (CROUCH AND SUSSEX 1981; SHEWRY *ET AL.,* 1995). Mass spectrometry signals of lower abundant proteins may be supressed by signals of such highly abundant proteins. One possibility to overcome this technical limitation is to minimise the overall sample complexity, *e.g.* by fractionation of the individual cellular compartments, which increases the resolution also for lower abundant proteins. Whereas different subcellular compartments are hard to isolate, protocols for the isolation of intact and functional mitochondria are well established for Arabidopsis seedlings (SWEETLOVE *ET AL.,* 2007). However, isolation of mitochondria will influence the mitochondrial metabolic activity, which finally may lead to metabolic quiescence, as the mitochondria are separated from their physiological cellular environment, which normally provides substrates to the active mitochondria, *e.g.* for fuelling respiration. Potential targets of the thiol redox machinery were already identified in isolated mitochondria (*e.g.* BALMER *ET AL.,* 2004), but with all known constraints of *in vitro* approaches their physiological relevance remains unclear (see section *1.3.2*). Yet, the physiological situation of isolated mitochondria may share certain characteristics of mitochondria in dry seeds, such as metabolic quiescence in the absence of substrates. As a consequence of the hypothesised low metabolic activity of isolated mitochondria, the NADPH regeneration, which is directly coupled to the primary metabolism by the oxidation of specific substrates (MOLLER AND RASMUSSON 1998; NOCTOR *ET AL.,* 2006), may be considerably low. The NADPH shortage may then cause oxidation of the thiol redox machinery, which is similar to seeds, where metabolic activity decreases during seed maturation process and thiols oxidise gradually at ageing (NAGEL *ET AL.,* 2015). External substrate application to isolated mitochondria should allow to resupply NADPH pools endogenously by a restarted primary metabolism, in which substrates are oxidised by regenerating $NADP^+$ to NADPH. Also seeds were resupplied with substrates at imbibition (see section *2.1.5*) restarting the primary metabolism (see sections *2.1.1* and *2.1.3*) and mitochondrial glutathione-linked redox machinery was rapidly rebooted (see section *2.1.6*). This hypothesised rebooting of the thiol redox machinery in isolated mitochondria at substrate application is monitored with the E_{GSH}-specific sensor roGFP2-Grx1 targeted to the matrix. Mitochondrial substrate oxidation may generate NADH and NADPH, but solely NADPH can be used by the mitochondrial NADPH-dependent GR2 (**Figure 21 c** and MARTY *ET AL.,* 2009) to establish a reduced glutathione pool, and by the NADPH-dependent NTRa/b (**Figure 21 c** and REICHHELD *ET AL.,* 2005; REICHHELD *ET AL.,* 2007) for reduction of the mitochondrial thioredoxins (**Figure 24**, **Figure 21 c**) and subsequently of their downstream target proteins.

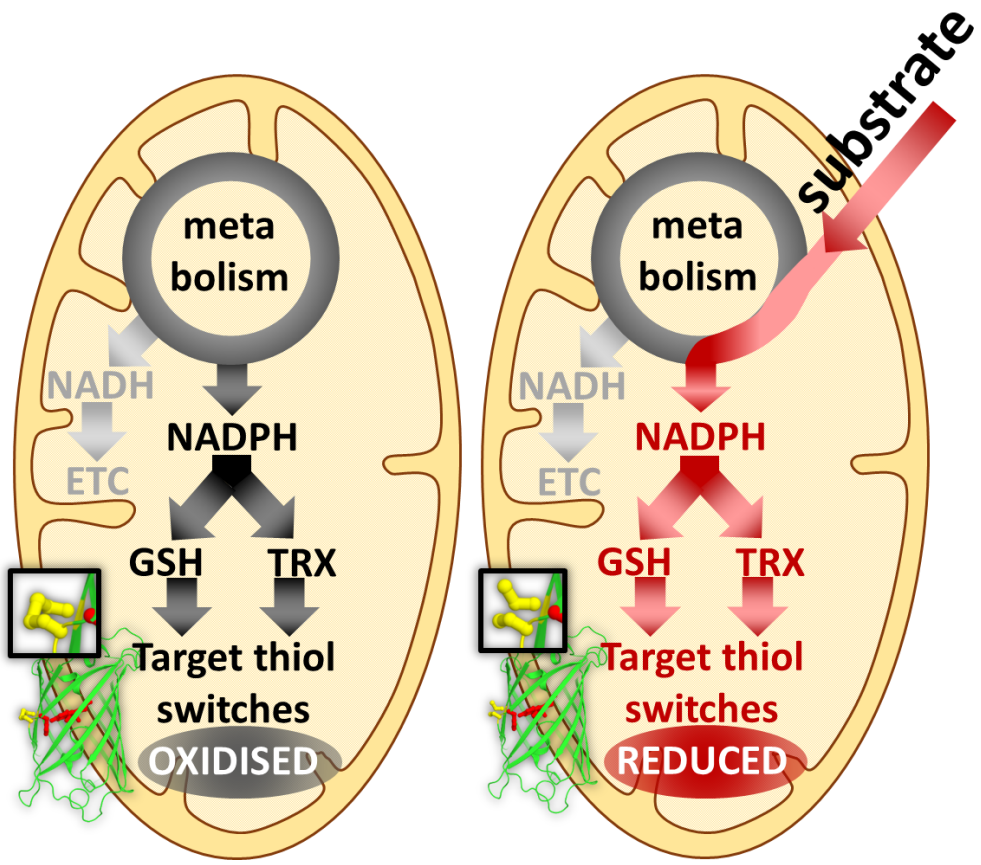

Figure 24: Model for restarting the matrix thiol redox machinery in isolated mitochondria through substrate feeding. Selected reactions of mitochondrial matrix metabolism can be restarted when substrates become available; substrate oxidation in specific reactions mediates reduction of NAD^+ as well as $NADP^+$ to NADH and NADPH, respectively. NADH fuels the mitochondrial electron transport chain (ETC). NADPH can act as an electron donor for thiol redox systems including NTR and GR2. The GR2 mediates the reduction of glutathione in the mitochondrial matrix, which can be followed in real-time via the E_{GSH}-specific fluorescent biosensor roGFP2-Grx1.

In germinating seeds β-oxidation of fatty-acids in the peroxisomes provides citrate to fuel downstream metabolic processes with reductant and carbon skeletons (PRACHAROENWATTANA *ET AL.,* 2005). Other organic acids were also proposed as potential metabolites exported from peroxisomes at β-oxidation, *e.g.* 2OG and succinate (ROTTENSTEINER AND THEODOULOU 2006). In line with the idea of active β-oxidation in germinating oily seeds, the concentration of citrate/isocitrate and of succinate responded remarkably to imbibition, whereas the concentration of 2OG remained unchanged (**Figure 14**). Hence, these substrates were tested for their capacity to trigger $NADP^+$ reduction and reduction of Cys moieties in the mitochondrial matrix, which was monitored via the E_{GSH} specific fluorescent biosensor roGFP2-Grx1 (**Figure 24**) *in organello*.

Feeding isolated mitochondria with 2OG, succinate and citrate as respiratory substrates triggered a rapid reductive response by the redox sensor (**Figure 25 a**). A steady-state plateau was reached within 25 min. Citrate feeding triggered a reduction of the roGFP2-Grx1 sensor by 43 %, succinate by 25 % and 2OG by 7 % (**Figure 25 b**). State II oxygen consumption rates were used to assess the ability of each of the organic acids to act as a respiratory substrate, *i.e.* to be taken up and to deliver electrons to the electron transport chain (ETC, **Figure 25 c**). Succinate feeding triggered an oxygen consumption rate of 70 nM O_2 min^{-1} mg^{-1}, while citrate and 2OG induced very similar rates of 22 and 20 nM O_2 min^{-1} mg^{-1}, respectively.

These data imply that isolated mitochondria were metabolically active and functional, indicated by active consumption of oxygen triggered by substrate oxidation. Application of different substrates to the isolated mitochondria caused distinct reduction of the matrix localised roGFP2-Grx1, although oxygen consumption rates were similar, as for citrate and 2OG. This suggests different capacities for $NADP^+$ reduction in the matrix. Citrate oxidation is accompanied by efficient reduction of the mitochondrial NADP pool restarting the mitochondrial redox machinery. Citrate is isomerised by aconitase (ACO) to isocitrate, which then is oxidised by isocitrate dehydrogenase (**Figure 26 a**). In Arabidopsis mitochondria a NADP-dependent isocitrate dehydrogenase (ICDH) or a NAD-dependent isocitrate dehydrogenase (IDH) is present (YOSHIDA AND HISABORI 2014). 2-oxoglutarate is decarboxylated in the presence of NAD^+ and CoA by the oxoglutarate dehydrogenase complex (OGDC) to Succinyl-CoA, CO_2 and NADH (**Figure 26 b**). Succinate is oxidised by the succinate dehydrogenase (SDH or Complex II of the ETC) to fumarate (**Figure 26 c**), which is hydrolysed to malate by fumarase (FUM). Malate is then oxidised by malate dehydrogenase (MDH) to oxaloacetate, or to pyruvate by NAD-malic enzyme (ME), reducing $NAD(P)^+$ to NAD(P)H. *In vivo* substrate-channelling between the individual enzymes of the Krebs-cycle involved in citrate and fumarate metabolism was reported for potato mitochondria, which may allow efficient control over metabolic pathway fluxes *in vivo* (ZHANG *ET AL.,* 2017). The lack of any pronounced reduction response by 2OG feeding, despite driving respiratory oxygen consumption at smaller rates as citrate, points to a strict specificity of OGDC to NAD^+ (and not $NADP^+$) as co-substrate. The exclusive generation of NADH cannot reduce the NADPH-specific thiol redox enzymes (GR and NTR), and transdehydrogenase activity appears to be lacking in Arabidopsis mitochondria (consistent with a lack of conservation of the mammalian transdehydrogenase gene). With the absence of transdehydrogenase in Arabidopsis mitochondria, only citrate and succinate oxidation triggers efficient $NADP^+$ reduction, whereas 2OG oxidation is mainly leading to the reduction of NAD^+. Matrix localised roGFP2-Grx1, an artificial redox target of the mitochondrial redox machinery, is significantly reduced as a response to citrate and succinate oxidation. This raises the hypothesis that also endogenous targets of the thiol redox machinery are redox-switched when mitochondrial NADPH production is restarted by application of citrate and succinate to isolated, functional mitochondria, which can be tested for in a global redox proteomic approach. 2OG was shown to not trigger any significant restart of the mitochondrial redox machinery while being still metabolised, as shown by causing similar oxygen consumption rates as citrate oxidation, making it a suitable control treatment for the redox proteomic approach.

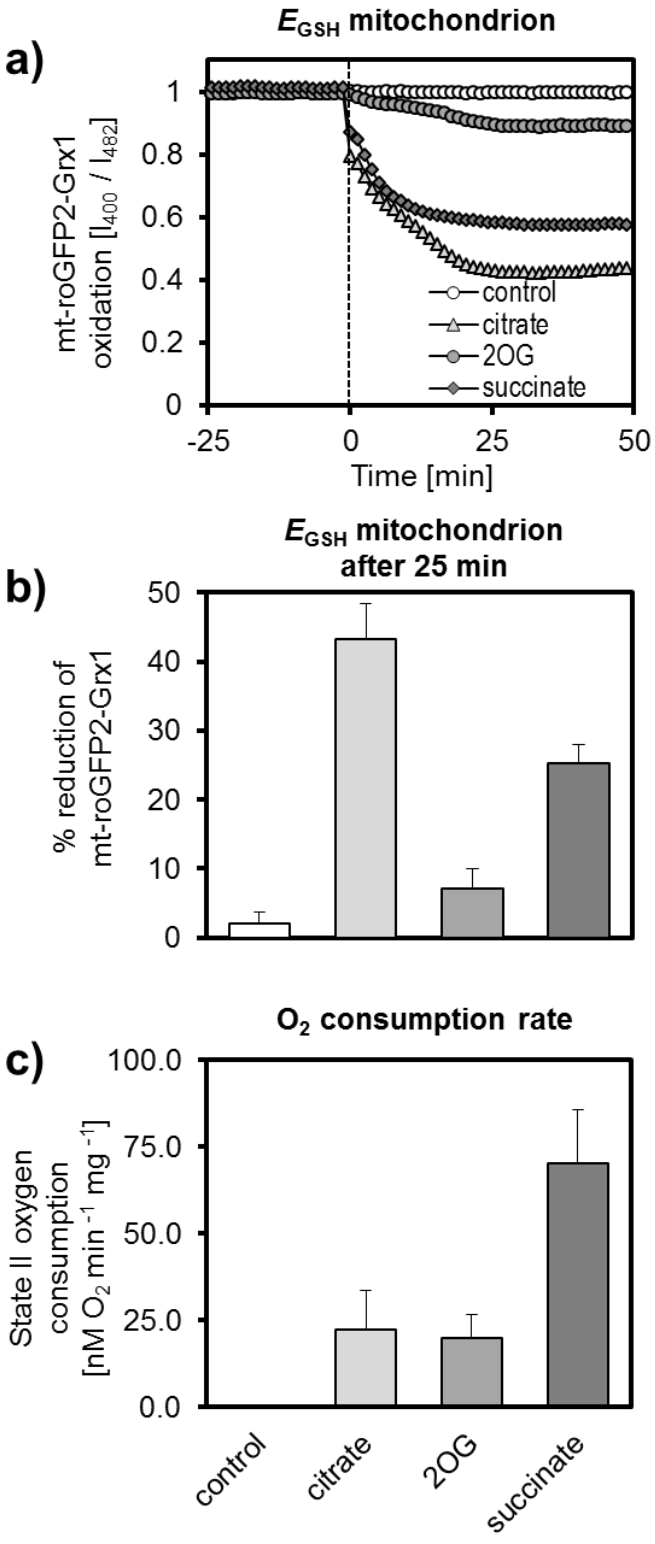

Figure 25: Glutathione redox dynamics in the mitochondrial matrix in response to substrate feeding. The E_{GSH} of isolated mitochondria was monitored using matrix localised roGFP2-Grx1 over time (sequential excitation at 400 and 482 ± 8 nm; emission at 530 ± 20 nm). Dashed black line in a) indicates substrate addition (10 mM citrate / 2OG or succinate) to isolated mitochondria to mimic the sudden substrate availability at seeds imbibition (**Figure 16 b** and **Figure 18**). Representative, normalised 400/482 nm ratios are plotted over time (average of four technical replicates). In b) the roGFP2-Grx1 reduction levels after 25 min of substrate addition were shown (*n* = 5, average +SD; full sensor oxidation with 5 mM DPS; full sensor reduction with 20 mM DTT). Oxygen consumption rates of isolated mitochondria supplemented with different substrates (state II without ADP, *n* = 4 average +SD). Respiration rate of quiescent mitochondria was used for background correction thus `control` mitochondria in c) show no oxygen consumption.

2.3.2 Identifying endogenous redox switches of mitochondrial matrix proteins

To identify endogenous targets of the matrix redox machinery, redox-switched and potentially redox-regulated peptides were identified employing a state-of-the-art thiol redox proteomics approach. Then similarities in thiol redox dynamics between imbibed seeds and the model of the quiescent-active transition in isolated mitochondria were exploited as conceptual basis. Differential labelling with iodoTMTs allows quantifying the redox state of individual Cys-peptides in a high-throughput manner with the capacity to pinpoint the individual redox-switched cysteine in a protein. Redox states of individual mitochondrial peptides before and after substrate application were quantified to identify peptides with altered redox states in response to restarting the endogenous redox machinery of the mitochondrial matrix.

2.3.2.1 Starting metabolic activity in mitochondria can trigger global, yet differential, reduction of proteins

Citrate, 2OG and succinate were used as metabolic substrates to quantify the redox-shifts of individual Cys-peptides in mitochondria after 25 min of respiratory activity by iodoTMT labelling. The MS/MS analysis was conducted with following criteria on the experimental design: only Cys-peptides of ≥7 amino acids length identified in three biological replicates for both, substrate supplemented isolated mitochondria and their untreated controls were considered, as this cut-off criteria was shown to increase the confidence in large-scale protein identifications by mass spectrometry (ELIAS AND GYGI 2007) and allows statistical analysis of the Cys-peptide redox-shifts. That means that each Cys-peptide was identified six times (three times for each treatment), except for succinate supplemented mitochondria, for which only two replicates could be recorded. Cys-oxidation values for peptides with >1 cysteines reflect the average Cys-oxidation state for all labelled cysteine residues in that particular peptide due to the reporter intensity quantification on the level of MS/MS detection. Reporter intensities cannot be assigned routinely to individual cysteine residues for these peptides. To avoid excluding important redox-active Cys-peptides, several of which contain two cysteine residues within close proximity, all Cys-peptides independent from their number of cysteine residues are taken into account for further analysis. Cys-peptides for which only one out of the two corresponding TMTs is identified by MS/MS lead to an apparent reduction of 0 % or 100 %, respectively. This may reflect the *in situ* situation of fully reduced or oxidised peptides, but would be indistinguishable from artefacts as a result of incomplete labelling or the sensitivity limit for tags of low abundant peptides. Yet, in all datasets complete absence of one tag was only found for a single peptide. For the Cys-peptide FCMFNDDVQGTAGVALAGLLGTVR of the mitochondrial NAD-malic enzyme 2 (At4g00570) only one tag in the citrate supplemented mitochondria was identified in all three replicates and thus the corresponding cysteine was 100 % reduced. As such, for the vast majority of identified Cys-peptides the percentage of Cys-oxidation could be validly quantified.

In mitochondria supplemented with citrate and their corresponding quiescent control the percentage of oxidation for 741 Cys-peptides were quantified, mapping to 425 proteins. In total 598 Cys-peptides contained a single cysteine residue, 139 Cys-peptides contained two and the remaining four Cys-peptides contained three cysteine residues. For the mitochondria supplemented with 2OG 734 Cys-peptides mapping to 443 proteins were quantified (one cysteine residue: 601 peptides, two cysteine residues: 130 peptides, three

cysteine residues: three peptides). For the succinate datasets, where only two replicates are available, 621 Cys-peptides mapping to 552 proteins were identified in total (511 peptides: one cysteine residue, 109 peptides: two cysteines, one peptide: three cysteines).

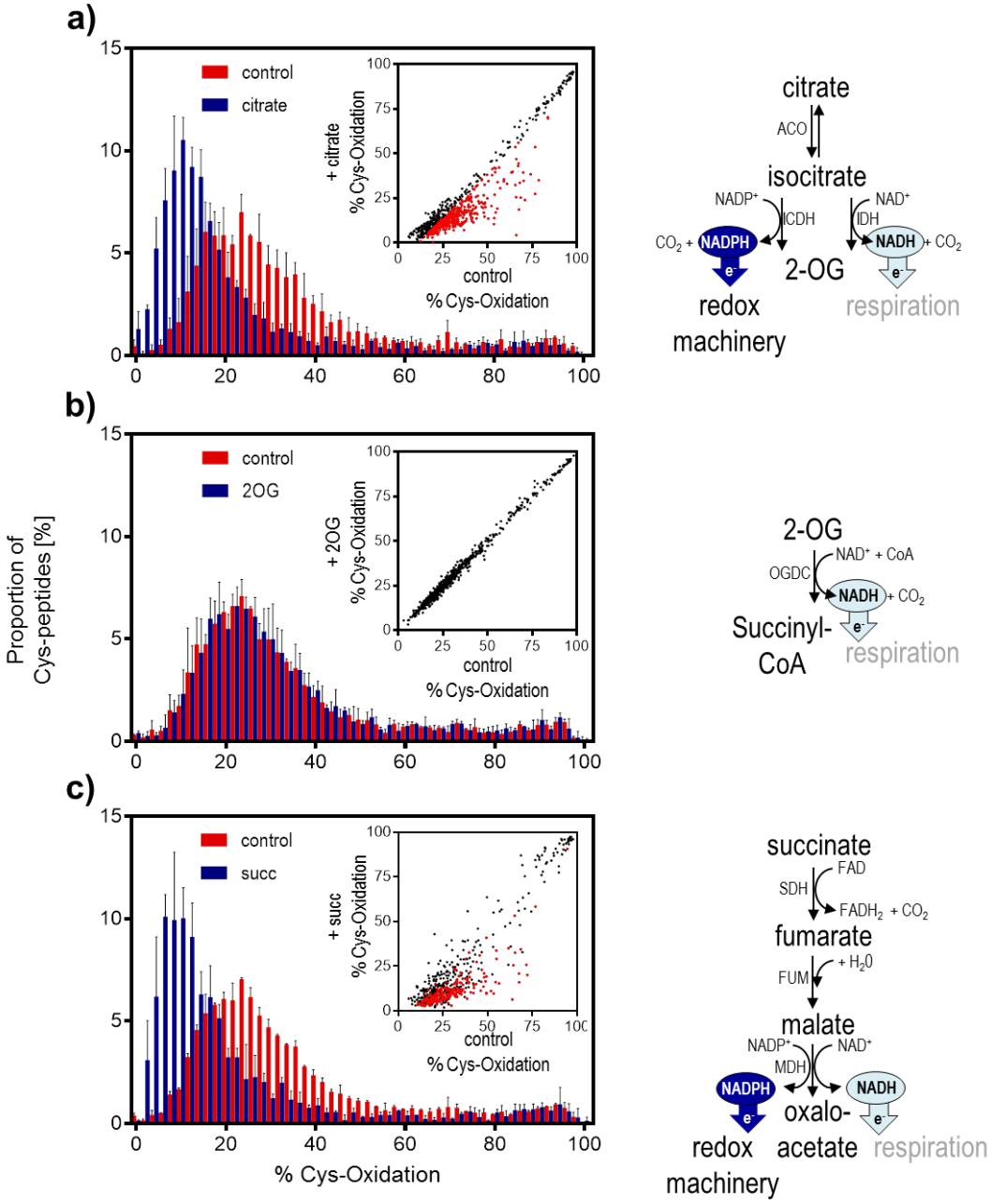

Figure 26: Abundance profiles of the redox states of Cys-peptides in quiescent and respiring isolated mitochondria. Isolated mitochondria from Arabidopsis seedlings were supplemented with citrate a), 2-oxoglutarate (2OG) b) or succinate (succ) c) and incubated for 25 min before labelling with iodoTMTs. Redox states of individual peptides were quantified by MS/MS for isolated mitochondria with and without respiratory substrate (blue and red bars, respectively). The distribution of cysteine peptide oxidation levels are given; the proportion of the total number of peptides in each 2 % quantile of percentage oxidation is plotted (n = 3, average +SD for citrate/2OG and n = 2 for succ). In insets, the percentage of Cys-oxidation without substrate addition is plotted against the percentage of Cys-oxidation after substrate addition for individual Cys-peptides. Cys-peptides with significant change in their Cys-oxidation state upon substrate application are marked in red (t-test corrected for multiple comparisons by Benjamini, Krieger & Yekutieli with <2 % FDR for citrate/2OG treatments and two-tailed, unpaired Students t-test with p<0.05 for succinate treatment). In the reaction schemes to the right the steps of the tricarboxylic acid cycle are shown, which are activated by the respective

substrate. Mitochondrial aconitase (ACO), NADP-dependent isocitrate dehydrogenase (ICDH), NAD-dependent isocitrate dehydrogenase (IDH). NAD-dependent oxoglutarate dehydrogenase complex (OGDC), succinate dehydrogenase (SDH), fumarase (FUM), NAD(P)-dependent malate dehydrogenase (MDH).

The Cys-peptides grouped into 2 % quantiles of Cys-oxidation states show a characteristic distribution with a median Cys-oxidation value of 27.1 % for the quiescent control, and 13 % in the mitochondria supplemented with citrate (**Figure 26 a**). By contrast mitochondria supplied with 2OG show an unchanged median of 27.0 % as compared to their corresponding control (27.1 %, **Figure 26 b**). Mitochondria supplied with succinate show a median Cys-oxidation of 12 %, as compared to the corresponding control (26.7 %, **Figure 26 c**). Hence, median Cys-oxidation is lowered by 14.1 % and 14.7 % by citrate and succinate, respectively, whereas practically no change (0.1 %) was found for 2OG.

The percentage of oxidation of individual Cys-peptides from quiescent mitochondria plotted against that of substrate supplemented mitochondria (**Figure 26 a**, **b** & **c** insets), results in an overall diagonal distribution for the Cys-peptides with unaltered redox state. Redox changes result in deviations by individual peptides from the diagonal distribution. For 2OG, not a single peptide differed in Cys-oxidation between treatment and control (t-test corrected for multiple comparisons by Benjamini, Krieger & Yekutieli with <2 % FDR). Citrate supply resulted in a significant reduction of 412 Cys-peptides mapping to 245 different proteins (**Figure 26 a**, red dots). For succinate supplementation valid statistics could not be performed due to availability of only two biological replicates; if does irrespectively, a significant reduction of 223 Cys-peptides mapping to 153 different proteins was obtained ($p<0.05$ with two-tailed, unpaired Student`s t-test).

Individual replicates (see replicates I, II & III in panels **a** and **b** of **Figure 27**, **Figure 28** and **Figure 29**), show high reproducibility, both globally and for the redox states of individual peptides, which underpins the technical validity of the approach. While in citrate supplemented mitochondria all changes were towards reduction, in succinate supplemented mitochondria (**Figure 29 b**), there were also a few peptides that appeared shifted slightly towards oxidation. Yet additional replication would be required to validate this effect statistically (**Figure 26 c**).

Boxplots of the Cys-oxidation states reveal that 50 % of all Cys-peptides show an average Cys-oxidation state of 19 - 40 % in all quiescent mitochondrial samples and in those supplemented with 2OG (panel **c** in **Figure 27**, **Figure 28** and **Figure 29**). At citrate supply 50 % of all Cys-peptides show an average Cys-oxidation state of 9 - 22 % (**Figure 27 c**) and 7 - 21 % at succinate supply (**Figure 29 c**).

Plotting the difference between the Cys-oxidation state between quiescent and 2OG supplemented mitochondria (% ΔCys-reduction) against the corresponding p-value (two-tailed, unpaired Student`s t-test; significantly different values plotted in red with $p<0.05$) show a two-tailed distribution (**Figure 28 d**). 399 and 335 peptides show a slight non-significant reduction or oxidation, respectively, resulting in even scattering around 0 % ΔCys-reduction. For the citrate experiment, the plot reveals uneven scattering with only two Cys-peptides showing a non-significant shift towards oxidation (**Figure 27 d**), and 739 Cys-peptides were shifted towards reduction (412 significant peptides with FDR<0.02 by t-test corrected for multiple comparisons by Benjamini, Krieger & Yekutieli; 423 significant peptides with $p<0.05$ by two-tailed Student`s t-test). The results were similar for the succinate experiment with slightly less pronounced one-sided scattering: here 49 Cys-peptides were non-significantly shifted towards oxidation and 572 were shifted towards reduction (223 significant peptides with $p<0.05$ by two-tailed Student`s t-test).

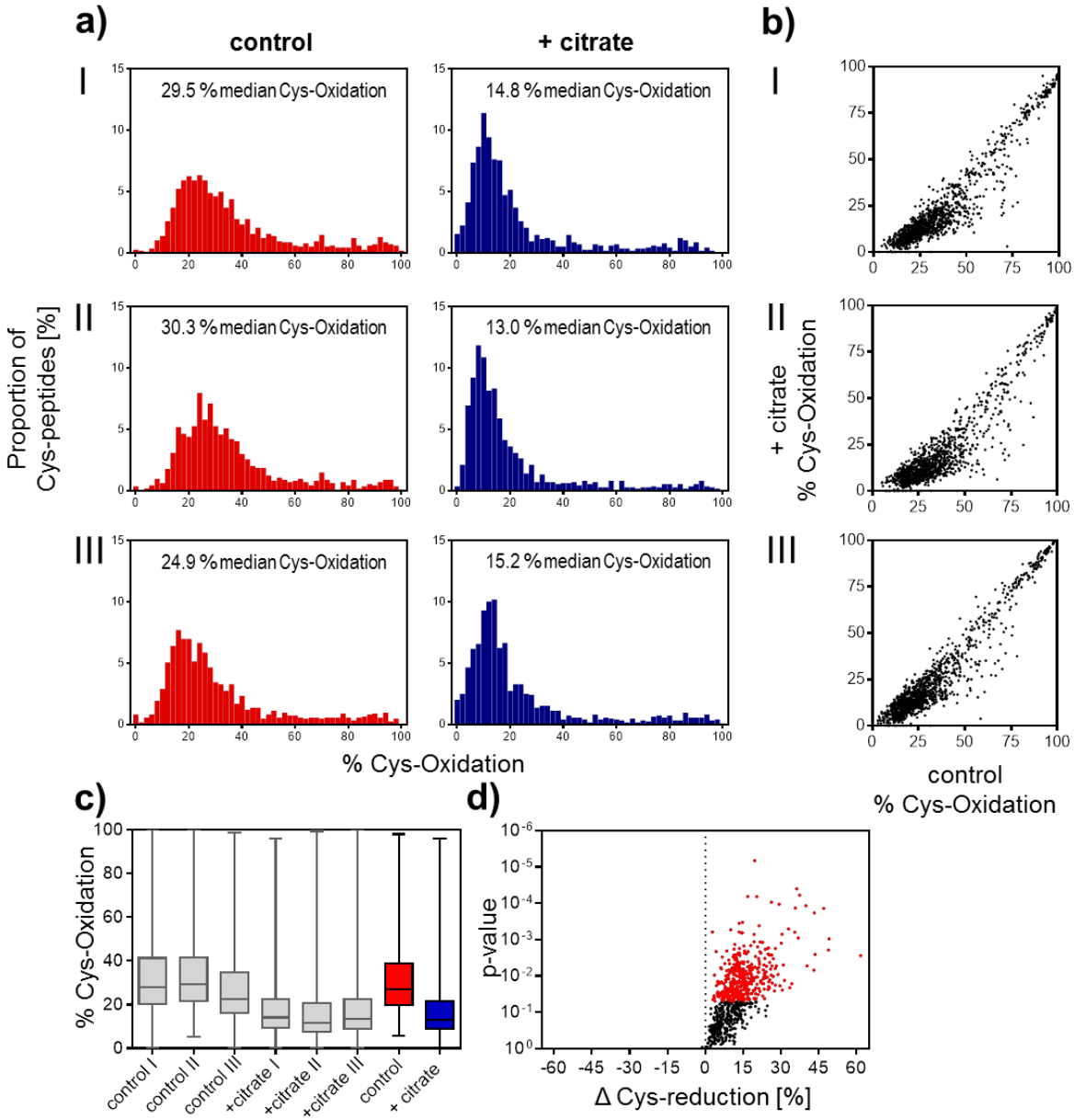

Figure 27: Individual replicates of the iodoTMT-based quantification of the redox states of isolated mitochondria supplemented with citrate and their corresponding quiescent controls. Mitochondria of Arabidopsis seedlings were supplemented with 10 mM citrate for 25 min. Percentage of Cys-reduction of individual peptides was quantified using MS/MS-analysis after iodoTMT-based labelling a) for quiescent mitochondria (control, red bars) and after citrate addition (+ citrate, blue bars). The distribution of oxidation-percentage is shown for replicates I, II & III; the proportion of the total number of peptides in each 2 % quantile of percentage oxidation is plotted. For all replicates the same data is also shown for individual Cys-peptides in b). Box-plots of the percentage in Cys-oxidation for the individual replicates and the total averages are shown in c). Volcano plots illustrating the the p-value (two-tailed, unpaired Student`s t-test) against the percentage change Cys-reduction at substrate supplementation in d). Peptides with p-values <0.05 are indicated in red.

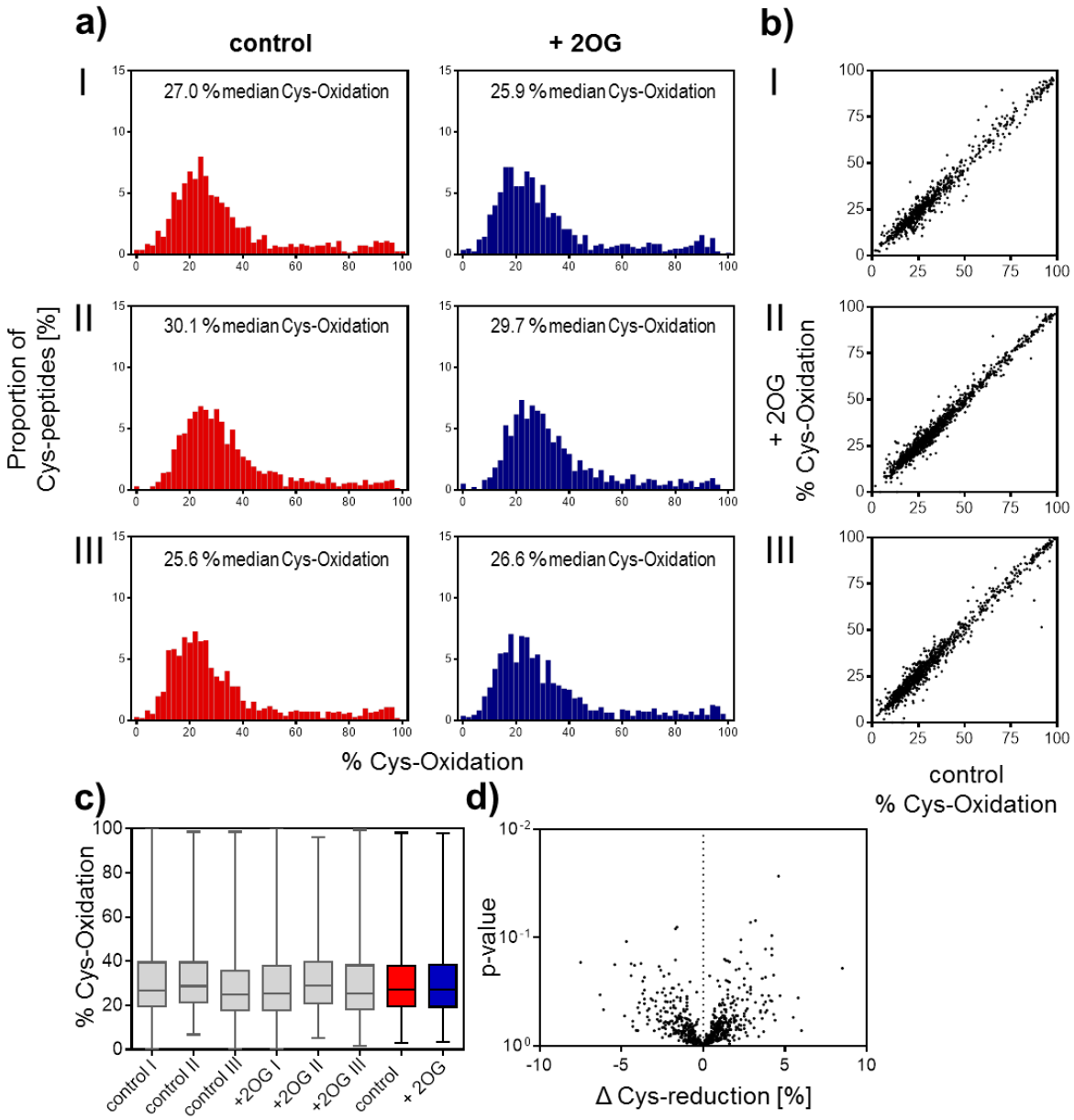

Figure 28: Individual replicates of the iodoTMT-based quantification of the redox states of isolated mitochondria supplemented with 2OG and their corresponding quiescent controls. Mitochondria of Arabidopsis seedlings were supplemented with 10 mM 2OG for 25 min. Percentage of Cys-reduction of individual peptides was quantified using MS/MS-analysis after iodoTMT-based labelling a) for quiescent mitochondria (control, red bars) and after 2OG addition (+ 2OG, blue bars). The distribution of oxidation-percentage is shown for replicates I, II & III; the proportion of the total number of peptides in each 2 % quantile of percentage oxidation is plotted. For all replicates the same data is also shown for individual Cys-peptides in b). Box-plots of the percentage in Cys-oxidation for the individual replicates and the total averages are shown in c). Volcano plots illustrating the the p-value (two-tailed, unpaired Student`s t-test) against the percentage change Cys-reduction at substrate supplementation in d). Peptides with p-values <0.05 are indicated in red.

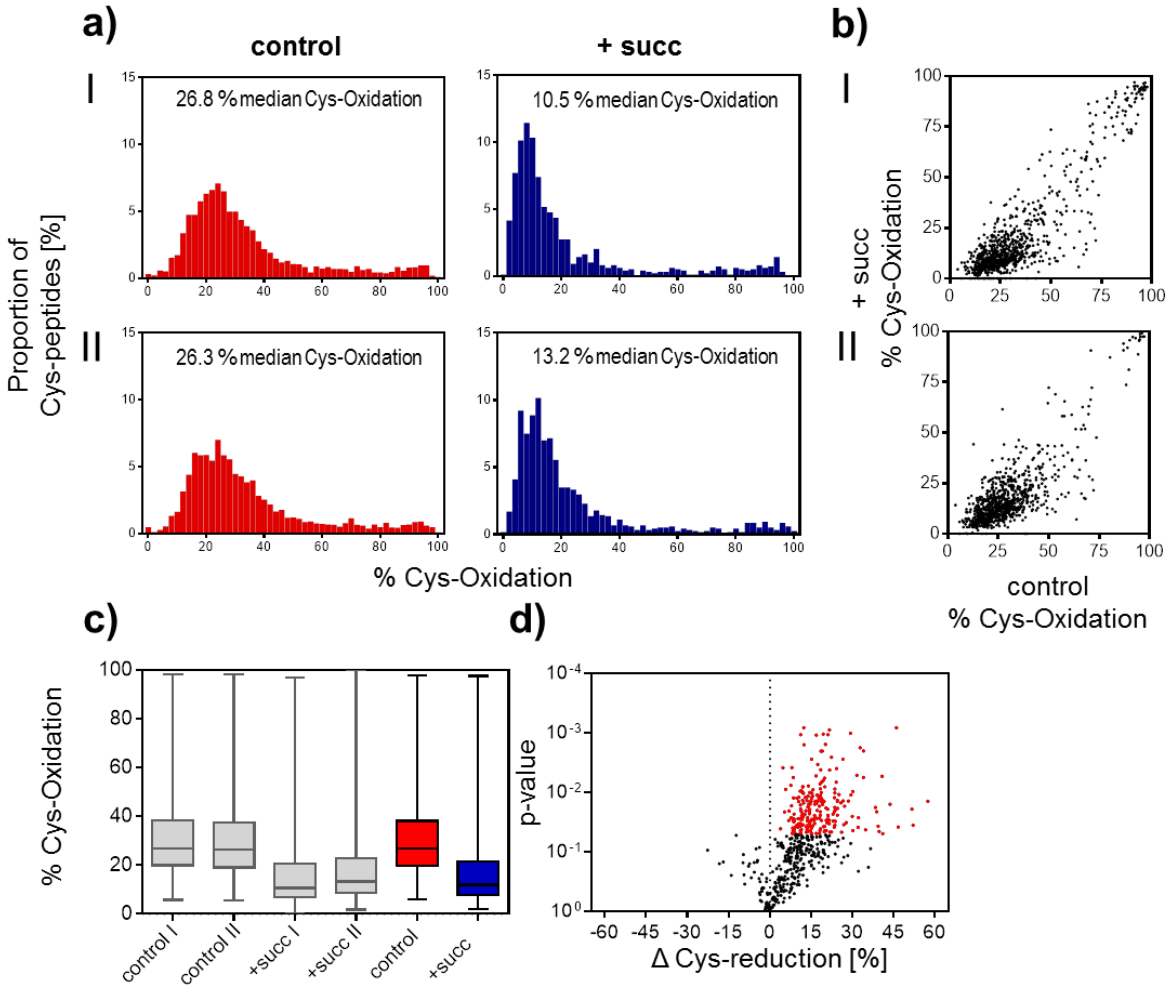

Figure 29: Individual replicates of the iodoTMT-based quantification of the redox states of isolated mitochondria supplemented with succinate and their corresponding quiescent controls. Mitochondria of Arabidopsis seedlings were supplemented with 10 mM succinate for 25 min. Percentage of Cys-reduction of individual peptides was quantified using MS/MS-analysis after iodoTMT-based labelling a) for quiescent mitochondria (control, red bars) and after succinate addition (+ succ, blue bars). Control I derives from the average of the controls in **Figure 27**, control II derives from the average of the controls in **Figure 28**. The distribution of oxidation-percentage is shown for replicates I, II; the proportion of the total number of peptides in each 2 % quantile of percentage oxidation is plotted. For all replicates the same data is also shown for individual Cys-peptides in b). Box-plots of the percentage in Cys-oxidation for the individual replicates and the total averages are shown in c). Volcano plots illustrating the the p-value (two-tailed, unpaired Student`s t-test) against the percentage change Cys-reduction at substrate supplementation in d). Peptides with p-values <0.05 are indicated in red.

Those data provide further evidence for an efficient restart of the matrix redox machinery as a result of the oxidation of specific substrates, confirming and generalising the observations using the roGFP2-Grx1 sensor (**Figure 25**). Oxidation of certain respiratory substrates, including citrate and succinate, trigger the reduction of a set of Cys-peptides. Other respiratory substrates, including 2OG, do not cause any reduction of any Cys-peptide. A reasonable interpretation is that NADPH as the sole substrate of the matrix thiol redox machinery is only provided by some dehydrogenases (*e.g.* by isocitrate dehydrogenase), while others specifically provide NADH (*e.g.* OGDC). Since the global pattern of Cys-peptide reduction appeared similar for citrate and succinate, the citrate dataset was chosen for

further in-depth analysis. Citrate supply caused the most pronounced reduction of roGFP2-Grx1 (**Figure 25 a** and **b**). This implies that the most negative E_{GSH} is reestablished by citrate oxidation, which is closest to the highly negative E_{GSH} values reported for Arabidopsis mitochondria *in vivo* (SCHWARZLÄNDER *ET AL.,* 2008). Citrate is also likely to act as the main respiratory substrate during seed imbibition *in vivo*. It was shown that citrate is exported from peroxisomes as a product of fatty acid β-oxidation in imbibed Arabidopsis seeds and this is critical for germination efficiency (PRACHAROENWATTANA *ET AL.,* 2005). Mutants impaired in the glyoxylate cycle, which was initially suggested to provide succinate to the mitochondria in germinating seeds, do not show germination impairment and can still germinate properly without any obvious deficiencies (EASTMOND *ET AL.,* 2000). The physiological relevance of citrate in early seed germination further underpins its utilisation as a model substrate.

2.3.2.2 Redox-switching of Cys-peptides may serve as an indicator of their subcellular (fine) localisation

The reduction of a Cys-peptide depends on its initial state in Cys-oxidation. Those Cys-peptides that are largely oxidised before the addition of the respiratory substrate can undergo large shifts in redox status, in principle, while the possible shift in redox status is limited for those that are already largely reduced to start with. Interestingly, none of the 24 Cys-peptides with a Cys-oxidation state >85 % in the quiescent control was found to get reduced at citrate supply. At least 16 of those are annotated as either localised to the intermembrane space or exposed to it. Of those eight Cys-peptides of different TIM-proteins (TIM 8, 9, 10 & 13) are exposed to the intermembrane space, and four Cys-peptides of different Complex I subunits are located in the membrane arm of Complex I facing the intermembrane space. The remaining four peptides correspond to proteins involved in the oxidation/reduction of cytochrome *c,* also implying exposition to the intermembrane space. The same principle holds true also for succinate experiment. Here, out of 34 peptides with a Cys-oxidation state of >85 %, eight peptides belong to TIM-proteins, and five to Complex I subunits with exposition to the intermembrane space and seven to proteins involved in the oxidation/reduction of cytochrome *c*.

Building on the idea that reduction can only be expected to Cys exposed to the mitochondrial matrix, the purity of the isolated mitochondria was estimated using annotation of subcellular localisation. It was hypothesised that even in the presence of contamination with proteins from other subcellular compartments, only proteins with mitochondrial localisation should undergo reduction by the reactivated matrix-localised thiol redox machinery.

For all individual peptides identified in the citrate experiment (n = 741), the consensus protein localisation (*in silico* predictions in many cases) was obtained from the Arabidopsis subcellular database (SUBA3; HOOPER *ET AL.,* 2014). 61 % of all identified peptides are annotated with mitochondrial localisation and 22 % with plastidic localisation (**Figure 30 a**, *Peptide level*). For the subgroup of peptides significantly reduced at citrate supply (412 peptides) 75 % are annotated with mitochondrial localisation and 13 % with plastidic localisation (**Figure 30 b**, *Peptide level*). In the subgroup of peptides that were not redox-shifted, only 44 % are annotated mitochondrial, while 33 % were annotated plastidic. For several proteins multiple Cys-peptides were identified. That considered, the annotated localisation of unique proteins reveals a smaller proportion of mitochondrial proteins as compared to the estimation at the peptide level (51 % in the control, **Figure 30 a**, *Protein level* and 67 % for redox-shifted proteins; **Figure 30 b**, *Protein level*). Hence, more mitochondrial proteins were identified by multiple peptides than proteins with an annotated localisation to

other compartments. In mitochondria supplemented with succinate, a slightly higher proportion of peptides are annotated with mitochondrial localisation (65 % in the control and 78 % for redox-shifted proteins). This indicates higher purity of the mitochondria, while the enrichment is similar (16 % increase for citrate and 13 % for succinate). At the protein level, 54 % of all identified proteins were annotated mitochondrial, whereas 72 % of the redox-switched proteins were annotated mitochondrial. It should be noted that the classification was performed at the basis of peptide identities and without their relative quantities. That leads to a bias towards low abundance contaminants, as the small absolute quantity of contaminating peptides is typically highly diverse even for highly pure preparations (SENKLER *ET AL.*, 2017). Yet, the relative enrichment of proteins and peptides annotated as mitochondrial proteins provides strong evidence for specific reduction of Cys-peptides with mitochondrial localisation. The absence of redox-shifting in highly oxidised proteins localised to the intermembrane space confirms that active reduction is limited to the matrix and that the inner mitochondrial membrane precludes reduction of non-matrix exposed Cys-peptides. Peptides that are not redox-shifted show enrichment for non-mitochondrial compartments, based on their annotation. Yet, there are also Cys-peptides identified that belong to well established matrix proteins, indicating that redox-switching in the matrix can be differential and specific.

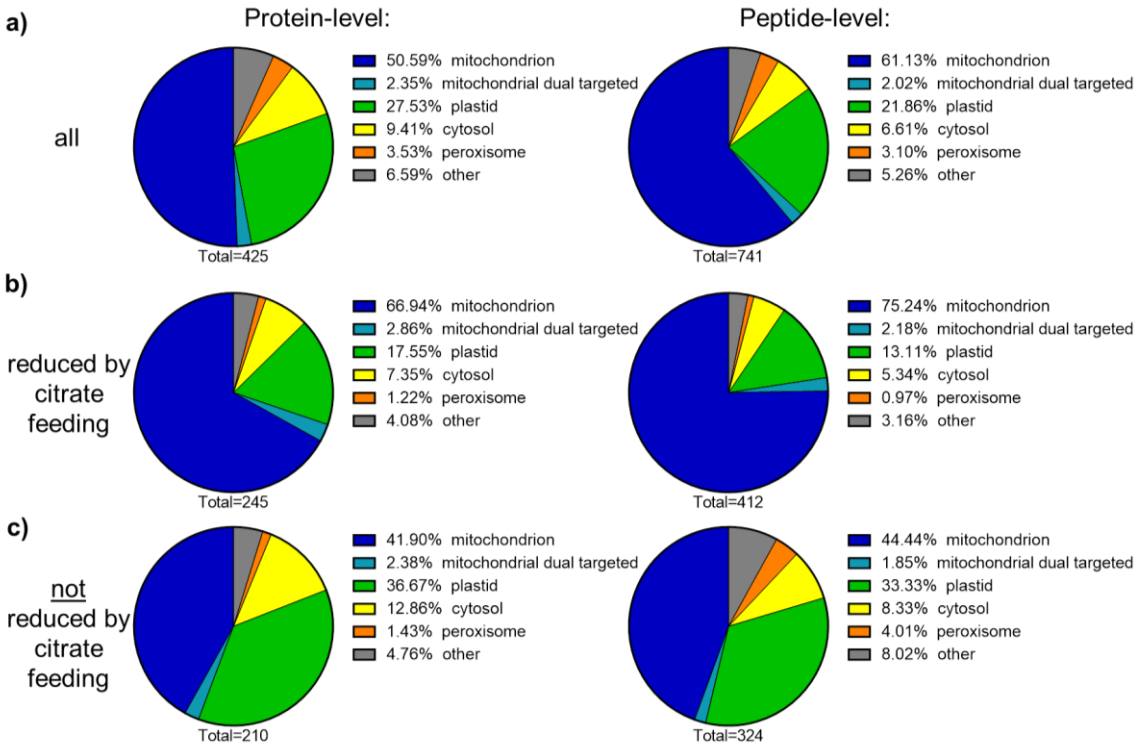

Figure 30: Annotated subcellular localisation of Cys-peptides and proteins identified in isolated mitochondria and redox-shifted by citrate addition. a) Annotated subcellular localisation of all identified proteins (*Protein-level*) and their individual detected Cys-peptides (*Peptide-level, n* = 3) based on the subcellular localisation database (SUBA3; HOOPER *ET AL.*, 2014). b) The annotated subcellular localisation for Cys-peptides significantly reduced at addition of respiratory substrate (t-test corrected for multiple comparisons by Benjamini, Krieger & Yekutieli with <2 % FDR) at *Protein-* and *Peptide-level*. c) The annotated subcellular localisation for non-redox-shifted Cys-peptides and corresponding proteins (t-test corrected for multiple comparisons by Benjamini, Krieger & Yekutieli with ≥2 % FDR).

2.3.2.3 *The most highly redox-shifted peptides belong to proteins of the mitochondrial thiol redox machinery*

To evaluate the functional roles of the identified redox-switched proteins, Cys-peptides were sorted according to their degree of redox-shifting, *i.e.* the differences between the Cys-oxidation percentage in quiescent control mitochondria and the percentage at addition of citrate as respiratory substrate (Δ%Cys-reduction). The 50 proteins with the most strongly redox-shifted Cys-peptides (all towards reduction) are listed in **Tab. 2**. The Cys-peptide showing the highest Δ%Cys-reduction with 61.7 % is unique and can be assigned to the mitochondrial/plastid dual-targeted GR 2. The Cys-oxidation value shifts from 66.0 % in the quiescent control to 4.3 % with citrate addition. A non-unique peptide of thioredoxin reductase NTR a and/or NTR b was identified as the second most reduced Cys-peptide with 49.1 % Δ%Cys-reduction (shifting from 76.5 % Cys-oxidation to 27.4 %). Both isoforms were described as dual-targeted to the cytosol and the mitochondria (REICHHELD *ET AL.,* 2005; REICHHELD *ET AL.,* 2007). The third most strongly shifted peptide belonged to mitochondrial TRX-o1, which underwent a redox change of 48.1 % (from 67.4 % Cys-oxidation to 18.6 %). Each of those three peptides featuring the strongest shifts contains two cysteine residues, preventing the distinct assignment of the shift to the individual cysteine. Instead the percentage represents an average between both Cys and may be even larger for one of the two; on the other hand formation of an intramolecular disulfide between the two Cys also remains a likely possibility, which would result in an equal contribution. For NTR and TRX-o1, peptides with the catalytic CxxC motive were identified. 12 out of the 50 most redox-shifted peptides showed this sequence motif. That included a unique peptide from TRX-o2. Experimental evidence for the expression of TRX-o2 had not been available before at the protein level, probably due to its low abundance. Its redox state was shifted by 24.5 %.

Three peptides of the heterologous expressed mitochondrial roGFP2-Grx1 were found redox-shifted. Two of them are amongst the 50 most reduced peptides. Two unique peptides can be assigned to the glutaredoxin domain and one peptide originates from the roGFP2 domain. The identified redox-switched Cys-peptides of the Grx1 domain contained either the peptide responsible for GSH-binding or the catalytic cysteine residues involved in the redox-relay with the roGFP2 domain. The identified redox-switched peptide deriving from the roGFP2-domain contains the Cys^{147} residue, which is involved in the disulfide bridge formation together with the Cys^{204} residue. No peptide containing the Cys^{204} residue was identified, likely due to the quality control thresholds applied for proteomic data analysis. Citrate supplementation triggered a Δ%Cys-reduction for the Cys^{147}-peptide of 30.4 %, which is smaller than the value measured via the optical properties of the roGFP2-Grx1 *in situ* (43 %, **Figure 25**).

Summarised, the most pronounced reductive shifts were observed for key players of the matrix redox machinery, identified by their catalytic cysteines. Only few metabolic enzymes were in the list of the 50 most redox-shifted Cys-peptides.

Tab. 2: The 50 most strongly redox-shifted peptides at restarting the thiol redox machinery of the mitochondrial matrix by citrate addition. Peptides with the highest difference between their Cys-oxidation state in isolated mitochondria with and without citrate addition; average Δ%Cys-reduction, *n* = 3. For non-unique peptides all matching identifiers were listed. Within the amino acid sequence of the identified peptides, cysteine residues are highlighted in bold and underlined.

% Δ Cys-Ox	identifier	name	AS-sequence
61.6	AT3G54660	Glutathione reductase 2, chloroplastic (GR2)	FATSFGASAAV**C**ELPFSTISSDTAGGVGGT**C**VLR
49.1	AT2G17420;AT4G35460	Thioredoxin reductase 2 (NADPH-dependent thioredoxin reductase 2) (NTR2; AtNTRA)	GISA**C**AV**C**DGAAPIFR
48.8	AT2G35010	Thioredoxin O1, mitochondrial (AtTrxo1)	AQDGSLPSVFYFTAAW**C**GP**C**R
46.9	AT4G37910	Heat shock 70 kDa protein 9, mitochondrial (Heat shock protein 70-9) (AtHsp70-9)	SP**C**QN**C**LK
43.5	AT1G66240	Homolog of anti-oxidant 1	VAMT**C**EG**C**VGAVK
43.2	AT1G51390;AT3G20970	NifU-like protein 5, mitochondrial (AtNfu-I) (AtNfu5)	MQGA**C**SG**C**PSSSVTLK
43.0	AT4G05400	At4g05400 (Copper ion binding protein) (Putative uncharacterized protein AT4g05400)	LYEQ**C**LNAP**C**PVR
40.3	AT1G58180	Beta carbonic anhydrase 6, mitochondrial (AtbCA6) (AtbetaCA6)	TQLASSHLSFDEQ**C**R
39.8	AT1G79230	Thiosulfate/3-mercaptopyruvate sulfurtransferase 1, mitochondrial	**C**IPFPQMFDS**C**NTLLPAEELKK
37.4		roGFP2-GRX1	D**C**IGG**C**SDLVSLQQSGELLTR
36.8	AT1G79230	Thiosulfate/3-mercaptopyruvate sulfurtransferase 1, mitochondrial	**C**IPFPQMFDS**C**NTLLPAEELK
36.2	AT5G13030	Putative uncharacterized protein At5g13030	PGV**C**MLS**C**SS
35.7	AT2G39270	Probable adenylate kinase 6, chloroplastic (ATP:AMP phosphotransferase)	I**C**SE**C**GGNYNVA**C**IDIK
35.4	AT1G48570	Putative uncharacterized protein At1g48570 (Zinc finger (Ran-binding) domain-containing protein)	TLAEPGDWE**C**PS**C**DFVNFR
34.3	AT1G04640	Octanoyltransferase (Lipoate biosynthesis protein)	**C**ETGVWVGDR
33.5	AT2G38660	Bifunctional protein FolD 1, mitochondrial (Methylenetetrahydrofolate dehydrogenase)	G**C**VELLIR
33.0	AT5G17790	Zinc finger protein VAR3, chloroplastic (Protein VARIEGATED 3)	QLTGSEWE**C**PQ**C**DFYNYGR
31.4	AT5G44730	At5g44730 (Dreg-2 like protein) (Haloacid dehalogenase-like hydrolase domain-containing protein)	AIGLP**C**PDYK
30.9	AT5G47630	Acyl carrier protein 3, mitochondrial (MtACP-3) (NADH-ubiquinone oxidoreductase 9.6 kDa subunit)	LT**CC**GDVATYILSETPTK
30.5	AT2G31240	Putative kinesin light chain (Tetratricopeptide repeat-containing protein)	**C**LEFA**C**EILEK
30.4		roGFP2-GRX1	LEYNYN**C**HNVYIMADK
30.1	AT4G22220	Iron-sulfur cluster assembly protein 1 (AtISU1) (NifU-like N-terminal domain-containing protein ISU1)	NDPNVGTGLVGAPA**C**GDVMK
29.6	AT4G16800	Probable enoyl-CoA hydratase 2, mitochondrial	I**C**GENAVFGLPETGLAIIPGAGGTQR
29.2	AT1G49660;AT1G49650	Probable carboxylesterase 5 (AtCXE5)	SAN**C**LAVSVQYR
28.8	AT4G22220	Iron-sulfur cluster assembly protein 1 (AtISU1) (NifU-like N-terminal domain-containing protein ISU1)	NVGSFDKNDPNVGTGLVGAPA**C**GDVMK
28.1	AT5G11350	Carbon catabolite repressor protein 4 homolog 6 (CCR4 homolog 6)	LWDDAPIVL**C**GDFN**C**TPK
27.8	AT2G43360	Biotin synthase (EC 2.8.1.6)	EVQQ**C**TLLSIK
27.8	AT2G26800	Hydroxymethylglutaryl-CoA lyase	GYVS**C**VVG**C**PVEGPVLPSK
27.7	AT5G46180	Ornithine aminotransferase, mitochondrial	TPVSHITE**C**DR
26.9	AT3G21300	RNA methyltransferase family protein (RNA methyltransferase-like protein)	**C**LLQSEPGNLVLAAVQD**C**WR
26.9	AT2G39670	Radical SAM domain-containing protein	LTA**C**VSSQVG**C**PLR
26.5	AT3G54826	Zim17-type zinc finger protein	HDFMMVFT**C**K
26.4	AT4G22220	Iron-sulfur cluster assembly protein 1 (AtISU1) (NifU-like N-terminal domain-containing protein ISU1)	TFG**C**GSAIASSSVATEWVK
26.3	AT1G04640	Octanoyltransferase (Lipoate biosynthesis protein)	YFEHIVP**C**GIADK
26.2	AT3G15590	Pentatricopeptide repeat-containing protein At3g15590, mitochondrial	GLQQTPWV**C**R
26.1	AT2G31060	At2g31060 (Elongation factor family protein)	LSLT**C**PSR
25.9	AT2G20830	Folic acid binding / transferase	TALDTINLELH**C**GSHPR
25.6	AT4G11600	Probable phospholipid hydroperoxide glutathione peroxidase 6, mitochondrial (AtGPX1)	GHGFEILAFP**C**NQFGNQEPGTNEEIVQFA**C**TR
25.5	AT5G47890	NADH dehydrogenase [ubiquinone] 1 alpha subcomplex subunit 2	ILL**C**QSSPASAPTR
25.5	AT1G79440	Succinate-semialdehyde dehydrogenase, mitochondrial (At-SSADH1)	NSGQT**C**V**C**ANR
25.4	AT2G30970	Aspartate aminotransferase, mitochondrial (EC 2.6.1.1) (Transaminase A)	VG**C**LSVL**C**EDPK
25.2	AT1G80270	Pentatricopeptide repeat-containing protein At1g80270, mitochondrial	TLLAN**C**VAAGNVK
25.1	AT5G65720	AT5G65720 protein (Cysteine desulfurase)	**C**VLDS**C**R
25.0	AT5G14580	Polyribonucleotide nucleotidyltransferase 2, mitochondrial (AtmtPNPase)	I**C**GQFVVNPTMDELSSSDLNLIYA**C**TR
25.0	AT2G43360	Biotin synthase (EC 2.8.1.6)	F**C**MGAAWR
24.9	AT1G80230	Cytochrome c oxidase subunit 5b-2, mitochondrial (AtCOX5b-2)	SFE**C**PV**C**TQYFK
24.9	AT4G01990	Pentatricopeptide repeat-containing protein At4g01990, mitochondrial	NQSTYGSLLN**C**Y**C**VEK
24.7	AT5G53140	Probable protein phosphatase 2C 76 (AtPP2C76)	NDDGSLS**C**GY**C**SFR
24.5	AT1G31020	Thioredoxin O2, mitochondrial (AtTrxo2)	DGSLPSVFYFTAAW**C**GP**C**R
24.5	AT4G00570	NAD-dependent malic enzyme 2, mitochondrial (AtNAD-ME2)	VMT**C**VQQ**C**DR

2.3.2.4 Multiple redox-switched Cys-peptides identified for unique proteins at key-positions of the mitochondrial metabolism

A total of 412 individual Cys-peptides corresponding to 245 proteins were significantly redox-shifted at citrate addition (**Figure 26 a**). Accordingly each protein was identified by 1.7 different Cys-peptides on average. For 151 proteins only a single specific Cys-peptide was identified. For the remaining proteins at least 2 Cys-peptides were significantly redox-switched. To highlight proteins identified by multiple redox-shifted Cys-peptides and to identify hotspots of redox-switching in known protein complexes and pathways, all redox-shifted peptides were filtered for identical corresponding Arabidopsis identifiers. With ten unique significantly redox-switched Cys-peptides, the 75 kDa subunit of the peripheral arm of Complex I was the richest in redox active Cys residues (**Figure 31 a**, blue dots).
Further significantly redox-switched Cys-peptides can be assigned to different proteins of the matrix-exposed peripheral arm of Complex I. In total 21 unique redox-switched peptides of the peripheral arm of Complex I were identified (**Figure 31 a**, blue dots), whereas three Cys-peptides were determined as non-switched (red dots). All other redox-switched Cys-peptides of the Complex I subunits identified belong to the matrix-exposed carbonic anhydrase domain, for which also a single non-switched cysteine residue was identified. All seven identified unique Cys-peptides located on the membrane arm are known to be exposed to the intermembrane space (BRAUN *ET AL.,* 2014) and were not redox-switched. Those observations are in agreement with the data obtained for highly oxidised peptides with >85 % Cys-oxidation states (**Figure 26 a**, **b** & **c** insets), which are often localised in the intermembrane space and which are not redox-switched in this model system. This reflects the clear separation of the two mitochondrial redox-machineries located in the intermembrane space and the mitochondrial matrix and makes the system unsuitable to analyse non-matrix exposed Cys-peptides.
In addition to Complex I subunits, also other proteins of the electron transport chain were identified as redox-switched (**Figure 31 b**). While for Complex II, IV and V at least two peptides were identified as redox-switched, no peptide of the Complex III was identified as being redox-switched, although the redox state of seven Cys-peptides could be quantified. This implies that these Cys-peptides are surface-exposed and therefore accessible for binding the tags during labelling procedure. Thus, their redox state can be quantified, although the redox state is not-shifted.
Redox-switching at most of the individual electron transport complexes may allow for sophisticated modulation of the electron fluxes down the respiratory chain with potential impacts on supercomplex dynamics and inner membrane architecture fine-tuning respiratory efficiency. Yet, although redox-switching of specific Cys-peptides is a prerequisite for redox regulation, its occurrence is not sufficient to predict regulatory significance; instead it may fulfil another function (as discussed in *1.3.2*).

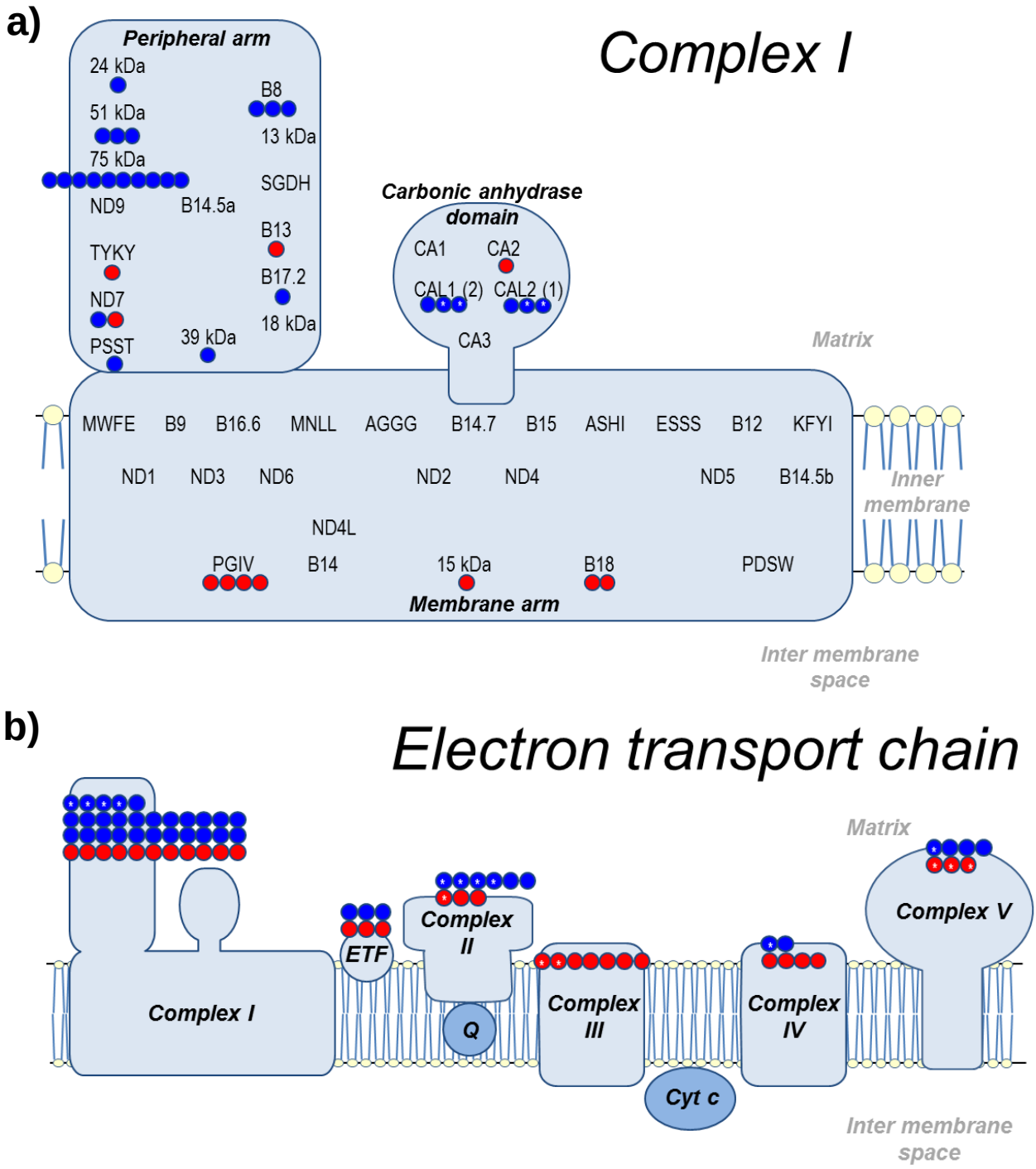

Figure 31: Schematic topology of identified Cys-peptides of mitochondrial Complex I and of other complexes of the respiratory chain. a) Schematic model of the internal subunit arrangement of plant Complex I according to BRAUN *ET AL.*, 2014. Subunits are named according to the bovine nomenclature. Identified peptides (*n* = 3) of Complex I are illustrated by circlets; blue circlets indicate Cys-peptides with significant change in their Cys-oxidation state at citrate addition (t-test corrected for multiple comparisons by Benjamini, Krieger & Yekutieli with <2 % FDR); red circlets represent Cys-peptides with no significant change in Cys redox state. White asterisks indicate non-unique Cys-peptides. Ancillary, possible isoforms of identified protein are given in parentheses. b) Schematic summary of all redox-switched peptides of known proteins of the electron transport chain according to CHROBOK *ET AL.*, 2016; SCHIKOWSKY *ET AL.*, 2017 and BRAUN *ET AL.*, 2014.

In addition to proteins of the electron transport chain, further respiration-associated proteins were identified by multiple redox-switched Cys-peptides. The E1-subunit of the oxoglutarate dehydrogenase complex (OGDC, AT5G65750, **Figure 32**) was identified with up to seven redox-switched Cys-peptides. However, three Cys-peptides are not unique and may also be assigned to the E1-subunit-derived from the protein AT3G55410. For other proteins of the TCA cycle, also multiple Cys-peptides were identified as redox-switched. 14 Cys-peptides for the different pyruvate dehydrogenase complex subunits were identified as redox-shifted. Furthermore, four Cys-peptides were identified but without any significant redox change. For the succinate dehydrogenase (SDH, also known as Complex II of the ETC, **Figure 31 b** and **Figure 32**) six out of nine quantified Cys-peptides were identified as redox-switched. Only three out of eight Cys-peptides assigned to the aconitase 1 and 2 were identified as redox-switched. Yet, for all enzymatic steps of the TCA cycle at least one peptide was identified as redox-switched.

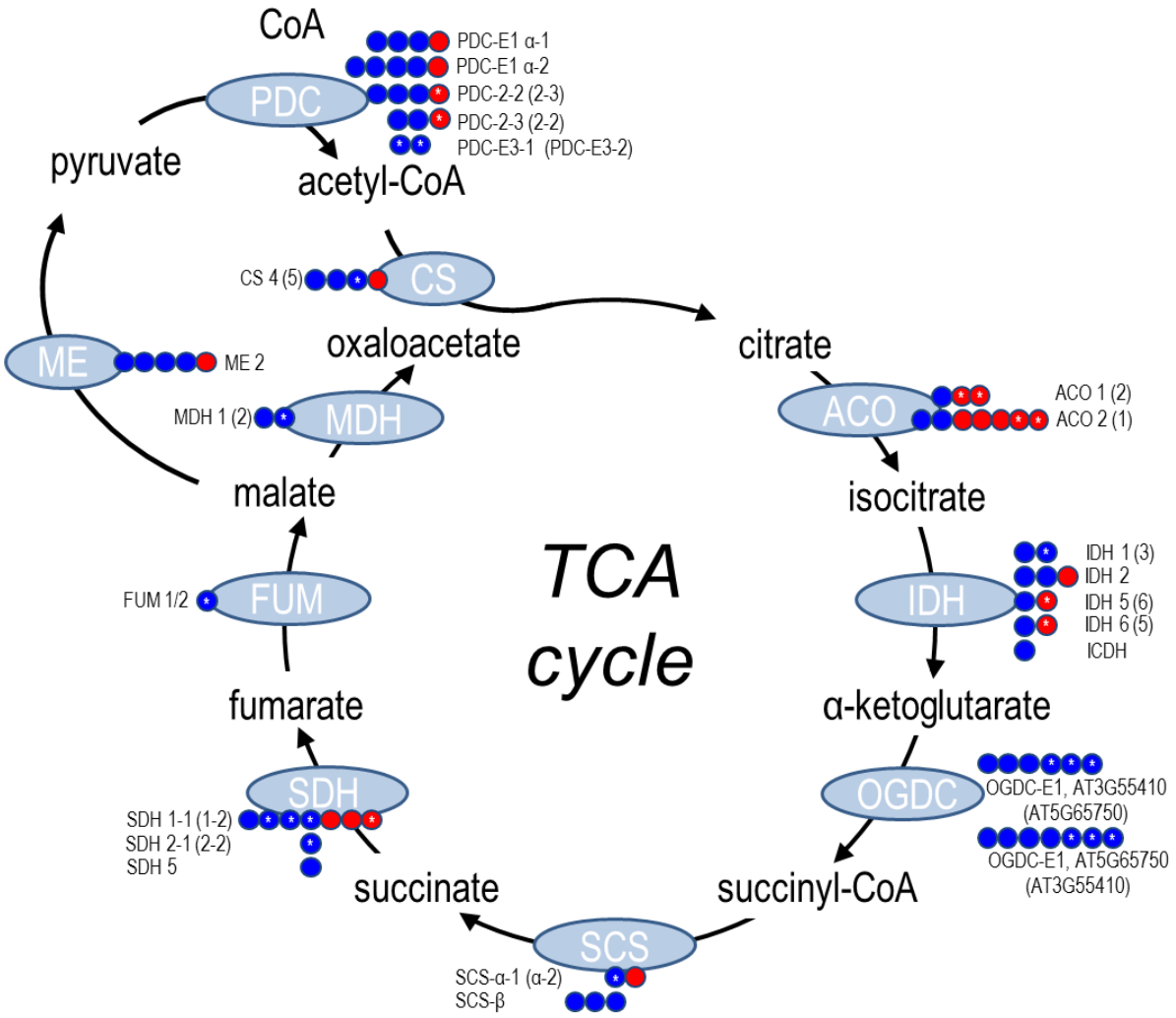

Figure 32: Schematic overview of identified Cys-peptides of TCA cycle associated proteins. Schematic summary of the TCA cycle to illustrate all quantified Cys-peptides (*n* = 3) by small circlets; blue circlets indicate peptides with a significant change in Cys redox state at citrate addition (t-test corrected for multiple comparisons by Benjamini, Krieger & Yekutieli with <2 % FDR); red circlets represent Cys-peptides with no significant change in Cys redox state. White asterisks indicate non-unique Cys-peptides. Ancillary, possible isoforms of identified protein are given in parentheses.

Furthermore, enzymes which are closely related to the TCA cycle function were identified as redox-switched by multiple Cys-peptides, *e.g.* the aspartate aminotransferase with five unique redox-switched Cys-peptides (**Figure 33**). Furthermore, five redox-switched Cys-peptides of the alanine aminotransferase 1 were identified. A single Cys-peptide identified for the alanine aminotransferase 1 is not unique and can be also assigned to the alanine aminotransferase 2, for which additionally two unique redox-switched Cys-peptides were identified. Aminotransferases catalyse the interconversion of amino acids and oxoacids of the TCA cycle, coupling the amino acid metabolism to the mitochondrial energy metabolism.

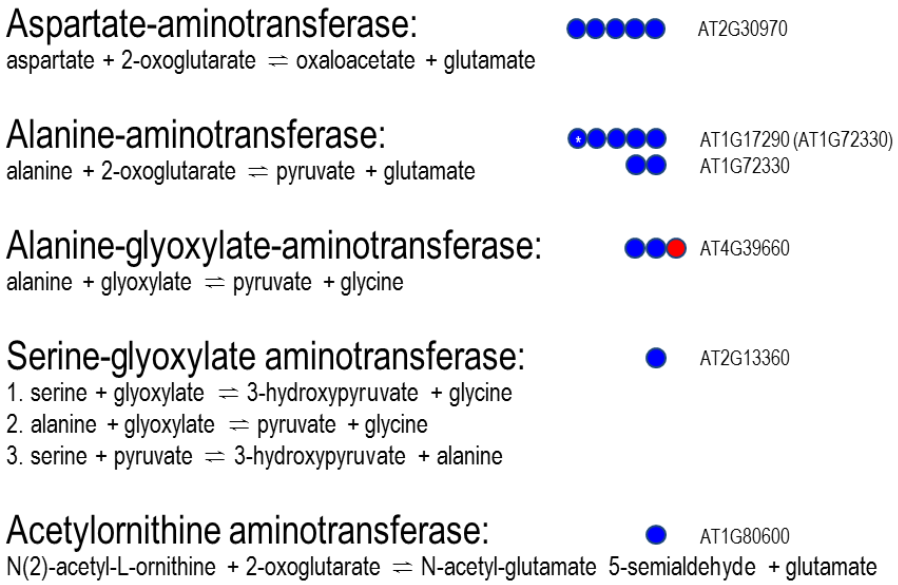

Figure 33: Overview of identified Cys-peptides of aminotransferases and their catalysed reactions. All quantified Cys-peptides of aminotransferases (*n* = 3) are illustrated by small circlets; blue circlets indicate Cys-peptides with significant change in their Cys redox state at citrate addition (t-test corrected for multiple comparisons by Benjamini, Krieger & Yekutieli with <2 % FDR); red circlets represent Cys-peptides with no significant change in Cys redox state. White asterisks indicate non-unique Cys-peptides. Ancillary, possible isoforms of identified protein are given in parentheses. Catalysed reactions are given for each identified transaminase below their name.

An overview of the proteinogenic amino acids and their metabolic precursors (according to www.genome.jp/kegg and HILDEBRANDT *ET AL.,* 2015) reveals that several further proteins of the mitochondrial amino acid metabolism were identified as redox-switched. Mainly proteins involved in the metabolism of valine/leucine, serine/glycine/cysteine and glutamate/proline/arginine were identified as redox-switched (blue dots in **Figure 34**), with proteins identified by most Cys-peptides as following:
The carboxyltransferase subunit of the 3-methylcrotonyl-CoA carboxylase was identified with five unique redox-switched Cys-peptides (AT4G34030, **Figure 34**). This enzyme is involved in leucine degradation within the mitochondrial matrix. For the mitochondrial glycine dehydrogenase 1/2 seven Cys-peptides were identified, of which four were redox-switched; as a part of the matrix localised glycine decarboxylase complex also four redox-switched Cys-peptides of the amino-methyltransferase were identified (AT1G11860). For the mitochondrial delta-1-pyrroline-5-carboxylate dehydrogenase 12A1 that catalyses proline degradation to glutamate, six unique Cys-peptides were identified, of which three were redox-switched (AT5G62530). Several other proteins involved in different steps of mitochondrial amino acid metabolism were also identified by up to three different redox-switched Cys-peptides (**Figure 34**).

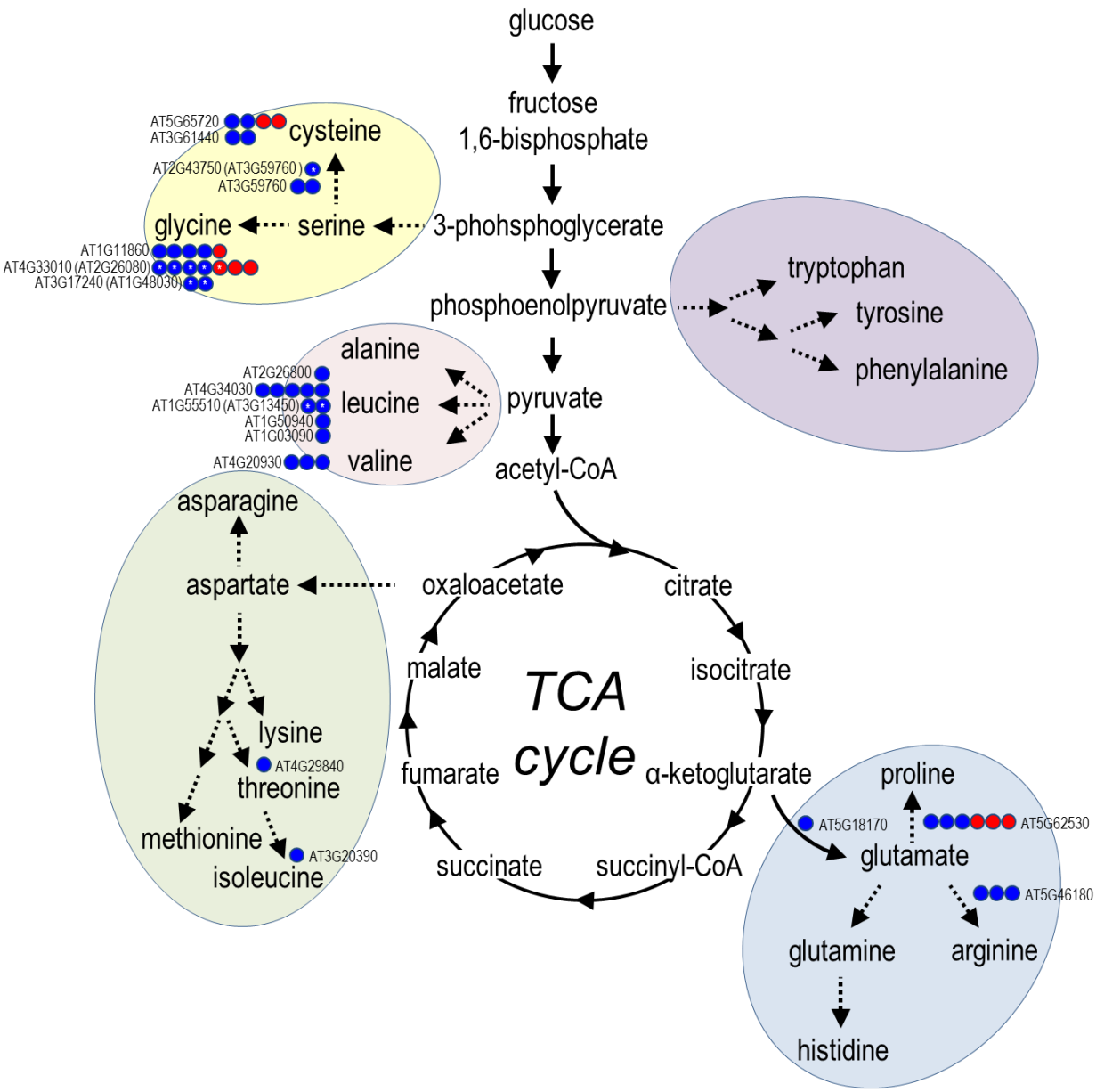

Figure 34: Overview of identified Cys-peptides of amino acid metabolism associated proteins. Schematic model of amino acid metabolism according to www.genome.jp/kegg and HILDEBRANDT *ET AL.*, 2015 including the proteinogenic amino acids and their precursors and/or degradation products. Amino acids derived from the same metabolic precursor were grouped and highlighted with coloured ovals. For simplicity, amino acid intermediates and corresponding enzymes are not illustrated. Identified peptides (n = 3) of proteins associated with amino acid metabolism are illustrated by circlets; blue circlets indicate peptides with a significant change in Cys redox state at citrate addition (t-test corrected for multiple comparisons by Benjamini, Krieger & Yekutieli with <2 % FDR); red circlets represent Cys-peptides with no significant change in Cys redox state. White asterisks indicate non-unique Cys-peptides. Ancillary, possible isoforms of identified protein are given in parentheses.

2.3.2.5 *Multiple non-redox-switched Cys-peptides identified for non-mitochondrial proteins*

Also within the subgroup of non-significantly redox-switched Cys-peptides, multiple different peptides can be assigned to the same proteins, *e.g*. for the large subunit of the ribulose bisphosphate carboxylase/oxygenase (RuBisCO) in total seven unique Cys-peptides were identified with unchanged Cys-peptide redox state. Four unique peptides of the peroxisomal glutamate-glyoxylate aminotransferase 1 were identified with unchanged Cys-peptide redox state. The small subunit of the RuBisCO was identified with in total three Cys-peptides with none of them being redox-shifted. This suggests that high abundant non-mitochondrial proteins, such as the different RuBisCO subunits of plastidic origin, were commonly identified within the isolated mitochondria, but these proteins/peptides were not significantly redox-switched given that functional and compartmentalised metabolism for NADPH provision to a co-localised redox machinery is needed for an active reduction of target proteins. This further supports the observations made for Cys-peptides identified with high Cys-oxidation states with >85 % (see insets in **Figure 26 a**, **b** & **c**) and for the subcellular predictions of the redox-switched Cys-peptides (**Figure 30 a, b** and **c**).
Together those lines of evidence draw a consistent picture implying redox-shifts associated to citrate addition for matrix-exposed Cys-peptides only, while non-matrix exposed mitochondrial Cys-peptides and contaminant proteins remain largely unaffected. Interestingly, also Cys-peptides of proteins with annotations for plastids were identified as redox-shifted at citrate addition, *e.g.* the Calvin cycle protein CP12 (WEDEL *ET AL.,* 1997) which raises the hypothesis that several proteins identified as redox-shifted in the mitochondria are indeed dual-targeted and not contaminating proteins of other compartments, such as of chloroplasts.

In summary several proteins of the mitochondrial energy metabolism, including the respiratory chain and the TCA cycle (the ETC: **Figure 31**, the TCA-cycle: **Figure 32**) and of the mitochondrial amino acid metabolism (aminotransferases: **Figure 33**, amino acid metabolism: **Figure 34**) were identified by multiple redox-switched Cys-peptides. For individual proteins up to ten unique Cys-peptides were identified as redox-switched by restarting the mitochondrial redox-machinery. These potential redox-regulated enzymes are diverse, which would allow complex regulation and flexible modulation of metabolic fluxes to control mitochondrial activity. Hypothetical redox regulation of the identified target proteins may allow concerted regulation and fine-tuning of central C, N and energy metabolism.
In addition, several Cys-peptides involved in iron-sulfur-cluster assembly/biogenesis were identified as highly redox-switched, but the most strongly reduced Cys-peptides represent catalytic cysteine residues of the redox machinery itself.
The question if redox-switching at the identified targets really affects organisation and/or activities and fluxes of the proteins and pathways remains to be investigated individually. Dedicated investigation of candidate proteins will be required, *e.g.* by site-directed mutagenesis of the specific cysteine residues followed by characterisation *in vitro* and *in vivo*. Yet, a critical advantage of the redox-switched peptides quantified here is that the conditions of sampling carry physiological meaning, because the isolated mitochondria system maintains steric and kinetic constraints and reestablishes thermodynamics. This is likely to be a decisive difference to the *in vitro* approaches to identify redox-regulated proteins that have been performed to identify target candidates so far (recently reviewed in NIETZEL *ET AL.,* 2017).

2.4 Physiological alterations of early seed germination in Arabidopsis redox mutants

2.4.1 Mutants impaired in the redox machinery show lowered respiratory efficiency

Multiple key-positions of the mitochondrial energy metabolism were identified as redox-switched at citrate addition to isolated mitochondria. This raises the hypothesis that respiration may be impaired in mutants with impaired redox machineries at early germination. Therefore different redox mutants were analysed for deviations in their respiratory performance at imbibition. After-ripened, synchronised seeds of different redox mutants (*gr1, gr2, trx-o1* & *ntr a/b*) and of their corresponding wildtype Col-0 were analysed using the oxygen sensitive fluorescent probe MitoXpress®Xtra (Luxcel Biosciences, **Figure 35**).
The Δ fluorescence lifetime was increased immediately in response to imbibition in all investigated seed samples in a similar manner as observed for Col-0 seeds (**Figure 35 a** and **Figure 7 a**). All redox mutants consistently showed an increase in oxygen consumption, as measured by an increase of the Δ fluorescence lifetime of the oxygen sensitive probe. Already during the very early time window that has been assessed by fluorescent protein sensors, elevated increase rates in Δ fluorescence lifetime were obvious (30 - 60 min). For the redox mutants the increase rates in Δ fluorescence lifetime were up to nearly double those of the wildtype control (**Figure 35 b**).
Elevated oxygen consumption rates are indicative of higher flux through respiratory metabolism. Since respiration is typically constraint by demand increased fluxes may be due to a decrease in respiratory efficiency (such as uncoupling and/or futile cycling) during early germination. This effect appears consistently correlated with defects at different positions in the cytosolic and mitochondrial redox machineries.

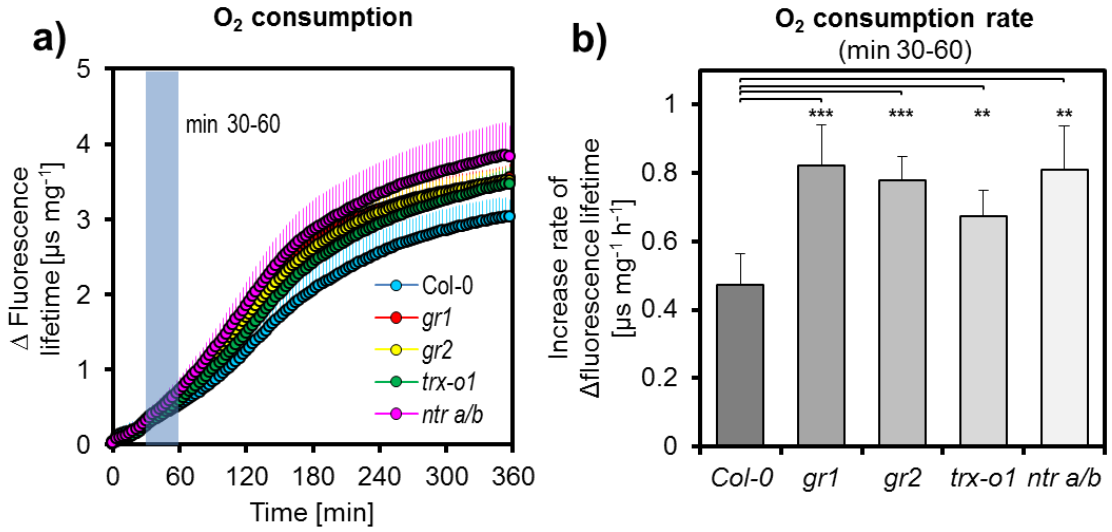

Figure 35: Oxygen consumption of imbibed Arabidopsis seeds from mutants of the redox machinery. The respiratory activity of Arabidopsis seeds in response to imbibition was measured a) using the MitoXpress®Xtra (Luxcel Biosciences) fluorescent probe. Probe lifetime increase (Δ Fluorescence lifetime) was calculated by subtraction of fluorescence lifetime at timepoint T_0 from the increasing fluorescence lifetime upon oxygen consumption during imbibition (*n* = 5; average +SD, normalised to seed weight). Light blue box indicates the time window, for which the average increase rate of Δ fluorescence lifetime was calculated as a measure of oxygen consumption rates in early germination. b) The increase rates of the Δ fluorescence lifetime in the time window marked in a) (30 - 60 min) are given (*n* = 5; average +SD, two-tailed, unpaired Student`s t-test: **p<0.01*, ***p<0.001). Measurements were performed by the group of Prof. Macherel.

2.4.2 The adenosine nucleotide energy charge is not affected in the redox mutants

The adenosine pools of seeds from the different redox mutants were investigated to obtain further information of their respiratory efficiency during early phases of germination. The amounts of free AMP, ADP and ATP were quantified in extracts from after-ripened, synchronised seeds before and after 1 h of imbibition (**Figure 36**).

AMP was the dominating adenosine in dry seeds of all lines ranging from about 145 to about 190 pmol mg^{-1}. In the *ntr a/b* mutant, the AMP concentration was higher as compared to the control. ADP content ranged from 65 to 89 pmol mg^{-1} and was slightly elevated in the *gr1* mutant. ATP was the lowest abundant adenosine in dry seeds with 13 - 20 pmol mg^{-1} in all lines, showing no differences in the redox mutants. In all lines the AMP concentration decreased at 1 h imbibition. AMP concentration were in the range between 51 - 94 pmol mg^{-1}, and the elevated AMP levels in the *ntr a/b* mutant were maintained. ADP concentration dropped to 30 - 38 pmol mg^{-1} at imbibition, without differences between the different lines. ATP concentration increased in all lines at imbibition reaching concentration of 74 - 103 pmol mg^{-1} without any differences between the different lines. The general pattern of establishment of adenosine energy charge was maintained in all lines. Although steady-state measurements cannot provide strict clues about adenosine fluxes, the increased rates of oxygen consumption observed in the mutants appear not to be mirrored in the establishment of energy charge.

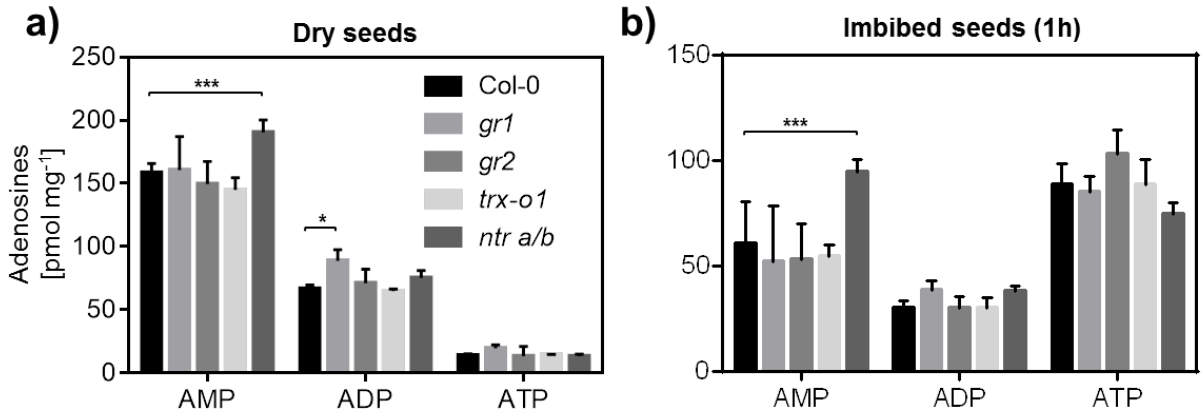

Figure 36: Adenosine pools of Arabidopsis seeds with impaired redox machinery. The adenosine pools of dry and imbibed Arabidopsis seeds were measured. AMP, ADP and ATP in dry seeds a) and after imbibition for 1 h b) were analysed by HPLC (average +SD, *n* = 4, seeds of two individuals were pooled). Col-0 values are the same as in **Figure 11**. Significantly different values of the mutants in comparison to the wildtype were indicated by asterisks (two-way ANOVA and Bonferroni`s multiple comparison test, *p<0.05, ***p<0.001). Measurements were performed by the group of Prof. Hell.

NADH concentration in dry and imbibed seeds were quantified to obtain a complementary read-out of the energy metabolism of the redox mutants (**Figure 37**) and to obtain further insight into the respiration phenotype of the redox mutants during early germination (**Figure 35**).

In comparison to the adenosine pools, total NADH concentration were small, as already observed for wildtype seeds (**Figure 13 b** and **Figure 37**) with 3.6 - 6.6 pmol mg^{-1} in the dry state and 4.0 - 8.5 pmol mg^{-1} after imbibition. The NADH concentration in the dry and imbibed *ntr a/b* seeds were increased in comparison to wildtype seeds, whereas the other

redox mutants did not show any alterations. A technical limitation is that HPLC-based analysis lacks subcellular resolution, which might restrict the sensitivity to detect potential subcellular molecular phenotypes in the redox mutants. Furthermore, the NADH/NAD^+ ratios were not estimated since a defined peak for NAD^+ was absent in the chromatogram of total seed extracts, which would have given further insight in the NAD redox state at imbibition.

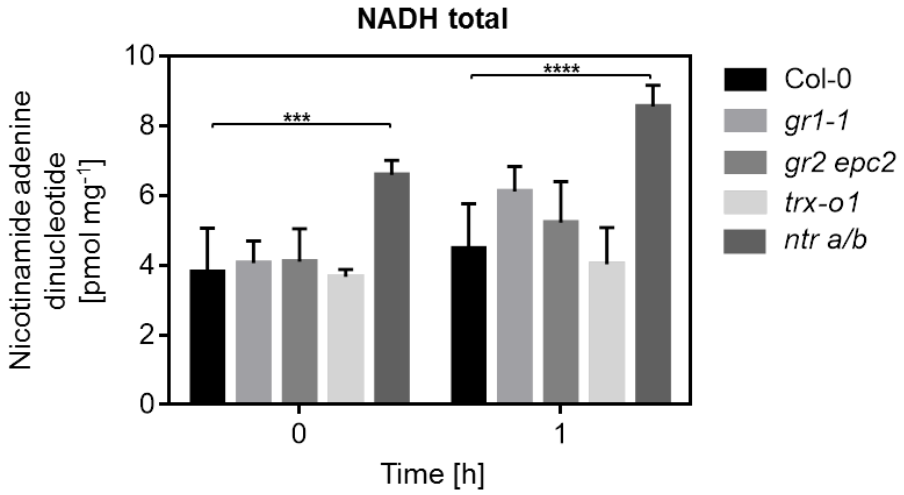

Figure 37: NADH concentration in seeds of Arabidopsis redox mutants. NADH concentration in extracts of seeds before (0 h) and after 1 h imbibition with water were determined by HPLC (average +SD, *n* = 4, seeds of two individuals were pooled; two-way ANOVA and Bonferroni`s multiple comparison test, ***p<0.001, ****p<0.0001). Col-0 values are the same as in **Figure 13 b**. Measurements were performed by the group of Prof. Hell.

2.4.3 TCA cycle associated intermediates dynamics are altered in in imbibed seeds of the redox mutants

The consistent respiration phenotype of the redox mutants during early seed germination without clear alterations in associated central redox metabolites suggests effective compensation, *e.g.* by increased flux rates through primary metabolism. While the measurements of metabolic fluxes is technically challenging, changes in flux are likely to generate imbalances in the metabolic network resulting in changed metabolic pool sizes also at steady-state. Therefore different organic acids of the TCA cycle and associated metabolic pathways were measured by GC-MS. Dry and imbibed seeds of all redox mutants were analysed.

In dry seeds malate was identified with highest quantities in all lines (**Figure 38 a**). The amounts were significantly increased in *gr1*, *gr2* and *trx-o1*, while in the *ntr a/b* mutant malate was slightly decreased. All other measured organic acids were not significantly altered when compared with the wildtype control, with the exception of citrate/isocitrate which were consistently absent in all dry seed samples. In imbibed seeds the amount of malate was significantly decreased in *gr2* background and was increased in the *ntr a/b* mutant (**Figure 38 b**). Even though absolute quantities of other metabolites were changed in response to imbibition, their amounts were not altered in the different redox mutants, except for citrate/isocitrate. Citrate/isocitrate was strongly increased in imbibed seeds of the wildtype, but amounts in all redox mutants were lower (**Figure 38 b**). This observation suggests that fluxes through primary metabolism, involved in the rapid accumulation of citrate/isocitrate at imbibition, are altered in redox-mutants. Changes in the fluxes to and from the pools of the unchanged steady-state metabolite levels remain possible and cannot be ruled out.

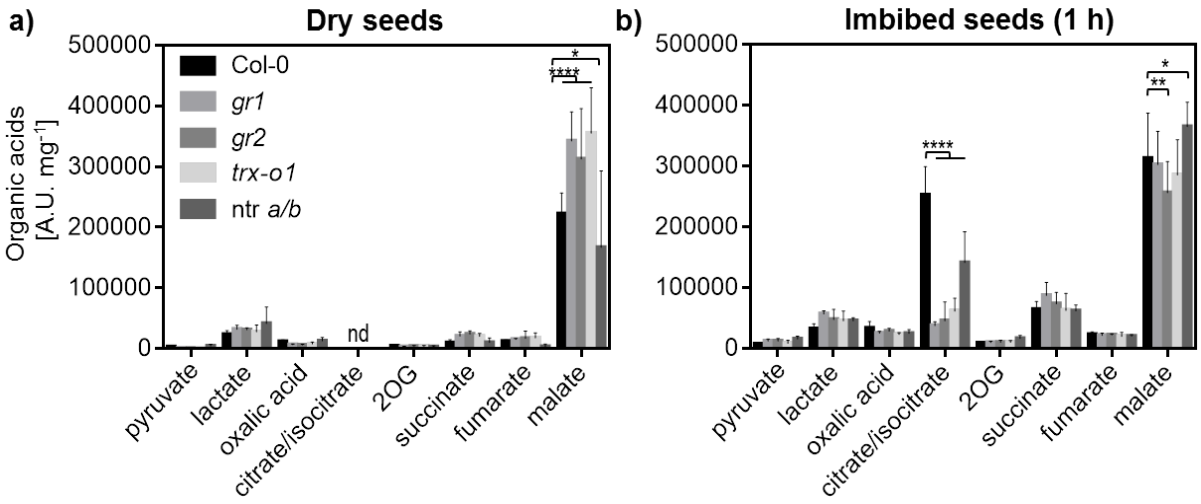

Figure 38: TCA cycle intermediates and associated organic acids in seeds of Arabidopsis redox mutants. Organic acids of total seed extracts were analysed by GC-MS (average +SD, *n* = 4, *p<0.05, ***p<0.001, ****p<0.0001; with two-way ANOVA and Bonferroni`s multiple comparison test). Seeds were either directly analysed before a), or after 1 h imbibition with water b). Col-0 values are the same as those shown in **Figure 14 b**. Water used for imbibition of seeds was measured as individual samples and values for individual organic acids were subsequently added to obtained values for the seeds to compensate for losses during imbibition based on the hydrophilic characteristics of organic acids. Measurements were performed by the group of Prof. Hell.

2.4.4 The amino acid fingerprint is altered in seeds of the redox mutants

In addition to energy metabolism-related enzymes identified as redox-switched when the mitochondrial redox machinery is restarted, also several enzymes participating in amino acid metabolism were identified as redox-switched. This raises the hypothesis that the amino acid metabolism may be impaired in seeds of the redox mutants at imbibition. Therefore the free amino acid composition was analysed in dry seeds of the redox mutants and after 1 h of imbibition (**Figure 39**).

The overall distribution of relative amino acid abundances in wildtype seeds was also observed for the redox mutants. Quantities of relatively low abundant amino acids (**Figure 39 a** and **c** and **Figure 20**) were not altered, neither in dry seeds nor in response to 1 h imbibition. However, specific high abundance amino acids showed differences between the wildtype control and the redox mutants in dry and imbibed seeds (**Figure 39 b** and **d**). In dry seeds concentration of glutamic acid (Glu) and asparagine (Asn) differed significantly in the *gr1* and *ntr a/b* lines. All other amino acids were unaffected in their concentration. The Glu concentration was also significantly increased in imbibed seeds of *gr1*, *gr2* and *ntr a/b* mutants. The Asn concentration was elevated in imbibed seeds of *gr1* and *gr2* mutants. Interestingly, proline (Pro) concentration was exclusively increased in imbibed *gr2* seeds.

These data further underpin a potential role for redox regulation of different enzymes involved in the amino acid metabolism. Yet, alterations in specific pools and mutants cannot provide direct evidence for redox regulation of a specific enzyme involved. The observed metabolic phenotypes may be alternatively explained, *e.g.* through unknown pleiotropic effects that impact on the metabolic network and such alterations are often not intuitive.

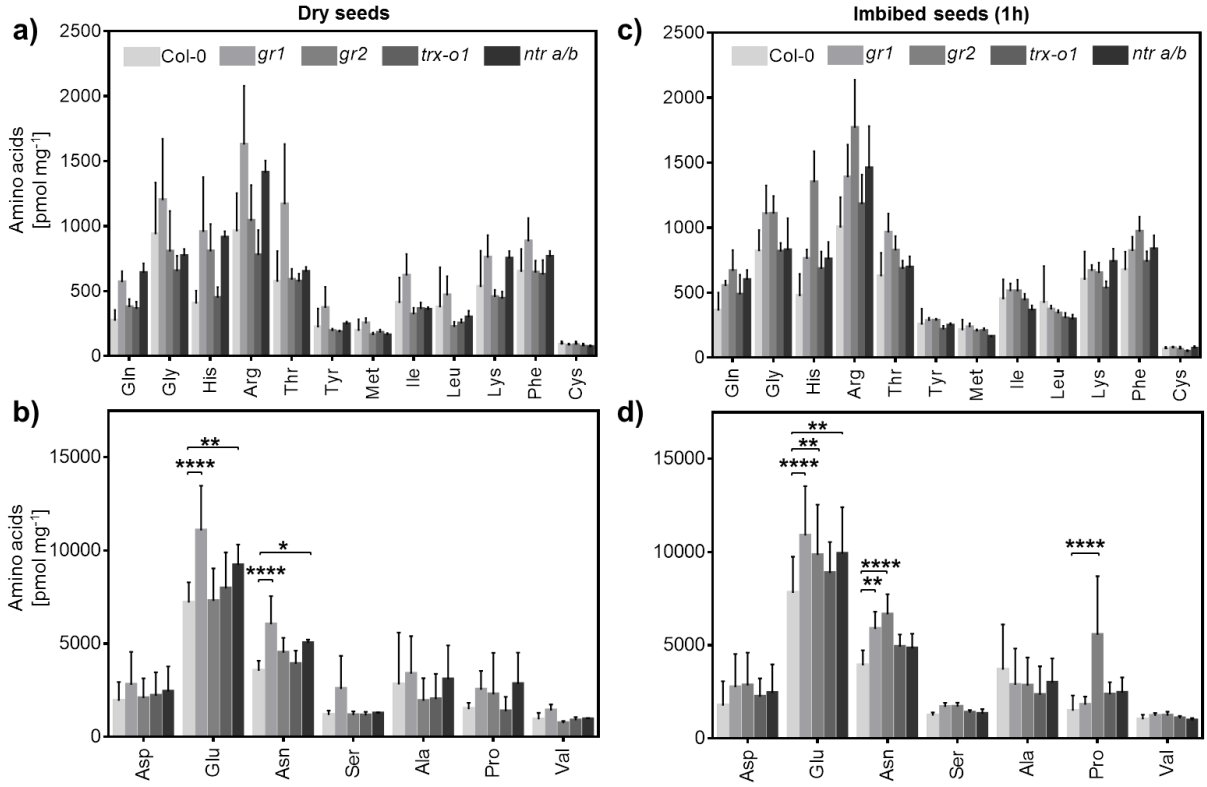

Figure 39: Amino acid pools of Arabidopsis seeds with impaired redox machinery. Free amino acid concentration in total extracts from seeds before a) and b) and after 1 h imbibition c) and d) analysed by HPLC. Low abundance amino acids are shown in a) and c), high abundance amino acids in b) and d) (average +SD, *n* = 4, seeds of two individuals were pooled). Free cysteine was quantified after derivatisation with monobromobimane by independent extraction and analysis. Col-0 values are the same as those shown in **Figure 20**. Significantly different values of the mutants in comparison to the wildtype seeds are indicated by asterisks (two-way ANOVA and Bonferroni`s multiple comparison test, *p<0.05, **p<0.01, ***p<0.001,****p<0.0001). Measurements were performed by the group of Prof. Hell.

Direct evidence for differences in the redox state of individual enzymes in the mutants is necessary to obtain deeper insight into the molecular mechanisms responsible for the observed metabolic phenotypes, *e.g.* changed pool sizes of specific organic acids and amino acids, as well as an overall elevation in respiration rate. The identified enzymes listed in **Figure 31, Figure 32**, **Figure 33** and **Figure 34** only provide hints as to which particular enzymes are redox-switched by the endogenous redox machinery under realistic redox conditions *in organello*, but whether and which of those thiol-switches are indeed differentially operated (and to what extent) in the different redox mutants requires experimental assessment.

2.5 Identification of differentially redox-switched peptides in the mutants of the redox machinery

2.5.1 Investigating mutants of the mitochondrial thioredoxin system to elucidate redox switches involved in germination efficiency

Key-positions of the mitochondrial energy metabolism were identified as targets of redox-switching (**Figure 31** and **Figure 32**). Several redox mutants exhibit respiration-related physiological and metabolic phenotypes (**Figure 35**, **Figure 36**, **Figure 37** and **Figure 38)**. Furthermore, several enzymes involved in the amino acid metabolism were identified as being redox-switched upon restarting the mitochondrial redox machinery (**Figure 33** and **Figure 34**). Mutants showing defects in the redox machinery actually exhibit significant alterations in their amino acid composition (**Figure 39**) with Glu, Asn and Pro contents being increased in different redox mutants. To further corroborate the causal link between the mutants impaired in the mitochondrial redox machinery leading to the germination phenotype, and to investigate the target specificities of the individual players of the mitochondrial redox machinery, the global Cys-peptide redox states in mitochondria of *ntr a/b* and *trx-o1* background were investigated. Targets of the mitochondrial thioredoxin were expected to be more oxidised in both mutants of the mitochondrial thioredoxin-linked redox machinery when compared with the corresponding wildtype controls.

2.5.1.1 Mitochondrial redox machinery is also kick-started in mutants of the thioredoxin-linked redox machinery

The redox proteomic approach to investigate the global Cys-peptide oxidation levels (*2.3*) was applied on isolated mitochondria of the *ntr a/b* and the *trxo1* mutants. The majority of all identified Cys-peptides in both mitochondrial fractions were identified in a partially oxidised state with a characteristic distribution with different median Cys-oxidation values for the quiescent controls and the citrate supplemented mitochondria (**Figure 40**). As already observed in wildtype mitochondria (**Figure 26 a**), citrate triggered a pronounced shift of the global Cys-peptide redox state (**Figure 40 a** and **b**) in both, the *ntr a/b* and the *trx-o1* mutant. In the *trx-o1* mutant, median Cys-oxidation was reduced by 14.4 % from 27.5 % before substrate addition to 13.1 % (**Figure 40 d**). Mitochondria lacking thioredoxin reductase (*ntr a/b*) showed a median Cys-oxidation of 28.5 % and were reduced by 13.1 % to a Cys-peptide oxidation state of 15.4 % (**Figure 40 c**). For wildtype mitochondria, the Cys-peptide oxidation state was reduced from 27.1 % to 13.0 % (**Figure 26**), indicating only a minor increase of the median Cys-oxidation state of the *ntr a/b* mutant, while the Cys-oxidation state of the *trx-o1* mutant was similar to that of the wildtype mitochondria.
In total 911 Cys-peptides were identified for the *ntr a/b* mutant, corresponding to 473 different proteins. 530 Cys-peptides were identified for the *trx-o1* mutant, corresponding to 307 different proteins. For the *ntr a/b* mutant in total 298 Cys-peptides were identified as significantly redox-switched, deriving from 193 different proteins (t-test corrected for multiple comparisons by Benjamini, Krieger & Yekutieli with <2 % FDR). For the *trx-o1* mutant 296 Cys-peptides of 179 proteins were identified as redox-switched. Individual replicates of the *ntr a/b* and the *trx-o1* mutants (

Figure 41 and **Figure 42**) revealed increased heterogeneity of the Cys-peptide oxidation states as compared to wildtype mitochondria (**Figure 27**, **Figure 28** and **Figure 29**). The median Cys-oxidation values between individual replicates differed by up to 10 % in both

mutants, but corresponding control Cys-oxidation values were shifted accordingly, resulting in comparable Δ % Cys-oxidation values for all replicates. The global Cys-oxidation values of the investigated mutants of the thioredoxin-based redox machinery show no obvious differences to those of wildtype mitochondria. Also on the basis of individual Cys-peptides no obvious differences are detectable (see small insets in **Figure 40 a** and **b**). Like in the experiment with wildtype mitochondria, no Cys-peptide with an initial oxidation state of >85 % underwent a redox-shift at substrate addition.

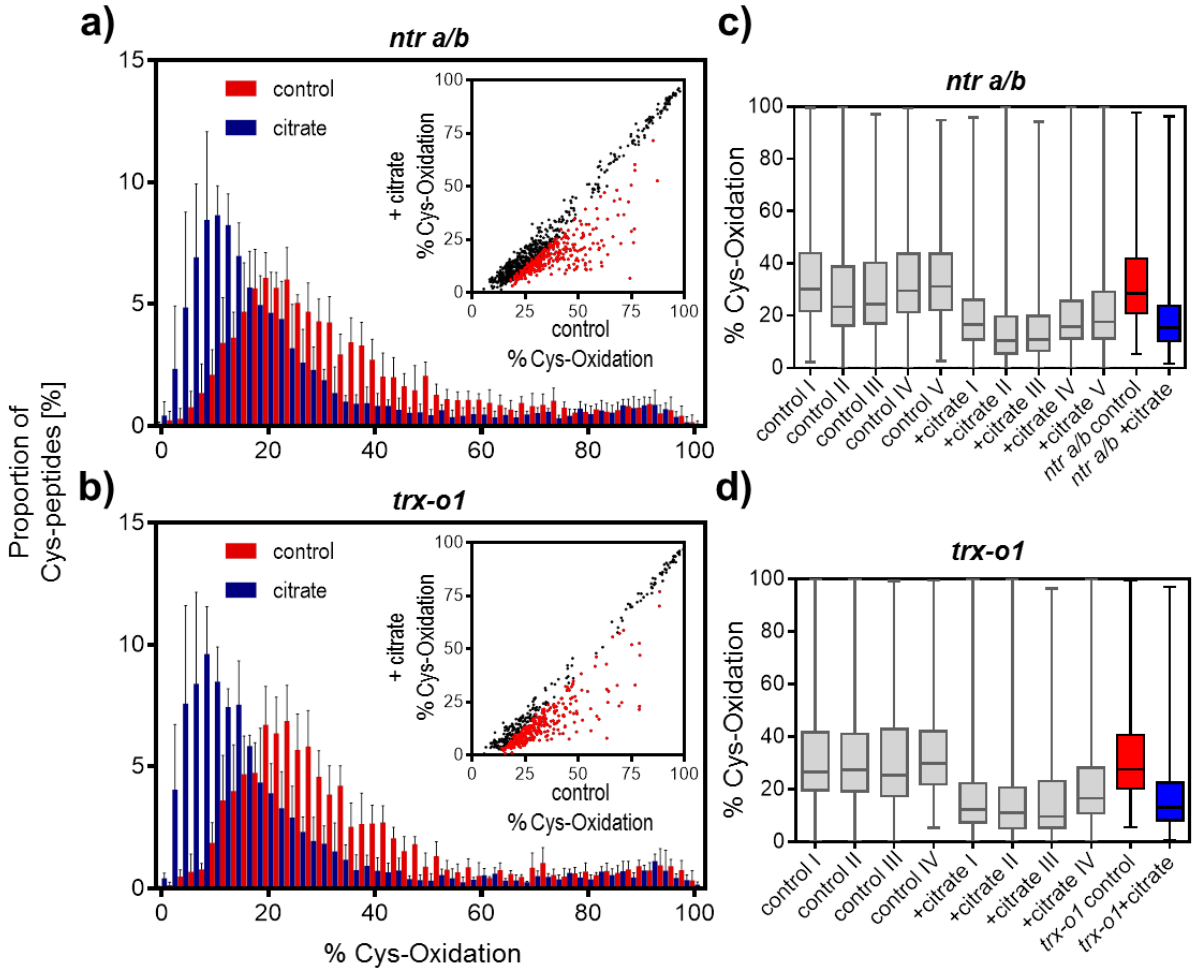

Figure 40: Global peptide redox state distributions of mitochondria from *ntr a/b* and *trx-o1* mutants. Mitochondria from *ntr a/b* a) and c) or *trx-o1* mutants b) and d), were supplemented with citrate for 25 min. Redox states of individual peptides were quantified using a MS/MS-based iodoTMT approach for mitochondria before (red bars) and after citrate addition (blue bars). The distribution of cysteine-peptide redox states are shown as the proportion of the total number of peptides in each 2 % quantile of percentage oxidation (n = 4 - 5, average +SD). In insets, the degree of Cys-oxidation without substrate addition is plotted against the degree of Cys-oxidation after substrate application for individual Cys-peptides. Red dots mark Cys-peptides with significant change in their Cys-oxidation state at substrate addition (t-test corrected for multiple comparisons by Benjamini, Krieger & Yekutieli with <2 % FDR). Box-plots in c) and d) of the Cys-oxidation state (in percent of total oxidation) are given for all individual replicates in grey and for their averages in red and blue.

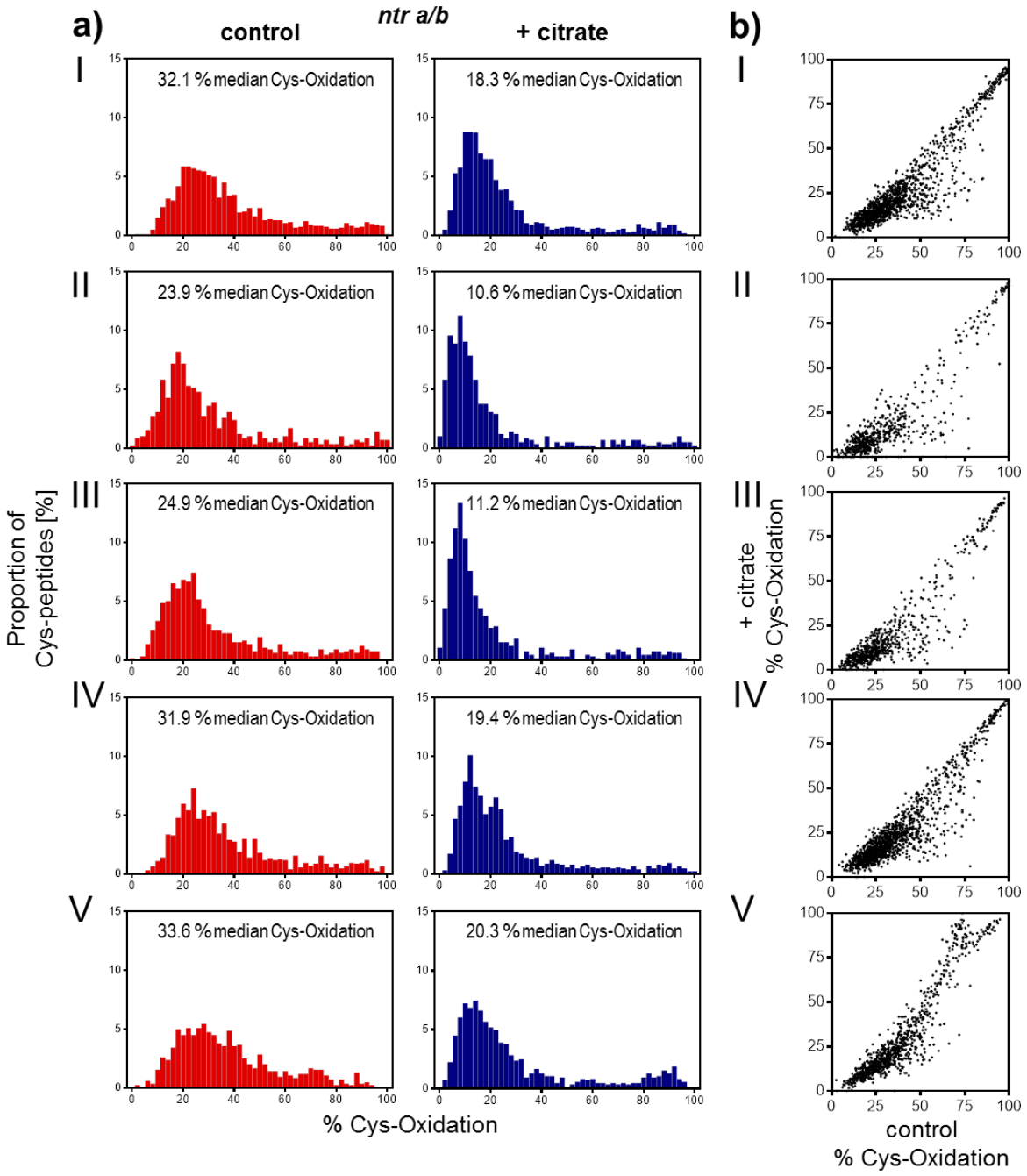

Figure 41: Individual replicates of the iodoTMT-based quantification of the redox states of isolated mitochondria of the *ntr a/b* mutant supplemented with citrate and their corresponding quiescent controls. Mitochondria of Arabidopsis seedlings of *ntr a/b* background were supplemented with 10 mM citrate for 25 min. Percentage of Cys-reduction of individual peptides was quantified using MS/MS-analysis after iodoTMT-based labelling a) for quiescent mitochondria (control, red bars) and after citrate addition (+ citrate, blue bars). The distribution of oxidation-percentage is shown for replicates I, II, III, IV & V; the proportion of the total number of peptides in each 2 % quantile of percentage oxidation is plotted. For all replicates the same data is also shown for individual Cys-peptides in b) by plotting the redox states of individual Cys-peptides at the quiescent state against the redox states after substrate application.

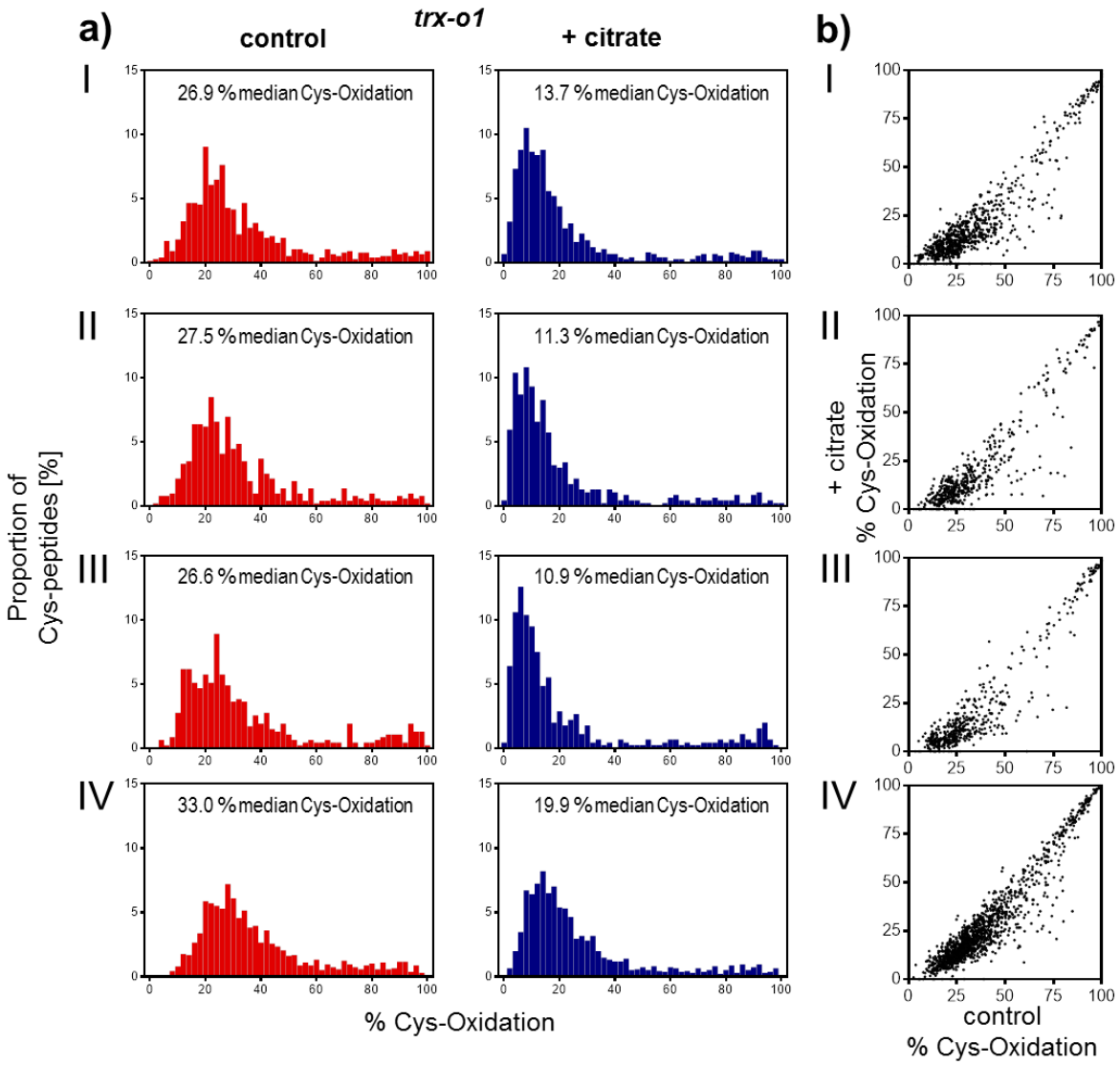

Figure 42: Individual replicates of the iodoTMT-based quantification of the redox states of isolated mitochondria of the *trx-o1* mutant supplemented with citrate and their corresponding quiescent controls. Mitochondria of Arabidopsis seedlings of *trx-o1* background were supplemented with 10 mM citrate for 25 min. Percentage of Cys-reduction of individual peptides was quantified using MS/MS-analysis after iodoTMT-based labelling a) for quiescent mitochondria (control, red bars) and after citrate addition (+ citrate, blue bars). The distribution of oxidation-percentage is shown for replicates I, II, III, & IV; the proportion of the total number of peptides in each 2 % quantile of percentage oxidation is plotted. For all replicates the same data is also shown for individual Cys-peptides in b) by plotting the redox states of individual Cys-peptides at the quiescent state against the redox states after substrate application.

While in wildtype mitochondria the three most reduced Cys-peptides were assigned to the GR2, the NTR a/b and TRX-o1, in the *ntr a/b* mutant no Cys-peptide was identified for the NTR a/b, confirming the absence of the protein. Surprisingly, a unique Cys-peptide of the mitochondrial TRX-o1 was identified as significantly redox-switched in mitochondria from the *trx-o1* line. While in isolated wildtype mitochondria up to eight unique peptides for the TRX-o1 protein (AT2G35010) were identified by MS analysis (including seven non-Cys-peptides), in the *trx-o1* background only a single peptide containing the catalytic CxxC motif was identified. The accumulated TMT reporter intensities of the first and the second label for this particular redox-switched Cys-peptide were decreased by factor four in mitochondria from the *trx-o1* line (**Figure 43 a**). In *ntr a/b* background not a single Cys-peptide of the

NTR a/b was identified, while this peptide was identified in all other experiments and its corresponding TMT reporter intensities were constant (**Figure 43 b**). The reporter ion intensity of specific Cys-peptides can only be considered as a crude estimate of the protein abundance, since Cys-peptides were enriched by antibodies during sample processing. However, these data suggest that the *ntr a/b* mutant is a true knock-out whereas in the *trx-o1* mutants still a potential truncated version of the Trx-o1 gene-product including the active-site motive can be identified. This is in contrast to a previous report in which this mutant was reported as a knockout (DALOSO *ET AL.,* 2015).
It appears remarkable that mutants impaired at key-positions of the mitochondrial redox machinery do not show severe alterations of the global Cys-peptide oxidation states. This suggests functional redundancy of the different redox machineries, which has been suggested for plant redox systems previously (REICHHELD *ET AL.,* 2007; MARTY *ET AL.,* 2009).

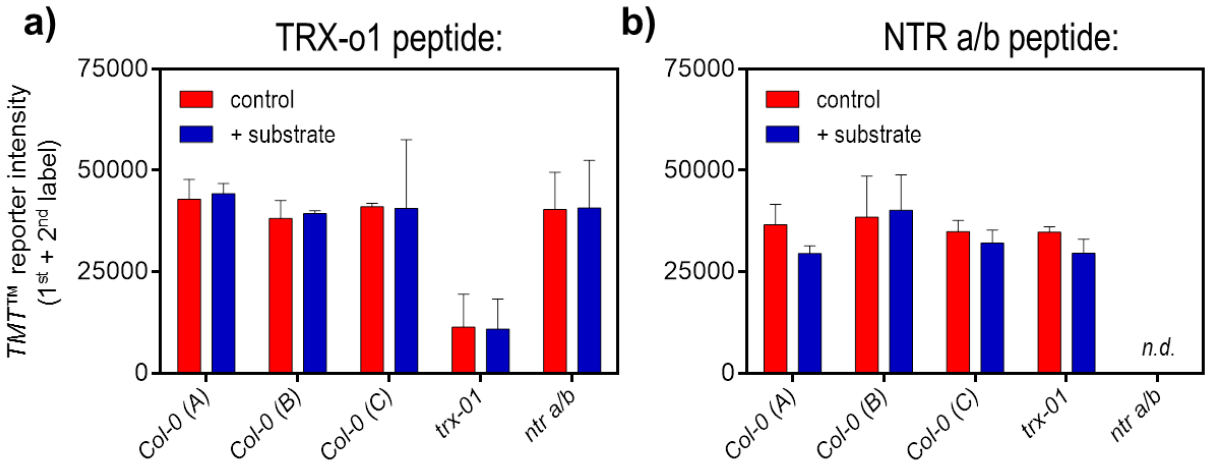

Figure 43: TMT reporter intensities of the THIOREDOXIN-o1- and NADP-dependent THIOREDOXIN REDUCTASE a/b-derived Cys-peptides identified in mitochondria of wildtype, *ntr a/b* and *trx-o1* mutant backgrounds. For the unique THIOREDOXIN-o1 (AT2G35010) -derived Cys-peptide, identified with the sequence AQDGSLPSVFYFTAAWCGPCR, corresponding TMT reporter intensities are given, a) for wildtype mitochondria of the individual experiments (A: with citrate; B: with 2OG; C: with succinate) and for mitochondria of the *trx-o1* and *ntr a/b* lines with citrate as metabolic substrate. Reporter intensities of the 1st and the 2nd label were added up as estimate of total peptide abundance. For the non-unique NADP-dependent THIOREDOXIN REDUCTASE a/b (AT2G17420, AT4G35460) -derived Cys-peptide, identified with the sequence GISACAVCDGAAPIFR, corresponding TMT reporter intensities are given in b). *n.d.* = not detectable.

2.5.1.2 Identification of individual Cys-peptides with altered Cys-oxidation state in mutants impaired in the mitochondrial thioredoxin system

To identify individual Cys-peptides altered in Cys redox state, corresponding values were compared to those of wildtype mitochondria in the same functional state, *i.e.* quiescent or supplemented with citrate. In a direct comparison of the global Cys-peptide redox profiles, no differences are obvious, indicated by almost perfect overlap of the histograms (**Figure 44**). Of the in total 911 Cys-peptides identified for the *ntr a/b* mutant, 633 Cys-peptides were also identified in the wildtype control, allowing to directly compare corresponding Cys-peptide redox states. For the 530 Cys-peptides identified for the *trx-o1* mutant 390 peptides were also identified in the wildtype control. A plot of the redox states of individual Cys-peptides in

wildtype background against the corresponding values of both redox mutants (*ntr a/b*: a) and c); *trx-o1*: b) and d)) reveals clear differences at the level of individual Cys-peptides (**Figure 44**, insets, red dots). In both states, quiescent and citrate supplemented mitochondria, several Cys-peptides differed significantly (t-test corrected for multiple comparisons by Benjamini, Krieger & Yekutieli with <2 % FDR). Interestingly, not all differentially reduced Cys-peptides showed increased Cys-oxidation values in the mutants, but several Cys-peptides also showed a reductive shift (see insets in **Figure 44**, red dots below the diagonal). This appears counterintuitive since the redox mutants may be expected to be impaired in reducing their target cysteines.

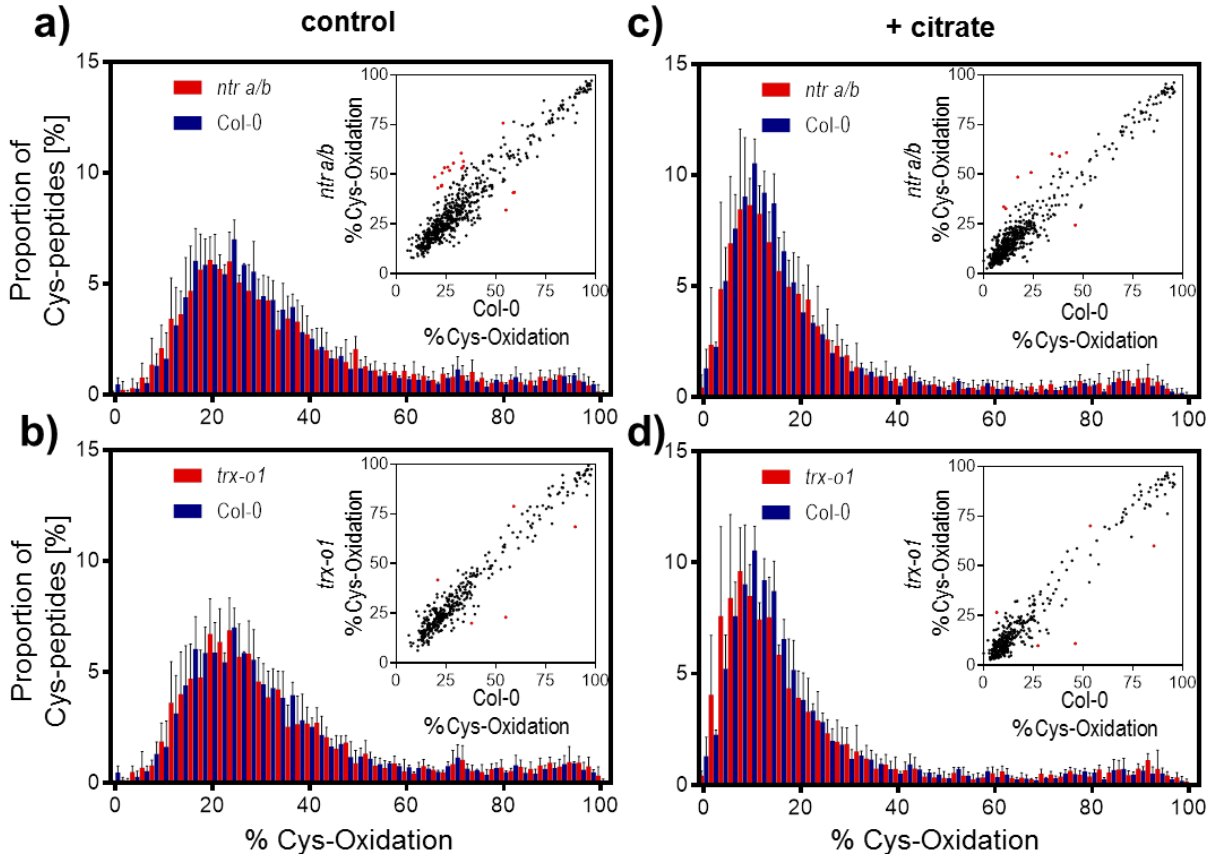

Figure 44: Differences in peptide redox states of mitochondria from *ntr a/b* and *trx-o1* mutants compared with wildtype mitochondria. Mitochondria from *ntr a/b* a) and c) (red bars) or *trx-o1* mutants b) and d) (red bars), were supplemented with citrate for 25 min. Redox states of individual peptides were quantified using a MS/MS-based iodoTMT approach for mitochondria before a) and b) and after citrate addition c) and d) and are compared with wildtype mitochondria (blue bars). The distribution of cysteine-peptide redox states are shown as the proportion of the total number of peptides in each 2 % quantile of percentage oxidation (n = 3 - 5, average +SD, data for wildtype mitochondria are the same as those in **Figure 26 a**). In insets, the degree of Cys-oxidation of the wildtype control is plotted against the degree of Cys-oxidation in the mutants for individual Cys-peptides. Red dots mark Cys-peptides with significant change in their Cys redox state between wildtype control and mutants (t-test corrected for multiple comparisons by Benjamini, Krieger & Yekutieli with <2 % FDR).

To visualise Cys-peptides with common changes in redox state under both metabolic conditions, the number of individual Cys-peptides with a significantly changed redox state were plotted for both mutants in a Venn-diagram (**Figure 45 a** for the *ntr a/b* mutant and **b** for the *trx-o1* mutant). In the *ntr a/b* mutant 17 unique Cys-peptides were significantly changed in their redox state compared to wildtype mitochondria under quiescence. Eight unique

Cys-peptides showed a different redox state in the *ntr a/b* background after citrate addition; five Cys-peptides (**Figure 45 a**, *overlapping*) were consistently changed in their Cys redox state in both metabolic conditions and are listed in **Tab. 3**.
In the *trx-o1* mutant only six peptides were identified with a significantly different Cys redox state as compared with the corresponding oxidation state of peptides in Col-0 mitochondria. In quiescent mitochondria five peptides were identified with significantly changed Cys-peptide redox state. In mitochondria supplemented with citrate, four of these peptides were also identified consistently (**Figure 45 b**); furthermore one Cys-peptide was identified as significantly redox-switched only in the *trx-o1* background after citrate addition, but not in the quiescent state.
Of the five identified Cys-peptides, that were consistently redox-shifted in the *ntr a/b* mutant (**Figure 45 a** and **Tab. 3**), two Cys-peptides were initially identified as not redox-switched in wildtype mitochondria (**Figure 26**), namely a peptide of the 30S ribosomal protein S13 and a peptide of the dihydrolipoyllysine-residue acetyltransferase component 2. One of the three remaining differentially redox-switched Cys-peptides, the NADP-dependent malic enzyme 4, is generally considered localising to the plastids and not the mitochondria (TRONCONI *ET AL.,* 2010). The Cys-peptide of the 2-oxoglutarate dehydrogenase E1 component is more oxidised in the *ntr a/b* mutant in both metabolic states than in the wildtype fractions, with an oxidative shift of 23 % in quiescent mitochondria and of 32 % after citrate addition. Also a peptide of the mitochondrial succinate-semialdehyde dehydrogenase showed significantly increased Cys-oxidation levels in the *ntr a/b* mutant, shifted by about 22 % at both metabolic states. Thus two proteins with annotated functions related to the TCA cycle were identified as differentially redox-switched in the *ntr a/b* mutant as compared to the wildtype.
Of the three peptides only identified with differentially redox-switched in the *ntr a/b* background after citrate application and not in the quiescent state, the corresponding proteins of two peptides were annotated to other compartments than the mitochondrion, the `Probable glutathione peroxidase 2` and the `Tubulin alpha-5 chain`, with the latter one also not identified as redox-switched in wildtype mitochondria (*2.3.2*). The third peptide can be uniquely assigned to the TRX-o2 and shows an increase of the Cys redox state from 34.4 % in wildtype mitochondria to 60.4 % in the ntr a/b mutant. This is in agreement with an impaired reduction of the thioredoxin system in the *ntr a/b* background, yet TRX-o1 shows no significant oxidative shift. This is counterintuitive, but it may suggest an efficient crosstalk of TRX- o1 with other redox machineries (*e.g.* REICHHELD *ET AL.,* 2007; MARTY *ET AL.,* 2009), but this crosstalk may not compensate for the oxidation of TRX- o2 in the *ntr a/b* background.

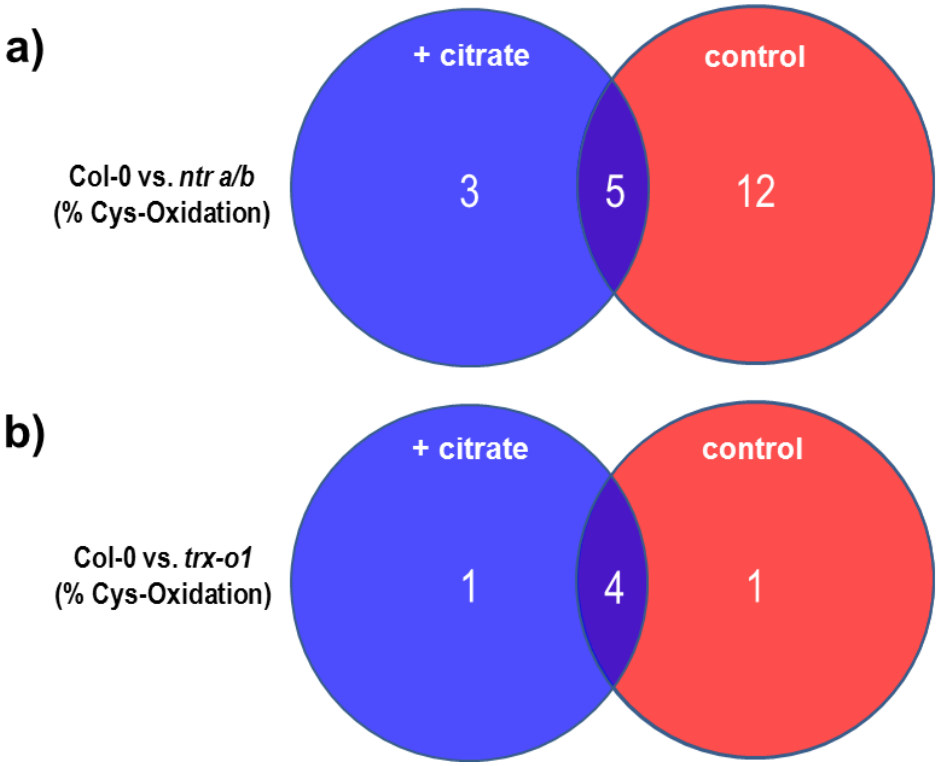

Figure 45: Significant redox-switched Cys-peptides in mitochondria of the *ntr a/b* and *trx-o1* mutants in different metabolic states. Venn-diagram shows the number of peptides differing significantly in their corresponding Cys-oxidation values in mitochondria of *ntr a/b* background (a) or of *trx-o1* background (b) when compared with corresponding Cys-oxidation states of the wildtype. Different peptides in the blue circle were identified after citrate addition (+ citrate), and in the red circle under quiescence without citrate addition (control) in the respective mutants.

Tab. 3: Cys-peptides in isolated mitochondria of the *ntr a/b* mutant with significantly different redox states. Peptides of the *ntr a/b* mutant, consistently changed in their Cys redox state when compared with the corresponding wildtype, are shown (peptides identified in **Figure 45 a,** overlapping Cys-peptides).

AA sequence	identifier	name
VPQ**C**NSSWTDEYIR	AT3G13930	Dihydrolipoyllysine-residue acetyltransferase component 2 of pyruvate dehydrogenase complex
LEQAY**C**GTIGYEYMHIADR	AT5G65750	2-oxoglutarate dehydrogenase, E1 component
HIQGLP**C**R	AT5G14320	30S ribosomal protein S13
ELEQ**C**AESSMYSPSYR	AT1G79750	NADP-dependent malic enzyme 4
VNNPATGEIIADVA**C**MGTK	AT1G79440	Succinate-semialdehyde dehydrogenase

Of the four identified Cys-peptides that were consistently identified showing a significant changed Cys redox state in the *trx-o1* mutant, when compared with the wildtype control (**Figure 45 b** and **Tab. 4**), only a single peptide, deriving from the cytochrome *c* oxidase subunit 5b-2, was initially identified as being redox-switched at citrate addition in wildtype mitochondria. Cys-oxidation values for the corresponding peptide of the cytochrome *c* oxidase subunit 5b-2 in quiescent mitochondria and in citrate supplemented mitochondria were both increased by about 20 %. The other three identified peptides were not significantly redox-switched in wildtype mitochondrial background. The one peptide solely identified redox-shifted in the citrate supplemented mitochondria of the *trx-o1* background and not in the quiescent state, is annotated as a plastidic `Dihydrolipoyl dehydrogenase 1` and its redox state in wildtype mitochondria was 53.7 % and 70.2 % in the *trx-o1* background.

Tab. 4: Cys-peptides in isolated mitochondria of the *trx-o1* mutant with significantly different redox states. Peptides of the *trx-o1* mutant, which are consistently changed in their Cys redox state when compared with the corresponding wildtype, are shown (peptides identified in **Figure 45 b,** overlapping Cys-peptides).

AA sequence	identifier	name
SL**C**PSEWVDR	AT1G22450	Cytochrome c oxidase subunit 6b-1 (AtCOX6b-1)
VPQ**C**NSSWTDEYIR	AT3G13930	Dihydrolipoyllysine-residue acetyltransferase component 2 of pyruvate dehydrogenase complex
CSDAHAIADAASK	AT4G33010	Glycine dehydrogenase [decarboxylating] 2
IVG**C**PGGEGEDEHDVVWFWLEK	AT1G80230	Cytochrome c oxidase subunit 5b-2, mitochondrial (AtCOX5b-2)

Summarising these observations made for both mutants of the mitochondrial thioredoxin-linked redox machinery, only a very small subset of redox-switched Cys-peptides in wildtype mitochondria was identified with significant altered Cys-oxidation states in mitochondria of the *trx-o1* or *ntr a/b* background. This may suggest that compensatory mechanisms can counteract the effect of impairments in the thioredoxin system and the observed phenotypes may be explained by these few alterations of a small subset of redox-shifted proteins. The list of identified redox-shifted Cys-peptides must be considered as incomplete and further differentially redox-switched Cys-peptides are likely to be lost due to technical limitations of the approach. Alternatively the sensitivity and reproducibility of the applied system may be too low to identify smaller, quantitative changes in redox-switched Cys-peptides, which may be of biological significance. Furthermore the biological relevance of the mitochondrial substrate application assay may be scrutinised, as it only recreates specific features of seed imbibition.

2.5.2 Investigating mutants of the mitochondrial glutathione-linked system to elucidate redox switches involved in germination efficiency

By restarting mitochondrial energy metabolism and endogenous NADPH production in the mitochondrial matrix as a result, both mitochondrial redox machineries are supplied with reductant (model in **Figure 21 c** or **Figure 24** and data in **Figure 25 a** and **Figure 26**). To dissect the interplay of both mitochondrial redox machineries, the thioredoxin-linked and the glutathione/glutaredoxin-linked systems, and to investigate their potential target specificities, also mutants of the mitochondrial GR2 (*gr2*) were investigated in the mitochondrial feeding assay. *Arabidopsis thaliana* mutants of the only known mitochondrial localised glutaredoxin GRXS15 have been found as embryo-lethal (MOSELER *ET AL.,* 2015) and were therefore not considered in our analysis due to lack of viable plants and, thus, material for mitochondria isolations. Moreover, mitochondrial GRXS15 was described to play a role in iron-sulfur cluster biogenesis, while its oxidoreductase activity was negligible (MOSELER *ET AL.,* 2015; STRÖHER *ET AL.,* 2016). Targets of the mitochondrial glutathione-linked redox machinery were expected to be more oxidised in the *gr2* mutant, although partial functional redundancy with or backup by the thioredoxin system appeared possible.

2.5.2.1 Mitochondrial glutathione redox state is partially reestablished in a mutant impaired in the mitochondrial glutathione reductase

The glutathione redox state in isolated mitochondria of the *gr2* background was assessed in response to substrate addition using matrix-localised roGFP2-Grx1 (**Figure 46**). However, reconstitution of the functional redox machinery in *gr2* background by application of the substrates succinate or citrate, both triggered reduction of the roGFP2-Grx1 sensor. Citrate triggered a higher reduction of the E_{GSH} biosensor than succinate application, indicating that the established E_{GSH} was supposed to be more negative. The redox state of the roGFP2-Grx1 sensor was indistinguishable in the wildtype and in the *gr2* background when supplied with citrate. This raises the hypothesis that not just the redox state of the artificial read-out, the roGFP2-Grx1, is unaltered in the mitochondria of *gr2* lines supplied with citrate, but also of *in situ* target proteins of the glutathione system. Therefore succinate application was used for the redox proteomics approach in *gr2* mitochondria, as here an oxidative shift was already observed for the artificial read-out roGFP2-Grx1.

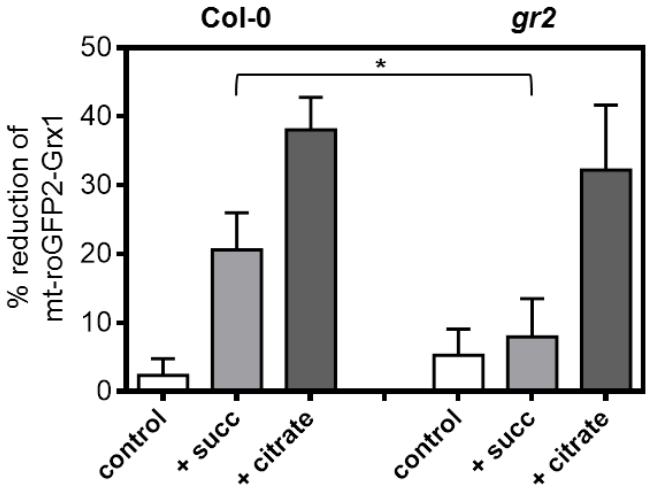

Figure 46: Mitochondrial glutathione redox state in *gr2* mutants. The glutathione redox state in isolated mitochondria of wildtype (Col-0) and *glutathione reductase 2* mutant (*gr2*) was analysed using

matrix localised roGFP2-Grx1 sensor by platereader-based assays (excitation at 400 ± 5 nm and 482 ± 8 nm; emission at 530 ± 20 nm for both excitation wavelengths). The roGFP2-Grx1 reduction after supplementation of different substrates for 25 min are shown (*n* = 3, average +SD, full sensor oxidation by addition of 5 mM DPS; full sensor reduction by addition of 20 mM DTT); *p<0.05 with two-tailed, unpaired Student`s t-test.

The majority of all identified Cys-peptides in isolated mitochondria of *gr2* background were identified in a partially oxidised state showing the characteristic distribution with different median Cys-oxidation values for the quiescent controls and for succinate addition (**Figure 47 a**). As already observed for the wildtype mitochondria (**Figure 26 c**), succinate application triggered a pronounced shift of the global distribution of Cys-peptide redox states (**Figure 47 a**). The median Cys-oxidation was reduced by 14.7 % from 31.9 % before succinate application to 17.2 % after (**Figure 47 c**), whereas the global distribution of redox states was shifted from 26.7 % to a median Cys-oxidation of 12 % in wildtype mitochondria (**Figure 29 c**). Half of all identified Cys-peptides in quiescent mitochondria show a Cys-oxidation between 24.6 % and 47.1 %; whereas half of the Cys-peptides in succinate supplemented mitochondria show a Cys-oxidation value between 11.6 % and 27.7 %. Yet for mitochondria supplemented with succinate only preliminary data are available (*n* = 1). In total 933 Cys-peptides were identified in mitochondria of the *gr2* mutant. Those peptides derived from 475 different proteins. Of the 933 peptides 780 peptides contained a single cysteine residue, 143 peptides two cysteines, nine peptides three cysteines and one peptide four cysteines. The quantified Cys-oxidation levels for the peptides containing more than one cysteine therefore represent the average of all cysteines in that particular peptide. The histograms and the box-plots of the individual replicates reveal that the global cysteine-oxidation values are well reproducible. In isolated mitochondria of the *gr2* background the catalytic Cys-peptide of the mitochondrial GLUTATHIONE REDUCTASE 2 was absent, whereas the peptide and the corresponding TMTs were detectable in all other experiments (**Figure 48**).

As observed for wildtype mitochondria, Cys-peptides with a Cys-oxidation of >85 % were coming from proteins located in the inter membrane space, *e.g*. several TIM-proteins (TIM 8, 9, 10 & 13), two different adenylate kinases (AK 1 & 3), but also of different proteins involved in the reduction/oxidation of cytochrome *c* (*e.g*. Ubiquinol-cytochrome *c* reductase hinge protein or cytochrome *c* oxidase subunit 6b-3). Although more definitive statements cannot be made because of missing replicates for the succinate supplemented *gr2* mitochondria, the available replicate suggests that none of these initially highly oxidised Cys-peptides are significantly reduced in response to succinate application. However, the plot of the individual Cys redox states under control conditions against the Cys-oxidation states after succinate addition shows again an overall shifted diagonal distribution with hardly any Cys-peptide showing an even slight increase of the Cys-oxidation state. This again indicates a degree of non-specific global reduction across all Cys-peptides, similar to what was observed in wildtype mitochondria.

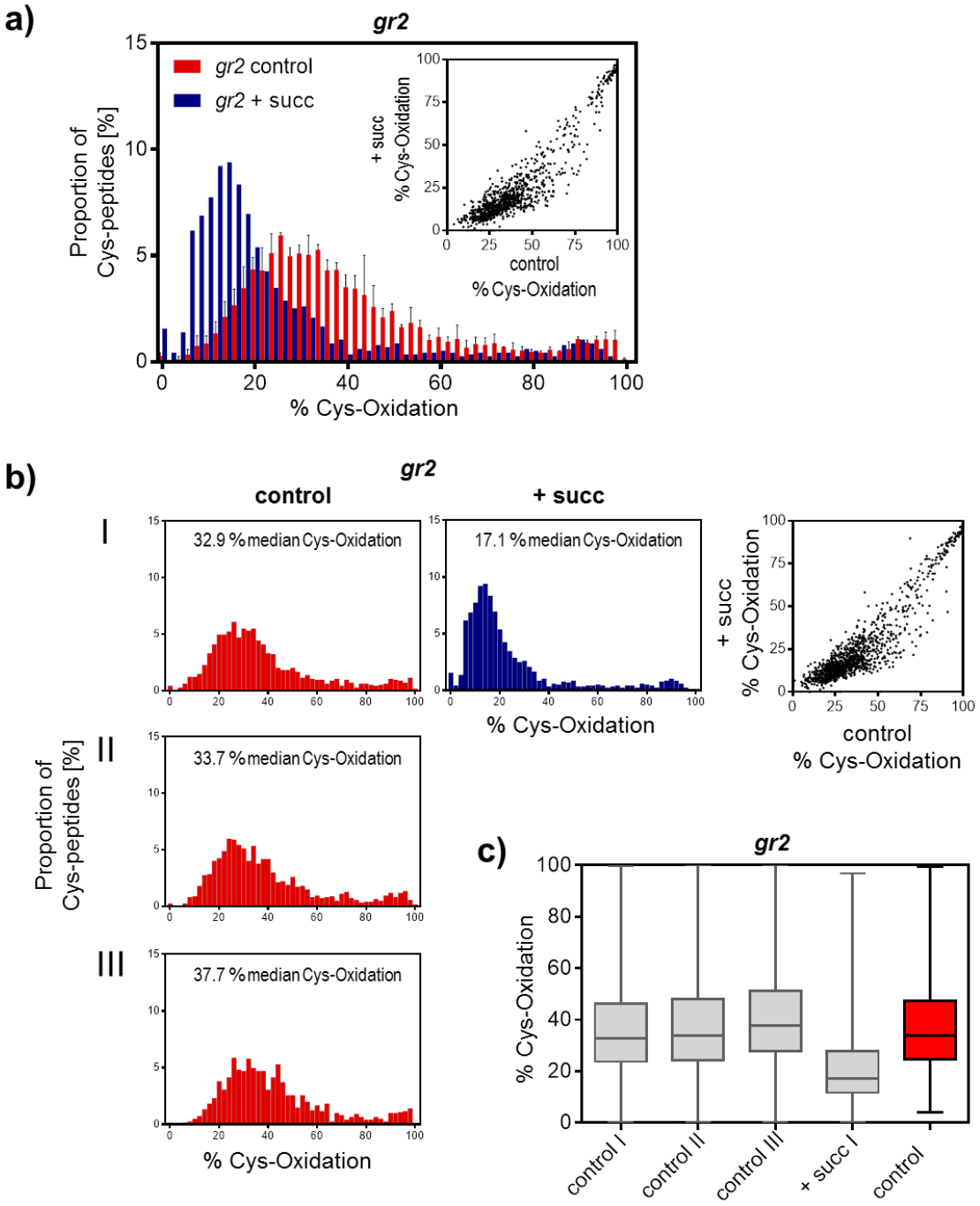

Figure 47: Global distribution of Cys-peptide redox states of mitochondria from *gr2* mutants. Isolated mitochondria from a *gr2* line a) were supplemented with succinate for 25 min. Redox states of individual peptides were quantified with MS/MS-based iodoTMT approach for quiescent mitochondria (red bars) and after succinate addition (blue bars). The global distribution of cysteine-peptide redox states are shown as the proportion of the total number of peptides in each 2 % quantile of percentage oxidation (n = 3 for mitochondria without succinate addition, average +SD; preliminary data with n = 1 for mitochondria supplemented with succinate). In the inset, the degree of Cys-oxidation without succinate application is plotted against the degree of Cys-oxidation after succinate application for individual Cys-peptides. In b) the global distribution of cysteine-peptide redox states are shown as the proportion of the total number of peptides in each 2 % quantile of percentage oxidation for the individual replicates. For replicate I the degree of Cys-oxidation of quiescent mitochondria is plotted against the degree of Cys-oxidation after succinate addition for individual Cys-peptides. Box-plots in c) of the Cys-oxidation state (in percent of total oxidation) are given for all individual replicates in grey and for the average of the quiescent control in red.

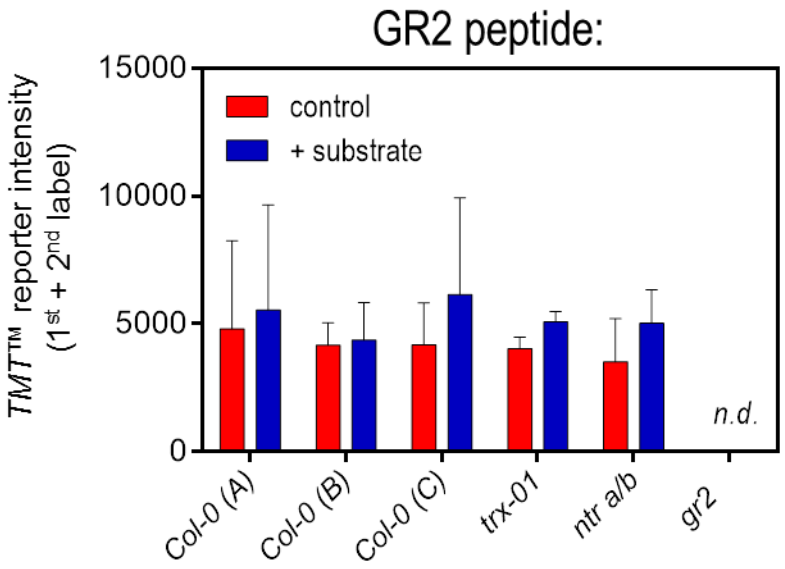

Figure 48: TMT reporter intensities of the GLUTATHIONE REDUCTASE 2-derived Cys-peptides identified in wildtype mitochondria and *gr2*-mutant background. For the unique GLUTATHIONE REDUCTASE (AT3G54660) -derived Cys-peptide, identified with the sequence FATSFGASAAVCELPFSTISSDTAGGVGGTCVLR, corresponding TMT reporter intensities are given for wildtype mitochondria of the individual experiments (A: with citrate; B: with 2OG; C: with succinate) and for mitochondria with *trx-o1*, *ntr a/b* and *gr2* background. Reporter intensities of the 1st and the 2nd label were added up as estimate of the total peptide-abundance. *n.d.* = not detectable.

2.5.2.2 Identification of individual Cys-peptides with altered Cys redox state in mitochondria lacking GLUTATHIONE REDUCTASE 2

To identify individual Cys-peptides, which are altered in their Cys-oxidation state in *gr2*, corresponding values were compared to those of wildtype mitochondria in the same energetic state. In a direct comparison of the global Cys-peptide oxidation state of wildtype mitochondria with those of the *gr2* mutant, a shift towards a more oxidised median Cys-oxidation can be observed (**Figure 49**). The median Cys-oxidation was shifted from 26.7 % in wildtype mitochondria (**Figure 29 c)** to 31.9 % in the *gr2* mutant (**Figure 47 c**). Of all 933 Cys-peptides identified in the *gr2* mutant, 633 were also identified in the wildtype mitochondria, allowing a direct comparison of the corresponding Cys redox states at the individual peptide level. 77 Cys-peptides were identified with significant differences in their redox states (n = 3 in both genomic backgrounds with t-test corrected for multiple comparisons by Benjamini, Krieger & Yekutieli and FDR < 2 %). Interestingly six of these peptides were significantly more reduced as compared to the wildtype mitochondria (**Tab. 5**). One of these peptides is the catalytic peptide of the NTR a/b, which shows an average Cys-oxidation of 76.5 % in the wildtype mitochondria and of only 61.1 % in the *gr2* mutant background. Only two of these six peptides were initially identified as redox-switched in the wildtype mitochondria in response to citrate application (**Figure 26 a**). Among the 71 peptides showing significantly increased Cys-oxidation in comparison to wildtype mitochondria, three peptides of the roGFP2-Grx1 were identified. Their increased oxidation is in agreement with the observations obtained by optical read-out of the sensor redox state, which was more oxidised at succinate addition in the *gr2* mitochondria (**Figure 46** and MARTY *ET AL.*, in preparation). The mitochondrial GRXS15 shows also an increased Cys-oxidation value in the

gr2 background, as well as different other proteins involved in the iron-sulfur cluster biogenesis, *e.g.* `protein BOLA4`, `NifU-like protein 5` or `Iron-sulfur cluster assembly protein 1`. Two enzymes of the mitochondrial TCA cycle were also identified as redox-shifted towards oxidation in the *gr2* background, the `malic enzyme 1` and different Cys-peptides of the `Pyruvate dehydrogenase`. The altered Cys-oxidation values of these enzymes may be caused by increased glutathionylation in the *gr2* background, as a consequence of a less reduced glutathione pool. However, crosstalk with other redox machineries or functional redundancy is likely to be not as efficient in the *gr2* line as in the *ntr a/b* and the *trx-o1* mutants, reasoned by several Cys-peptides showing alterations in their Cys-oxidation level, whereas only very few proteins were identified redox-shifted in the *ntr a/b* and *trx-o1* lines. Unfortunately the analogous comparison could not be performed for succinate supplemented mitochondria with *gr2* background due to lack of replicates for a statistical analysis.

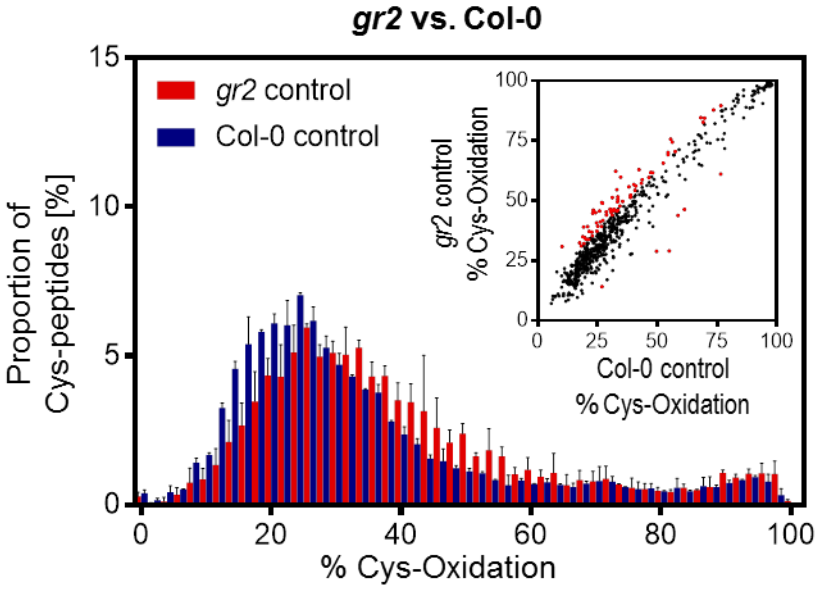

Figure 49: Differences in redox state of individual Cys-peptides of mitochondria from *gr2* mutants. Redox state of isolated and quiescent mitochondria from *gr2* background (red bars) and of the corresponding wildtype (blue bars) were analysed. Redox states of individual peptides were quantified using an MS/MS- based iodoTMT approach. The distribution of cysteine-peptide oxidation levels are shown as the proportion of the total number of peptides in each 2 % quantile of percentage oxidation (*n* = 3, average +SD; values for Col-0 control are the same as in **Figure 26 a**). In insets, the degree of Cys-oxidation of the Col-0 background is plotted against the degree of Cys-oxidation of the mutant for the individual Cys-peptides (*n* = 3, average). Dots marked in red indicate Cys-peptides with significant change in their Cys redox state between wildtype control and *gr2* mutant (t-test corrected for multiple comparisons by Benjamini, Krieger & Yekutieli with <2 % FDR).

Tab. 5: Cys-peptides in quiescent mitochondria of the *gr2* mutant with significantly more reduced redox states. Peptides of the *gr2* mutant, which are consistently more reduced as compared with the corresponding wildtype, are listed (peptides identified in **Figure 49**).

AA sequence	identifier	name
VPQ**C**NSSWTDEYIR	AT3G13930	Dihydrolipoyllysine-residue acetyltransferase component 2 of pyruvate dehydrogenase complex
TF**C**SGADVLSLYHSINEGNTEESK	AT4G31810	3-hydroxyisobutyryl-CoA hydrolase-like protein 2
GISA**C**AV**C**DGAAPIFR	AT2G17420	Thioredoxin reductase 2 (NTR a)
EAIW**C**GSTNSATEEGK	AT4G08900	Arginase 1 (Arginine amidohydrolase 1)
NVV**C**NFTEGAMYSFPQIR	AT1G23310	Glutamate--glyoxylate aminotransferase 1 (AtGGT2
TFDV**C**FAQLK	AT2G21170	Triosephosphate isomerase

Tab. 6: Cys-peptides in quiescent mitochondria of the *gr2* mutant with significantly more oxidised redox states. Peptides of the *gr2* mutant, which are consistently more oxidised as compared with corresponding wildtype, are listed (peptides identified in **Figure 49**).

AA sequence	identifier	name
YFSNVA**C**AK	AT4G13360	3-hydroxyisobutyryl-CoA hydrolase-like protein 3
G**C**YVGQELIAR	AT4G12130	Putative transferase At4g12130
CSGSLAVR	AT5G06580	D-lactate dehydrogenase [cytochrome]
D**C**GVESFGADRK	AT1G24180	Pyruvate dehydrogenase E1 component subunit
AQAANFPF**C**TIEPNVGIVAVPDSR	AT1G56050	Obg-like ATPase 1
ELEQ**C**AESSMYSPSYR	AT1G79750	NADP-dependent malic enzyme 4
GS**C**HIGGNVSTNAGGLR	AT4G36400	D-2-hydroxyglutarate dehydrogenase
D**C**GVESFGADR	AT1G24180	Pyruvate dehydrogenase E1 component subunit alpha-2
LVTVEEGFPQHGV**C**AEI**C**ASVVEESFSYLDAPVER	AT5G50850	Pyruvate dehydrogenase E1 component subunit
LIPPHV**C**F	AT5G06580	D-lactate dehydrogenase [cytochrome]
AGGSDPLEEY**C**NDNPETDE**C**R	AT2G47400	Calvin cycle protein CP12-1
G**C**VANIAAK	AT3G59760	Cysteine synthase
VDASGPED**C**PEEGR	AT4G08390	L-ascorbate peroxidase S
TPVSDKEIESIMLGG**C**I	AT5G24165	At5g24165 (Putative uncharacterized protein At5g24165)
LYVEAG**C**NVEEAQR	AT5G49840	CLP protease regulatory subunit CLPX2
CVVHAAWSSPTGLPAQTLIDR	AT3G48680	Gamma carbonic anhydrase-like 2
YIVVDV**C**YPEAPVGSIR	AT2G04940	Expressed protein (Putative uncharacterized protein At2g04940)
GWVPTLLGYSAQGA**C**K	AT5G14040	Mitochondrial phosphate carrier protein 3
PT**C**PY**C**R		roGFP2-GRX1
EIESIMLGG**C**I	AT5G24165	At5g24165 (Putative uncharacterized protein At5g24165)
NHYLSS**C**PSPSIK	AT3G19740	AAA-type ATPase domain-containing protein
EDYLE**C**LHHSK	AT3G62790	NADH dehydrogenase [ubiquinone] iron-sulfur protein 5-B
ED**C**WGGSNLGSDFPTPK	AT5G53350	CLP protease regulatory subunit CLPX1
FITPEGELEVE**C**DDDVYVLDAAEEAGIDLPYS**C**R	AT1G60950	Ferredoxin-2
CTILPQEDKIPAIVDR	AT1G17290	Alanine aminotransferase 1
IRPSVQDDGGDIEY**C**GFDTETGIVK	AT1G51390	NifU-like protein 5
VLINNIEEYAPIVYTPTVGLV**C**QNYSGLFR	AT2G13560	NAD-dependent malic enzyme 1
TPVSNEEMEAILLGG**C**I	AT4G23885	At4g23885 (Uncharacterized protein)
D**C**IGG**C**SDLVSLQQSGELLTR		roGFP2-GRX1
HV**C**INVVSSAFEGQSAVNR	AT5G17560	Protein BOLA4
LLQTSS**C**L	AT1G56000	AT1G56000 protein (FAD/NAD(P)-binding oxidoreductase domain-containing protein)
LNPEKDTFVL**C**K	AT5G19370	Rhodanese-like/PpiC domain-containing protein 12, (Sulfurtransferase 12)
NDPNVGTGLVGAPA**C**GDVMK	AT4G22220	Iron-sulfur cluster assembly protein 1 (AtISU1
CEEAIPLDAWVPADDVLPL**C**K	AT2G15620	Ferredoxin--nitrite reductase
LSSVNLAFIA**C**K	AT4G36400	D-2-hydroxyglutarate dehydrogenase
AAGMALAQHPVVNAS**C**K	AT3G25860	Dihydrolipoyllysine-residue acetyltransferase component 4 of pyruvate dehydrogenase complex
VAGQIGDAYL**C**YDR	AT1G30680	Twinkle homolog protein (DNA helicase)
YKEQGLEILAFP**C**NQFLGQEPGNNEEIQQTV**C**TR	AT2G31570	Probable glutathione peroxidase 2
CMALSTVVFVGDAK	AT2G14170	Methylmalonate-semialdehyde dehydrogenase [acylating]
TIQHEAVEAASASAAPAGSAMLSST**C**DIHAK	AT5G64400	Uncharacterized protein
CTWATPEER	AT3G28700	Uncharacterized protein
TLLAN**C**VAAGNVK	AT1G80270	Pentatricopeptide repeat-containing protein At1g80270
WASIAFGAGIGIGSAYTD**C**SR	AT1G22520	Uncharacterized protein
VVVFIKPT**C**PY**C**R		roGFP2-GRX1
VNNPATGEIIADVA**C**MGTK	AT1G79440	Succinate-semialdehyde dehydrogenase
GVPESPQ**C**GFSSLAVR	AT3G15660	Monothiol glutaredoxin-S15, mitochondrial
IYSV**C**TSTYTGFGALISEELS**C**K	AT3G06790	Multiple organellar RNA editing factor 3
KVPQ**C**NSSWTDEYIR	AT3G13930	Dihydrolipoyllysine-residue acetyltransferase component 2 of pyruvate dehydrogenase complex
TVD**C**YSPGQGLMPASFK	AT1G56560	Alkaline/neutral invertase A
GLQQTPWV**C**R	AT3G15590	Pentatricopeptide repeat-containing protein At3g15590
HDFMMVFT**C**K	AT3G54826	Zim17-type zinc finger protein
LH**C**SMLAEDAIK	AT4G22220	Iron-sulfur cluster assembly protein 1 (AtISU1)
GFGADVIMTSES**C**R	AT1G53000	3-deoxy-manno-octulosonate cytidylyltransferase
GITIQSAATY**C**TWK	AT2G45030	Elongation factor G-2
SLVPGVF**C**AGADLK	AT4G16800	Probable enoyl-CoA hydratase 2
VVIFGLPGAYTGV**C**SQQHVPSYK	AT3G06050	Peroxiredoxin-2F, mitochondrial
SQVLDETAWSDQDY**C**K	AT2G33600	At2g33600 (Cinnamoyl coa:nadp oxidoreductase-like 2)
TAIIEGDVVGGT**C**VNR	AT3G16950	Dihydrolipoyl dehydrogenase 1
VLAESESSAFEDQ**C**GR	AT5G14740	Carbonic anhydrase
AMATLNVPAEAGHYGVLIENQ**C**K	AT2G37230	Pentatricopeptide repeat-containing protein At2g37230
GFLA**C**QAHR	AT3G13110	Serine acetyltransferase 3, mitochondrial
AG**C**DVTVWNR	AT1G17650	Glyoxylate/succinic semialdehyde reductase 2
GFNIS**C**VGIIVYR	AT3G08580	ADP,ATP carrier protein 1, mitochondrial
GFTVLQA**C**EVAGVDIPR	AT5G37510	AT5G37510 protein (NADH-ubiquinone oxidoreductase subunit)
TYYLTLEAL**C**K	AT3G02650	Pentatricopeptide repeat-containing protein At3g02650
ISI**C**GVSK	AT4G31810	3-hydroxyisobutyryl-CoA hydrolase-like protein 2
CFGENYVQEIIDK	AT4G26860	Putative pyridoxal phosphate-dependent enzyme, YBL036C type
D**C**GPMVLDALIK	AT3G27380	Succinate dehydrogenase [ubiquinone] iron-sulfur subunit 1
Y**C**GSPVGTVAANDPGDK	AT1G56560	Alkaline/neutral invertase A, mitochondrial
NAGGV**C**IADEVQTGFGR	AT4G39660	Alanine:glyoxylate aminotransferase 2 homolog
Y**C**IVAGK	AT5G46290	Beta-ketoacyl-[acyl carrier protein] synthase I

2.6 *In vitro* characterisation of the hydrogen peroxide sensor roGFP2-Orp1

A general attribute of orthodox, dry seeds are oxidised glutathione pools of the plasmatic compartments (*e.g.* **Figure 16**) and a global proteome. Both, the plasmatic glutathione pools and the proteome are actively reduced early during germination (*e.g.* ALKHALFIOUI *ET AL.,* 2007, **Figure 16** and **Figure 18**). Prior to the reduction during germination, oxidation of the seed thiols needs to occur during the maturation and desiccation (*e.g.* JOB *ET AL.,* 2005). Since O_2 is unreactive with thiols, hydrogen peroxide has been suggested as a key electron acceptor to mediate oxidation, *e.g.* of the protein thiols. Furthermore, hydrogen peroxide release was described in germinating seeds (*1.4* and SCHOPFER *ET AL.,* 2001). Through its reactivity with specific chemical groups hydrogen peroxide has been proposed to act as a major signalling molecule crucial for many developmental processes, such as root hair formation (FOREMAN *ET AL.,* 2003). For *in vivo* monitoring of hydrogen peroxide different fluorescent probes are available. Yet, when this work was started, there was no tool available for dynamic and reliable hydrogen peroxide monitoring in plants. Here roGFP2-Orp1 (GUTSCHER *ET AL.,* 2009) is characterised to enable dynamic and specific hydrogen peroxide measurements with subcellular resolution *in planta*. Even though HyPer was already characterised in Arabidopsis (COSTA *ET AL.,* 2010), its underlying chromophore cpYFP was found highly pH-sensitive (SCHWARZLÄNDER *ET AL.,* 2011; SCHWARZLÄNDER *ET AL.,* 2014) complicating the interpretation of measurements. RoGFP2-based sensors are largely pH-inert in a physiological meaningful range, when used ratiometrically, providing an important advantage (SCHWARZLÄNDER *ET AL.,* 2016). Characterisation of roGFP2-Orp1 under *in vitro* conditions was performed prior to *in planta* measurements.

2.6.1 Expression and purification of roGFP2-Orp1 protein

6x His-tagged roGFP2-Orp1 was purified from IPTG-induced Origami DE3 cells. The culture appeared green after IPTG induction, suggesting expression and maturation of the recombinant roGFP2-Orp1 protein to high amounts. After sonication and centrifugation of the cells also the supernatant appeared green, suggesting solubility of roGFP2-Orp1, although the pellet was also green, indicative of an insoluble proportion. After nickel affinity chromatography, all obtained protein fractions were separated by 1D-SDS-PAGE to estimate the apparent molecular masses and the purity of the eluted protein fractions (**Figure 50**). The eluted fractions (**Figure 50** `Elu. I` and `Elu. II`) showed two strong bands with apparent molecular masses of about 50 and 40 kDa, while other bands were decreased after washing with increasing concentration of imidazole (**Figure 50** `W I`, `W II` and `W III`). No other strong protein bands were visible in the Coomassie stained SDS-PAGE of the eluted fractions I and II (**Figure 50** `Elu I` and `Elu II`). An estimated apparent molecular mass of about 50 kDa matches with the expected size of the His-tagged roGFP2-Orp1 with 49.6 kDa suggesting successful purification of recombinant roGFP2-Orp1 protein. However, a defined band with a lower molecular mass was detected, which might be explained either by contamination with a different protein species or, more likely, by partial degradation of the roGFP2-Orp1 sensor. Gel filtration chromatography would allow to specifically separate the 50 kDa fraction. Since the required chromatography setup was not available when the work was done, the extract was employed without any further purification step for characterisation.

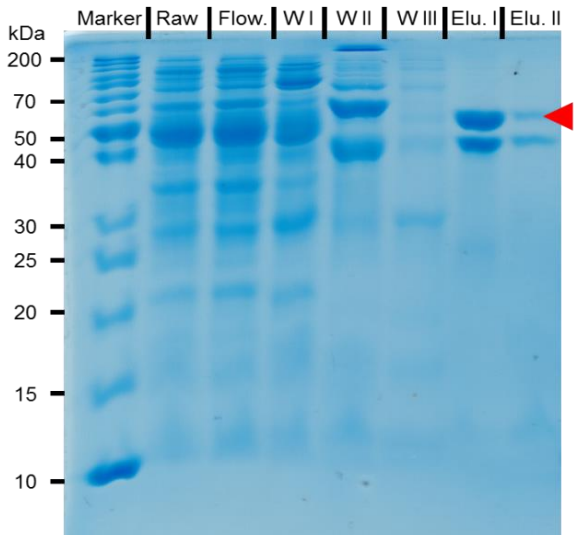

Figure 50: Heterologous expression of the hydrogen peroxide sensor roGFP2-Orp1. Expression of N-terminal 6x His-tagged roGFP2-Orp1 in Origami DE3 cells induced with 0.1 mM IPTG for 16 h at 20°C and purification by binding to a nickel-NTA column. Raw cell extract after IPTG induction (`Raw`), unbound flow-through (`Flow.`), fractions after washing with increasing amounts of imidazole (`W I`: 20 mM, `W II`: 40 mM, `W III`: 60 mM) and two subsequent fractions after elution with 250 mM imidazole (`Elu. I` & `Elu. II`) separated by 10 % (v/v) 1D-SDS-PAGE. PageRuler™ Unstained Protein Ladder was used for estimation of apparent molecular masses, indicated by `Marker`. Red marker: expected molecular mass of 6x His-tagged roGFP2-Orp1 protein (49.6 kDa).

2.6.2 Optical characteristics of roGFP2-Orp1 protein

Excitation and emission scans of purified roGFP2-Orp1 were performed (**Figure 51**) to validate the typical dual excitation and single emission properties of roGFP2-based probes (DOOLEY *ET AL.*, 2004; HANSON *ET AL.*, 2004) and to verify the sensor characteristics described by Gutscher and colleagues (GUTSCHER *ET AL.*, 2009).

The reduced roGFP2-Orp1 (roGFP2-Orp1$_{red}$) sensor showed a characteristic peak in its excitation spectrum around 490 nm, while the excitation spectrum of the oxidised sensor (roGFP2-Orp1$_{ox}$) revealed the two characteristic peaks at about 400 nm and 490 nm, with the latter showing less relative intensities as compared to the reduced sensor (**Figure 51 a**). The spectroscopic dynamic range (δ) of the roGFP2-Orp1 protein between its fully oxidised and its fully reduced state was about 6.1, when excited at 405 and 488 nm. The isobestic point of unchanged fluorescence intensities between the reduced and the oxidised protein was at 423 nm.

Emission spectra of roGFP2-Orp1$_{red}$ and roGFP2-Orp1$_{ox}$ revealed an emission peak at around 515 nm (**Figure 51 b**). Fluorescence intensity emitted from the roGFP2-Orp1$_{red}$ was higher than for roGFP2-Orp1$_{ox}$ when excited at 488 nm. When excited at 405 nm, emitted light of roGFP2-Orp1$_{ox}$ was higher than of roGFP2-Orp1$_{red}$.

The purified protein fraction showed similar spectral properties, as other roGFP2-based probes, yet with a lower dynamic range. This was already reported by Gutscher and colleagues (GUTSCHER *ET AL.*, 2009).

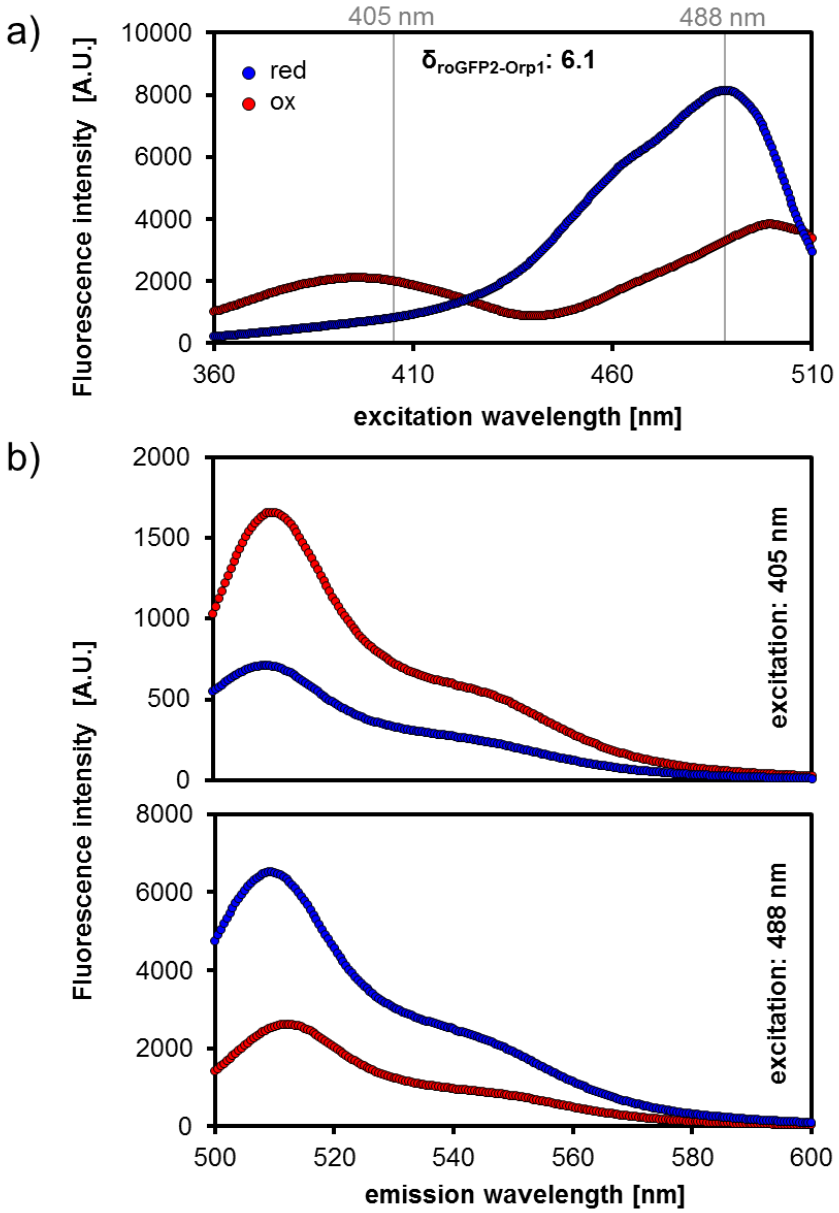

Figure 51: Excitation and emission spectra of purified roGFP2-Orp1 protein *in vitro*. RoGFP2-Orp1 was oxidised (dots marked in red, `ox`) or reduced (dots marked in blue, `red`) by addition of 1 mM DPS or 20 mM DTT, respectively. a) Excitation spectra of roGFP2-Orp1; emission at 515 nm. The spectroscopic dynamic range (δ) calculated from the 405/488 nm excitation ratios assuming fully oxidised and fully reduced sensor. Excitation wavelengths are indicated by vertical, grey lines. b) Emission spectra of oxidised and reduced roGFP2-Orp1 with excitation at 405 nm (upper panel) and at 488 nm (lower panel). Data was recorded in 0.5 nm steps and 5 nm bandwidth for both, excitation and emission spectra (n = 4, technical replicates).

2.6.3 pH sensitivity of roGFP2-Orp1 protein

The chromophore of another family of hydrogen peroxide sensors, HyPer, was shown to be pH sensitive confounding hydrogen peroxide measurements (*e.g.* ROMA *ET AL.,* 2012; SCHWARZLÄNDER *ET AL.,* 2014). To investigate the pH-sensitivity of roGFP2-Orp1, the oxidised or reduced sensor was incubated in buffers of different pH (5.3 - 8.3). After equilibration 400/482 nm excitation ratios were monitored and pH was measured thereafter for validation (**Figure 52**).

Absolute fluorescence intensities for both excitation wavelengths were quenched by lowering the pH independently from the sensor oxidation state (data not shown), consistent with the pH sensitivity of wildtype GFP (PATTERSON *ET AL.,* 1997). Yet, the 400/482 nm excitation ratios were constant in the pH range of 6.5 - 8.3 for both redox states of the sensor, resulting in a constant spectroscopic dynamic range of about 8. The spectroscopic dynamic range is dependent on the wavelength used for excitation, thus the discrepancy to the values estimated in *2.6.2* (~6.1) can be reasoned, as roGFP2-Orp1 was here excited at 405 nm and 488 nm. With decreasing pH under 6.0, the 400/482 nm ratio of the oxidised sensor dropped slightly, while the ratio of the reduced sensor increased. This resulted in a lower dynamic range for the sensor in the more acidic pH range of 5.3 – 6. These data indicate that the roGFP2-Orp1 sensor is pH inert in a physiological meaningful pH range of most cell compartments of the plant, providing an advantage over HyPer variants. This appears of particular importance in cell compartments, such as the chloroplast and the mitochondria, where pH can fluctuate considerably depending on external conditions.

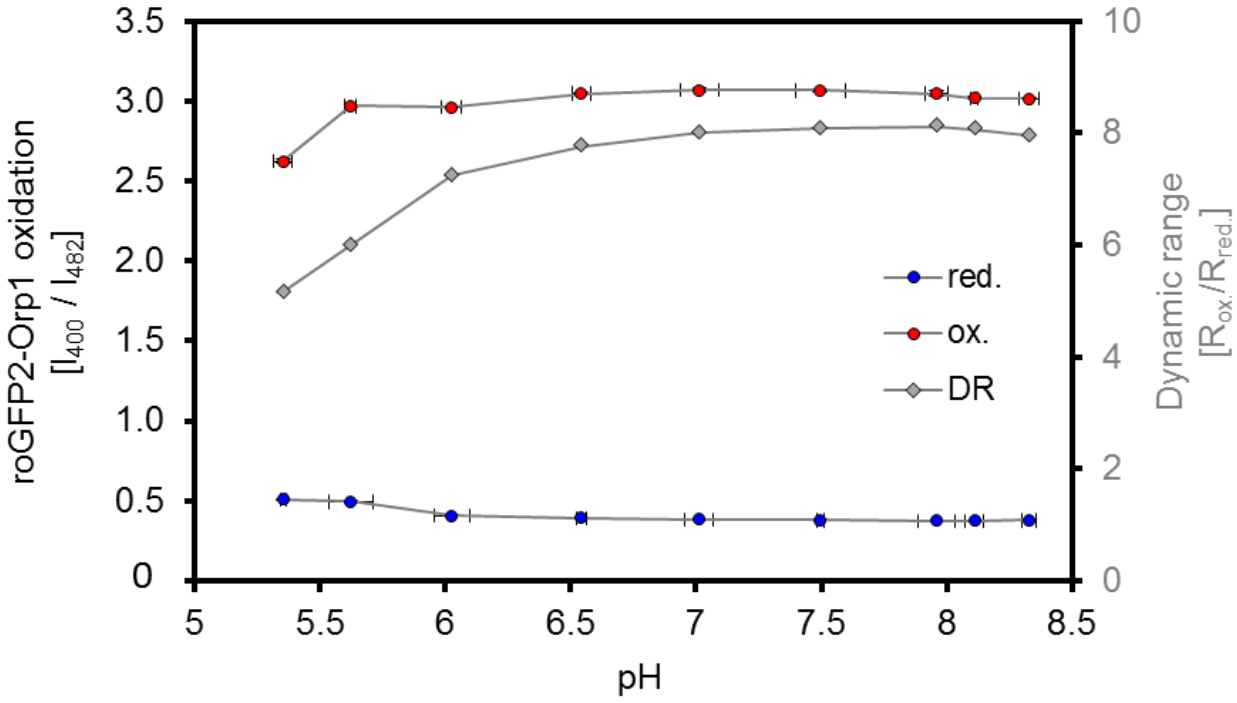

Figure 52: pH dependence of the 400/482 nm excitation ratio of roGFP2-Orp1 *in vitro*. RoGFP2-Orp1 fluorescence ratios in the pH range of 5.3 - 8.3 are shown (*n* = 3 technical replicates; vertical error bars: SD, but too small to be visible); excitation at 400/482 nm; emission at 530 ± 20 nm. Purified sensor was either reduced with 20 mM DTT (blue circles) or oxidised with 1 mM DPS (red circles) for 20 min in a buffer containing 100 mM MES-KOH (pH 5.3 - 6.5), HEPES-KOH (pH 7 - 8) or Tris-HCl (pH 8.1 - 8.3). pH was controlled after the spectroscopic measurements with a micro pH-electrode (*n* = 3 technical replicates; horizontal error bars: SD). Dynamic range ($R_{ox.}/R_{red.}$) of roGFP2-Orp1 is plotted on the secondary axis (grey diamonds).

2.6.4 Hydrogen peroxide oxidises roGFP2-Orp1 effectively and reversible in vitro

RoGFP2-Orp1 protein extract was assayed for its sensitivity for hydrogen peroxide *in vitro*. 0.3 µM reduced roGFP2-Orp1 was titrated with increasing concentration of hydrogen peroxide (**Figure 53**). Untreated, reduced roGFP2-Orp1 showed a slight but steady rate of increase in 400/482 nm ratio over time. At the time point of hydrogen peroxide addition (grey arrow), the sensor population was already partially oxidised. 0.3 µM of sensor extract treated with different concentration of hydrogen peroxide in the range of 0 to 100 µM revealed a dose-dependent increase of the 400/482 nm ratio. Application of 1 µM of hydrogen peroxide was sufficient to completely oxidise the roGFP2-Orp1 sensor *in vitro*, while less than equimolar amounts caused only partial oxidation of the sensor extract. Full sensor response was achieved in less than 15 min after hydrogen peroxide application. Addition of the reductant DTT in excess (white arrow) caused complete reduction of the roGFP2-Orp1 extract, indicating fully reversible oxidation of the protein sensor. These data confirm the dynamic responsiveness of roGFP2-Orp1 to hydrogen peroxide in the µM range as already described by Gutscher and colleagues (GUTSCHER *ET AL.*, 2009).

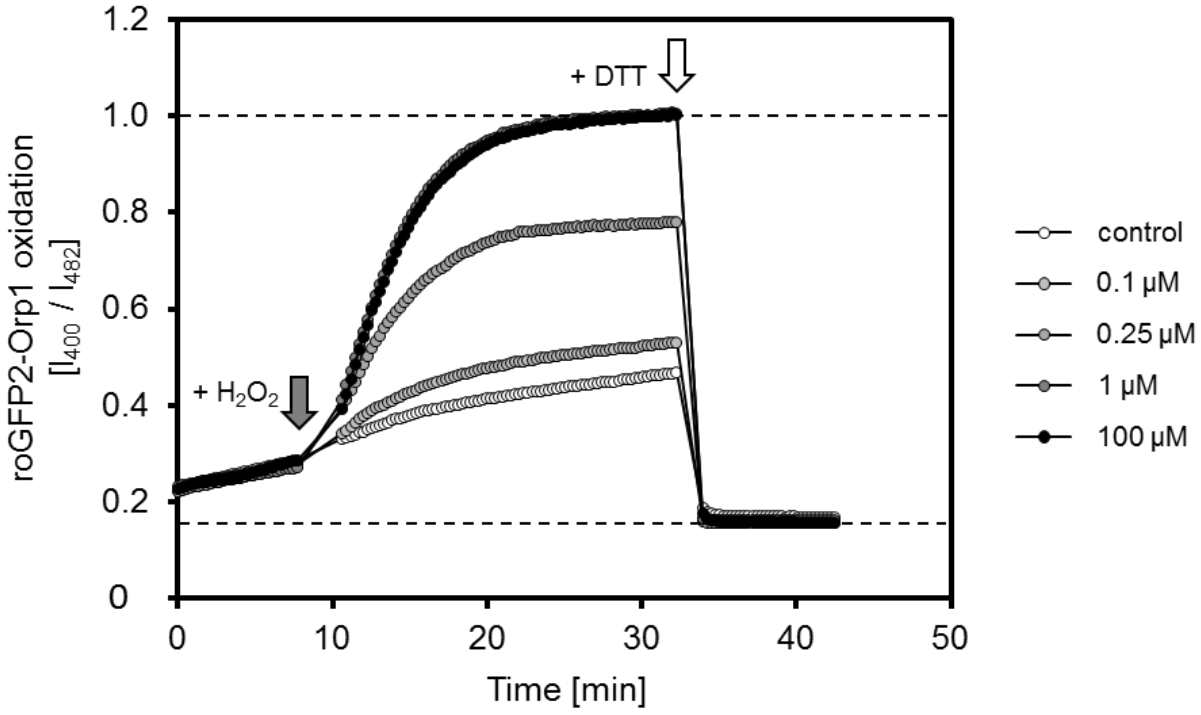

Figure 53: Hydrogen peroxide responses of pre-reduced roGFP2-Orp1 protein *in vitro*. The fluorescence ratios (400/482 nm, *n* = 3 technical replicates, mean normalised to the highest value) of roGFP2-Orp1 (0.3 µM) were plotted over time (emitted light at 530 ± 20 nm). Purified roGFP2-Orp1 was pre-reduced with 20 mM DTT for 20 min on ice; DTT was then removed using by size exclusion column. The grey arrow indicates the addition of hydrogen peroxide to a final concentration of 0 µM (white circles), 0.1 µM (light grey circles), 0.25 µM (grey circles), 1 µM (dark grey circles) and 100 µM (black circles). The white arrow indicates the addition of 20 mM DTT for reduction of the sensor. Upper dashed line indicates fully oxidised state (1 mM DPS for 20 min), lower dashed line fully reduced state of roGFP2-Orp1 (20 mM DTT for 20 min).

2.6.5 Reduction of roGFP2-Orp1 by reconstituted redox machineries

Reversibility of the sensor response is the basis for dynamic hydrogen peroxide monitoring. Yet, the reduction depends on the endogenous redox systems when the sensor is used *in vivo*. Hence, the identification of the endogenous redox systems involved in the sensor reduction is critical for an appropriate interpretation of roGFP2-Orp1-based *in vivo* measurements. This is of particular interest since the Orp1 peroxidase was shown to be reduced by the thioredoxin machinery in yeast cells (DELAUNAY *ET AL.,* 2002), while the fused roGFP2 is known to interact with the glutathione/glutaredoxin systems (*e.g*. DOOLEY *ET AL*., 2004; HANSON *ET AL*., 2004). As a result the sensor links both thiol redox machineries.
The cellular redox systems were reconstituted *in vitro* using purified Arabidopsis proteins to estimate the respective contribution of each system to the reduction of the sensor. The roGFP2-Orp1 population was in its oxidised state after purification, indicated by equal 400/482 nm ratios of DPS treated sensor fractions and untreated sensor fractions (**Figure 54**). Reconstitution of the thioredoxin machinery by addition of NADPH, NTR b and TRX-o1 caused a slow but steady reduction of the sensor population, indicated by a decreasing 400/482 nm ratio over time. Addition of reduced glutathione to the oxidised sensor caused a decrease in 400/482 nm ratio. The ratio dropped instantly at glutathione addition and reached a plateau after 120 min, while reduction by the reconstituted thioredoxin machinery was still ongoing at this time point and reached higher levels of reduction. In the presence of human GRXC1, addition of glutathione caused a much faster reduction of the 400/482 nm ratio. The reduction reached a plateau after 120 min, but did not reach the same reduction level as completely reduced roGFP2-Orp1 at DTT treatment. Both cellular redox machineries are capable of reducing the roGFP2-Orp1 *in vitro*, but glutaredoxin-mediated reduction with reduced glutathione was kinetically more effective than the thioredoxin-dependent reduction. As such it is likely that the GSH/GRX system dominates the reduction of the sensor *in vivo*.

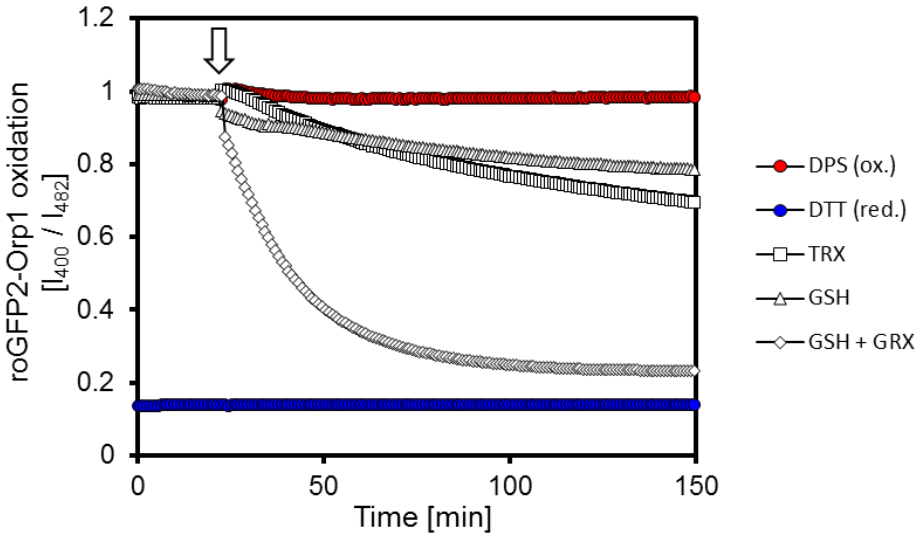

Figure 54: Reduction of roGFP2-Orp1 protein extracts by reconstituted TRX and GSH/GRX machineries *in vitro*. The fluorescence ratios (400/482 nm) of roGFP2-Orp1 were plotted over time (*n* = 3 technical replicates, mean normalised to the highest value). As controls for full reduction and oxidation, purified sensor was either treated with 20 mM DTT (DTT, blue circles) or 1 mM DPS (DPS, red circles) for 20 min, respectively. The white arrow indicates the addition of either 10 mM reduced glutathione (GSH, triangles), 10 mM reduced glutathione in presence of excess GRXC1 (50 µM; GSH+GRX, diamonds) or TRX-o1 (50 µM), NADPH (0.1 mM) and excess of NTRb (50 µM; TRX, squares), respectively. NADPH (0.1 mM) and excess of yeast glutathione reductase (50 µM) was added to maintain a highly negative redox potential of the supplemented glutathione.

2.7 Characterisation of the roGFP2-Orp1 protein sensor *in planta*

RoGFP2-Orp1 was effectively oxidised by µM levels of hydrogen peroxide *in vitro*. It was next tested if the sensor can also respond to hydrogen peroxide in plants. Hence, stable Arabidopsis sensor lines with roGFP2-Orp1 constructs for different subcellular compartments were generated, to enable measurements with subcellular resolution.

2.7.1 Arabidopsis sensor lines for cytosolic and nuclear expression of the roGFP2-Orp1 sensor

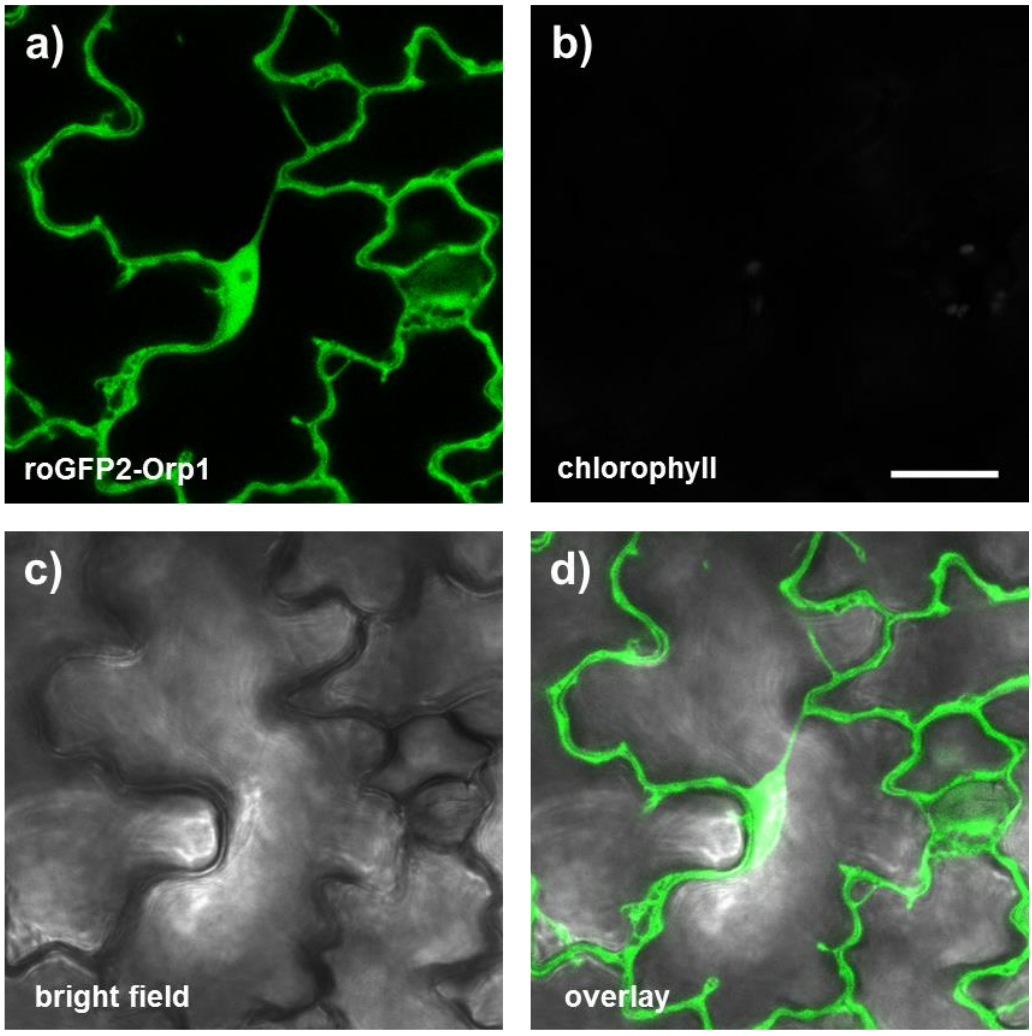

Figure 55: *35S*:roGFP2-Orp1 in epidermis cells of cotyledons of five-day-old Arabidopsis seedlings. Arabidopsis seedlings with stable expression of *35S*:roGFP2-Orp1 were analysed by CLSM. a) roGFP2-Orp1 fluorescence signal in green (excitation at 488 nm, emission at 520 ± 15 nm), b) auto-fluorescence of chlorophyll in white (excitation at 488 nm, emission at 675 ± 25 nm), c) bright field (T-PMT), d) overlay of a-c. Size bar = 20 µm.

Epidermal cells of young seedlings stably expressing roGFP2-Orp1 under the control of a *35S* promotor showed clear fluorescence at 488 nm excitation (**Figure 55**). RoGFP2-Orp1 fluorescence was distinct to the chlorophyll auto-fluorescence, which was hardly detectable due to the low chlorophyll content of plastids in epidermal pavement cells. Fluorescence was restricted to the nucleoplasm counterstaining the nucleolus and the cytosol, as evident from trans-vacuolar strands. Together this suggests strong and specific expression of the roGFP2-Orp1 sensor in the cytosol and the nucleoplasm of Arabidopsis cells. Five independent cytosolic roGFP2-Orp1 lines were selected, showing no obvious growth phenotypes, yet different sensor expression levels, as indicated by different fluorescence intensities. For further characterisation of cytosolic roGFP2-Orp1 *in planta*, the line with brightest sensor signal was selected.

2.7.2 Arabidopsis lines for expression of the roGFP2-Orp1 sensor in the mitochondrial matrix

Root cells of young seedlings transformed with roGFP2-Orp1 C-terminal fused to the target peptide (TP) of the β-subunit of the ATP-Synthase of *Nicotiana plumbaginifolia* under the control of a *35S* promotor showed a clear fluorescence-signal at 488 nm excitation (**Figure 56**). Chlorophyll auto-fluorescence was not detectable in roots. RoGFP2-Orp1 fluorescence was prominent in round to bean shaped structures of 1 - 2 µm in size, which were also stained with the mitochondrial matrix specific fluorescent dye MitoTracker® Orange CMTMRos. The organelles were highly dynamic and moved rapidly. Lower fluorescence intensities were also detected in the cytosol for both excitation wavelengths. These observations suggest expression of roGFP2-Orp1 in the mitochondrial matrix, with residual amounts in the cytosol. Five independent mitochondrial roGFP2-Orp1 lines were selected, showing typical growth phenotypes, as often associated with the heterologous expression of fluorescent biosensors in the mitochondrial matrix, *e.g.* early leaf-senescence and delayed germination and growth in early seedling stages (SCHWARZLÄNDER *ET AL.,* 2016; DE COL *ET AL*., 2017, *in preparation*). The five independent lines show different sensor expression levels, as indicated by different fluorescence intensities. For further characterisation of mitochondrial roGFP2-Orp1 *in planta,* the line with the brightest sensor signal was chosen. Together the cytosolic and the mitochondrial sensor lines promise to establish hydrogen peroxide measurements with subcellular resolution in living Arabidopsis tissues.

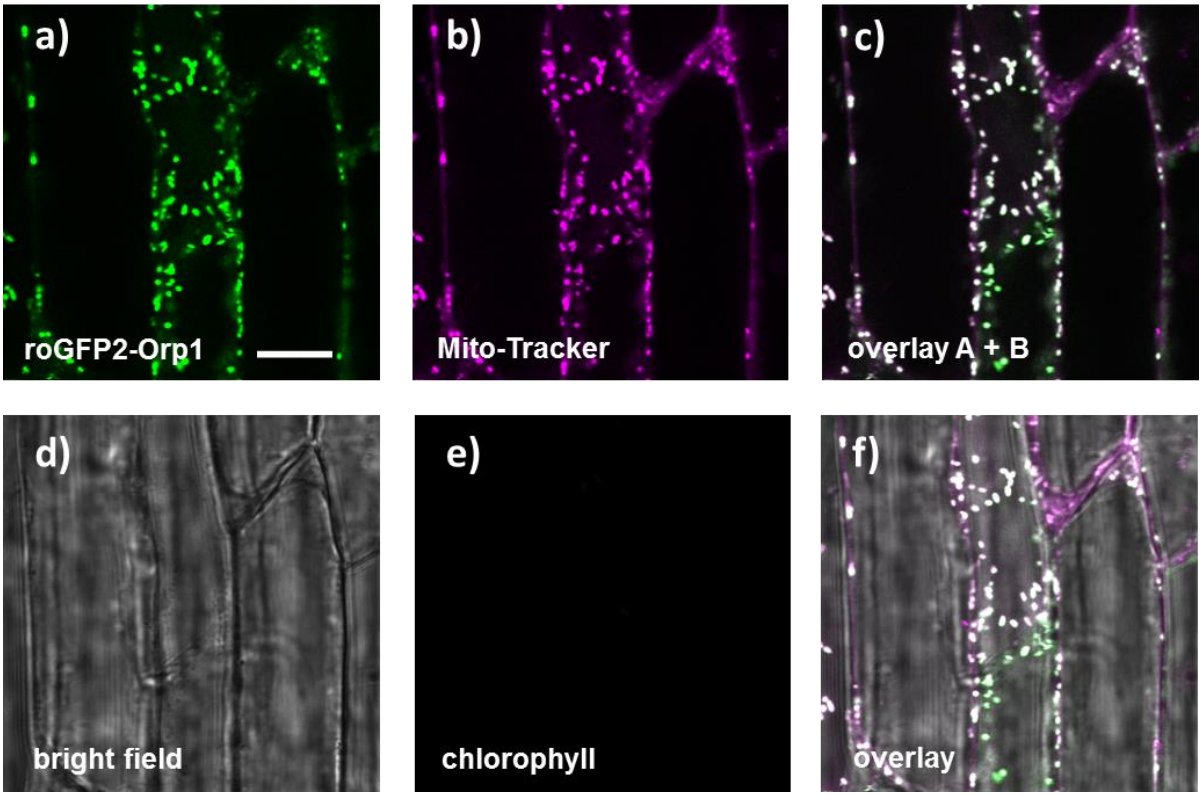

Figure 56: *35S*:TP-β-subunit-ATP-Synthase-roGFP2-Orp1 in root cells of five-day-old Arabidopsis seedlings. Arabidopsis seedlings with stable expression of *35S*:TP-β-subunit-ATP-Synthase-roGFP2-Orp1 were analysed by CLSM. a) roGFP2-Orp1 fluorescence signal in green (excitation at 488 nm, emission at 520 ± 15 nm), b) fluorescence of the mitochondrial marker 'MitoTracker® Orange CMTMRos' in magenta (excitation at 543 nm, emission at 595 ± 25 nm), c) overlay image of a) and b), d) bright field (T-PMT), e) auto-fluorescence of chlorophyll in white (excitation at 488 nm, emission at 675 ± 25 nm), f) overlay of a) - e). Size bar = 10 µm.

2.7.3 RoGFP2-Orp1 responds to external applied oxidative stress in living Arabidopsis tissues

It was tested to what extent the roGFP2-Orp1 sensor was able to respond to externally applied reductant and oxidant *in planta*.

The sensor targeted to the cytosol or the mitochondrial matrix was responsive to external application of high concentration of DTT and hydrogen peroxide (**Figure 57**). Hydrogen peroxide caused an increase in 405/488 nm ratio in both, the cytosolic and the mitochondrial roGFP2-Orp1 lines. DTT addition led to a slight, but significant reduction of the 405/488 nm ratio in the mitochondrial roGFP2-Orp1 line, as compared to the control, while for the cytosolic roGFP2-Orp1 no further reduction was observed. The spectroscopic dynamic range (δ) of both sensor populations was slightly lower than estimated using purified roGFP2-Orp1 *in vitro* (**Figure 51 a**) with 5.0 for the cytosolic roGFP2-Orp1 and 3.9 for the mitochondrial roGFP2-Orp1. The reason for this is not known, but similar effects were observed for roGFP2 before (*e.g.* SCHWARZLÄNDER *ET AL.*, 2008). These data suggest that the redox state of roGFP2-Orp1 responds dynamically *in planta*. It further shows that mitochondrial roGFP2-Orp1 is not completely reduced *in vivo*. Yet both sensors are highly reduced under control conditions, which is a prerequisite for measurements of oxidation by hydrogen peroxide.

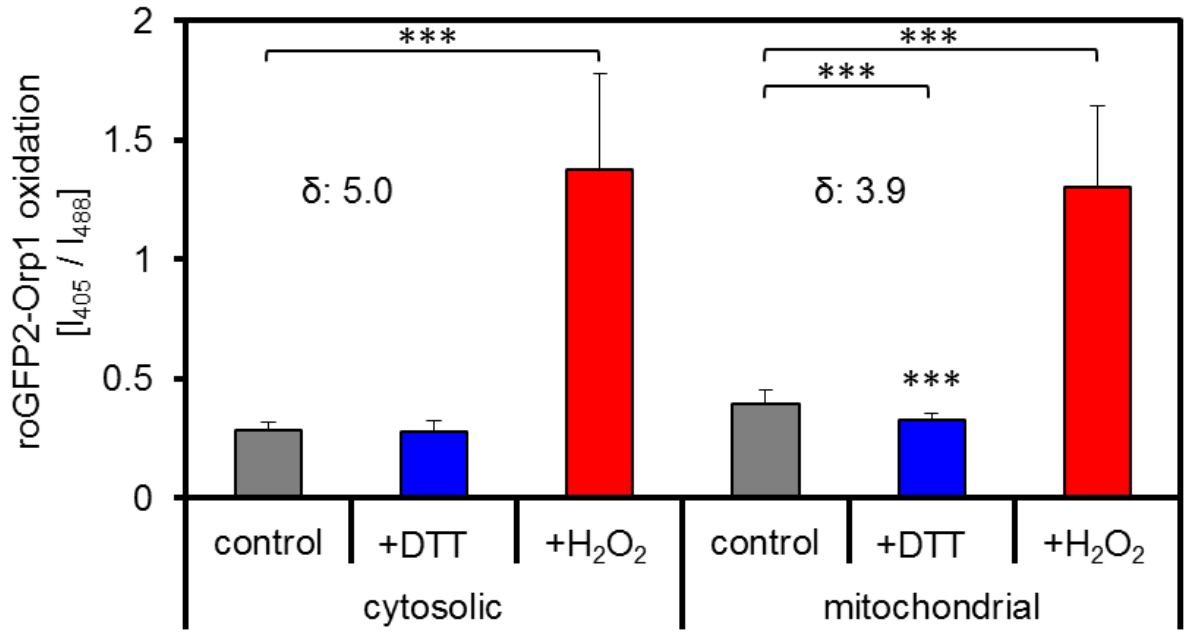

Figure 57: *In vivo* calibration of cytosolic and mitochondrial roGFP2-Orp1 in root tips of five-day-old Arabidopsis seedlings. RoGFP2-Orp1 expressed in the cytosol and in the mitochondrial matrix of Arabidopsis seedlings were investigated by CLSM. 405/488 nm ratios (average +SD, *n* = 12, emission at 520 ± 15 nm) were plotted for untreated plants (control), after addition of 20 mM DTT for 15 min (+DTT) or 100 mM hydrogen peroxide (+H_2O_2). The spectroscopic dynamic range is given for each line (δ). ***p<0.001 with two-tailed, unpaired Student`s t-test.

2.7.4 Response of mitochondrial roGFP2-Orp1 to the redox cycling agent menadione

External application of high amounts of reductant and oxidant led to a response of the roGFP2-Orp1 *in planta* (**Figure 57**). To investigate if also endogenously produced hydrogen peroxide can oxidise roGFP2-Orp1 *in vivo*, menadione was applied to young Arabidopsis seedlings. The redox cycling compound menadione triggers continuous formation of superoxide through the catalytic transfer of electrons from endogenous donors, such as the ubiquinone pool of the mitochondrial ETC, to molecular oxygen, while menadione itself is regenerated. Superoxide is then dismutated to hydrogen peroxide by superoxide dismutases. Arabidopsis seedlings treated with 30 µM menadione for 20 min showed an increase in 405/488 nm ratio of matrix targeted roGFP2-Orp1 (**Figure 58**). Oxidation was investigated in cells of the cotyledons, the hypocotyl, the upper-root and the root tip. All tissue types showed an increase in 405/488 nm ratio and the increase was most pronounced in the cotyledon epidermis. This shows that also endogenously produced hydrogen peroxide is capable of triggering a roGFP2-Orp1 response. Yet, menadione application leads to an excessive formation of hydrogen peroxide, which is why the response of the sensor to physiological changes in hydrogen peroxide fluxes *in planta* remains open.

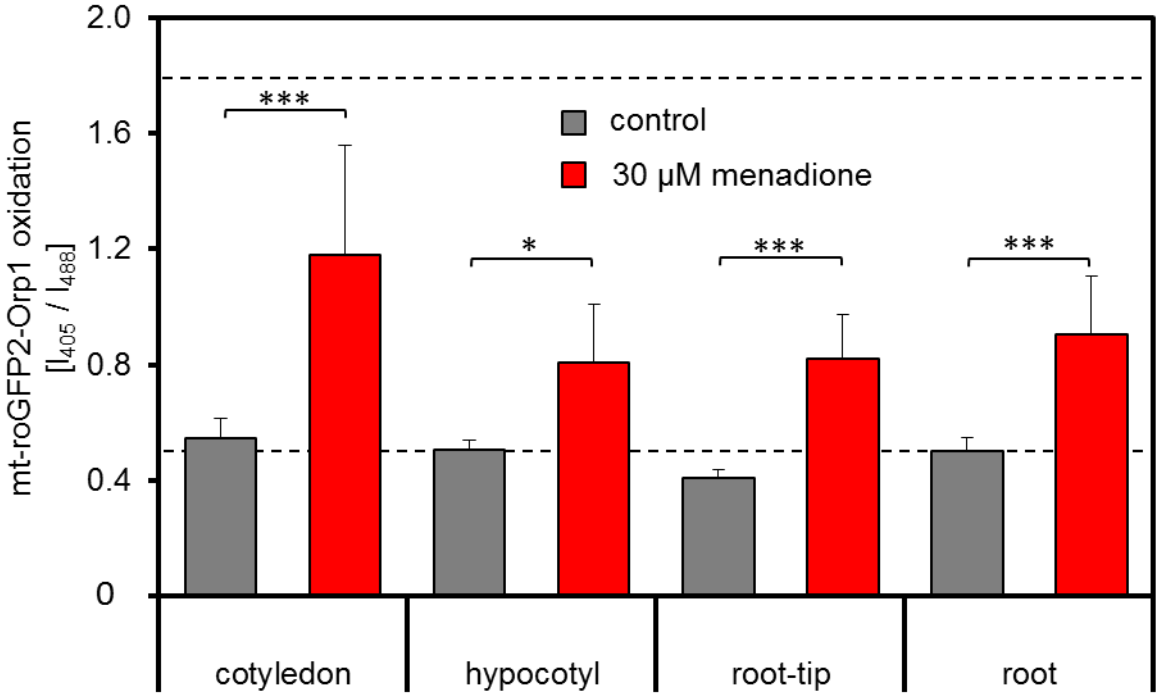

Figure 58: The response of mitochondrial roGFP2-Orp1 to menadione-mediated hydrogen peroxide production. Five-day-old seedlings were treated with 30 µM menadione for 20 min and analysed by CLSM. The fluorescence ratios (sequential excitation: 405 and 488 nm, emission: 520 ± 15 nm) of roGFP2-Orp1 in the mitochondrial matrix of different tissues are shown (n = 5 - 10 biological replicates, mean +SD; two-tailed, unpaired Student`s t-test: *p<0.05, ***p<0.001). Upper dashed line indicates fully oxidised state (1 mM DPS for 20 min), lower dashed line fully reduced state (20 mM DTT for 20 min) of mitochondrial roGFP2-Orp1 in the cotyledons.

2.7.5 Mutants with impaired redox homeostasis investigated with roGFP2-Orp1

To further explore the response characteristics of roGFP2-Orp1 *in vivo,* the sensor was introduced into different mutants with impairments in their cellular redox machineries (FINKEMEIER *ET AL.,* 2005; QUEVAL *ET AL.,* 2007; REICHHELD *ET AL.,* 2007; DALOSO *ET AL.,* 2015; MARTY *ET AL*., in preparation; see also **Figure 59**). T-DNA insertion mutants of the main peroxisomal catalase isoform CAT2 were expected to show increased steady-state-levels of hydrogen peroxide (QUEVAL *ET AL.,* 2007). The mitochondrial peroxiredoxin II-F is the only known Arabidopsis mitochondrial peroxiredoxin (FINKEMEIER *ET AL.,* 2005). Consequently mitochondrial hydrogen peroxide levels may be expected to be increased in the corresponding mutant (*prx II-F*). Mutants of the cellular glutathione/- and thioredoxin-based redox machineries (*gr2*, MARTY *ET AL*., in preparation; *ntr a/b*, REICHHELD *ET AL.,* 2007 and *trx-o1,* DALOSO *ET AL.,* 2015) may affect the reduction of the roGFP2-Orp1 sensor directly (*2.6.5*). These mutants also may have an additional impact on the basal hydrogen peroxide levels, because they are part of the antioxidant machinery, supplying electrons for hydrogen peroxide detoxification by different peroxidases (*e.g.* Apx, Prx, Gpx-like). Furthermore, perturbed electron flux via the thioredoxin-dependent redox machinery can affect the redox dynamics of the glutathione-dependent redox machinery, and *vice versa* via redox crosstalk (REICHHELD *ET AL.,* 2007; MARTY *ET AL.,* 2009), with potential impacts on the roGFP2-Orp1 redox state, as well as the antioxidant systems.

The redox state of cytosolic roGFP2-Orp1 was unchanged in all lines, while mitochondrial roGFP2-Orp1 showed a strongly increased 405/488 nm ratio in the *gr2* background. The 405/488 nm ratio was also slightly elevated in the *ntr a/b* and *cat2* lines. These data suggest that *in vivo* the reduction of the roGFP2-Orp1 sensor is mainly dependent on the glutathione redox state, in agreement with the findings *in vitro* (*2.6.5*). While the thioredoxin-dependent redox machinery appears not to strongly contribute to sensor reduction, clear differences can be observed for the *ntr a/b* mutant, indicating that the thioredoxin systems nevertheless contributes. Furthermore, there was no alteration in the mutant impaired in the mitochondrial peroxiredoxin, indicating that the lack of antioxidant potential was well compensated for and/or sensor sensitivity was not sufficient to detect changes. Although genetic interference with redox and antioxidant machineries has been used in other studies (ALBRECHT *ET AL.*, 2011), this approach comes with the problem of interfering with both, the reduction pathways for the sensor, as well as the antioxidant machinery, making it hard to draw clear-cut conclusions with respect to cause and effect. Yet, the mutant of the peroxisomal catalase 2 (*cat2*), does not interfere with the sensor reduction, as its activity is independent from electrons donated from the metabolism. Indeed, the mitochondrial roGFP2-Orp1 is slightly shifted towards oxidation as compared to control conditions, although the sensor is located to the mitochondrial matrix and not to the peroxisomes, where CAT2 is located. Thus hydrogen peroxide is likely to diffuse across different membranes. Localisation of the sensor directly to peroxisomes may increase the sensitivity for altered hydrogen peroxide levels in *cat2* background by lowering hydrogen peroxide dilution effects, but peroxisomal sensor lines were not available when the work was done.

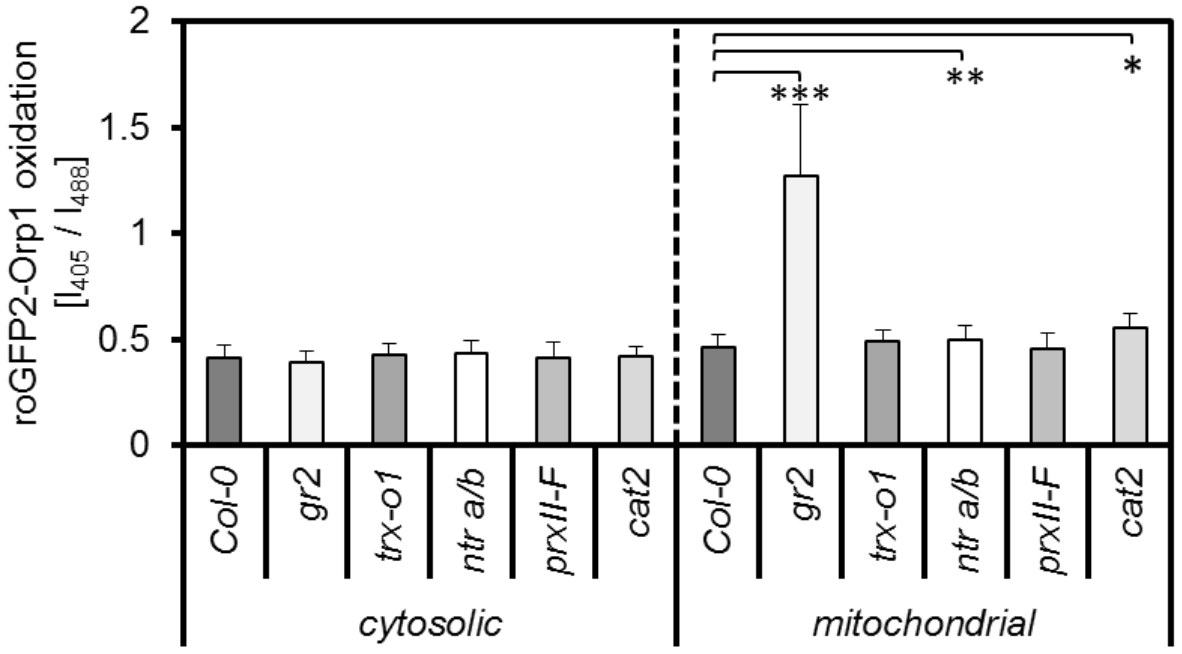

Figure 59: Steady-state of roGFP2-Orp1 in redox mutants. CLSM analysis of T-DNA insertion mutants of glutathione reductase 2 (*gr2*), thioredoxin-o1 (*trx-o1*), thioredoxin reductases a/b (*ntr a/b*), peroxiredoxin II-F (*prxII-F*) and catalase 2 (*cat-2*), expressing the roGFP2-Orp1 construct either in the cytosol or the mitochondrial matrix. Five-day-old Arabidopsis seedlings were investigated. The fluorescence ratios (sequential excitation: 405 and 488 nm; emission: 520 ± 15 nm) of roGFP2-Orp1 are shown (average +SD; *n* = 6 - 12 biological replicates; four images obtained per individual plant were pooled: one for the cotyledons, one for the hypocotyl, one for the root and one for the root tip; two-tailed, unpaired Student`s t-test: *p<0.05, **p<0.01, ***p<0.001).

2.7.6 Cytosolic roGFP2-Orp1 redox homeostasis in seeds in response to imbibition

The roGFP2-Orp1 sensor was characterised *in vitro* (*2.6*) and its *in vivo* responsiveness to endogenous produced hydrogen peroxide could be established (**Figure 58**). However, the glutathione-linked redox machinery in particular was shown to have a strong impact on the redox state of the sensor, as shown by using the matrix-localised sensor in the *gr2* background (**Figure 59**). Changes in glutathione redox potential may hence interfere with the read-out. Yet, monitoring hydrogen peroxide dynamics is expected feasible, if alterations in the E_{GSH} are controlled by simultaneously monitoring the E_{GSH} with the Grx1- roGFP2 sensor side-by-side (ALBRECHT *ET AL.*, 2011).
Hydrogen peroxide formation during quiescence release of imbibed seeds was reported by H_2-DCF-DA (SCHOPFER *ET AL.,* 2001). It was therefore attempted to monitor the roGFP2-Orp1 sensor response during seed quiescence release.
Seeds with cytosolic expression of roGFP2-Orp1 were analysed in response to imbibition analogously to the measurements performed with Grx1-roGFP2 and roGFP2 expressing seeds (**Figure 16 a** and **b)**. Also the cytosolic roGFP2-Orp1 sensor was reduced in a rapid manner biphasic at imbibition with water, indicated by an immediate decrease of the 400/482 nm ratio (**Figure 60**). The reduction of the sensor was initiated directly after imbibition, reaching a first plateau after 20 - 30 min. After 75 min of imbibition, the roGFP2-Orp1 sensor reached a second plateau. Generally the shape of the curve of roGFP2-Orp1 reduction fits to the curve of Grx1-roGFP2, showing no obvious differences in shape (**Figure 16 a**). This suggests that the redox state of the cytosolic roGFP2-Orp1 sensor in imbibed seeds is mostly influenced by the glutathione redox state and not by hydrogen peroxide produced during the onset of metabolism. Although roGFP2-Orp1 acts as a E_{GSH} sensor in early germination, the absence of any hydrogen peroxide effects on its kinetic fingerprint, as well as the strong reductive shift of the proteomes, suggest that the question of any significant hydrogen peroxide mediated oxidation during early germination may deserve re-visiting with suitable methodologies and rigour.

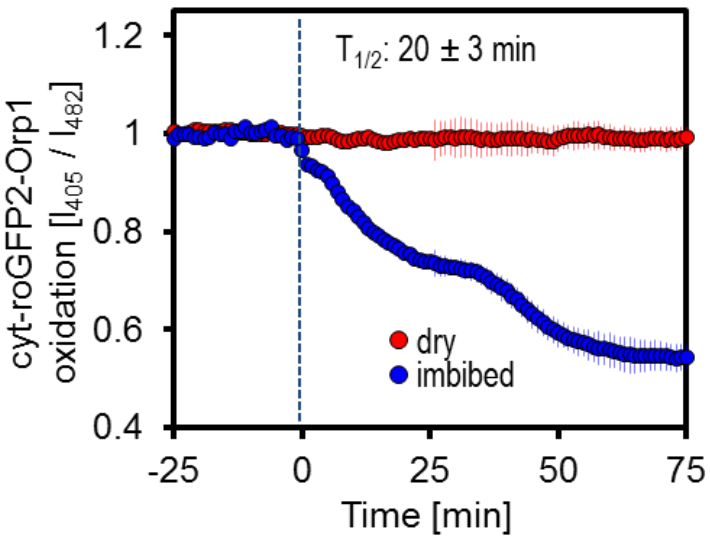

Figure 60: *In vivo* response of roGFP2-Orp1 to seed imbibition. Cytosolic roGFP2-Orp1 redox state of Arabidopsis seeds was monitored in a platereader. Wildtype seeds without sensor expression (Col-0) were used for auto-fluorescence correction. Dashed blue lines indicate start of imbibition with water. Seeds excited at 400 ± 5 nm and 482 ± 8 nm, emission at 530 ± 20 nm. The 400/482 nm ratio of whole seeds is plotted over time (average ±SD, *n* = 5 different seed batches). $T_{1/2}$ gives time point of half-maximal sensor response.

3. DISCUSSION

3.1 Rapid restart of the energy metabolism in imbibed seeds requires a refined concept of mitochondria in early germination

Dry seeds of spermatophytes were considered to be largely metabolically quiescent (BEWLEY 1997; HOLDSWORTH *ET AL.,* 2008; WEITBRECHT *ET AL.,* 2011). In response to imbibition, energy metabolism of seeds is restarted within minutes, indicated by a strong and immediate increase of the oxygen consumption (**Figure 7**) and the simultaneous phosphorylation pf AMP and ADP to ATP (**Figure 10** and **Figure 11**). This goes in line with observations by Paszkiewicz and colleagues (PASZKIEWICZ *ET AL.,* 2017), suggesting intact and differentiated mitochondria in dry seeds, which become metabolically and respiratorily active in response to imbibition. Observed respiration of imbibed seeds was temperature-dependent and was inhibited by the application of cyanide, an inhibitor of Complex IV of the mitochondrial respiratory chain. Already in 1981 similar observations were made in lettuce seeds (HOURMANT AND PRADET 1981), showing an increase of the oxygen consumption of imbibed seeds, while energy charge of adenosines was increased within 60 minutes. The described increase of adenosine energy charge was sensitive to cyanide and to a nitrogen atmosphere, suggesting that mitochondrial respiration is critical for the early establishment of energy charge. Furthermore, an increase of cytochrome *c* oxidase and ATPsynthase activity was described for maize embryos in response to imbibition, while oxygen was consumed (EHRENSHAFT AND BRAMBL 1990). Attucci and colleagues were able to detect oxidative phosphorylation in isolated mitochondria from dry sunflower seeds *in vitro* by supplementing different mitochondrial substrates (ATTUCCI *ET AL.,* 1991), and a proportion of the ATP formed in this study was dependent on the activity of the adenylate kinase located in the intermembrane space of mitochondria. The combined, cyclic activity of the adenylate kinase and of oxidative phosphorylation (**Figure 61**) may be also responsible for the rapid interconversion of AMP and ADP to ATP in Arabidopsis seeds in response to imbibition, observed here (*2.1.3,* **Figure 11**). Neither adenylate kinase activity, nor oxidative phosphorylation on their own are capable of converting AMP to ATP, making it reasonable to hypothesise about concerted action of both processes. Total adenylate pool sizes remained largely unchanged during imbibition, suggesting a dominating role of phosphorylation and not *de novo* synthesis. It must be emphasised that also substrate level phosphorylation (*e.g.* by glycolysis or by the TCA cycle) is very likely to contribute, and a clear discrimination cannot be made based on the available data. This is also supported by the occurrence of lactate in the imbibed seeds, emphasising the contribution of fermentation during early germination.

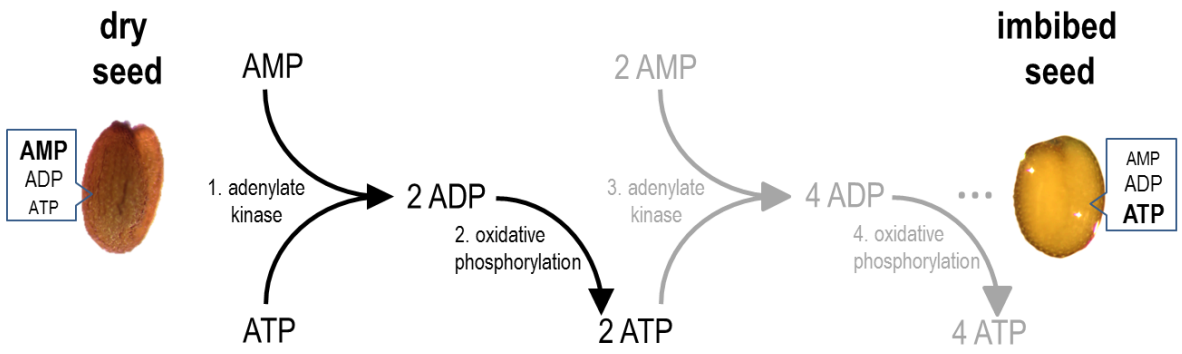

Figure 61: Model for the rapid phosphorylation of adenosines in seeds in response to imbibition. Dry seeds show a characteristic adenosine fingerprint with high amounts of AMP, intermediate amounts of ADP and low amounts of ATP. In response to imbibition, especially AMP levels are significantly diminished while ATP amounts increase. A cyclic, synchronised activity of the adenylate kinase and oxidative phosphorylation may explain the rapid interconversion of high amounts of AMP to ATP.

These observations for seeds of monocotyledons and dicotyledons suggest that the rapid restart of the (mitochondrial) energy metabolism in response to imbibition is a general phenomenon of orthodox seeds of spermatophytes. The rapid interconversion of AMP and ADP to ATP establishes an energy charge to fuel early germination processes with energy. Storage of high amounts of ATP in dry seeds would be unfeasible due to its instability. In addition to providing energy for germination processes, the energetic state of adenosine nucleotides regulates essential metabolic enzymes directly via cofactor availability or by substrate/product inhibition or activation (ATKINSON AND WALTON 1967; GEIGENBERGER *ET AL.*, 2010; NUNES-NESI *ET AL.*, 2013). Cofactor changes in seeds at imbibition are likely to impact directly on the regulation of different enzyme activities to regulate germinating-promoting processes.

These observations of seeds at imbibition give rise to several intriguing questions: do dormant seeds also show a rapid restart of energy metabolism or does distinct metabolic regulation contribute to dormancy? How is the start of energy metabolism regulated in commonly submerged seeds, *e.g.* of *Oryza sativa,* which can germinate under a normal oxygen atmosphere but also under hypoxic conditions? Is the diminished germination vigour of aged seeds associated with an impaired adenosine nucleotide energy charge and/or total pool size? The latter question was investigated by Kibinza and colleagues in aged sunflower seeds (KIBINZA *ET AL.*, 2006). Artificially aged seeds showed lowered total adenosine nucleotide pools, while their energetic state was not significantly affected at increasing moisture. Whether diminished adenosine nucleotide pools contributed to the lowered seed vigour or if it was just correlated with ageing was not examined in that study. But it has been shown that seed quality and germination vigour are associated with the respiratory capacity (WOODSTOCK AND GRABE 1967).

This work provides conclusive and consistent evidence suggesting that mitochondria in dry seeds are metabolically competent and energy metabolism is restarted immediately at imbibition (**Figure 7, Figure 10**, **Figure 11**, **Figure 14**, **Figure 16**, **Figure 17**, **Figure 18**). Yet, the question as to the status of mitochondria in dry seeds has been discussed controversial in recent times. There have been a number of reports suggesting that energetically-competent mitochondria were absent in dry seeds and that substantial biogenesis of pro-mitochondria is initially required before mitochondrial energy metabolism could commence (HOWELL *ET AL.*,

2006; LAW *ET AL.,* 2012; LAW *ET AL.,* 2014). Yet a membrane potential and ATP is required to drive protein import across the mitochondrial membranes (GEISSLER *ET AL.,* 2000; PFANNER AND GEISSLER 2001). Substantial mitochondrial biogenesis at imbibition of dry seeds is not in conflict with the observation of stored, respiratory competent mitochondria that are activated directly at imbibition. Stored pro-mitochondria that are respiratory competent, yet at limited capacity and/or efficiency, are likely to require a high degree of protein import to allow for the establishment of fully functional mitochondria and to boost mitochondrial number and volume. As such a refined concept of mitochondria in seeds is proposed in the light of the observations presented here, which brings together the strong points of both previously conflicting models.

3.2 The role of the cellular redox machinery on germination

Already in 1943, the fast appearance of reduced glutathione during the first four hours of germination was reported as a universal attribute of spermatophytes (HOPKINS AND MORGAN 1943), suggesting an important function of reduced glutathione in early germination. Using buthionine sulphoximine (BSO) treatment, inhibiting gamma-glutamylcysteine synthase catalysing the first step of glutathione biosynthesis, it could be shown that the rapid increase of reduced glutathione is mainly based on the reduction of stored, oxidised glutathione and not on *de novo* biosynthesis (TOMMASI *ET AL.,* 2001). This is in line with the observations made in this work using roGFP2-based fluorescent biosensors in the cytosol and in mitochondria at imbibition of Arabidopsis seeds (*2.1.6;* **Figure 16** and **Figure 18**) and HPLC-based measurements suggesting stable total glutathione content (**Figure 19**). In addition to its function in ROS detoxification, the glutathione pool can also modulate enzyme activities at central hubs of the primary metabolism in a redox-dependent manner through (de-)glutathionylation (*e.g.* HURD *ET AL.,* 2005). Although most evidence stems from mammalian systems, similar regulatory functions appear likely also in plants (DIXON *ET AL.,* 2005; MICHELET *ET AL.,* 2005). For several plant enzymes, also a thioredoxin-mediated redox regulation has been established. In chloroplasts, redox regulation of several Calvin-Benson-cycle enzymes is mediated via the ferredoxin/thioredoxin system in a light-dependent manner (WOLOSIUK AND BUCHANAN 1977). In the cytosol and in mitochondria, however, the thioredoxin-based redox systems are thermodynamically coupled to the primary carbon metabolism as source of NADPH, rather than photosynthetic electron transport (REICHHELD *ET AL.,* 2005; REICHHELD *ET AL.,* 2007). As such, the rapid reduction of the subcellular glutathione pools in seeds at imbibition (*2.1.6;* **Figure 16** and **Figure 18**) requires the formation of NADPH, since glutathione reductase 1 is strictly NADPH-dependent (MARTY *ET AL*., 2009). This implies that also the thioredoxin-based redox machinery is restarted in imbibed seeds when NADPH becomes available. Indeed *Medicago truncatula* seeds show an increased reduction of thioredoxin-linked proteins at imbibition (ALKHALFIOUI *ET AL.,* 2007) and similar findings were also made in germinating wheat seeds (BYKOVA *ET AL.,* 2011 a; BYKOVA *ET AL*., 2011 b). These observations, which appear largely consistent across monocotyledonous and dicotyledonous plant species, suggest that the rapid restart of the cellular redox machineries is a general characteristic of spermatophytes during early germination of orthodox seeds.

The physiological relevance of functional redox machineries for efficient germination in Arabidopsis was demonstrated by decreased germination rates for different mutant lines defective in thiol redox systems. The effects were particularly pronounced in aged seeds (*2.2.1* and *2.2.2;* **Figure 21**, **Figure 23** and **Tab. 1**). This germination phenotype is consistent

with previous observations in two of the mutants (DALOSO *ET AL.,* 2015). The specific underlying mechanism of the germination phenotype remains speculative given that the mutants affect different subcellular localisations (**Figure 21 c**), *e.g.* GR1 is dual-targeted to the cytosol and the peroxisomes (MARTY *ET AL.,* 2009; KATAYA AND REUMANN 2010), NTR a/b is dual-targeted to mitochondria and the cytosol (REICHHELD *ET AL.,* 2007) and GR2 is dual-targeted to plastids and mitochondria, although plastidic GR2 was complemented by expression under the endogenous promotor (MARTY *ET AL*., in preparation). Impairment of a single cell compartment only is expected in the *trx-o1* mutant (DALOSO *ET AL.,* 2015). That suggests that perturbation of redox homeostasis in the mitochondrial matrix is sufficient to cause an impairment of germination vigour. Yet, clear effects also in the *gr1* mutants suggest that the mitochondria are not the only compartment where redox regulation affects germination, and that thiol redox regulation may provide a more general mechanism across the cell to underpin efficient germination. The current data cannot distinguish if the decreased germination vigour is due to processes in early germination or is already set during seed filling and/or maturation. To that end, knowledge about *in situ* targets of the mitochondrial redox machinery provides critical clues towards the underlying molecular mechanisms of the redox regulation in germination.

Pioneering studies for the identification of *in vitro* targets of the different plant mitochondrial redox machineries were performed using isolated mitochondrial extracts (BALMER *ET AL.,* 2004; ROUHIER *ET AL.,* 2005; WINGER *ET AL.,* 2007; MARTI *ET AL.,* 2009; YOSHIDA *ET AL.,* 2013); a large number of potential targets were identified, but for most candidate proteins redox regulation was not verified under physiologically relevant conditions. A major constraint of the *in vitro* studies is that the endogenous thermodynamics, kinetics and structural constraints, which are at the centre of determining specificity in redox regulation are lost (reviewed in NIETZEL *ET AL.,* 2017). Those conditions were reconstituted in the isolated mitochondria system optimised in this work: intact and actively respiring mitochondria were used to establish rapid transition to a highly negative potential of the thiol redox machineries (as inferred by roGFP2-based measurements in the matrix) similar to the transition occurring in seeds *in vivo*. That is in contrast to the usage of mitochondrial protein extracts, in which structural organisation, including micro-compartmentalisation is lost, redox potentials of thiol pools are uncontrolled, *i.e.* strongly oxidising, and the reaction between the redoxins are irreversible rather than competitive. In an assay of similar design, addition of different TCA cycle substrates to isolated rat mitochondria successfully triggered the reduction of the mitochondrial glutathione pool (GARCIA *ET AL.,* 2010). This conceptual design was also applied with a different rationale in tobacco leaf mitochondria: Vanlerberghe and colleagues supplemented isolated mitochondria with different TCA cycle substrates to restart mitochondrial primary metabolism and the mitochondrial (thioredoxin) redox machinery in turn (VANLERBERGHE *ET AL.,* 1995). Application of specific substrates efficiently reduced mitochondrial alternative oxidase (AOX), while other substrates showed no reductive effect, suggesting effective reconstitution of the mitochondrial thioredoxin-linked redox machinery. Both mitochondrial redox machineries are dependent on the endogenous production of NADPH and reduction of the NADP pool requires substrates of NADP-dependent oxidoreductases, *e.g.* the NADP - dependent isocitrate dehydrogenase (MOLLER AND RASMUSSON 1998). Although supply with specific substrates to isolated Arabidopsis mitochondria triggered a marked decrease in matrix E_{GSH}, the E_{GSH} was not as negative as observed in mitochondria of intact tissues of green plants (SCHWARZLÄNDER *ET AL.,* 2008), indicated by only partial reduction of the matrix targeted roGFP2-Grx1 after citrate or succinate addition (*2.3.1;* **Figure 25**). The reason for this effect remains unclear, but potential

causes may include lowered internal glutathione concentration due to impaired glutathione import and/or partial loss during the mitochondrial purification procedure. In that case substrate addition still mimics the initial reduction phase of the oxidised mitochondrial glutathione pool in seeds at imbibition (**Figure 16**, **Figure 18** and **Figure 24**), even though not the full thermodynamic shift may be achieved for glutathione-dependent redox-switching, while thioredoxin-dependent targets would not be expected to be affected. The suitability of the isolated mitochondria as a model is further underpinned by the application of citrate, since this organic acid is particularly relevant as substrate of mitochondrial carbon metabolism in germinating seeds. When stored triacylglycerols of seeds are metabolised in peroxisomes by β-oxidation of fatty-acids, citrate is exported to mitochondria to fuel respiration of the germinating embryo (PRACHAROENWATTANA *ET AL.,* 2005).

3.3 Thiol-switched mitochondrial proteins at the global level

The quantification of the *in vivo* Cys-peptide redox states at a global scale has been established almost a decade ago (LEICHERT *ET AL.,* 2008), by making use of differential labelling with thiol-specific mass-tags and subsequent identification and quantification by mass spectrometry. The versatility of the differential thiol labelling technique OxICAT has been shown in several studies (LEICHERT *ET AL.,* 2008; BRANDES *ET AL.,* 2011; KNOEFLER *ET AL.,* 2012; BRANDES *ET AL.,* 2013; MENGER *ET AL.,* 2015) and OxICAT has often been considered the current gold standard for thiol redox proteomics. It offers many advantages over common gel-based approaches, with respect to sensitivity, reproducibility and the possibility to identify individual redox-switched cysteine residues. However, only two different isotopic mass-tags are available for the OxICAT strategy, which prohibits sample multiplexing. Hence an iodoTMT-based analysis of redox-switched Cys-peptides of the Arabidopsis mitochondria was chosen, which allows multiplexing and minimises technical variability as a result of sample preparation (THOMPSON *ET AL.,* 2003). While the redox state of ICAT-labelled peptides is quantified based on the characteristic mass differences of both mass-tags in the MS^1-step, iodoTMTs are isobaric and need to be fragmented to generate specific reporter ions with different molecular masses in the MS^2-step. The ICAT reagents have a molecular weight of 442 and 451 Da, respectively. All applied iodoTMTs have a molecular weight of 457 Da, but generate characteristic reporter ions of 126, 127, 128, 129, 130 or 131 kDa at MS/MS fragmentation. The ICAT-reagent and iodoTMTs differ in their chemical compositions and structures, which might cause different repulsion characteristics for native proteins affecting the binding affinity to certain proteins. For biotinylated iodoacetamide it has been suggested that its bulky structure prevents binding to certain cysteine residues (KIM *ET AL.,* 2000). Yet, the thiol-reactive groups of both tags are chemically identical.

IodoTMT-based quantification of the Cys-peptide redox state at a global scale was already successfully applied in mouse tissues (CHOUCHANI *ET AL.,* 2016) and embryonic kidney cells (ARAKI *ET AL.,* 2016). Both commonly used thiol-specific mass-tags for the differential thiol labelling strategy revealed a similar global Cys-oxidation pattern of identified peptides in several different organisms: in *Mus musculus*, *Homo sapiens*, *Drosophila melanogaster*, *Caenorhabditis elegans, Saccharomyces cerevisiae* and *Escherichia coli* peptides were on average partially oxidised with a mean Cys-oxidation of 5-25 %. These values mirror the same range as observed here for the substrate supplemented isolated mitochondria (**Figure 26**, **Figure 40** and **Figure 47**), suggesting a reasonable representation of

physiological redox conditions in this model. This is in agreement with observations based on genetically encoded fluorescent biosensors for E_{GSH} showing a highly reducing glutathione redox state in most subcellular compartments including the cytosol, the mitochondrial matrix and the peroxisomes (DOOLEY *ET AL.,* 2004; HANSON *ET AL.,* 2004; SCHWARZLÄNDER *ET AL*., 2008). An exception makes the ER (MEYER *ET AL.,* 2007), where more oxidising conditions have been consistently observed. This is also reflected by increased Cys-oxidation of peptides of the secretory pathway (BRANDES *ET AL.,* 2011; KNOEFLER *ET AL.,* 2012). Also in the isolated Arabidopsis mitochondria Cys-peptides with high oxidation levels of >85 % were identified (**Figure 26**, **Figure 40** and **Figure 47**). Several of these highly oxidised Cys are known to be exposed to the mitochondrial intermembrane space. There oxidation can be explained by the presence of an independent redox machinery allowing oxidative protein folding similar to the ER (RIEMER *ET AL.,* 2009; CARRIE *ET AL.,* 2010). For the reduction of protein thiols in response to the addition of respiratory substrates, functional endogenous machineries for metabolism and thiol reduction are required. None of the highly oxidised intermembrane space proteins were significantly reduced by the reactivated thiol redox machinery of the matrix, suggesting strict compartmentalisation and separation by the inner mitochondrial membrane. Redox-switched peptides of respiratory Complex I were orientated to the mitochondrial matrix, whereas peptides facing the intermembrane space were not redox-switched (**Figure 31 a**). Additionally, peptides that did not undergo redox-switching were overrepresented in proteins with plastidic or cytosolic annotation, while redox-switched peptides were typically annotated mitochondrial (**Figure 30**). For instance, several Cys-peptides of different RuBisCO subunits were identified as not redox-switched. Taken together these findings strongly argue for reduction specifically of matrix-exposed protein thiols triggered by the metabolically dependent restart of the matrix thiol redox machinery. The observed preferential reduction of matrix exposed proteins may allow the identification of proteins with so far unknown mitochondrial localisation *e.g.* caused by incorrect predictions or annotations or yet unknown dual-targeting. Dual-targeting has been reported as commonly underestimated for proteins targeted to organelles with endosymbiotic origin (BAUDISCH *ET AL.,* 2014). Yet, about 22.5 % of the identified redox-switched peptides were annotated as not mitochondrial and may be considered as a result of a non-specific reduction (**Figure 30 b**). Reduction of a non-mitochondrial protein thiol may be caused by during a very short time period of sample preparation: highly reactive protein thiols of non-mitochondrial origin may be partially reduced through redox equilibration with proteins previously reduced in the mitochondrial matrix and then released as a result of organelle lysis. The one-sided volcano plot for citrate supplemented mitochondria (**Figure 27 d**) reveals an uneven distribution of the Cys-oxidation states and almost all Cys-peptides were shifted towards reduction. This suggests unspecific reduction also of non-target proteins, providing evidence to a certain degree of redox equilibration. The volcano-plot for succinate supplemented mitochondria, does not show the same general shift and a more even distribution of Cys redox states, which may be explained by more rapid sample processing and/or better maintenance of mitochondrial integrity (**Figure 29 d**). A less negative redox potential established by succinate addition may also contribute, since the capacity for redox equilibration decreases with a smaller thermodynamic driving force of the genuine targets.

The histograms of mitochondrial Cys-peptides redox states show a typical and reproducible distribution with almost no peptide completely reduced or oxidised (**Figure 26**, **Figure 40** and **Figure 47**). Although intermediate redox states also dominated redox proteomes in several organisms investigated by OxICAT and iodoTMTs (LEICHERT *ET AL.,* 2008; BRANDES *ET AL.,* 2011; KNOEFLER *ET AL.,* 2012; BRANDES *ET AL.,* 2013; MENGER *ET AL.,*

2015; ARAKI *ET AL.,* 2016; CHOUCHANI *ET AL.,* 2016) this phenomenon raises further questions that have not yet been adequately discussed in the recent literature. *In vitro* OxICAT analysis of individual recombinant proteins, *e.g.* of the heat shock protein 33 (Hsp33), showed a rapid and complete conversion from full oxidation to full reduction, and *vice versa* (LEICHERT *ET AL.,* 2008). Such a binary situation may be intuitively expected for many Cys-peptides of the Arabidopsis mitochondrial proteome (and for any other proteome) as well. This would give rise to a distribution of redox states with two maxima close to 0 and 100 % oxidation. Yet, a majority of all identified Cys-peptides showed partial oxidation, similar to previous studies in different organisms (LEICHERT *ET AL.,* 2008; BRANDES *ET AL.,* 2011; KNOEFLER *ET AL.,* 2012; BRANDES *ET AL.,* 2013; MENGER *ET AL.,* 2015; ARAKI *ET AL.,* 2016; CHOUCHANI *ET AL.,* 2016). This suggests that during thiol-trapping by mass-tags, while proteins solubilise and denature, equilibration of the protein thiol redox states occurs allowing highly reduced protein thiols to react with highly oxidised Cys-peptides before the mass-tags can prevent further exchange by modification. This may be optimised in the future by using higher excess of mass-tags or novel tags with higher reactivity. This may also lower the impact of redox equilibration with non-mitochondrial proteins to minimise their unspecific reduction. The expected impact of redox equilibration on the data is a masking of small genuine redox-shifts, while strong redox-shifts are unlikely due to secondary equilibration. As such the observed redox-shifts may underestimate the endogenous values and may be regarded as a conservative measure for the most strongly shifted peptides. This is consistent with observations for the matrix located roGFP2-Grx1 sensor that showed a strong reductive shift when quantified spectroscopically, but this shift was slightly less pronounced at the level of Cys-peptides (*2.3.1*, **Figure 25 b**). Further, a technical effect commonly observed for MS^2-based quantification of reporter ions may also contribute to the observation of a Cys-peptide redox profiles dominated by partial oxidation: multiple, different peptides can be accidentally co-selected at the same retention time as a target peptide for fragmentation of MS/MS identification, an effect called *ion-suppression* (CHRISTOFOROU AND LILLEY 2012). This leads to the simultaneous generation of reporter ions from different Cys-peptides with different redox states and thus, to the determination of the average redox state of both co-selected peptides. The chance for co-selection of peptides increases with sample complexity. Yet, although this affect may contribute, it cannot alone account for the observed partial oxidation at the global scale. Also OxICAT-based studies, where label quantification occurs at the MS^1-level showed similar characteristics (*e.g.* MENGER *ET AL.*, 2015).

Although a systematic, technical component to the observed redox-shifts appears likely and the data must be critically appraised accordingly, potential systematic artefacts are likely to be small at the quantitative level. This is confirmed by the identification of archetypical redox proteins amongst the most strongly redox-shifted Cys-peptides and the highly oxidised peptides with Cys exposed to the mitochondrial intermembrane space (**Tab. 2**). Further the measurements showed very high reproducibility allowing for a robust quantification and comparison of global effects in protein thiol redox states (*e.g.* **Figure 26**, **Figure 27**, **Figure 28** and **Figure 29**).

3.4 Thiol-switched proteins involved in primary metabolism

Among the most strongly redox-shifted Cys-peptides, several catalytic cysteine residues were identified, *e.g.* of the GR2, NTR a/b and TRX-o1 (**Tab. 2**). Utilisation of immunoenrichment of TMT-labelled Cys-peptides allows for the identification also of low abundant thiol proteins, such as TRX-o2 (**Tab. 2**). So far this protein had not been identified at the proteomic level and evidence for its expression had been solely based on the mRNA level. Here a peptide of the TRX-o2 with the AA sequence DGSLPSVFYFTAAWCGPCR was identified. Although this peptide is not unique based on its AA sequence, since TRX-o1 contains an identical sequence, it can be unambiguously assigned to the TRX-o2, due to a unique N-terminal trypsin-recognition-site. By contrast, tryptic digest of TRX-o1 can only give rise to a distinct peptide (AQDGSLPSVFYFTAAWCGPCR). Although TRX-h2 was previously also reported mitochondrial (MENG *ET AL.,* 2010), this localisation has been a matter of controversial discussion and no corresponding peptide was identified in this work. While the absence of a peptide in a proteomics approach should not be taken as evidence for its absence *in situ*, the other two mitochondrial TRXs were reliably detected and TRX-h2 was recently shown to localise to the secretory pathway (TRAVERSO *ET AL.,* 2013). Several Cys-proteins were identified by their catalytic CxxC motif, which is present in many thiol-based oxidoreductases. This shows the effective restart of the different thiol-based redox machineries of the mitochondrial matrix but does not necessarily reflect regulatory redox-switching.

In addition to the proteins that are well-established players of the mitochondrial thiol redox machinery, several peptides involved in mitochondrial iron-sulfur-cluster-assembly were identified. High reactivity of functional cysteines involved in iron-sulfur-cluster-assembly was already described in human cancer cells (WEERAPANA *ET AL.,* 2010). In a similar recent screen for highly reactive cysteines in isolated mitochondria of human cancer cells, several proteins of the electron transport chain and of the TCA cycle were identified, albeit under non-physiological thermodynamic conditions (BAK *ET AL.,* 2017). Yet, those findings are in line with this work on Arabidopsis mitochondria, where enzymes of the TCA cycle and of the respiratory chain were also identified as hotspots of redox-switching (**Figure 31** and **Figure 32**). Redox-switched and potentially redox-regulated enzymes of mitochondrial energy metabolism may enable fine-tuning of respiration to ensure efficient usage of the limited stored resources of the seed for effective provision of carbon skeletons and energy to drive germination (working-model in **Figure 62**). Efficient germination to enable rapid growth and competition for environmental resources is likely to be a trait under strong selection.

Redox regulation of different TCA cycle associated enzymes was studied *e.g*. for citrate synthase (SCHMIDTMANN *ET AL.,* 2014), fumarase and succinate dehydrogenase (DALOSO *ET AL.,* 2015), as well as isocitrate dehydrogenase (YOSHIDA AND HISABORI 2014). Interestingly, mutants of the mitochondrial redox machinery show pronounced alterations in the citrate/isocitrate content in imbibed seeds (**Figure 38 b**). It may be speculated that changes in citrate/isocitrate content are associated with redox regulation of mitochondrial isocitrate dehydrogenase, although in more general cause and effect are often less directly linked in the metabolic network. Although peptides of mitochondrial MDH were redox-switched in the reconstituted, isolated mitochondria (**Figure 32**), MDH activity was found insensitive to thiol redox changes *in vitro* (YOSHIDA AND HISABORI 2016). Yet, this does not rule out redox regulation *in vivo*, because redox-switching may not always result in direct changes of activity, but may also affect protein localisation, folding or complex formation (see *1.3*.).

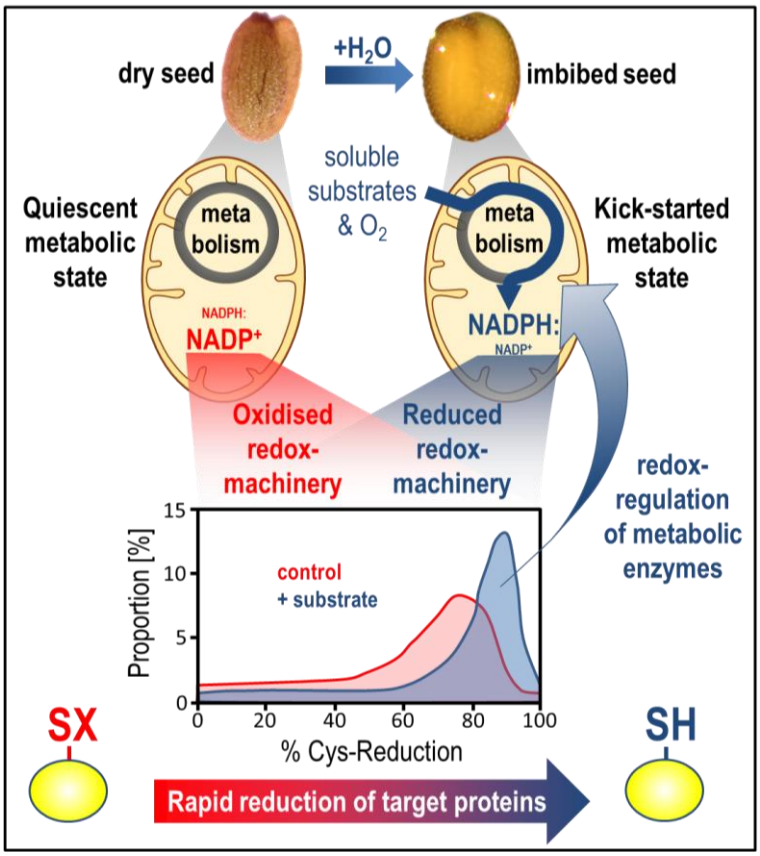

Figure 62: Working model for kick-starting the mitochondrial redox control in Arabidopsis seeds at imbibition. Dry *Arabidopsis* seeds show quiescent metabolism, due to internal hypoxia and/or lack of available substrates. At imbibition, oxygen and soluble substrates become available, allowing for onset of flux through mitochondrial metabolism. $NADP^+$ is reduced to NADPH, due to flux through specific dehydrogenases, providing reductant to the matrix thiol redox machinery and allowing reduction of downstream target protein cysteines. Reduction may result in redox regulation, either activating or inactivating specific proteins. MS-based thiol labelling techniques, *e.g.* differential thiol labelling with iodoTMTs, allow for the identification of protein cysteines that undergo redox-switching. Among all identified redox-switched proteins, key-positions of the mitochondrial energy metabolism are prominent, suggestive of a role for redox regulation of energy metabolism during early phases of imbibition.

The AOX of the inner mitochondrial membrane is often considered the classic example of a redox-regulated enzyme in plant mitochondria (*e.g.* VANLERBERGHE *ET AL.*, 1995). Yet, no Cys-peptide for any AOX isoform was identified by the iodoTMT labelling approach. A technical constraint of the proteomics may account for the absence: only TMT-tagged Cys-peptides were considered for peptide identification and quantification. The AA sequences of the most highly expressed AOX isoforms (AOX1a - AT3G22370; AOX1b - AT3G22360 and AOX1c - AT3G27620) contain trypsin cleavage sites directly upstream and downstream of the cysteine residue involved in the disulfide bridge formation, predicting a tryptic peptide of five AA. Yet, peptides with less than seven AA are excluded from the analysis to allow for the unambiguous identification of proteins (*4.4.9*). As a result many peptides are lost from analysis and proteins were typically identified by a small number of peptides, covering only short stretches on the full length protein. To increase the number of unique peptides from a sample other proteases with distinct cleavage sites could be utilised in conjunction to trypsin to generate an orthogonal set of Cys-peptides. Depending on the specific protease, such an approach would be likely to identify also the redox-active AOX peptide.

Several enzymes involved in mitochondrial amino acid metabolism were also identified as redox-switched, *e.g.* different aminotransferases (**Figure 33** and **Figure 34**). In addition, seeds from mutant lines impaired in their thiol redox machineries showed pronounced alterations in amino acid contents at imbibition (**Figure 39**). Aminotransferases catalyse reactions, in which an amino group from one amino acid is transferred to an α-keto acid. Thus, the turn-over of different amino acids is tightly coupled to the content of different organic acids of the TCA cycle. The interconversion of amino acids and organic acids may contribute to the metabolic fine-tuning and the C/N balance during early germination. When storage proteins are degraded and free amino acids were mobilised and accumulate during germination, metabolic adjustments are necessary to match supply and demand. Of particular interest may be the mitochondrial Δ-1-pyrroline-5-carboxylate dehydrogenase 12A1 (AT5G62530), a protein involved in the degradation of proline to glutamate. For this protein in total three unique Cys-peptides were identified as redox-shifted. Interestingly, in seeds of the *gr2* background the amount of proline was increased at imbibition, whereas the other redox mutants did not show significant alterations in their proline content. This may suggest glutathionylation-dependent redox regulation of the enzyme. Proline was frequently described as an important osmo-protectant accumulating in dehydrated plants counteracting the effects of osmotic stress, and proline degradation is particularly active at rehydration (YOSHIBA *ET AL.,* 1997). Also mature plant embryos face dehydration during seed maturation, making proline degradation after imbibition plausible. Indeed proline contents of Arabidopsis seeds are high and an important role of proline for germination was suggested (VERBRUGGEN AND HERMANS 2008; SZABADOS AND SAVOURE 2010).

Cysteines identified as redox-switched by thiol redox proteomics have to be tested individually for the impact on enzyme activity *in vitro* and *in vivo*. For specific identified proteins, *e.g.* for mitochondrial sulfurtransferase, thiol-switching has already been shown to have a direct impact on the enzyme activity. Interaction with the thioredoxin redox machinery was recently shown and mutation of the individual cysteines affected enzyme activity (BUROW *ET AL.,* 2002; HENNE *ET AL.,* 2015). Interestingly a germination phenotype was reported for the double mutant of the mitochondrial and the cytosolic sulfurtransferases (mitochondrial STR1 and cytosolic STR2; MAO *ET AL.,* 2011). As such, impaired sulfurtransferase activity may contribute to the observed lowered germination vigour described in *2.2.1* and *2.2.2* as a direct consequence to disturbed redox regulation in the redox mutants. If sulfurtransferases are indeed differentially redox-regulated in the mitochondrial redox mutants was not resolved by the redox proteomics approach applied in this work. Nevertheless, specifically redox-switched protein thiols may be assumed to show perturbed redox states in mutants with impaired redox machineries, unless redundancy of other redox systems can compensate. Based on the clear germination vigour phenotypes, especially in artificially aged seeds of the different redox machineries, only partial redundancy appears to exist between the redox systems.

3.5 Differentially thiol-switched proteins in mutants of the thiol redox systems

Only very few proteins were identified with significantly changed Cys-oxidation states in both mutants with impaired thioredoxin-based redox machinery (*2.5.1*). The *ntr a/b* mutant was characterised as a complete, functional knock-out (REICHHELD *ET AL.,* 2007) and indeed no peptides were identified in the corresponding isolated mitochondria (**Figure 43 b**). Consequently pronounced oxidation of all mitochondrial thioredoxin targets was expected, given that the reductant supply of the mitochondrial thioredoxins should be blocked. A similar experimental rationale applied to the *trx-o1* mutants, the only plant mitochondrial thioredoxin that had been unambiguously confirmed at the protein level (DALOSO *ET AL.,* 2015). The lack of stronger redox perturbations in the thiol redox proteome of the *trx-o1* background may be due to residual TRX-o1 activity, given that the active side peptide was still detectable at low abundance (**Figure 43**) and/or functional redundancy between the two mitochondrial thioredoxin isoforms, given that TRX-o2 could be detected in the dataset (see *2.3.2,* **Tab. 2**). Analysis of a now available *trx-o1* x *trx-o2* double mutant (YOSHIDA AND HISABORI, 2016) will avoid potential isoform redundancy in the future. However, for Arabidopsis mitochondria no thioredoxin reductase other than NTR a and NTR b is known. This suggests partial functional backup in the *ntr a/b* background by other redox systems, *e.g.* by the GR/glutathione-system, as previously suggested by Reichheld and colleagues (REICHHELD *ET AL*., 2007). Effective crosstalk and functional backup between the glutathione-dependent and the thioredoxin-dependent redox machineries was described in both directions (REICHHELD *ET AL.,* 2007; MARTY *ET AL*., 2009 and **Figure 63 b**). For mutants impaired in one of the two mitochondrial redox machineries only, no pronounced germination phenotype is observable when seeds are fresh, but germination vigour is negatively affected in aged seeds. Yet, the simultaneous disruption of both, the mitochondrial thioredoxin-/ and the glutathione-dependent redox systems leads to severe germination defects. Most seeds fail to germinate and those that germinate, die within the next days, as shown by BSO treatment of *ntr a/b* seeds (REICHHELD *ET AL.,* 2007) or by crossing of the *gr2* mutant (complemented for plastid expression) with the *ntr a/b* double mutant (MARTY *ET AL*., in preparation). The observation that roGFP2-Grx1 can still be reduced in isolated mitochondria of *gr2* background (**Figure 46**), suggests that the matrix glutathione pool can receive electrons from the thioredoxin system similar to what has been found previously for the cytosol (MARTY *ET AL*., 2009). RoGFP2-Grx1 sensor reduction in the absence of GR2 is in line with the redox proteomics of *gr2* mitochondria, in which median Cys-peptide oxidation was only slightly increased (*2.5.2*) and only a small group of Cys-peptides showed altered Cys-oxidation. Albeit statistics could only be performed for non-energised *gr2* mitochondria, the available data from succinate supplemented mitochondria of *gr2* background show pronounced reduction of the median Cys-oxidation state by a degree comparable to wildtype mitochondria. This suggests that crosstalk between the thioredoxin-/ and glutathione-dependent redox-machineries is very efficient making identification of specific endogenous targets of either system a challenge. Yet, the presence of one of the systems appears essential to allow seed germination and seedling growth, since disruption of both systems in parallel leads to lethality (see working-model in **Figure 63 a**).

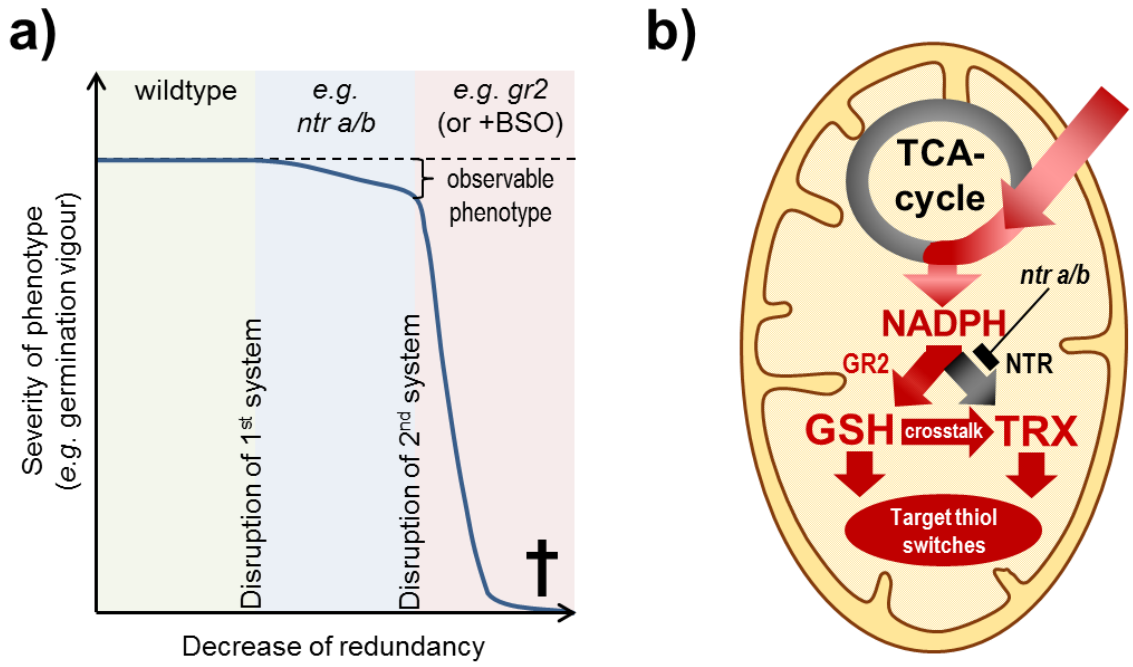

Figure 63: Model of the relationship between phenotype and redundancy of the mitochondrial thiol redox systems in Arabidopsis. a) Arabidopsis mutants with defects in a single redox pathway, *e.g.* impaired in the NADPH-dependent thioredoxin reductase (*ntr a/b* background) are viable, which suggests partial redundancy of the different redox-machineries. Phenotypes are only caused under added pressure to the system, *e.g.* by seed ageing. Additional disruptions of the second redox pathway, *e.g.* by knockout of matrix glutathione reductase (*gr 2* background), or glutathione depletion by buthionine sulphoximine treatment (BSO), leads to lethality directly after germination (MARTY *ET AL.*, in preparation; REICHHELD *ET AL.,* 2007). b) Exemplary model for the crosstalk between the glutathione and the thioredoxin-dependent redox systems in *ntr a/b* background. Similar crosstalk applies for the *gr2* mutant, *vice versa*, yet with inverse direction of the backup electron flux.

3.6 Monitoring of hydrogen peroxide with the probe roGFP2-Orp1

The hydrogen peroxide sensor roGFP2-Orp1 (GUTSCHER *ET AL.,* 2009) was successfully applied in several organisms including flies (ALBRECHT *ET AL.,* 2011) and mice (FUJIKAWA *ET AL.,* 2016), but not yet in plants. Sensors of the HyPer family have seen more usage, including in Arabidopsis, despite severe risks of pH artefacts (*e.g.* ROMA *ET AL.*, 2012; SCHWARZLÄNDER *ET AL.,* 2014). RoGFP2-Orp1 was unresponsive to pH changes in the physiological range, which makes for a decisive advantage over the sensors of the HyPer family. In this work, the roGFP2-Orp1 steady-state read-out was found to be dominated by E_{GSH} -dependent reduction *in vitro* and *in vivo*. Reduction by the thioredoxin system had a minor impact, probably due to less efficient kinetics of the interaction. Hence, the *in vivo* probe response reflects the steady-state balance between the rates of oxidation and reduction and consequently an oxidative shift of the probe might be caused by different hypothetical scenarios:

1. by an increased rate of oxidation by hydrogen peroxide, as a result of increased production and/or decreased scavenging

2. by a decreased rate of reduction by the endogenous thiol redox systems; under conditions that lead to oxidation of the thiol redox machineries even draining electrons from the sensor may occur, due to the reversible nature of the thiol exchange reaction

The different factors that influence the redox state of the probe requires caution with the mechanistic interpretation of recorded data. Side-by-side comparisons with the E_{GSH} biosensor Grx1-roGFP2 appear sensible to explore the impact of potential changes in the glutathione redox potential. Especially in physiological situations characterised by a highly dynamic E_{GSH}, *e.g.* as observed in this work at seed imbibition (*2.1.6*), side-by-side comparisons with Grx1-roGFP2 appear critical to estimate the specific contributions to the sensor read-out by hydrogen peroxide. However, the impact of the endogenous thioredoxin-dependent redox systems on the probe cannot be controlled for, since currently no thioredoxin redox sensor is available. That said, endogenous hydrogen peroxide detoxification may also affect the reduction of the glutathione and thioredoxin systems, leading to a situation where cause and effect are notoriously difficult to disentangle, owing to the interconnected topology of the cellular antioxidant network. Hence roGFP2-Orp1 (like the HyPer sensors) may be more appropriately regarded as integrative sensor for the interface between hydrogen peroxide and thiol redox balance. As such it reports what endogenous proteins with similar sensitivities would undergo when changes in the redox network occur.

Both peroxidases, Orp1 of roGFP2-Orp1 and OxyR of the HyPer-sensor are characterised by a reactivity for hydrogen peroxide that is about 100 times slower than that of the typical 2-Cys peroxiredoxins (MORGAN *ET AL.,* 2016). In combination with a highly negative E_{GSH} *in vivo*, the sensitivity of the roGFP2-Orp1 sensor for the detection of hydrogen peroxide is likely too low to monitor baseline hydrogen peroxide levels; instead the sensor may be most suitable to transient of high hydrogen peroxide concentration with subcellular resolution. This limitation in sensitivity may be overcome by the application of recently developed sensors with improved sensitivity for hydrogen peroxide, *e.g.* the roGFP2-Tsa2, which is based on the fusion of roGFP2 to a 2-Cys peroxiredoxin (MORGAN *ET AL.,* 2016). Yet, the expression of artificial peroxidases with high affinity for hydrogen peroxide, which allows baseline hydrogen peroxide monitoring, may alter the endogenous hydrogen peroxide homeostasis and thus, the development of `passive` probes, which do not react with hydrogen peroxide, would be beneficial.

Taken together the Arabidopsis roGFP2-Orp1 sensor lines established and characterised in this work enable monitoring of hydrogen peroxide in plants, minimising the risk of *e.g.* pH caused artefacts; but measurement require careful setup and interpretation to obtain results that carry specific mechanistic meaning. That will avoid problems as those that have been observable in several published reports using the HyPer sensors, while opening the door to novel and meaningful discovery on subcellular redox dynamics in plants.

4. MATERIAL & METHODS

4.1 Technical equipment and consumables

4.1.1 Laboratory equipment

A1000 plant growth chamber	Conviron, www.conviron.com
Airstream® Class II Biological Safety Cabinet	ESCO, www.escoglobal.com
Analytical Balance Summit SI-234	Denver Instrument, www.denverinstrument.com
Beckman Centrifuge Avanti® J-26-XP	Beckman, www.beckmancoulter.com
Beckman Rotor JA-25.50	Beckman, www.beckmancoulter.com
Beckman Rotor JA-10	Beckman, www.beckmancoulter.com
CLARIOstar® platereader	BMG, www.bmglabtech.com
Electroporator MicroPulser™	Bio-Rad, www.bio-rad.com
Eppendorf BioPhotometer Plus	Eppendorf, www.eppendorf.de
Eppendorf Centrifuge 5430	Eppendorf, www.eppendorf.de
Eppendorf Centrifuge 5424 R	Eppendorf, www.eppendorf.de
Eppendorf Thermomixer™ Comfort	Eppendorf, www.eppendorf.de
Eppendorf Thermomixer™ Compact	Eppendorf, www.eppendorf.de
Gel documentation MF-ChemiBIS 2.0	DNR Bio-Imaging Systems, www.dnr-is.com
GC-MS-QP2010 Plus	Shimadzu, www.shimadzu.de
HPLC Autosampler 717 plus	Waters, www.waters.com
HPLC column Nova-Pak™ C18, 4.6 x 250 mm	Waters, www.waters.com
HPLC Controler and pump 600E	Waters, www.waters.com
HPLC fluorescenc-detector Shimadzu RF 551	Shimadzu, www.store.shimadzu.com
Incubators 37 °C Ecotron Typ ET25-TA-00	INFORS HT, www.infors-ht.com
Labculture® Vertical laminar flow cabinet	ESCO, www.escoglobal.com
Leica M165FC stereomicroscope	Leica, www.leica-microsystems.com
Leica DCF425C camera	Leica, www.leica-microsystems.com
Magnetic Stirrer MR Hei-Mix L	Heidolph, www.heidolph-instruments.de
MS/MS Thermo-Scientific Orbi Trap Velos Pro™	Thermo Scientific, www.thermoscientific.com
MS/MS Thermo-Scientific Orbi Trap Q-Exactive™	Thermo Scientific, www.thermoscientific.com
Nanodrop™ 2000c	Thermo Scientific, www.thermoscientific.com
Orbital platform shaker Unimax 1010	Heidolph, www.heidolph-instruments.de
Oxygraph Clark-type oxygen electrode	Hansatech Instruments, www.hansatech-instruments.com
pH-Meter FE20 – FiveEasy™	Mettler Toledo, www.mt.com
Plant growth chambers	Jan Weiler GmbH
POLARstar® Omega platereader	BMG, www.bmglabtech.com
Precision Balance TP1502	Denver Instrument, www.denverinstrument.com
Spectro-fluorometer JASCO FP-8300	JASCO, www.jasco.de

TKA LabTower EDI water purification system	Thermo Electron LED, www.thermofisher.com
UV-lamp, portable	M&S, www.m-und-s-laborgeraete.de
Vacuum concentrator Savant® DNA 120	Thermo Scientific, www.thermofisher.com
Vortex mixers Scientific Industries	Scientific Industries, www.scientificindustries.com
Zebron ZB 5MS column	Phenomenex, www.phenomenex.com
Zeiss Axio Observer Z1 Zeiss	Zeiss, www.zeiss.de
Zeiss confocal microscope LSM780	Zeiss, www.zeiss.de
Zeiss Plan-Apochromat 63x/1.40 Oil DIC M27	Zeiss, www.zeiss.de

4.1.2 Consumables

General chemicals were purchased from Applichem (www.applichem.com/home), Sigma-Aldrich (www.sigmaaldrich.com), Duchefa (www.duchefa-biochemie.com), Merck (www.merckmillipore.de) and Roth (www.carlroth.com). General plastic ware was purchased from Sarstedt (www.sarstedt.com/home) and VWR (de.vwr.com/store). Micropore™ tape was purchased from 3M (www. 3mdeutschland.de).

4.1.3 Enzymes

Proteinase K, BP and LR clonase II enzyme mix for Gateway® cloning were purchased from Invitrogen™ (www.thermofisher.com). Phusion® High-Fidelity DNA Polymerase and Taq™ DNA Polymerase were obtained from New England Biolabs (www.neb.com). Pierce™ Trypsin Protease was purchased by Thermo Scientific™ (www.fishersci.de).

4.1.4 Specific chemicals, antibodies, materials and commercial kits

HisTrap™ Chelating HP column	GE Healthcare Life Sciences, www.gelifesciences.com
Immobilised Anti-TMT™ Antibody Resin	Thermo Scientific, www.thermofisher.com
iodoTMT™ Elution Buffer	Thermo Scientific, www.thermofisher.com
iodoTMTsixplex™ Isobaric Mass Tagging Kit	Thermo Scientific, www.thermofisher.com
MitoXpress®Xtra oxygen detection kit	Luxcel Biosciences, www.luxcel.com
NucleoBond® PC 100	Macherey-Nagel, www.mn-net.com
NucleoSpin® Plasmid mini	Macherey-Nagel, www.mn-net.com
NucleoSpin® Gel and PCR Clean-up	Macherey-Nagel, www.mn-net.com
Zeba™ Spin Desalting Columns	Thermo Scientific, www.thermofisher.com

4.1.5 Software

BMG Omega MARS Data analysis v2.10 R3	BMG, www.bmglabtech.com
BMG Omega MARS Data analysis v3.10 R4	BMG, www.bmglabtech.com
EndNote X5	Thomson Reuters, www.endnote.com

FinchTV v. 1.4.0 sequence viewer	PerkinElmer www.geospiza.com/ftvdlinfo.html
GraphPad Prism® 6.01 and 7.01	GraphPad Software, www.graphpad.com
Leica Application Suite	Leica, www.leica-microsystems.com
MatLab-based ratiometric imaging software	Prof. M. Fricker, www.markfricker.org
MaxQuant v. 1.5.5.1	Prof. J. Cox, www.coxdocs.org/
Oxygraph Plus v. 1.02	Hansatech Instruments, www.hansatech-instruments.com
SerialCloner 2.6.1	SerialCloner, serialbasics.free.fr
ZEN 2011 black and blue edition	Zeiss, www.microscopy.zeiss.com

4.1.6 Online resources and databases

Arabidopsis subcellular database	SUBA3, suba3.plantenergy.uwa.edu.au
Kyoto Encyclopedia of Genes and Genomes	KEGG pathways, www.genome.jp/kegg/pathway.html
The Arabidopsis Information Resource	TAIR10, www.arabidopsis.org
Universal Protein Resource database	UniProt, www.uniprot.org

4.2 Plant methods

4.2.1 Plant material

Arabidopsis thaliana ecotype Columbia-0 (Col-0; referred to as wildtype) was used as control for plant experiments. Analysed mutants are listed in **Tab. 7**. Additionally, Col-0 plants and mutants highlighted with a black dot (●) were transformed with pBinCM:SHMT-roGFP2-Grx1 (Ubi10) for the redox proteomics approach. Col-0 plants and mutants labelled with a white dot (○) were additionally transformed with pH2GW7:mt-roGFP2-Orp1 and pH2GW7:cyt-roGFP2-Orp1. Acronyms of the mutants are used within this thesis.

Tab. 7: *Arabidopsis thaliana* T-DNA insertion lines.

acronym	name	locus	line	characteristics
gr1	*gr1-1*	At3g24170	SALK_105794	*gr1* T-DNA insertion (MARTY *ET AL.*, 2009)
gr2 *(●○)*	*gr2-1 epc. 2*	At3g54660	SALK_040170	*gr2* T-DNA insertion, complemented with plastidic GR2 under endogenous promoter (MARTY *ET AL.*, in preparation)
ntr a/b *(●○)*	*ntr a x ntr b*	At2g17420 At4g35460	SALK_539152 SALK_545978	double mutant of *ntra* and *ntrb* T-DNA insertions (REICHHELD *ET AL.*, 2007)
trx-o1 *(●○)*	*trx-o1*	At2g35010	SALK_042792	*trx-o1* T-DNA insertion (DALOSO *ET AL.*, 2015)
prxII-F *(○)*	*prxII-F-1*	At3g06050	GK-114G01	*prxII-f* T-DNA insertion (FINKEMEIER *ET AL.*, 2005)
cat2 *(○)*	*cat2-1*	At4g35090	SALK_057998	*cat2-1* T-DNA insertion (QUEVAL *ET AL.*, 2007)

4.2.2 Stable transformation of Arabidopsis by `floral dip`

Arabidopsis plants were transformed according to the protocol established by CLOUGH AND BENT 1998. Plants were grown on soil under long-day conditions for five to six weeks. After bolting, first stems were removed to trigger the formation of multiple secondary stems with an increased number of flowers. *Agrobacterium tumefaciens* C58C1 cells transformed with the desired binary expression vector system were cultured in 5 ml LB-medium (1 % (w/v) tryptone, 0.5 % (w/v) yeast extract, 1 % (w/v) NaCl, pH 7.0 with NaOH) under antibiotic selection (*e.g.* 100 µg/ml ampicillin, 50 µg/ml kanamycin and 50 µg/ml rifampicin) for about 24 h at 28°C and 180 rpm. The pre-culture was then used to inoculate 250 ml of fresh selective medium. After a further 24 h of cultivation under the same conditions, cells were harvested by centrifugation for 10 min at 5.000 *g*. Supernatant was discarded and bacterial pellet was resuspended in dipping medium (5 % (w/v) sucrose and 0.02 % (v/v) of the surfactant Silwett *L-77*, www.momentive.com) to a final $OD_{600\,nm}$ of 0.8 - 1.0. The flower buds were dipped into the Agrobacteria solution for about 10 s. Dipped plants were stored in the dark overnight at room temperature and under high humidity. Plants were then cultivated under standard long-day conditions for fast development of seeds. Optionally, dipping procedure was repeated after one week to increase the transformation efficiency. Seeds were harvested and grown on half-strength MS-medium supplemented with 0.8 % (w/v) Phytagel™ for selection of successfully transformed plants making use of sensor fluorescence marker (*4.6.6*).

4.2.3 Harvesting of Arabidopsis seeds and long-term storage

After one month of after-ripening at 20°C in the siliques, seeds of synchronised Arabidopsis plants were harvested side-by-side and individually for each plant. Because seeds of the same plant originating from different siliques can be in different maturation stages, only dry seeds falling out of the siliques without usage of inadequate external force were harvested to minimise biological heterogeneity. Seeds were either directly used or prepared for long-term storage to preserve germination vigour. Seeds were stored in paper envelopes in a sealed plastic box containing dry silica gel to reduce air moisture. For long-term storage, the plastic box containing the dry seeds was stored at -20°C.

4.2.4 Surface sterilisation of Arabidopsis seeds and in vitro *cultivation*

Arabidopsis seeds were incubated in 70 % (v/v) ethanol for 2 min and dispersed on sterile filter paper for complete drying under a laminar flow hood. Individual seeds were picked with a sterile toothpick and transferred to growth medium (0.5x MS-medium, 0.8 % (w/v) Phytagel™, ±1 % (w/v) sucrose, 10 mM MES pH 5.8 with KOH) in a petri dish. Seeds were either directly transferred to the growth cabinet or initially stratified in the dark at 4°C for 48 h. Growth cabinet was set to a diurnal cycle (16 h light at 22°C followed by 8 h darkness at 18°C; light intensity of about 50 - 75 $\mu Em^{-2}s^{-1}$). After a growth phase of ten to twelve days, individual seedlings were transferred to soil.

4.2.5 Estimation of the germination efficiency of Arabidopsis seeds

Synchronised, non-dormant Arabidopsis seeds were grown on 0.5x MS-media as described in *4.2.4* without prior stratification. Media was either prepared with or without 1 % (w/v) sucrose. Seeds of different mutant lines were grown on the same petri-dish

side-by-side to compensate for plate effects. Germination rates were recorded daily at the same time point for a timeframe of five days. Penetration of the testa and the endosperm was used as the criterion for successful germination (**Figure 22**) and was determined with a stereomicroscope (Zeiss, Stemi 2000).

4.2.6 Plant growth on soil for seed propagation

After ten to twelve days of synchronous *in vitro* culture (*4.2.4*), seedlings were transferred individually to imbibed Jiffy-7® pellets or to imbibed soil mixture (ten parts of Floradur® B-seed, one part of Perlite Perligran 0-6 and one part of quartz sand). Plants were grown under long-day conditions with a diurnal cycle of 16 h light at 22°C and 8 h darkness at 18°C. Growth chamber humidity was set to 50 % with a light intensity of 120 $\mu Em^{-2}s^{-1}$. Plant positions in the growth chamber were randomised twice a week to compensate for positioning effects to minimise plant growth-heterogeneity. Plants were cultivated for ten weeks and transferred to 20°C for after-ripening (*4.2.3*).

4.2.7 Hydroponic culture of Arabidopsis seedlings

Arabidopsis seedlings were cultivated in hydroponic culture as described in SWEETLOVE *ET AL.,* 2007, to rapidly obtain sufficient biomass for the isolation of mitochondria. Detergent-free, sterile glass pots were filled with 60 ml of liquid media (1x MS-media including vitamins, 2 % (w/v) sucrose, 0.04 % (w/v) MES pH 5.8 with KOH, 0.1 % (w/v) microagar). After autoclaving, pots were transferred to 4°C allowing slight solidification of the microagar. About 5 - 10 mg of Arabidopsis seeds were cultivated per individual pot. Seed surface was sterilised by incubation in 70 % (v/v) ethanol for 2 min. Ethanol was replaced by a sterilisation solution (5 % (v/v) sodium hypochlorite, 0.1 % (v/v) TWEEN®-20) and subsequent incubation for 30 - 45 min with overhead rotation. In a laminar flow hood, sterilised seeds were washed with H_2O three times. For each glass pot 500 µl of H_2O was added. After resuspension of the seeds in H_2O, 500 µl of seed-containing solution was transferred to the surface of the culture media. Seeds should remain on the surface allowing efficient gas exchange to not limit respiration during heterotrophic growth phases. Glass pots were closed with a transparent lid and were sealed with Micropore™ tape. Seeds were stratified in the dark for 48 h at 4°C. Growth cabinet was set to a diurnal cycle (16 h light at 22°C followed by 8 h darkness at 18°C with light intensity of about 50 - 75 $\mu Em^{-2}s^{-1}$). Seedlings were grown for about twelve days with gentle agitation (80 - 110 rpm).

4.2.8 Imbibition of seeds

Synchronised, after-ripened seeds of three individual plants were thoroughly mixed in the same proportion to minimise biological variation during later analysis (*e.g.* 3x 10 mg of each plant). 2 ml of H_2O was added to a sterile filter paper in a petri dish. Seeds were dispersed on the wet filter paper. Seeds of different mutants were imbibed on the same filter paper side-by-side to minimise positioning effects. After 1 or 4 h of imbibition, imbibed seeds were used for further analysis. For extraction of highly hydrophilic metabolites, such as most organic acids, seeds were directly imbibed in an unsealed reaction tube with 250 µl of H_2O at 25°C for 0, 1 and 4 h of imbibition while gently shaking. Water used for imbibition was analysed separately. (Values measured for the individual eluted organic acids in the aqueous fraction were added to the values obtained for the seed fraction to compensate for losses based on solving of the hydrophilic acids.)

4.3 Bacteriological methods

4.3.1 Bacterial strains

Agrobacterium tumefaciens C58C1	C58 (Rif^R), pTiC58 cured, pGV2260 (Carb^R) (DEBLAERE *ET AL.,* 1985)
Escherichia coli DH5α	F-, 80lacZdeltaM15 Δ (lacZYA-argF)U169 deoR recA1 endA1 hsdR17 (rK-, mK+) phoA supE44 thi-1 gyrA96 relA1 lambda-(Stratagene)
Escherichia coli Origami DE3	Δ(ara–leu)7697 ΔlacX74 ΔphoA PvuII phoR araD139 ahpC galE galK rpsLF'[lac$^+$ lacI^q pro] (DE3) gor522::Tn10 trxB: pLysS (Cam^R, Str^R, Tet^R) (Novagen)

4.3.2 Bacterial growth

Bacteria were grown in liquid LB-medium (1 % (w/v) tryptone, 0.5 % (w/v) yeast extract, 1 % (w/v) NaCl pH 7.0 with NaOH) or on solid LB-medium supplemented with 2 % (w/v) agar agar. *Escherichia coli* were grown at 37°C with 220 rpm on selective media (either 100 µg/ml ampicillin or 10 µg/ml gentamycin, **Tab. 12** and **Tab. 13**). *Agrobacterium tumefaciens* strains were cultivated at 28°C and 180 rpm. 100 µg/ml ampicillin and 50 µg/ml rifampicin were added to select for the C58C1 strain expressing the binary helper plasmid. To select for the respective plant transformation vectors (**Tab. 14**), either 50 µg/ml kanamycin or 100 µg/ml spectinomycin was applied to the LB-media.

4.3.3 Glycerol stocks

Bacteria were inoculated to 5 ml selective LB-media and were grown overnight (*4.3.2*). 500 µl of the overnight culture was added to 500 µl of 50 % (v/v) glycerol in a 2 ml reaction tube and was gently mixed. Bacteria supplemented with glycerol were frozen in liquid nitrogen and stored at -85°C.

4.3.4 Preparation of competent cells and transformation of bacteria

Agrobacterium tumefaciens were transformed by electroporation. Agrobacteria were grown overnight at 28°C in 25 ml selective LB-medium. 5 ml of the overnight culture were used to inoculate 250 ml of LB-medium. Reaching an $OD_{600\ nm}$ of 0.8, the culture was chilled on ice for 30 min and pelleted by centrifugation at 2.000 *g* for 10 min at 4°C. Bacterial pellet was washed twice with 250 ml and once with 125 ml ice-cold H_2O. Pellet was then washed twice with 125 ml and once with 50 ml of 10 % (v/v) sterile glycerol, pre-chilled at 4°C. Finally, pellet was resuspended in 2 ml of 10 % (v/v) glycerol. Aliquots of 40 µl each were frozen in liquid nitrogen and stored at -85°C.
Electroporation of competent Agrobacteria cells was performed with the MicroPulser™. 1 µl of plasmid DNA was added to 40 µl of competent cells on ice and thoroughly mixed. After 10 min of incubation bacteria suspension was transferred to an electroporation cuvette and pulsed with 2.2 kV for 5 ms according to manufacturers` protocol. Immediately after pulsing, 500 µl of sterile LB-medium was added. Pulsed bacterial suspension was transferred to new reaction tubes and was cultivated for 2 - 3 h at 28°C and 180 rpm. To select for transformed bacteria, suspension was cultivated on selective agar medium overnight.

Escherichia coli were transformed by heat shock. For the production of competent *E. coli* cells, 5 ml of an overnight culture was used to inoculate 250 ml of pre-warmed selective LB-medium. Bacterial suspension was grown at 37°C to an $OD_{600\ nm}$ of 0.8. Culture was chilled on ice for 15 min and pelleted by centrifugation for 15 min at 2.000 *g* and 4°C. Cells were resuspended in 20 ml pre-chilled TSS-medium (85 % (v/v) LB-medium, 10 % (w/v) PEG 4000, 5 % (v/v) DMSO, 50 mM $MgCl_2$). 100 µl aliquots were immediately frozen in liquid nitrogen and stored at -85°C. For transformation, competent cells were thawed on ice and 1 µl of plasmid was added. After 30 min of incubation on ice, bacteria were heat-shocked at 42°C for 30 s. 500 µl of LB-medium was added. Bacteria were grown for 1 h at 37°C without any antibiotic selection. Bacteria were then grown on selective LB-agar overnight. Single colonies were picked and cultivated in selective LB-medium (*4.3.2*).

4.3.5 Plasmid isolation from E. coli *cultures*

Plasmids were isolated according to the manufacturers` protocol of the NucleoSpin® Plasmid mini kit (Macherey-Nagel, www.mn-net.com). Instead of using the supplied elution buffer, H_2O was used for the elution of plasmids.

4.3.6 Recombinant protein expression and affinity-based purification

For the expression of recombinant proteins, *e.g.* roGFP2-Orp1 in Origami DE3 cells, a 5 ml pre-culture was grown overnight at 37°C and 220 rpm on selective LB-medium. 200 ml of selective LB-medium was inoculated with the pre-culture and was grown to an $OD_{600\ nm}$ of 0.6 – 0.8. Expression of the recombinant protein was induced by the addition of IPTG to a final concentration of 0.1 mM. Culture was grown at 20°C and 220 rpm for 24 h.
Bacteria were harvested by centrifugation for 10 min at 5.000 *g* and 4°C. Bacterial pellet was resuspended in 10 ml extraction buffer (50 mM Tris-HCl pH 8.0, 250 mM NaCl) and cells were sonicated for 10 min on ice. Lysate was centrifuged for 15 min at 18.000 *g* and 4°C to remove insoluble cell debris. To ensure complete removal of insoluble particles, supernatant was filtered through a 45 µm aseptic filter and protease inhibitor PMSF was added to a final concentration of 100 mM. Supernatant was circulated over the HiTrap™ Chelating HP column at a constant flow rate of 1 ml/min on ice for 60 min to allow efficient binding of 6xHis-tagged proteins to the Ni^{2+}-column. Bound proteins were washed with increasing concentration of imidazole containing wash buffer (50 mM Tris-HCl pH 8.0, 250 mM NaCl and 20/40/60 mM imidazole) to remove non-specific bound proteins. 6xHis-tagged proteins were eluted with elution buffer (50 mM Tris-HCl pH 8.0, 250 mM NaCl and 250 mM imidazole) and were collected in reaction tubes. Finally, column was washed with 10 mM EDTA to remove the nickel. For prohibiting microorganism growth during storage of the column, 0.02 % (w/v) azide was loaded on the column.

4.4 Protein methods and biochemical assays

4.4.1 Isolation of coupled and functional mitochondria

Arabidopsis seedlings cultivated in liquid culture were harvested after twelve days of cultivation (*4.2.7*). Seedlings were removed from the liquid culture and were washed with pre-chilled H_2O to remove remaining media. All following procedures were performed on ice or at 4°C to decrease protease activity and to obtain coupled and functional mitochondria. All buffers and gradient solutions were prepared one day in advance allowing efficient pre-chilling. Equipment, *e.g.* mortar and pistil, were chilled at 4°C. Beforehand, equipment was only washed with water without soap to keep it detergent-free. About 20 g of seedlings were used per extraction. 300 ml of pre-chilled extraction buffer (**Tab. 8**) was added to the seedlings into a pre-chilled mortar. Tissue was grinded extensively for about 3 min; extract was filtered through one layer of `Miracloth` into a pre-chilled beaker. Remaining tissue was grinded in the remaining extraction medium (about 100 ml) after addition of about 2 g of sea sand. Extract was filtered and slightly squeezed to collect as much of filtered extract as possible, which was combined with the previous filtrate. Filtered extract was centrifuged for 5 min at 1.300 *g* to pellet cell debris, *e.g.* cell wall fragments or nuclei. Supernatant was carefully filtered through one layer of Miracloth and collected in a new centrifugation tube. During 20 min of centrifugation at 18.000 *g*, mostly mitochondria, chloroplasts and peroxisomes were pelleted, whereas mainly the cytosolic and endoplasmic fractions remain in the supernatant. The supernatant was discarded and the green pellet was dispersed using residual extraction medium and a fine wet brush. Resuspended pellet was filled into a new tube and 350 ml of 1x wash buffer (**Tab. 8**) was added. Both steps were repeated to minimise contaminations of non-mitochondrial compartments. The pellet was then dispersed in about 1 to 3 ml of the remaining 1x wash buffer using a fine wet brush. Resuspended fraction was loaded on a 0 - 6 % (w/v) PVP gradient (**Tab. 8**). Deceleration of the centrifuge was switched off to not dislocate the gradient. After 40 min of centrifugation at 40.000 *g*, upper green layers of the gradient were discarded. Mitochondrial fractions were yellowish/brownish and sediment slightly above the bottom of the tube. The mitochondrial fraction was collected by a pipette without touching the undefined debris at the bottom of the tube. Mitochondrial fractions were split into three new tubes. About 20 ml of final wash medium (**Tab. 8**) was added to each tube. After centrifugation for 15 min at 23.700 *g*, supernatant was discarded. 5 ml of final wash medium was added to each tube and pellets were resuspended by gently shaking. All mitochondrial fractions were combined in a single tube. After a final centrifugation step at 23.700 *g* for 15 min, as much supernatant as possible was discarded. Mitochondrial fractions were resuspended in the smallest possible volume of final wash buffer. To maintain highly coupled mitochondria, the tube was stored on ice until it was used for further analysis.

Tab. 8: Buffers and gradients for the isolation of Arabidopsis mitochondria. All buffers and gradients for isolation of mitochondria were prepared one day in advance. DTT and ascorbic acid were added to the extraction buffer freshly on the day of usage. The pH was adjusted after dissolving of ascorbic acid. 2x wash buffer was used for preparation of the gradients; remaining buffer was diluted to 1x wash buffer by addition of H_2O.

	component	molarity/quantity
Extraction medium (pH 7.4 with KOH) 400 ml per extraction	sucrose	0.25 M
	EDTA	1.5 mM
	MOPS	15 mM
	BSA	0.4 % (w/v)
	PVP-40	0.6 % (w/v)
	DTT (fresh)	10 mM
	ascorbic acid (fresh)	100 mM
2x wash buffer (pH 7.5 with KOH) 200 ml per extraction	sucrose	0.6 M
	TES	20 mM
	BSA	0.2 % (w/v)
Final wash medium (pH 7.5 with KOH) 200 ml per extraction	sucrose	0.3 M
	TES	10 mM
Heavy gradient solution 35 ml for 2 gradients	2x wash buffer	17.5 ml
	Percoll®	11.2 ml (32 % v/v)
	PVP-40	2.1 g (6 % w/v)
	H_2O	fill to 35 ml
Light gradient solution 35 ml for 2 gradients	2x wash buffer	17.5 ml
	Percoll®	11.2 ml (32 % v/v)
	H_2O	6.3 ml

4.4.2 Mitochondrial substrate supplementation assay

The protein concentration of freshly isolated mitochondria in `final wash medium` was quantified by Bradford assay (*4.4.10*). For labelling of the Cys-peptides with iodoTMTs, 400 µg of mitochondrial proteins were dissolved in basic incubation medium (BIM: 0.3 M sucrose, 10 mM NaCl, 2 mM $MgSO_4$, 5 mM KH_2PO_4, 10 mM TES pH 7.5 with KOH) and filled up to a total volume of 2 ml. Suspension was transferred to the reaction chamber of a Clark-type oxygen electrode without closing the lid to allow gas exchange with the atmosphere. Magnetic stirrer was used to avoid sedimentation of mitochondria and to diminish oxygen gradients (set to 100 rpm). To restart mitochondrial respiration, 10 mM of substrate was added (citrate, succinate or 2-oxoglutarate; pH 7.5 with KOH), whereas a quiescent control fraction derived from the same isolation procedure and was treated identically without substrate addition. After 25 min of incubation at 25°C, mitochondria were pelleted by centrifugation for 1 min at 13.000 *g*. Supernatant was discarded and mitochondrial pellet was resuspended in the first labelling buffer containing iodoTMTs (*4.4.5*).
To visualise the reduction of the mitochondrial glutathione pool, isolated mitochondria with matrix localised roGFP2-Grx1 were analysed synchronously in a platereader with time-shifted dual excitation at 400 ± 5 nm and 482 ± 8 nm and emission at 530 ± 20 nm for both excitation wavelengths. About 10 µg of mitochondrial protein was added to 185 µl of BIM and fluorescence was recorded for 20 min before addition of 10 mM of substrates. Sensor reduction was tracked for 45 min. For calibration of the roGFP2-Grx1 sensor, 5 mM DPS was added for 30 min. Finally an excess of 20 mM DTT was added to completely reduce the sensor. The degree of oxidation of the roGFP2-Grx1 sensor ($OxD_{roGFP2\text{-}Grx1}$) was calculated according to the formula given in SCHWARZLÄNDER *ET AL.,* 2008:

$$\text{OxDroGFP2-Grx1} = \frac{R - Rred}{\frac{\text{I482ox}}{\text{I482red}}(Rox - R) + (R - Rred)}$$

with R as the ratio of excitation at 400/482 nm, R_{red} as the ratio of fully reduced sensor after reduction with 20 mM DTT, R_{ox} as the ratio of the fully oxidised sensor after oxidation with 5 mM DPS and I_{482ox} and I_{482red} as the intensities with excitation at 482 nm of the sensor in its fully oxidised and fully reduced state, respectively. The raw values were corrected by subtracting the respective blank values.

4.4.3 Respiration assay of isolated mitochondria

Respiration of isolated mitochondria (*4.4.1*) was analysed in a Clark-type oxygen electrode (Oxygraph, Hansatech) according to SWEETLOVE *ET AL.,* 2007. Mitochondria were isolated according to *4.4.1*. Respiration was estimated before and after substrate addition to isolated mitochondria in basic incubation medium (*4.4.2*) supplemented with 0.1 % (w/v) BSA. In a final volume of 1 ml, about 30 - 50 µg of mitochondrial proteins were solubilised under constant stirring to avoid sedimentation of individual mitochondria. Baseline oxygen consumption of isolated mitochondria without substrate supplementation was quantified. Addition of 10 mM substrate (citrate, 2OG or succinate at pH 7.5 with KOH) initiated mitochondrial respiration. Maximal respiration rate after substrate oxidation was quantified and was normalised to the amount of total mitochondrial protein estimated with Bradford assay (*4.4.10*).

4.4.4 Extraction of seed proteins with conserved redox state

Dry seeds of three individual plants were pooled (10 mg each) and mixed thoroughly. In total 3.5 mg of seeds were used per replicate (n = 4). Dry and imbibed seeds (*4.2.8*) were directly transferred to a reaction tube containing 200 µl of 25 % (v/v) TCA. Seeds were completely solubilised by using a drilling machine for 3 min. As a strong acid, TCA efficiently conserves the endogenous redox state of proteins by quenching the deprotonation of protein thiols to the reactive thiolate anion. After 15 min of incubation, extracts were centrifuged for 20 min at 18.000 *g* and 4°C. Precipitated protein pellets were washed twice with 500 µl of ice-cold 100 % (v/v) acetone. After the final centrifugation step, protein pellets were dried with a slight but constant flow of nitrogen to avoid oxygenation and consequent modification of protein thiols. Dried protein pellets were immediately used to label reduced thiols with iodoTMT (*4.4.5*).

4.4.5 Labelling of the endogenous redox state with iodoTMT

One vial containing 0.2 mg of iodoTMT was sufficient to label up to 400 µg of extracted proteins. Freeze-dried, light-sensitive iodoTMTs were resolved in 10 µl of 100 % (v/v) methanol and subsequently added to the first labelling buffer (8 M urea, 20 mM HEPES pH 8.0, 1 mM EDTA and 0.01 % (v/v) Triton™-*X-100*). Proteins were solubilised efficiently in the presence of 8 M urea. Triton™-*X-100* is added to crack membranes allowing labelling of organellar proteins, which would be shielded by intact lipid bilayers. Slightly basic pH of 8.0 efficiently deprotonates reduced thiol groups to the more reactive thiolate anions and maintains high specificity of the iodoTMT for irreversible binding to cysteines rather than to other amino acids. EDTA binds to divalent metal ions preventing Fenton-type reactions forming reactive oxygen species and consequent artificial oxidation of reduced protein thiols.

Ideal protein concentration for iodoTMT labelling is between 1 - 2 µg/µl. For labelling of mitochondrial proteins, in total 300 µl were used, whereas seed proteins were labelled in 200 µl of labelling buffer. Proteins were labelled for 1.5 h at 30°C in the dark while gently shaking. Insoluble proteins were removed by centrifugation for 10 min at 18.000 *g*. Unbound iodoTMT was removed by acetone protein precipitation. A 4-fold volume of pre-chilled 100 % (v/v) acetone was used for overnight precipitation. Samples were brought to room temperature and extensively mixed by vortexing. After centrifugation for 10 min at 18.000 *g*, the supernatant was discarded. Protein pellet was washed twice with 80 % (v/v) acetone and finally with 100 % (v/v) acetone, which allows fast drying of the protein pellet. To efficiently dissolve the protein pellet in acetone during the washing steps, reaction tubes were sonicated for up to 15 s. In between, proteins were pelleted by centrifugation for 5 min at 18.000 *g*. For the second labelling of proteins with iodoTMT, protein pellets were resuspended in 100 µl of labelling buffer (8 M urea, 20 mM HEPES pH 8.0, 1 mM TCEP freshly added). TCEP is a mild non-thiol reductant used for the reduction of oxidised cysteines making them reactive to the second iodoTMT. TCEP was chosen instead of thiol-containing reducing agents to prohibit quenching of the labelling reaction by irreversible binding to the iodoTMTs. Protein concentration was estimated with Bradford reagent prior to second labelling (*4.4.10*). Protein quantities within all replicates were adjusted to a final protein amount of 175 µg. Second labelling was performed in a total volume of 200 µl of labelling buffer containing the second corresponding iodoTMT. A typical labelling scheme of the iodoTMT approach is shown in **Tab. 9**. For the different biological replicates and treatments, labels were swapped to compensate for hypothetical label biases. Proteins were labelled for 1.5 h at 30°C in the dark with gentle agitation. After 2nd labelling, proteins were multiplexed with respect to their mass-tags (**Tab. 9**). Remaining, unbound iodoTMT would impair immunoprecipitation during later sample clean-up. Hence, unbound 2nd iodoTMT was removed by acetone protein precipitation at -20°C. A 4-fold volume of pre-chilled 100 % (v/v) acetone was used for overnight incubation directly after sample combination. Samples were brought to room temperature and extensively mixed by vortexing. After centrifugation for 10 min at 18.000 *g*, the supernatant was discarded. Protein pellet was washed twice with 80 % (v/v) acetone and finally with 100 % (v/v) acetone. Dry protein pellet was used for trypsination (*4.4.6*).

Tab. 9: Representative iodoTMT labelling scheme. A typical iodoTMT labelling scheme for a comparison of two conditions with four replicates each. Label swaps were performed to avoid potential label biases. Although multiplexing of three individual samples is possible, only two samples of each condition were combined.

		1st label	2nd label	multiplexing
Condition A	1st replicate	iodoTMT # 126	iodoTMT # 129	1st replicates
	2nd replicate	iodoTMT # 128	iodoTMT # 131	2nd replicates
	3rd replicate	iodoTMT # 130	iodoTMT # 127	3rd replicates
	4th replicate	iodoTMT # 129	iodoTMT # 126	4th replicates
Condition B	1st replicate	iodoTMT # 128	iodoTMT # 131	
	2nd replicate	iodoTMT # 130	iodoTMT # 127	
	3rd replicate	iodoTMT # 126	iodoTMT # 129	
	4th replicate	iodoTMT # 131	iodoTMT # 128	

4.4.6 Trypsination of precipitated proteins

Dry protein pellets were dissolved in ABC buffer (25 mM ammonium bicarbonate pH 7 - 8). For 350 µg of proteins (2x 175 µg per replicate), 350 µl of ABC buffer was used (1 µl of ABC buffer per 1 µg of protein). Trypsin was added in a protein to trypsin ratio of 100:1. Proteins were trypsinated at 37°C for 2 h with gentle agitation. Again the same amount of trypsin was added to a final protein to trypsin ratio of 50:1. The second trypsin addition should compensate for trypsin losses due to auto-cleavage of the protease allowing efficient trypsination of the precipitated proteins. After overnight incubation at 37°C, trypsinated peptides were centrifuged briefly. Addition of 1/20 volume of 20 % (v/v) TFA is leading to a complete denaturation and inactivation of trypsin. After centrifugation for 10 min at 18.000 *g*, samples were placed in a centrifugal evaporator until TFA containing ABC buffer was completely evaporated.

4.4.7 Immunoprecipitation of iodoTMT-labelled peptides

Dry peptides were dissolved in TBS buffer (50 mM Tris-HCl pH 7.6, 150 mM NaCl). For 350 µg of trypsinated protein, 350 µl of TBS buffer was used (1 µl of TBS buffer per 1 µg of peptides). The pH of the resuspended peptide solution was checked and adjusted to a final pH of 7 - 8 with NaOH to minimise negative effects of an acidic pH on the immunoprecipitation efficiency. Peptides were resuspended - if necessary, sonication for 15 s was performed. Not resuspended particles were pelleted by centrifugation for 10 min at 18.000 *g*. Not mandatory but recommended is the control of efficient trypsination before starting the immunoprecipitation. While proteins can be sensed via Bradford reagent, quantification of efficiently trypsinated peptides is not possible. Yet, trypsinated peptides can be quantified with absorbance at 280 nm with a NanoDrop™. Ideally no protein can be identified with Bradford reagent whereas protein/peptide amount analysed with NanoDrop™ is in the range of the total protein amount initially used for trypsination (about 350 µg per replicate). For 350 µg of peptides, 350 µl of antibody resin was used; hence 50 % (v/v) of the total antibody resin volume is slurry. Before usage, the antibody resin was washed three times with TBS. 1 min of centrifugation at 1.500 *g* is sufficient for sedimentation of the immobilised antibodies. Before the supernatant of centrifuged samples were given to the washed antibody resin, the slurry volume was replaced by addition of 175 µl TBS. IodoTMT-labelled Cys-peptides bind to the antibody resin during overnight incubation with overhead rotation at 4°C. Unbound Cys-peptides were removed by centrifugation for 2 min at 1.500 *g*. To loose unspecific bound peptides, antibody resin was incubated for 30 min with 1 ml TBS and gentle agitation. After centrifugation for 1 min at 1.500 *g*, supernatant was discarded and antibody resin was washed in total three times with 1 ml TBS and two times with H_2O. To elute specifically bound iodoTMT-labelled Cys-peptides, 400 µl of the iodoTMT elution solution was added and incubated for 10 min with gentle agitation. After centrifugation for 2 min at 1.500 *g*, supernatant containing the eluted peptides were transferred to new reaction tubes. To avoid incompatibility of unknown components of the iodoTMT elution solution with mass spectrometry, samples were placed in a centrifugal evaporator. After complete evaporation of the iodoTMT elution solution, samples were either stored at -80°C or were directly used for mass spectrometry analysis.

4.4.8 Sample clean-up for mass spectrometry

IodoTMT-labelled peptides were dissolved in 20 µl of 5 % (v/v) acetonitrile and 0.1 % (v/v) TFA. After short centrifugation, 20 µl of 0.1 % (v/v) TFA was added. Samples were loaded on non-polar Pierce™ C18 StageTips to remove salts and other non-peptide contaminations. Pierce™ C18 StageTips were activated prior the loading by addition of 20 µl of 100 % (v/v) acetonitrile. The C18-material was equilibrated with 20 µl of 0.1 % (v/v) TFA. The sample was than loaded to the StageTip twice to ensure complete binding of the peptides. Peptides bound to the non-polar StageTip were washed with 20 µl of 0.1 % (v/v) TFA; salts and other non-peptide contaminations in the flow-through were discarded. Bound peptides were eluted by addition of 40 µl of 60 % (v/v) acetonitrile and 0.1 % (v/v) TFA solution. Eluted peptides were placed in a centrifugal evaporator to completely remove the acetonitrile/TFA solution. For mass spectrometry analysis, iodoTMT-labelled peptides were finally dissolved in 20 µl of 5 % (v/v) acetonitrile and 0.1 % (v/v) acetic acid.

4.4.9 Mass spectrometry-based identification of peptides and quantification of TMT reporter ion intensity with subsequent data analysis

Quantification of labelled peptides requires a mass spectrometer capable of MS/MS detection. The different iodoTMT are isobar and labelled peptides cannot be distinguished by a defined shift in the corresponding MS spectra, as it is routinely done for OxICAT analysis (LEICHERT *ET AL.,* 2008). For quantification of the different isobaric iodoTMT, their specific reporter ions have to be fragmented and identified via MS/MS. By fragmentation of the iodoTMT, specific reporter ions are generated, which are differing in their molecular masses due to their different isotope distribution.
Either a Thermo-Scientific Orbi Trap Velos Pro™ or Thermo-Scientific Orbi Trap Q-Exactive™ was used for peptide identification and TMT quantification. 10 µl of the peptide solution (*4.4.8*) were injected; peptides were separated in a liquid chromatography in a 180 min gradient. While the first MS quantification is fast, fragmentation and MS/MS-based identification is relatively slow, allowing just a limited number of fragmentations in a certain retention time-window. Based on the necessity of fragmentation of the iodoTMTs for the reporter ion generation and quantification, only for fragmented peptides the estimation of the redox state is possible. Therefore peptides for HCD-based fragmentation were chosen by a Top10 analysis – selecting always the ten most abundant peptides for MS/MS fragmentation at a certain retention time-window. Identified and quantified via MS, high abundant peptides eluting in a broader timeframe will be excluded for further MS/MS fragmentation once their corresponding MS/MS spectra is recorded. Thereby the resolution for low-abundant peptides at similar retention times is increased, while multiple quantifications of reporter ions derived from always the same high-abundant peptides are excluded.
MaxQuant version 1.5.5.1 was used to analyse the raw-files for each LC-MS/MS run. Beside the iodoTMT-based modifications, methionine oxidation and acetylation of the N-terminus were allowed as potential peptide modifications, whereas C-terminal carbamidomethyl was set as a fixed modification in the MaxQuant parameters. As a reference sequence database, a FASTA file containing recent *Arabidopsis thaliana* annotations was downloaded from www.Arabidopsis.org (TAIR-10; containing 27.416 protein coding genes). Additionally, a FASTA file with the sequence of roGFP2-Grx1 was used for analysing the isolated mitochondria expressing matrix roGFP2-Grx1 (**Tab. 10**).

Tab. 10: Amino acid sequence of matrix located roGFP2-Grx1. Amino acid sequence of roGFP-Grx1 expressed in the mitochondrial matrix without N-terminal mitochondrial targeting sequence is given in single letter code. Sequence was used to complete the TAIR10 FASTA file obtained from www.Arabidopsis.org to allow the assigning of roGFP2-Grx1-derived trypsinated peptides to their belonging hypothetical masses.

VSKGEELFTGVVPILVELDGDVNGHKFSVSGEGEGDATYGKLTLKFISTTGKLPVPWPTLVTTLTYGV QCFSRYPDHMKQHDFFKSAMPEGYVQERTIFFKDDGNYKTRAEVKFEGDTLVNRIELKGIDFKEDGNI LGHKLEYNYN**C**HNVYIMADKQKNGIKVNFKIRHNIEDGSVQLADHYQQNTPIGDGPVLLPDNHYLST**C** SALSKDPNEKRDHMVLLEFVTAAGITLGMDELYKTSGGSGGGGSGGGGSGGGGSGGGGSGGGGS GGEFAQEFVNCKIQPGKVVVFIKPT**C**PY**C**RRAQEILSQLPIKQGLLEFVDITATNHTNEIQDYLQQLTGA RTVPRVFIGKDCIGG**C**SDLVSLQQSGELLTRLKQIGALQ

In the MaxQuant parameters, the reporter ion mass tolerance was set to 0.01 Dalton. The minimal peptide length for identification was set to ≥ 7 amino acids with a max. peptide mass of 4600 Dalton at Trypsin/P digestion. Up to two missed cleavages during trypsination were allowed. 2x charged peptides identified with <1 % FDR were considered for quantification of the corresponding reporter ions. The peptide identification FDR was based on the *target-decoy* search strategy. For the *target-decoy* strategy, obtained peptide spectra were additionally assigned to the reversed protein sequences generated *in silico* based on the TAIR-10 FASTA file. The FDR based on the *target-decoy* search strategy allows the estimation of how many false positive peptide spectra are associated to an entire data set (ELIAS AND GYGI 2007). All other MaxQuant parameters were not changed. The *Peptide-table* generated by the MaxQuant software contains all reporter ion intensities quantified for each identified peptide in each experiment. For further analysis peptides containing not a single cysteine residue were excluded from the dataset. In average, 60 - 65 % of all identified peptides contained at least a single cysteine. Potential known contaminants *e.g.* keratin or trypsin-derived peptides were removed from the dataset. TAIR10 identifiers were transcribed to their corresponding protein names according to www.uniprot.org. Consensus localisations of all identified Cys-peptides are given according to www.suba3.plantenergy.uwa.edu.au. The Cys-oxidation state (in %) of the corresponding peptide was calculated by dividing the reporter ion intensity of the 2nd label by the sum of both label intensities, finally multiplied by 100 ((Intensity 2nd label / sum of Intensity of 1st and 2nd label) * 100). The average % Cys-oxidation for individual peptides was calculated for three to five biological replicates. Peptides identified in less than three replicates were excluded from further analysis. The Δ% Cys-oxidation was calculated by subtracting the % Cys-oxidation states after substrate supplementation of those without substrate addition. Peptides significantly differing in their Cys-oxidation states were identified with a t-test corrected for multiple comparisons by Benjamini, Krieger & Yekutieli with <2 % FDR using GraphPad Prism 7.0. For bar charts plotting the proportion of Cys-peptide oxidation levels, the number of Cys-peptides in each 2 % quantile of % Cys-oxidation was counted based on the average Cys-oxidation state of three to five replicates. In total the number of Cys-peptides for 51 quantiles was calculated and normalised to the total number of identified Cys-peptides in each experiment. To check for variability between different replicates, each replicate was analysed additionally on its own. The overall distribution of all Cys-peptide oxidation levels, for all individual replicates as well as for their averages, was also plotted in boxplots using GraphPad Prism 7.0.

In scatter plots of the % Cys-oxidation level of individual Cys-peptides in one condition plotted against its corresponding % Cys-oxidation value under another condition, those peptides, which are significantly shifted in their % Cys-oxidation levels were plotted in red.

For a functional classification of all identified redox-switched proteins, identified peptides were mapped on schematic structures of the mitochondrial Complex I (according to BRAUN

ET AL., 2014), on a schematic overview of all other electron transport chain associated proteins (CHROBOK *ET AL.,* 2016; SCHIKOWSKY *ET AL.,* 2017), of all enzymes of the TCA cycle (www.genome.jp/kegg) and to all enzymes participating in amino acid metabolism (www.genome.jp/kegg and HILDEBRANDT *ET AL.,* 2015).

4.4.10 Determination of protein concentration

The protein concentration *e.g.* of isolated mitochondria (*4.4.1*) was determined using a classical Bradford assay (BRADFORD 1976). Bovine serum albumin (BSA) standards (0, 0.1, 0.2, 0.4 and 0.8 µg/µl) were used for calibration. 5 µl of adequately diluted protein solution were mixed with 195 µl 1x Roti®-Quant (Carl-Roth, www.carlroth.com) for 5 min in a 96-wellplate at room temperature. Absorbance was measured for triplicates at 595 nm with the POLARstar® Omega or CLARIOstar® microplate reader (BMG, www.bmglabtech.com). Protein concentration was calculated with consideration of the absorbance of the standard curve.
Trypsinated peptides were quantified using the typical absorbance characteristics of proteins and peptides at 280 nm in a NanoDrop™ (Thermo Scientific, www.thermoscientific.com).

4.4.11 SDS-PAGE and Coomassie-staining

2.5 - 10 µg of protein was used for the separation in a reducing, denaturating polyacrylamide gel according to LAEMMLI 1970. Proteins in 1x SDS-loading buffer (250 mM Tris-HCl pH 6.8, 10 % (w/v) SDS, 0.01 % (w/v) bromphenol blue, 25 % (v/v) β-mercaptoethanol, 50 % (v/v) glycerol) were boiled at 95°C for 5 min before loading to the gel. Samples were separated in a discontinuous 10 % SDS-PAGE covered with a 4 % stacking gel. Separation was achieved at constant voltage of 110 V in SDS-running-buffer (25 mM Tris-HCl pH 8.3, 192 mM glycine, 0.1 % (w/v) SDS) until loading front reached the bottom of the separation gel. As molecular mass standards, PageRuler™ Unstained Protein Ladder was used (www.thermofisher.com).
Separated proteins were stained with Coomassie blue (50 % (v/v) ethanol, 1 % (v/v) acetic acid, 0.1 % (w/v) Coomassie G250, 10 % (w/v) SDS, 20 % (v/v) glycerol) over night. On the next day the polyacrylamide gel was incubated in destaining solution (50 % (v/v) ethanol, 20 % (v/v) acetic acid) until background appeared clear. Gel was documented by usage of a scanner.

4.4.12 Determination of the total thiol concentration in seeds

For the quantification of the total glutathione content and of the free amino acid cysteine, 50 mg of seeds were used for the extraction with 1 ml of 0.1 M HCl. Grinded seed material was incubated for 15 min at 4°C with agitation. Supernatant was cleared twice by centrifugation for 5 min at 14.000 rpm and 4°C. The pH of 25 µl extract was increased by addition of 235 µl 1 M Tris-HCl pH 8.3 and 0.08 M NaOH allowing efficient reduction of all thiols by supplementing 10 mM DTT to a final volume of 270 µl. After a short centrifugation step, samples were reduced for 1 h at room temperature in the dark. 25 µl of 10 mM monobromobimane (mBBr) in acetonitrile were added to label all reduced thiols. After 15 min of incubation in the dark with gentle agitation, derivatisation was stopped by lowering the pH by addition of 700 µl of 5 % (v/v) acetic acid. Insoluble precipitates were removed by centrifugation for 45 min at 4°C and maximal speed. Supernatant was transferred to HPLC-compatible vials. 20 µl of each sample was loaded onto the HPLC column Nova-Pak™ C18; 4 µM; 60 Å; 4.6 x 250 mm (www.waters.com) for separation in a flow with 1.3 ml/min of

91 % (v/v) 100 mM potassium acetate pH 5.3 with KOH and 9 % (v/v) methanol at 37°C. Samples were excited at 380 nm and emission was recorded at 480 nm in a Shimadzu RF 551 fluorescence detector (www.store.shimadzu.com). Standards with known quantities of mBBr-tagged cysteine and glutathione were used for the quantification of the samples.
Acidic extraction, as used for total thiol determination, was also applied for the quantification of adenosines and the different amino acids.

4.4.13 Determination of organic acids in seeds

After seed imbibition (*4.2.8*) seeds were grinded with a small pistil in 180 µl of 100 % (v/v) methanol. For increasing yield of extraction, samples were vigorously shaken at 70°C for 15 min. Extract was supplemented with 100 µl of 100 % (v/v) chloroform and further incubated for 5 min at 37°C while shaking. For the separation of the polar and organic phases, 200 µl of H_2O was added and samples were centrifuged for 10 min at 11.000 *g*. The upper phase represents the polar phase containing the organic acids. 300 µl of the polar phase were transferred to fresh tubes and solvent was evaporated by a centrifugal evaporator without heating of the samples. Samples were derivatised by methoximation and silylation. Therefore dry pellets were dissolved in 20 µl methoximation reagent containing 20 mg/ml methoxyamine hydrochloride in pyridine and incubated for 2 h at 37°C with gently shaking. For silylation, 32.2 µl N- Methyl-N-(trimethylsilyl)trifluoroacetamide and 2.8 µl alkane standard mixture (50 mg/ml C10-C40) were added to each sample. After incubation for 30 min at 37°C, samples were transferred to glass vials for GC-MS analysis. A GC-MS-QP2010 Plus (Shimadzu®) fitted with a Zebron ZB 5MS column (Phenomenex®; 30 meter x 0.25 mm x 0.25 µm) was used for GC/MS analysis. The GC was operated with an injection temperature of 230°C and 2 µl sample were injected in the split mode (1:10). The GC temperature program started with a 1 min hold at 70°C followed by a 6°C/min ramp to 310°C, a 20°C/min ramp to 330°C and a bake-out for 5 min at 330°C using Helium as carrier gas with constant linear velocity. The MS was operated with ion source and interface temperatures of 250°C, a solvent cut time of 6.3 min and a scan range (m/z) of 40 - 1000 with an event time of 0.3 s. The “GC-MS solution” software (Shimadzu®) was used for data processing.

4.5 DNA methods

4.5.1 Oligonucleotides

Primers were synthesised by MWG (MWG, www.eurofinsgenomics.eu). Freeze-dried primers were resuspended in H_2O to a final concentration of 20 pmol/µl and were stored at -20°C.

Tab. 11: Primers used for cloning of cyt-roGFP2-Orp1 and mt-roGFP2-Orp1. The primers # 2660 and # 2680 were used for attaching the GATEWAY®-sites to the roGFP2-Orp1 sequence. Primers # 2662, # 2663, # 2664, # 2666, # 2681 and # 2682 were used for the fusion of the mitochondrial targeting sequence to the roGFP2-Orp1 construct and to simultaneously attach GATEWAY®-sites to the termini. Primers # 689 and # 690 were used for sequencing of the insert in the pDonR207 entry-vector.

primer ID	sequence
# 2660	GGGGACAAGTTTGTACAAAAAAGCAGGCTTCACCATGGTGAGCAAGGGC GAGGAG
# 2680	GGGGACCACTTTGTACAAGAAAGCTGGGTTCTATTCCACCTCTTTCAAAAG TTC
# 2662	TACAAAAAAGCAGGCTTCACCATGGCTTCTCGGAGGCTTCTC
# 2663	GAACAGCTCCTCGCCCTTGCTCACACCAGCGCCGGTGAACTCATCGGTA
# 2664	TACCGATGAGTTCACCGGCGCTGGTGTGAGCAAGGGCGAGGAGCTGTTC
# 2681	GTACAAGAAAGCTGGGTTCTATTCCACCTCTTTCAAAAGTTCTTC
# 2666	GGGGACAAGTTTGTACAAAAAAGCAGGCTTCACC
# 2682	GGGGACCACTTTGTACAAGAAAGCTGGGTTCTA
# 689	TCGCGTTAACGCTAGCATGGATCTC
# 690	GTAACATCAGAGATTTTGAGACAC

4.5.2 Plasmids

Plasmids used for the transformation of *E. coli* Origami DE3 for the expression of recombinant proteins are listed in **Tab. 12**. Plasmids obtained from cooperation partners were highlighted accordingly.

Tab. 12: Plasmids used for the heterologous expression of proteins in *E. coli*.

plasmid	resistance	constructed / provided by	description
pET16b:NTRb	Amp^R	J.P. Reichheld Perpignan, France	heterologous expression of NTRb in *E. coli*
pET16b:TRXo1	Amp^R	J.P. Reichheld Perpignan, France	heterologous expression of TRX-o1 in *E. coli*
pET16b:GRXC1	Amp^R	J.P. Reichheld Perpignan, France	heterologous expression of GRX-C1 in *E. coli*
pET16b:GR2	Amp^R	J.P. Reichheld Perpignan, France	heterologous expression of GR2 in *E. coli*
pETG10a: roGFP2-Orp1	Amp^R	T. Nietzel Bonn, Germany	heterologous expression of roGFP2-Orp1 in *E. coli*

Plasmids used as templates or as destination-vectors for cloning of the roGFP2-Orp1 construct are listed in **Tab. 13**. Plasmids obtained from cooperation partners were highlighted accordingly. Plasmid for PCR-based amplification of the N-terminal transit peptide of the ATP-synthase β-subunit (first 87amino acids) of *Nicotiana plumbaginifolia* was obtained from David Logan (LOGAN AND LEAVER 2000).

Tab. 13: Plasmids used for GATEWAY®-cloning of the roGFP2-Orp1 construct.

plasmid	resistance	constructed / provided by	description
pBSSK: roGFP2-Orp1	Amp^R	I. Aller Bonn, Germany	template of the roGFP2-Orp1 construct
pDonR207	$Gent^R$	Invitrogen www.thermofisher.com	GATEWAY® entry-vector
pH2GW7	$Spec^R$ (Hyg^R in plants)	Laboratory of Plant Systems Biology Ghent, Belgium	GATEWAY® destination-vector for stable plant transformation
pETG-10a	Amp^R	EMBL AG (www.embl.de)	over-expression of recombinant proteins in *E. coli*

Plasmids used for the stable transformation of *Arabidopsis thaliana* were listed in **Tab. 14**. Plasmids obtained from cooperation partners were highlighted accordingly.

Tab. 14: Plasmids used for the stable transformation of Arabidopsis plants.

plasmid	resistance	constructed / provided by	description
pH2GW7:cyt-roGFP2-Orp1	$Spec^R$ (Hyg^R in plants)	T. Nietzel Bonn, Germany	stable expression of cytosolic roGFP2-Orp1 under *CaMV 35 S* promoter
pH2GW7:mt-roGFP2-Orp1	$Spec^R$ (Hyg^R in plants)	T. Nietzel Bonn, Germany	stable expression of mitochondrial roGFP2-Orp1 under *CaMV 35 S* promoter
pBinCM:SHMT-roGFP2-Grx1	Kan^R (Kan^R in plants)	C. Müller Heidelberg, Germany	stable expression of mitochondrial roGFP2-Grx1 under *Ubi-10* promotor
pH2GW7:cyt-ATeam1.03nD/nA	$Spec^R$ (Hyg^R in plants)	M. Schwarzländer Bonn, Germany	stable expression of cytosolic ATeam under *CaMV 35 S* promotor
pSS02:cyt-Peredox-mCherry	Kan^R (Hyg^R in plants)	M. Schwarzländer Bonn, Germany	stable expression of cytosolic Peredox-mCherry under *Ubi-10* promotor

4.5.3 DNA gel electrophoresis and DNA purification

DNA fragments were separated on agarose gels. 1 % (w/v) agarose was dissolved in 1x TBE buffer (90 mM boric acid, 90 mM Tris-HCl pH 8.0, 2 mM EDTA) by heating in a microwave. Ethidium bromide was added to a final concentration of 500 ng/ml. DNA was mixed with 5x loading buffer (40 % (v/v) glycerol, 0.25 % (w/v) bromophenol blue, 0.25 % (w/v) xylene cyanole) in a 5:1 ratio. As molecular mass standard, GeneRuler™ DNA Ladder Mix (www.thermoscientificbio.com) was used. Gels run at 110 V in TBE buffer for 30 - 60 min and ethidium bromide fluorescence was documented with a MF-ChemiBIS2.0 gel-documentation. For excision of defined gel slices with the PCR product of interest, agarose gel was illuminated with 254 nm by a portable UV-lamp (M&S, www.m-und-s-laborgeraete.de). DNA was purified using the NucleoSpin® Gel and PCR clean-up system according to the manufacturers` manual (Macherey-Nagel, www.mn-net.com).

4.5.4 Quantification of DNA content

DNA concentration, *e.g.* of isolated plasmids, was quantified with Nanodrop™ spectrophotometer based on the characteristic absorption of DNA at specific wavelengths.

4.5.5 DNA sequencing

Sequencing was performed by StarSeq (www.starseq.com). Samples were prepared according to the company's guidelines; primers # 689 and # 690 (**Tab. 11**) were used for sequencing the inserts in pDonR207 background. The obtained sequences were analysed with FinchTV sequence viewer.

4.5.6 GATEWAY® cloning strategies

GATEWAY® cloning was performed according to the manufacturers` instructions (www.thermofisher.com/de/de/home/life-science/cloning/gateway-cloning/protocols.html) to clone roGFP2-Orp1 in a bacterial expression vector as well as in vectors for the stable transformation of *Arabidopsis thaliana*. Vectors used for GATEWAY® cloning were listed in **Tab. 13**. Primers for attaching the GATEWAY®-sites (and the mitochondrial targeting sequence) to the roGFP2-Orp1 sequence were listed in **Tab. 11**. For attaching GATEWAY®-sites to the roGFP2-Orp1 construct without any N-terminal targeting sequence, primers # 2660 and # 2680 were used. For attaching fragmentary GATEWAY®-sites to the mitochondrial targeting sequence as well as to the roGFP2-Orp1 construct, primer pairs # 2662/2663 and # 2664/2681 were used in separate PCR reactions. In a final PCR-based elongation, GATEWAY®-sites were elongated to their full length and the mitochondrial targeting sequence was fused to the roGFP-Orp1 construct via overlapping sequences. For amplification of DNA, Phusion® High-Fidelity DNA Polymerase was used in 50 µl reactions according to the manufacturers` protocol. GATEWAY® entry clones were generated by BP-reaction of donor vectors (**Tab. 13**) and PCR products with attached GATEWAY®-sites according to the manufacturers` protocol. Entry clones were transformed to DH5α cells for plasmid amplification (*4.3.4*). Entry clones were sequenced (*4.5.5*) before generating the GATEWAY® expression clones (**Tab. 13**) via LR-reaction according to the manufacturers` protocol. The pETG10a:roGFP2-Orp1 vector was transformed into Origami DE3 cells for the heterologous production of roGFP2-Orp1 (*4.3.6*) while the pH2GW7:cyt-roGFP2-Orp1 and the pH2GW7.mt-roGFP2-Orp1 vectors where transformed into C58C1 cells for the stable transformation of *Arabidopsis thaliana* (*4.2.2*).

4.6 Imaging methods (microscopy methods & platereader assays)

4.6.1 Seed respiration assay

The respiratory activity of after-ripened and synchronised Arabidopsis seeds during imbibition in water was measured using the MitoXpress®Xtra (Luxcel Biosciences, www.luxcel.com) fluorescent probe as described in SECHET *ET AL.,* 2015 and WILL *ET AL.,* 2006. Seeds in the 1 - 2 mg range were precisely weighed using an ultra-balance (*AD6 Autobalance*, Perkin Elmer) and placed in the wells of a 96-well plate (n = 5). 150 µl of deionised water supplemented with 100 nM MitoXpress®Xtra was added in each well. After 5 min of gently shaking (800 rpm) on a multi-well plate shaker, 100 µl mineral oil was added to prevent resolving of oxygen from the surrounding gas phase. Oxygen depletion in the medium was estimated from the increase in fluorescence lifetime (FLT) of the probe using a CLARIOstar® Omega plate spectro-fluorometer equipped with a time-resolved fluorescence head (BMG LABTECH GmbH). At each time point, fluorescence relative units (Ex: 340 nm, Em: 605-705 nm) were recorded (50 light flashes per measurement and well) for 30 µs after 30 and 70 µs, and probe lifetime (LT) calculated from the ratio of fluorescence intensity at 30 µs delay and 70 µs delay as follows. LT = (70-30)/ Ln (W1 / W2) where 70 is W2 delay time (70 µs) and 30 is W1 delay time (30 µs). W1 is RFU signal measured after W1 delay, W2 is RFU signal measured after W2 delay. MitoXpress®Xtra LT data were analysed using the MARS Data analysis software version 3.1 R2 (BMG LABTECH GmbH). Probe lifetime increase (Δ Fluorescence lifetime) was calculated by subtraction of fluorescence lifetime at timepoint T_0 from the increasing fluorescence lifetime at oxygen consumption during imbibition. Δ Fluorescence lifetime was normalised to the respective amount of seeds. The average fluorescence lifetime increase rate was calculated, derived from the average of the fluorescence lifetime increase rates in a 3 min timeframe.

4.6.2 Platereader-based emission and excitation scans of Arabidopsis seeds

Excitation and emission scans for seeds expressing different fluorescent biosensors were performed with a CLARIOstar® platereader equipped with a monochromator and a spectro-fluorometer. Dry seeds were filled into a well plate (Greiner Bio-one GmbH; multiwall plates, clear and flat bottom) with help of a small spoon until well bottoms were completely covered. 384-wellplates were used to minimise the amount of seeds needed. Electrostatic repulsion of dry seeds was prevented by covering the well plate with a sheet of paper and infilling of seeds via a small punched hole just as big as the opening of an individual well. Col-0 seeds without sensor expression were used as control and for background subtraction. For imbibition of the seeds, built-in injection pumps were used for fast addition of 75 µl of H_2O. After 1 h of starting the imbibition, emission/excitation scans were performed.
For cyt-ATeam seeds, emission scans were performed. Seeds were excited at 435 ± 5 nm and emission was recorded in 1 nm steps with an emission bandwidth of 10 nm in the range of 460 – 590 nm. For cyt-Peredox-mCherry seeds, emission scan was performed separately for both fluorophores, the T-Sapphire and the mCherry. mCherry was excited at 550 ± 7.5 nm, T-Sapphire at 400 ± 10 nm. Emission was recorded for both fluorophores with 0.5 nm resolution and with a bandwidth of 15 nm. The emission of T-Sapphire was recorded in the range of 450 – 600 nm, whereas for mCherry the emission was recorded in the range of 580 - 670 nm. Based on the different sensor principles, for roGFP2-expressing seeds excitation scans were performed, whereas emission wavelength was set constantly to 530 ± 20 nm. Seeds were excited in 1 nm steps in a range from 360 - 495 ± 5 nm.

4.6.3 Emission and excitation scans of purified roGFP2-Orp1 in a spectro-fluorometer

The fluorescence characteristics of heterologous expressed roGFP2-Orp1 were analysed in a spectro-fluorometer (JASCO FP-8300, www.jasco.de). 5 µM of purified sensor was either reduced with 20 mM DTT or oxidised by 1 mM DPS in `standard reaction buffer` (5 mM EDTA, 100 mM potassium phosphate pH 7.0). Excitation spectra of roGFP2-Orp1 in the range of 360 - 510 nm (with 0.5 nm resolution and 5 nm bandwidth) was recorded with emission in the range of 510 - 540 nm. The spectroscopic dynamic range (δ) was calculated from the 405/488 nm excitation ratios for fully oxidised and fully reduced probe. Emission spectra of oxidised and reduced roGFP2-Orp1 in the range of 500 - 600 nm were recorded with 0.5 nm resolution at excitation at either 405 nm or 488 nm.

4.6.4 Platereader-based dynamic monitoring of fluorescent biosensors

The different sensor kinetics during early imbibition of seeds were recorded in a CLARIOstar® platereader. Dry seeds were filled into individual wells as described in *4.6.2*. Col-0 seeds were used for background normalisation. Fluorescence was recorded for at least 25 min before addition of 75 µl H_2O with the built-in injection pumps. Seeds expressing the cytosolic ATeam were excited at 450 ± 5 nm, emission was recorded in the range of 490 ± 10 nm for the CFP domain and 535 ± 10 nm for the cpYFP domain. The normalised FRET-ratio (cpYFP/CFP) of whole seeds is plotted over time. Cyt-Peredox-mCherry seeds were excited at 570 ± 10 nm for the mCherry domain and at 400 ± 10 nm for the T-Sapphire domain simultaneously. Emission of mCherry was recorded in the range of 620 ± 15 nm and 520 ± 10 nm for T-Sapphire. The normalised T-Sapphire/mCherry ratio is plotted over time. RoGFP2 seeds were excited at 400 ± 5 nm and 482 ± 8 nm. Emission was recorded for both excitation wavelengths at 530 ± 20 nm. The normalised 400/482 nm ratio is plotted over time. Measurements for all sensor-expressing seeds were repeated in several assays of independent seed-batches (n = 4 - 6).

For dynamic monitoring of the 400/482 nm ratio of purified roGFP2-Orp1, same settings were used as for measurement of roGFP2-Grx1 in seeds. For estimating the pH-sensitivity of roGFP2-Orp1, 1 µM of purified sensor was either reduced with 20 mM DTT or oxidised by 1 mM DPS in standard reaction buffer with differently adjusted pH (5 mM EDTA, 100 mM MES-KOH for pH 5.3 - 6.5, HEPES KOH for pH 7 - 8 or Tris-HCl for pH 8.1 - 8.3). pH was controlled after measurement directly in the 96-wellplate with pH-microelectrode.
For the hydrogen peroxide titration of pre-reduced roGFP2-Orp1, 0.3 µM purified sensor was reduced with 20 mM DTT in standard reaction buffer for 20 min on ice. Excess DTT was removed by size exclusion chromatography (Zeba™ Spin Desalting Columns, www.thermofisher.com). Fluorescence was recorded over time in a CLARIOstar® platereader. To minimise artificial oxidation of the reduced roGFP2-Orp1 by oxygen, standard reaction buffer was degassed and saturated with nitrogen before usage. Furthermore, 96-wellplate was covered with argon for sealing it from the oxygen containing atmosphere. Fluorescence was recorded for 10 min before different amounts of hydrogen peroxide were added (0 µM, 0.1 µM, 0.25 µM, 1 µM and 100 µM final concentration). For estimation of the dynamic range of roGFP2-Orp1, 20 mM DTT was added for full sensor reduction.
For analysing the *in vitro* reduction of purified roGFP2-Orp1 by different cellular redox systems, fluorescence of 1 µM purified sensor in standard reaction buffer was tracked with a

CLARIOstar® platereader. The reduction of the purified roGFP2-Orp1 was initiated by addition of 0.1 mM NADPH to each sample. 10 mM reduced glutathione in presence of 50 µM yeast glutathione reductase, 10 mM reduced glutathione in presence of 50 µM GRXC1 and 50 µM yeast glutathione reductase, as well as 50 µM TRX-o1 in presence of 50 µM NTRb were tested for its capacity to reduce roGFP2-Orp1. As controls, fully reduced and oxidised roGFP2-Orp1 was used.

4.6.5 CLSM-based monitoring of fluorescent biosensors (in isolated embryos or in Arabidopsis seedlings)

Dry seeds were imbibed on a wet filter paper (*4.2.8*) for 10 - 240 min. Testa and the endosperm were carefully removed with scalpel and forceps under a stereomicroscope (Zeiss, Stemi 2000). Embryos were mounted on an inverted Zeiss confocal microscope LSM780 (WAGNER *ET AL.,* 2015) using a 63x objective (Plan-Apochromat 63x/1.40 Oil-immersion DIC M27). Pinhole was set to 1 airy unit to minimise auto-fluorescence contribution from different z-levels. 12 bit images with 512 x 512 pixel resolution were obtained.
For mitochondrial roGFP2-Grx1 biosensor, confocal was set to multi-track mode with line switching between excitation at 405 nm and 488 nm. Emission was recorded in the range of 520 ± 15 nm for both excitation wavelengths; auto-fluorescence was detected in the range of 450 ± 20 nm after excitation at 405 nm. For ATeam biosensor, confocal was set to single-track mode. Samples were excited at 458 nm, emission was recorded in the range of 475 - 500 nm for the CFP domain and 525 – 550 nm for the cpYFP domain.
Images were exported in .lsm format with the Zeiss ZEN 2011 software. For the ratiometric analysis images were loaded into a MatLab-based analysis software (FRICKER 2016) and analysed according to the provided user manual (www.markfricker.org). Ratiometric analysis was performed on a pixel-by-pixel basis with spatial averaging of 3 x 3 pixels. Background fluorescence of individual images in regions without sensor fluorescence was quantified. Overall fluorescence intensities of individual pixels were adjusted accordingly by background subtraction. As a cut-off, fluorescence intensities of individual pixels with less than 2x of the standard deviation of the average background fluorescence intensity were excluded from further analysis. Saturated pixels and pixels within the 10 % quantile of highest fluorescence intensity were excluded for further analysis. Auto-fluorescence correction for the mt-roGFP2-Grx1 data analysis was applied based on a fixed correction factor of 0.5 of the built-in correction mechanism. For mt-roGFP2-Grx1 the 405/488 nm ratio was calculated, whereas for cyt-ATeam the cpYFP/CFP FRET-ratio was determined.
For confocal imaging of five days old seedlings (*4.2.4*) expressing either mitochondrial or cytosolic roGFP2-Orp1, same confocal settings were used as for roGFP2-Grx1 biosensor (see above). For external application of chemicals, *e.g.* menadione or hydrogen peroxide, seedlings were incubated for 20 min in reaction tubes at room temperature. Ratiometric analysis was performed as described above. For co-localisation of mitochondrial targeted roGFP2-Orp1 with the mitochondrial specific fluorescent dye *MitoTracker® Orange CMTMRos* (www.thermofisher.com), seedlings were vacuum-infiltrated in a 500 nM solution of the fluorescent dye for 10 min. Afterwards seedlings were incubated for 2 h in the same solution allowing efficient uptake of the fluorescent dye and an enrichment to mitochondria driven by their membrane potential. Seedlings were mounted on a confocal microscope (WAGNER *ET AL.,* 2015) and the dye was excited at 543 nm while emission was collected in the range of 570 - 620 nm. Chlorophyll auto-fluorescence was collected in the range of 650 - 700 nm at excitation at 488 nm.

4.6.6 Screen for fluorescent, transgenic plants

Seeds dipped with a construct for fluorescent biosensors (T_0-generation, s. *4.2.2*) were cultivated according to *4.2.4*. Five to seven days old seedlings were screened for fluorescence with a Leica M165 FC stereomicroscope equipped with a Leica DFC425 C camera for imaging and standard GFP filters with 470 ± 40 nm for excitation and 525 ± 50 nm for emission. Fluorescent, transgenic T_1 seedlings were put on soil (*4.2.6*) for proliferation of seeds and for the identification of homozygous plants. T_1 generation is uniformly hemizygous for the inserted sensor constructs, whereas the T_2 generation segregates according to Mendel in a 1:2:1 pattern. Because plants homozygous for the sensor construct cannot be distinguished from heterozygous plants by its fluorescence characteristics, propagation of the T_2 plants is mandatory to obtain pure homozygous seed material. T_3 seeds were harvested for each plant separately. Seeds of twelve plants of each T_2 plant were cultivated *in vitro* individually. This allows fluorescence-based screening for homozygous plants: homozygous T_2 plants show no segregation in the corresponding T_3 generation and thus all seedlings show fluorescence, whereas heterozygous T_2 plants segregate, resulting in 25 % non-fluorescent plants in the T_3 generation.

4.6.7 Documentation of different germination stages

Seeds were placed on MS-media plates according to *4.2.4*. Seeds in different stages of germination were documented with a Leica M165 FC stereomicroscope equipped with a Leica DFC425 C camera and a Leica KL 1500 compact bright-field lamp.

4.7 Cooperation partners

All experiments in this thesis were drafted and conceptual designed independently. Technical expertise and equipment from colleagues and cooperation partners were used to expand the technical possibilities. However, all obtained data were analysed and interpreted independently. For the iodoTMT experiments, mitochondria were isolated and labelled independently. Samples were prepared for mass spectrometry analysis during a one week stay in the lab of Dr. Hochgräfe. For the *ntr a/b*, *trx-o1* and *gr2* redox proteomics experiment, samples were labelled and then sent to Dr. Hochgräfe for further processing and mass spectrometry-based analysis. For the seed respiration assay and the quantification of seed metabolites by HPLC and GC-MS, plants were grown and synchronised and seeds were then analysed in the lab of Prof. Macherel and Prof. Hell. Cooperation partners (heads of the corresponding groups) and their contribution to this thesis:

Seed respiration assay		Prof. Dr. David Macherel University of Angers, INRA
Measurements of:	- adenosines - amino acids - organic acids - glutathione	Prof. Dr. Rüdiger Hell University of Heidelberg, COS
MS/MS-based iodoTMT quantification		Dr. Falko Hochgräfe University of Greifswald, ZIK

5. REFERENCES

AKTER, S., HUANG, J. J., BODRA, N., DE SMET, B., WAHNI, K., ROMBAUT, D., PAUWELS, J., GEVAERT, K., CARROLL, K., VAN BREUSEGEM, F. & MESSENS, J. (**2015**). DYn-2 based identification of Arabidopsis sulfenomes. *Molecular & Cellular Proteomics* 14, 1183-1200, doi:10.1074/mcp.M114.046896

ALBRECHT, S. C., BARATA, A. G., GROSSHANS, J., TELEMAN, A. A. & DICK, T. P. (**2011**). *In vivo* mapping of hydrogen peroxide and oxidised glutathione reveals chemical and regional specificity of redox homeostasis. *Cell Metabolism* 14, 819-829, doi:10.1016/j.cmet.2011.10.010

ALKHALFIOUI, F., RENARD, M., VENSEL, W. H., WONG, J., TANAKA, C. K., HURKMAN, W. J., BUCHANAN, B. B. & MONTRICHARD, F. (**2007**). Thioredoxin-linked proteins are reduced during germination of *Medicago truncatula* seeds. *Plant Physiology* 144, 1559-1579, doi:10.1104/pp.107.098103

ARAKI, K., KUSANO, H., SASAKI, N., TANAKA, R., HATTA, T., FUKUI, K. & NATSUME, T. (**2016**). Redox sensitivities of global cellular cysteine residues under reductive and oxidative stress. *Journal of Proteome Research* 15, 2548-2559, doi:10.1021/acs.jproteome.6b00087

ARC, E., GALLAND, M., CUEFF, G., GODIN, B., LOUNIFI, I., JOB, D. & RAJJOU, L. (**2011**). Reboot the system thanks to protein post-translational modifications and proteome diversity: How quiescent seeds restart their metabolism to prepare seedling establishment. *Proteomics* 11, 1606-1618, doi:10.1002/pmic.201000641

ATKINSON, D. E. & WALTON, G. M. (**1967**). Adenosine triphosphate conservation in metabolic regulation - rat liver citrate cleavage enzyme. *Journal of Biological Chemistry* 242, 3239

ATTUCCI, S., CARDE, J. P., RAYMOND, P., SAINTGES, V., SPITERI, A. & PRADET, A. (**1991**). Oxidative-phosphorylation by mitochondria extracted from dry sunflower seeds. *Plant Physiology* 95, 390-398, doi:10.1104/Pp.95.2.390

BAILLY, C. (**2004**). Active oxygen species and antioxidants in seed biology. *Seed Science Research* 14, 93-107, doi:10.1079/Ssr2004159

BAK, D. W., PIZZAGALLI, M. D. & WEERAPANA, E. (**2017**). Identifying functional cysteine residues in the mitochondria. *ACS Chemical Biology*, doi:10.1021/acschembio.6b01074

BALMER, Y., VENSEL, W. H., TANAKA, C. K., HURKMAN, W. J., GELHAYE, E., ROUHIER, N., JACQUOT, J. P., MANIERI, W., SCHUURMANN, P., DROUX, M. & BUCHANAN, B. B. (**2004**). Thioredoxin links redox to the regulation of fundamental processes of plant mitochondria. *Proceedings of the National Academy of Sciences of the United States of America* 101, 2642-2647, doi:10.1073/pnas.0308583101

BAUDISCH, B., LANGNER, U., GARZ, I. & KLOSGEN, R. B. (**2014**). The exception proves the rule? Dual-targeting of nuclear-encoded proteins into endosymbiotic organelles. *New Phytologist* 201, 80-90, doi:10.1111/nph.12482

BAZIN, J., LANGLADE, N., VINCOURT, P., ARRIBAT, S., BALZERGUE, S., EL-MAAROUF-BOUTEAU, H. & BAILLY, C. (**2011**). Targeted mRNA oxidation regulates sunflower seed dormancy alleviation during dry after-ripening. *Plant Cell* 23, 2196-2208, doi:10.1105/tpc.111.086694

BELOUSOV, V. V., FRADKOV, A. F., LUKYANOV, K. A., STAROVEROV, D. B., SHAKHBAZOV, K. S., TERSKIKH, A. V. & LUKYANOV, S. (**2006**). Genetically encoded fluorescent indicator for intracellular hydrogen peroxide. *Nature Methods* 3, 281-286, doi:10.1038/NMETH866

BERNDT, C., SCHWENN, J. D. & LILLIG, C. H. (**2015**). The specificity of thioredoxins and glutaredoxins is determined by electrostatic and geometric complementarity. *Chemical Science* 6, 7049-7058, doi:10.1039/c5sc01501d

BEWLEY, J. D. (**1997**). Seed germination and dormancy. *Plant Cell* 9, 1055-1066, doi:10.1105/Tpc.9.7.1055

BIENERT, G. P., MØLLER, A. L. B., KRISTIANSEN, K. A., SCHULZ, A., MØLLER, I. M., SCHJOERRING, J. K. & JAHN, T. P. (**2007**). Specific aquaporins facilitate the diffusion of hydrogen peroxide across membranes. *Journal of Biological Chemistry* 282, 1183-1192, doi:10.1074/jbc.M603761200

BILAN, D. S., PASE, L., JOOSEN, L., GOROKHOVATSKY, A. Y., ERMAKOVA, Y. G., GADELLA, T. W. J., GRABHER, C., SCHULTZ, C., LUKYANOV, S. & BELOUSOV, V. V. (**2013**). HyPer-3: A genetically encoded H_2O_2 probe with improved performance for ratiometric and fluorescence lifetime imaging. *ACS Chemical Biology* 8, 535-542, doi:10.1021/cb300625g

BITEAU, B., LABARRE, J. & TOLEDANO, M. B. (**2003**). ATP-dependent reduction of cysteine-sulphinic acid by *S. cerevisiae* sulphiredoxin. *Nature* 425, 980-984, doi:10.1038/nature02075

BRADFORD, M. M. (**1976**). A rapid and sensitive method for the quantitation of microgram quantities of protein utilising the principle of protein-dye binding. *Analytical Biochemistry* 72, 248-254, doi:10.1016/0003-2697(76)90527-3

BRANDES, N., REICHMANN, D., TIENSON, H., LEICHERT, L. I. & JAKOB, U. (**2011**). Using quantitative redox proteomics to dissect the yeast *redoxome*. *Journal of Biological Chemistry* 286, 41893-41903, doi:10.1074/jbc.M111.296236

BRANDES, N., TIENSON, H., LINDEMANN, A., VITVITSKY, V., REICHMANN, D., BANERJEE, R. & JAKOB, U. (**2013**). Time line of redox events in ageing postmitotic cells. *Elife* 2, e00306, doi:10.7554/eLife.00306

BRAUN, H. P., BINDER, S., BRENNICKE, A., EUBEL, H., FERNIE, A. R., FINKEMEIER, I., KLODMANN, J., KÖNIG, A. C., KUHN, K., MEYER, E., OBATA, T., SCHWARZLÄNDER, M., TAKENAKA, M. & ZEHRMANN, A. (**2014**). The life of plant mitochondrial complex I. *Mitochondrion* 19 Pt B, 295-313, doi:10.1016/j.mito.2014.02.006

BUROW, M., KESSLER, D. & PAPENBROCK, J. (**2002**). Enzymatic activity of the Arabidopsis sulfurtransferase resides in the C-terminal domain but is boosted by the N-terminal domain and the linker peptide in the full-length enzyme. *Biological Chemistry* 383, 1363-1372, doi:10.1515/Bc.2002.155

BYKOVA, N. V., HOEHN, B., RAMPITSCH, C., BANKS, T., STEBBING, J. A., FAN, T. & KNOX, R. (**2011 a**). Redox-sensitive proteome and antioxidant strategies in wheat seed dormancy control. *Proteomics* 11, 865-882, doi:10.1002/pmic.200900810

BYKOVA, N. V., HOEHN, B., RAMPITSCH, C., HU, J. J., STEBBING, J. A. & KNOX, R. (**2011 b**). Thiol redox-sensitive seed proteome in dormant and non-dormant hybrid genotypes of wheat. *Phytochemistry* 72, 1162-1172, doi:10.1016/j.phytochem.2010.12.021

CARRIE, C., GIRAUD, E., DUNCAN, O., XU, L., WANG, Y., HUANG, S., CLIFTON, R., MURCHA, M., FILIPOVSKA, A., RACKHAM, O., VRIELINK, A. & WHELAN, J. (**2010**). Conserved and novel functions for *Arabidopsis thaliana* MIA40 in assembly of proteins in mitochondria and peroxisomes. *Journal of Biological Chemistry* 285, 36138-36148, doi:10.1074/jbc.M110.121202

CHOUCHANI, E. T., JAMES, A. M., FEARNLEY, I. M., LILLEY, K. S. & MURPHY, M. P. (**2011**). Proteomic approaches to the characterisation of protein thiol modification. *Current Opinion in Chemical Biology* 15, 120-128, doi:10.1016/j.cbpa.2010.11.003

CHOUCHANI, E. T., KAZAK, L., JEDRYCHOWSKI, M. P., LU, G. Z., ERICKSON, B. K., SZPYT, J., PIERCE, K. A., LAZNIK-BOGOSLAVSKI, D., VETRIVELAN, R., CLISH, C. B., ROBINSON, A. J., GYGI, S. P. & SPIEGELMAN, B. M. (**2016**). Mitochondrial ROS regulate thermogenic energy expenditure and sulfenylation of UCP1. *Nature* 532, 112-116, doi:10.1038/nature17399

CHRISTOFOROU, A. L. & LILLEY, K. S. (**2012**). Isobaric tagging approaches in quantitative proteomics: the ups and downs. *Analytical and Bioanalytical Chemistry* 404, 1029-1037, doi:10.1007/s00216-012-6012-9

CHROBOK, D., LAW, S. R., BROUWER, B., LINDEN, P., ZIOLKOWSKA, A., LIEBSCH, D., NARSAI, R., SZAL, B., MORITZ, T., ROUHIER, N., WHELAN, J., GARDESTROM, P. & KEECH, O. (**2016**). Dissecting the metabolic role of mitochondria during developmental leaf senescence. *Plant Physiology* 172, 2132-2153, doi:10.1104/pp.16.01463

CLOUGH, S. J. & BENT, A. F. (**1998**). Floral dip: a simplified method for Agrobacterium-mediated transformation of *Arabidopsis thaliana*. *Plant Journal* 16, 735-743, doi:10.1046/j.1365-313x.1998.00343.x

COSTA, A., DRAGO, I., BEHERA, S., ZOTTINI, M., PIZZO, P., SCHROEDER, J. I., POZZAN, T. & LO SCHIAVO, F. (**2010**). H_2O_2 in plant peroxisomes: an *in vivo* analysis uncovers a Ca^{2+}-dependent scavenging system. *Plant Journal* 62, 760-772, doi:10.1111/j.1365-313X.2010.04190.x

CROUCH, M. L. & SUSSEX, I. M. (**1981**). Development and storage-protein synthesis in *Brassica napus* L. embryos *in vivo* and *in vitro*. *Planta* 153, 64-74, doi:10.1007/BF00385319

DALOSO, D. M., MÜLLER, K., OBATA, T., FLORIAN, A., TOHGE, T., BOTTCHER, A., RIONDET, C., BANAT, L., CARRARI, F., NUNES-NESI, A., BUCHANAN, B. B., REICHHELD, J. P., ARAUJO, W. L. & FERNIE, A. R. (**2015**). Thioredoxin, a master regulator of the tricarboxylic acid cycle in plant mitochondria. *Proceedings of the National Academy of Sciences of the United States of America* 112, E1392-E1400, doi:10.1073/pnas.1424840112

DE VOS, C. H. R., KRAAK, H. L. & BINO, R. J. (**1994**). Ageing of tomato seeds involves glutathione oxidation. *Physiologia Plantarum* 92, 131-139, doi:10.1111/j.1399-3054.1994.tb06664.x

DEBLAERE, R., BYTEBIER, B., DEGREVE, H., DEBOECK, F., SCHELL, J., VANMONTAGU, M. & LEEMANS, J. (**1985**). Efficient octopine Ti plasmid-derived vectors for Agrobacterium-mediated gene-transfer to plants. *Nucleic Acids Research* 13, 4777-4788, doi:10.1093/nar/13.13.4777

DEKKERS, B. J. W., SCHUURMANS, J. A. M. J. & SMEEKENS, S. C. M. (**2008**). Interaction between sugar and abscisic acid signalling during early seedling development in Arabidopsis. *Plant Molecular Biology* 67, 151-167, doi:10.1007/s11103-008-9308-6

DELAUNAY, A., PFLIEGER, D., BARRAULT, M. B., VINH, J. & TOLEDANO, M. B. (**2002**). A thiol peroxidase is an H_2O_2 receptor and redox-transducer in gene activation. *Cell* 111, 471-481, doi:10.1016/S0092-8674(02)01048-6

DIXON, D. P., SKIPSEY, M., GRUNDY, N. M. & EDWARDS, R. (**2005**). Stress-induced protein S-glutathionylation in Arabidopsis. *Plant Physiology* 138, 2233-2244, doi:10.1104/pp.104.058917

DOOLEY, C. T., DORE, T. M., HANSON, G. T., JACKSON, W. C., REMINGTON, S. J. & TSIEN, R. Y. (**2004**). Imaging dynamic redox changes in mammalian cells with green fluorescent protein indicators. *Journal of Biological Chemistry* 279, 22284-22293, doi:10.1074/jbc.M312847200

EASTMOND, P. J., GERMAIN, V., LANGE, P. R., BRYCE, J. H., SMITH, S. M. & GRAHAM, I. A. (**2000**). Postgerminative growth and lipid catabolism in oilseeds lacking the glyoxylate cycle. *Proceedings of the National Academy of Sciences of the United States of America* 97, 5669-5674, doi:10.1073/pnas.97.10.5669

EHRENSHAFT, M. & BRAMBL, R. (**1990**). Respiration and mitochondrial biogenesis in germinating embryos of maize. *Plant Physiology* 93, 295-304, doi:10.1104/Pp.93.1.295

EL-MAAROUF-BOUTEAU, H. & BAILLY, C. (**2008**). Oxidative signaling in seed germination and dormancy. *Plant Signalling & Behavior* 3, 175-182

ELIAS, J. E. & GYGI, S. P. (**2007**). Target-decoy search strategy for increased confidence in large-scale protein identifications by mass spectrometry. *Nature Methods* 4, 207-214, doi:10.1038/nmeth1019

ENGELHARD, J., CHRISTIAN, B. E., WEINGARTEN, L., KUNTZ, G., SPREMULLI, L. L. & DICK, T. P. (**2011**). *In situ* kinetic trapping reveals a fingerprint of reversible protein thiol oxidation in the mitochondrial matrix. *Free Radical Biology and Medicine* 50, 1234-1241, doi:10.1016/j.freeradbiomed.2011.01.035

ERMAKOVA, Y. G., BILAN, D. S., MATLASHOV, M. E., MISHINA, N. M., MARKVICHEVA, K. N., SUBACH, O. M., SUBACH, F. V., BOGESKI, I., HOTH, M., ENIKOLOPOV, G. & BELOUSOV, V. V. (**2014**). Red fluorescent genetically encoded indicator for intracellular hydrogen peroxide. *Nature Communications* 5, doi:10.1038/Ncomms6222

FINKEMEIER, I., GOODMAN, M., LAMKEMEYER, P., KANDLBINDER, A., SWEETLOVE, L. J. & DIETZ, K. J. (**2005**). The mitochondrial type II peroxiredoxin F is essential for redox homeostasis and root growth of *Arabidopsis thaliana* under stress. *Journal of Biological Chemistry* 280, 12168-12180, doi:10.1074/jbc.M413189200

FOREMAN, J., DEMIDCHIK, V., BOTHWELL, J. H. F., MYLONA, P., MIEDEMA, H., TORRES, M. A., LINSTEAD, P., COSTA, S., BROWNLEE, C., JONES, J. D. G., DAVIES, J. M. & DOLAN, L. (**2003**). Reactive oxygen species produced by NADPH oxidase regulate plant cell growth. *Nature* 422, 442-446, doi:10.1038/nature01485

FRICKER, M. D. (**2016**). Quantitative redox imaging software. *Antioxidants & Redox Signaling* 24, 752-762, doi:10.1089/ars.2015.6390

FUJIKAWA, Y., ROMA, L. P., SOBOTTA, M. C., ROSE, A. J., DIAZ, M. B., LOCATELLI, G., BRECKWOLDT, M. O., MISGELD, T., KERSCHENSTEINER, M., HERZIG, S., MÜLLER-DECKER, K. & DICK, T. P. (**2016**). Mouse redox histology using genetically encoded probes. *Science Signalling* 9, rs1, doi:10.1126/scisignal.aad3895

GALLAND, M., HUGUET, R., ARC, E., CUEFF, G., JOB, D. & RAJJOU, L. (**2014**). Dynamic proteomics emphasizes the importance of selective mRNA translation and protein turnover during Arabidopsis seed germination. *Molecular & Cellular Proteomics* 13, 252-268, doi:10.1074/mcp.M113.032227

GARCIA, J., HAN, D., SANCHETI, H., YAP, L. P., KAPLOWITZ, N. & CADENAS, E. (**2010**). Regulation of mitochondrial glutathione redox status and protein glutathionylation by respiratory substrates. *Journal of Biological Chemistry* 285, 39646-39654, doi:10.1074/jbc.M110.164160

GEIGENBERGER, P., RIEWE, D. & FERNIE, A. R. (**2010**). The central regulation of plant physiology by adenylates. *Trends in Plant Science* 15, 98-105, doi:10.1016/j.tplants.2009.11.004

GEISSLER, A., KRIMMER, T., BOMER, U., GUIARD, B., RASSOW, J. & PFANNER, N. (**2000**). Membrane potential-driven protein import into mitochondria - The sorting sequence cytochrome b_2 modulates the Δpsi-dependence of translocation of the matrix-targeting sequence. *Molecular Biology of the Cell* 11, 3977-3991, doi:10.1091/mbc.11.11.3977

GOMES, A., FERNANDES, E. & LIMA, J. L. F. C. (**2005**). Fluorescence probes used for detection of reactive oxygen species. *Journal of Biochemical and Biophysical Methods* 65, 45-80, doi:10.1016/j.jbbm.2005.10.003

GUBLER, F., MILLAR, A. A. & JACOBSEN, J. V. (**2005**). Dormancy release, ABA and pre-harvest sprouting. *Current Opinion in Plant Biology* 8, 183-187, doi:10.1016/j.pbi.2005.01.011

GUTSCHER, M., PAULEAU, A. L., MARTY, L., BRACH, T., WABNITZ, G. H., SAMSTAG, Y., MEYER, A. J. & DICK, T. P. (**2008**). Real-time imaging of the intracellular glutathione redox potential. *Nature Methods* 5, 553-559, doi:10.1038/Nmeth.1212

GUTSCHER, M., SOBOTTA, M. C., WABNITZ, G. H., BALLIKAYA, S., MEYER, A. J., SAMSTAG, Y. & DICK, T. P. (**2009**). Proximity-based protein thiol oxidation by H_2O_2-scavenging peroxidases. *Journal of Biological Chemistry* 284, 31532-31540, doi:10.1074/jbc.M109.059246

GYGI, S. P., RIST, B., GERBER, S. A., TURECEK, F., GELB, M. H. & AEBERSOLD, R. (**1999**). Quantitative analysis of complex protein mixtures using isotope-coded affinity tags. *Nature Biotechnology* 17, 994-999, doi:10.1038/13690

HANSON, G. T., AGGELER, R., OGLESBEE, D., CANNON, M., CAPALDI, R. A., TSIEN, R. Y. & REMINGTON, S. J. (**2004**). Investigating mitochondrial redox potential with redox-sensitive green fluorescent protein indicators. *Journal of Biological Chemistry* 279, 13044-13053, doi:10.1074/jbc.M312846200

HENNE, M., KÖNIG, N., TRIULZI, T., BARONI, S., FORLANI, F., SCHEIBE, R. & PAPENBROCK, J. (**2015**). Sulfurtransferase and thioredoxin specifically interact as demonstrated by bimolecular fluorescence complementation analysis and biochemical tests. *FEBS Open Bio* 5, 832-843, doi:10.1016/j.fob.2015.10.001

HERRMANN, J. M. & RIEMER, J. (**2012**). Mitochondrial disulfide relay: redox-regulated protein import into the intermembrane space. *Journal of Biological Chemistry* 287, 4426-4433, doi:10.1074/jbc.R111.270678

HILDEBRANDT, T. M., NESI, A. N., ARAUJO, W. L. & BRAUN, H. P. (**2015**). Amino acid catabolism in plants. *Molecular Plant* 8, 1563-1579, doi:10.1016/j.molp.2015.09.005

HOFFMANN, C., PLOCHARSKI, B., HAFERKAMP, I., LEROCH, M., EWALD, R., BAUWE, H., RIEMER, J., HERRMANN, J. M. & NEUHAUS, H. E. (**2013**). From endoplasmic reticulum to mitochondria: absence of the Arabidopsis ATP antiporter endoplasmic reticulum adenylate transporter1 perturbs photorespiration. *Plant Cell* 25, 2647-2660, doi:10.1105/tpc.113.113605

HOLDSWORTH, M. J., BENTSINK, L. & SOPPE, W. J. (**2008**). Molecular networks regulating Arabidopsis seed maturation, after-ripening, dormancy and germination. *New Phytologist* 179, 33-54, doi:10.1111/j.1469-8137.2008.02437.x

HOLSCHER, C., MEYER, T. & VON SCHAEWEN, A. (**2014**). Dual-targeting of Arabidopsis 6-phosphogluconolactonase 3 (PGL3) to chloroplasts and peroxisomes involves interaction with Trx m2 in the cytosol. *Molecular Plant* 7, 252-255, doi:10.1093/mp/sst126

HOOPER, C. M., TANZ, S. K., CASTLEDEN, I. R., VACHER, M. A., SMALL, I. D. & MILLAR, A. H. (**2014**). SUBAcon: a consensus algorithm for unifying the subcellular localisation data of the Arabidopsis proteome. *Bioinformatics* 30, 3356-3364, doi:10.1093/bioinformatics/btu550

HOPKINS, F. G. & MORGAN, E. J. (**1943**). Appearance of glutathione during the early stages of the germination of seeds. *Nature* 152, 288-290, doi:10.1038/152288a0

HOURMANT, A. & PRADET, A. (**1981**). Oxidative-phosphorylation in germinating lettuce seeds (*Lactuca-Sativa*) during the 1st hours of imbibition. *Plant Physiology* 68, 631-635, doi:10.1104/Pp.68.3.631

HOWELL, K. A., MILLAR, A. H. & WHELAN, J. (**2006**). Ordered assembly of mitochondria during rice germination begins with promitochondrial structures rich in components of the protein import apparatus. *Plant Molecular Biology* 60, 201-223, doi:10.1007/s11103-005-3688-7

HUNG, Y. P., ALBECK, J. G., TANTAMA, M. & YELLEN, G. (**2011**). Imaging cytosolic NADH-NAD^+ redox state with a genetically encoded fluorescent biosensor. *Cell Metabolism* 14, 545-554, doi:10.1016/j.cmet.2011.08.012

HURD, T. R., COSTA, N. J., DAHM, C. C., BEER, S. M., BROWN, S. E., FILIPOVSKA, A. & MURPHY, M. P. (**2005**). Glutathionylation of mitochondrial proteins. *Antioxidants & Redox Signaling* 7, 999-1010, doi:10.1089/ars.2005.7.999

HURD, T. R., PRIME, T. A., HARBOUR, M. E., LILLEY, K. S. & MURPHY, M. P. (**2007**). Detection of reactive oxygen species-sensitive thiol proteins by redox difference gel electrophoresis - Implications for mitochondrial redox signaling. *Journal of Biological Chemistry* 282, 22040-22051, doi:10.1074/jbc.M703591200

IGLESIAS-BAENA, I., BARRANCO-MEDINA, S., LAZARO-PAYO, A., LOPEZ-JARAMILLO, F. J., SEVILLA, F. & LAZARO, J. J. (**2010**). Characterization of plant sulfiredoxin and role of sulphinic form of 2-Cys peroxiredoxin. *Journal of Experimental Botany* 61, 1509-1521, doi:10.1093/jxb/erq016

IMAMURA, H., NHAT, K. P., TOGAWA, H., SAITO, K., IINO, R., KATO-YAMADA, Y., NAGAI, T. & NOJI, H. (**2009**). Visualization of ATP levels inside single living cells with fluorescence resonance energy transfer-based genetically encoded indicators. *Proceedings of the National Academy of Sciences of the United States of America* 106, 15651-15656, doi:10.1073/pnas.0904764106

JOB, C., RAJJOU, L., LOVIGNY, Y., BELGHAZI, M. & JOB, D. (**2005**). Patterns of protein oxidation in Arabidopsis seeds and during germination. *Plant Physiology* 138, 790-802, doi:10.1104/pp.105.062778

KADOKURA, H., TIAN, H. P., ZANDER, T., BARDWELL, J. C. A. & BECKWITH, J. (**2004**). Snapshots of DsbA in action: Detection of proteins in the process of oxidative folding. *Science* 303, 534-537, doi:10.1126/science.1091724

KALLIO, P. & PIIROINEN, P. (**1959**). Effect of gibberellin on the termination of dormancy in some seeds. *Nature* 183, 1830-1831, doi:10.1038/1831830a0

KATAYA, A. R. & REUMANN, S. (**2010**). Arabidopsis glutathione reductase 1 is dually targeted to peroxisomes and the cytosol. *Plant Signalling & Behavior* 5, 171-175, doi:10.4161/psb.5.2.10527

KIBINZA, S., VINEL, D., COME, D., BAILLY, C. & CORBINEAU, F. (**2006**). Sunflower seed deterioration as related to moisture content during ageing, energy metabolism and active oxygen species scavenging. *Physiologia Plantarum* 128, 496-506, doi:10.1111/j.1399-3054.2006.00771.x

KIM, J. R., YOON, H. W., KWON, K. S., LEE, S. R. & RHEE, S. G. (**2000**). Identification of proteins containing cysteine residues that are sensitive to oxidation by hydrogen peroxide at neutral pH. *Analytical Biochemistry* 283, 214-221, doi:10.1006/abio.2000.4623

KNOEFLER, D., THAMSEN, M., KONICZEK, M., NIEMUTH, N. J., DIEDERICH, A. K. & JAKOB, U. (**2012**). Quantitative *in vivo* redox sensors uncover oxidative stress as an early event in life. *Molecular Cell* 47, 767-776, doi:10.1016/j.molcel.2012.06.016

KOBREHEL, K., WONG, J. H., BALOGH, A., KISS, F., YEE, B. C. & BUCHANAN, B. B. (**1992**). Specific reduction of wheat storage proteins by thioredoxin-h. *Plant Physiology* 99, 919-924, doi:10.1104/Pp.99.3.919

KRANNER, I. & GRILL, D. (**1993**). Content of low-molecular-weight thiols during the imbibition of pea-seeds. *Physiologia Plantarum* 88, 557-562, doi:10.1034/j.1399-3054.1993.880404.x

LAEMMLI, U. K. (**1970**). Cleavage of structural proteins during the assembly of the head of bacteriophage T4. *Nature* 227, 680-685, doi:10.1038/227680a0

LAW, S. R., NARSAI, R., TAYLOR, N. L., DELANNOY, E., CARRIE, C., GIRAUD, E., MILLAR, A. H., SMALL, I. & WHELAN, J. (**2012**). Nucleotide and RNA metabolism prime translational initiation in the earliest events of mitochondrial biogenesis during Arabidopsis germination. *Plant Physiology* 158, 1610-1627, doi:10.1104/pp.111.192351

LAW, S. R., NARSAI, R. & WHELAN, J. (**2014**). Mitochondrial biogenesis in plants during seed germination. *Mitochondrion* 19, 214-221, doi:10.1016/j.mito.2014.04.002

LEICHERT, L. I. & JAKOB, U. (**2006**). Global methods to monitor the thiol-disulfide state of proteins *in vivo*. *Antioxidants & Redox Signaling* 8, 763-772, doi:10.1089/ars.2006.8.763

LEICHERT, L. I., GEHRKE, F., GUDISEVA, H. V., BLACKWELL, T., ILBERT, M., WALKER, A. K., STRAHLER, J. R., ANDREWS, P. C. & JAKOB, U. (**2008**). Quantifying changes in the thiol redox proteome upon oxidative stress *in vivo*. *Proceedings of the National Academy of Sciences of the United States of America* 105, 8197-8202, doi:10.1073/pnas.0707723105

LINKIES, A. & LEUBNER-METZGER, G. (**2012**). Beyond gibberellins and abscisic acid: how ethylene and jasmonates control seed germination. *Plant Cell Reports* 31, 253-270, doi:10.1007/s00299-011-1180-1

LOGAN, D. C. & LEAVER, C. J. (**2000**). Mitochondria-targeted GFP highlights the heterogeneity of mitochondrial shape, size and movement within living plant cells. *Journal of Experimental Botany* 51, 865-871, doi:10.1093/jexbot/51.346.865

LOZANO, R. M., WONG, J. H., YEE, B. C., PETERS, A., KOBREHEL, K. & BUCHANAN, B. B. (**1996**). New evidence for a role for thioredoxin h in germination and seedling development. *Planta* 200, 100-106, doi:10.1007/BF00196655

MAGNESCHI, L. & PERATA, P. (**2009**). Rice germination and seedling growth in the absence of oxygen. *Annals of Botany* 103, 181-196, doi:10.1093/aob/mcn121

MAILLOUX, R. J., JIN, X. L. & WILLMORE, W. G. (**2014**). Redox regulation of mitochondrial function with emphasis on cysteine oxidation reactions. *Redox Biology* 2, 123-139, doi:10.1016/j.redox.2013.12.011

MAO, G., WANG, R., GUAN, Y., LIU, Y. & ZHANG, S. (**2011**). Sulfurtransferases 1 and 2 play essential roles in embryo and seed development in *Arabidopsis thaliana*. *Journal of Biological Chemistry* 286, 7548-7557, doi:10.1074/jbc.M110.182865

MARCHESI, E., ROTA, C., FANN, Y. C., CHIGNELL, C. F. & MASON, R. P. (**1999**). Photoreduction of the fluorescent dye 2 '-7 '-dichlorofluorescein: A spin trapping and direct electron spin resonance study with implications for oxidative stress measurements. *Free Radical Biology and Medicine* 26, 148-161, doi:10.1016/S0891-5849(98)00174-9

MARKVICHEVA, K. N., BILAN, D. S., MISHINA, N. M., GOROKHOVATSKY, A. Y., VINOKUROV, L. M., LUKYANOV, S. & BELOUSOV, V. V. (**2011**). A genetically encoded sensor for H_2O_2 with expanded dynamic range. *Bioorganic & Medicinal Chemistry* 19, 1079-1084, doi:10.1016/j.bmc.2010.07.014

MARTI, M. C., OLMOS, E., CALVETE, J. J., DIAZ, I., BARRANCO-MEDINA, S., WHELAN, J., LAZARO, J. J., SEVILLA, F. & JIMENEZ, A. (**2009**). Mitochondrial and nuclear localisation of a novel Pea thioredoxin: Identification of its mitochondrial target proteins. *Plant Physiology* 150, 646-657, doi:10.1104/pp.109.138073

MARTY, L., SIALA, W., SCHWARZLÄNDER, M., FRICKER, M. D., WIRTZ, M., SWEETLOVE, L. J., MEYER, Y., MEYER, A. J., REICHHELD, J. P. & HELL, R. (**2009**). The NADPH-dependent thioredoxin system constitutes a functional backup for cytosolic glutathione reductase in Arabidopsis. *Proceedings of the National Academy of Sciences of the United States of America* 106, 9109-9114, doi:10.1073/pnas.0900206106

MARX, C., WONG, J. H. & BUCHANAN, B. B. (**2003**). Thioredoxin and germinating barley: targets and protein redox changes. *Planta* 216, 454-460, doi:10.1007/s00425-002-0857-7

MENG, L., WONG, J. H., FELDMAN, L. J., LEMAUX, P. G. & BUCHANAN, B. B. (**2010**). A membrane-associated thioredoxin required for plant growth moves from cell to cell, suggestive of a role in intercellular communication. *Proceedings of the National Academy of Sciences of the United States of America* 107, 3900-3905, doi:10.1073/pnas.0913759107

MENGER, K. E., JAMES, A. M., COCHEME, H. M., HARBOUR, M. E., CHOUCHANI, E. T., DING, S. J., FEARNLEY, I. M., PARTRIDGE, L. & MURPHY, M. P. (**2015**). Fasting, but not aging, dramatically alters the redox status of cysteine residues on proteins in *Drosophila melanogaster*. *Cell Reports* 11, 1856-1865, doi:10.1016/j.celrep.2015.05.033

MEYER, A. J., BRACH, T., MARTY, L., KREYE, S., ROUHIER, N., JACQUOT, J. P. & HELL, R. (**2007**). Redox-sensitive GFP in *Arabidopsis thaliana* is a quantitative biosensor for the redox potential of the cellular glutathione redox buffer. *Plant Journal* 52, 973-986, doi:10.1111/j.1365-313X.2007.03280.x

MICHELET, L., ZAFFAGNINI, M., MARCHAND, C., COLLIN, V., DECOTTIGNIES, P., TSAN, P., LANCELIN, J. M., TROST, P., MIGINIAC-MASLOW, M., NOCTOR, G. & LEMAIRE, S. D. (**2005**). Glutathionylation of chloroplast thioredoxin f is a redox signaling mechanism in plants. *Proceedings of the National Academy of Sciences of the United States of America* 102, 16478-16483, doi:10.1073/pnas.0507498102

MØLLER, I. M. & RASMUSSON, A. G. (**1998**). The role of NADP in the mitochondrial matrix. *Trends in Plant Science* 3, 21-27, doi:10.1016/S1360-1385(97)01156-4

MOREIRA, B. & PAUSAS, J. G. (**2012**). Tanned or burned: The role of fire in shaping physical seed dormancy. *PLOS ONE* 7, doi:10.1371/journal.pone.0051523

MORGAN, B., VAN LAER, K., OWUSU, T. N. E., EZERINA, D., PASTOR-FLORES, D., AMPONSAH, P. S., TURSCH, A. & DICK, T. P. (**2016**). Real-time monitoring of basal H_2O_2 levels with peroxiredoxin-based probes. *Nature Chemical Biology* 12, 437-U495, doi:10.1038/Nchembio.2067

MOSELER, A., ALLER, I., WAGNER, S., NIETZEL, T., PRZYBYLA-TOSCANO, J., MÜHLENHOFF, U., LILL, R., BERNDT, C., ROUHIER, N., SCHWARZLÄNDER, M. & MEYER, A. J. (**2015**). The mitochondrial monothiol glutaredoxin S15 is essential for iron-sulfur protein maturation in *Arabidopsis thaliana*. *Proceedings of the National Academy of Sciences of the United States of America* 112, 13735-13740, doi:10.1073/pnas.1510835112

MOTOHASHI, K., KONDOH, A., STUMPP, M. T. & HISABORI, T. (**2001**). Comprehensive survey of proteins targeted by chloroplast thioredoxin. *Proceedings of the National Academy of Sciences of the United States of America* 98, 11224-11229, doi:10.1073/pnas.191282098

MURPHY, M. P. (**2009**). How mitochondria produce reactive oxygen species. *Biochemical Journal* 417, 1-13, doi:10.1042/Bj20081386

NAGEL, M., KRANNER, I., NEUMANN, K., ROLLETSCHEK, H., SEAL, C. E., COLVILLE, L., FERNANDEZ-MARIN, B. & BORNER, A. (**2015**). Genome-wide association mapping and biochemical markers reveal that seed ageing and longevity are intricately affected by genetic background and developmental and environmental conditions in barley. *Plant Cell and Environment* 38, 1011-1022, doi:10.1111/pce.12474

NÉE, G., XIANG, Y. & SOPPE, W. J. (**2017**). The release of dormancy, a wake-up call for seeds to germinate. *Current Opinion in Plant Biology* 35, doi:10.1016/j.pbi.2016.09.002

NEILL, S., DESIKAN, R. & HANCOCK, J. (**2002**). Hydrogen peroxide signalling. *Current Opinion in Plant Biology* 5, 388-395, doi:10.1016/S1369-5266(02)00282-0

NIETHAMMER, P., GRABHER, C., LOOK, A. T. & MITCHISON, T. J. (**2009**). A tissue-scale gradient of hydrogen peroxide mediates rapid wound detection in zebrafish. *Nature* 459, 996-U123, doi:10.1038/nature08119

NIETZEL, T., MOSTERTZ, J., HOCHGRÄFE, F. & SCHWARZLÄNDER, M. (**2017**). Redox regulation of mitochondrial proteins and proteomes by cysteine thiol switches. *Mitochondrion*, doi:10.1016/j.mito.2016.07.010

NOCTOR, G., QUEVAL, G. & GAKIERE, B. (**2006**). NAD(P) synthesis and pyridine nucleotide cycling in plants and their potential importance in stress conditions. *Journal of Experimental Botany* 57, 1603-1620, doi:10.1093/jxb/erj202

NUNES-NESI, A., ARAUJO, W. L., OBATA, T. & FERNIE, A. R. (**2013**). Regulation of the mitochondrial tricarboxylic acid cycle. *Current Opinion in Plant Biology* 16, 335-343, doi:10.1016/j.pbi.2013.01.004

ORACZ, K., EL-MAAROUF-BOUTEAU, H., KRANNER, I., BOGATEK, R., CORBINEAU, F. & BAILLY, C. (**2009**). The mechanisms involved in seed dormancy alleviation by hydrogen cyanide unravel the role of reactive oxygen species as key factors of cellular signaling during germination. *Plant Physiology* 150, 494-505, doi:10.1104/pp.109.138107

PASZKIEWICZ, G., GUALBERTO, J. M., BENAMAR, A., MACHEREL, D. & LOGAN, D. C. (**2017**). Arabidopsis seed mitochondria are bioenergetically active immediately upon imbibition and specialize via biogenesis in preparation for autotrophic growth. *Plant Cell* 29, 109-128, doi:10.1105/tpc.16.00700

PATTERSON, G. H., KNOBEL, S. M., SHARIF, W. D., KAIN, S. R. & PISTON, D. W. (**1997**). Use of the green fluorescent protein and its mutants in quantitative fluorescence microscopy. *Biophysical Journal* 73, 2782-2790, doi:10.1016/S0006-3495(97)78307-3

PAULSEN, C. E., TRUONG, T. H., GARCIA, F. J., HOMANN, A., GUPTA, V., LEONARD, S. E. & CARROLL, K. S. (**2012**). Peroxide-dependent sulfenylation of the EGFR catalytic site enhances kinase activity. *Nature Chemical Biology* 8, 57-64, doi:10.1038/nchembio.736

PFANNER, N. & GEISSLER, A. (**2001**). Versatility of the mitochondrial protein import machinery. *Nature Reviews Molecular Cell Biology* 2, 339-349, doi:10.1038/35073006

POTOCKY, M., JONES, M. A., BEZVODA, R., SMIRNOFF, N. & ZARSKY, V. (**2007**). Reactive oxygen species produced by NADPH oxidase are involved in pollen tube growth. *New Phytologist* 174, 742-751, doi:10.1111/j.1469-8137.2007.02042.x

PRACHAROENWATTANA, I., CORNAH, J. E. & SMITH, S. M. (**2005**). Arabidopsis peroxisomal citrate synthase is required for fatty acid respiration and seed germination. *Plant Cell* 17, 2037-2048, doi:10.1105/tpc.105.031856

QUEVAL, G., ISSAKIDIS-BOURGUET, E., HOEBERICHTS, F. A., VANDORPE, M., GAKIERE, B., VANACKER, H., MIGINIAC-MASLOW, M., VAN BREUSEGEM, F. & NOCTOR, G. (**2007**). Conditional oxidative stress responses in the Arabidopsis photorespiratory mutant *cat2* demonstrate that redox state is a key modulator of daylength-dependent gene expression, and define photoperiod as a crucial factor in the regulation of H_2O_2-induced cell death. *Plant Journal* 52, 640-657, doi:10.1111/j.1365-313X.2007.03263.x

RAJJOU, L., LOVIGNY, Y., GROOT, S. P. C., BELGHAZ, M., JOB, C. & JOB, D. (**2008**). Proteome-wide characterisation of seed aging in Arabidopsis: A comparison between artificial and natural aging protocols. *Plant Physiology* 148, 620-641, doi:10.1104/pp.108.123141

RAYMOND, P., ALANI, A. & PRADET, A. (**1985**). ATP production by respiration and fermentation, and energy-charge during aerobiosis and anaerobiosis in 12 fatty and starchy germinating-seeds. *Plant Physiology* 79, 879-884, doi:10.1104/Pp.79.3.879

REICHHELD, J. P., MEYER, E., KHAFIF, M., BONNARD, G. & MEYER, Y. (**2005**). AtNTRB is the major mitochondrial thioredoxin reductase in *Arabidopsis thaliana*. *FEBS Letters* 579, 337-342, doi:10.1016/j.febslet.2004.11.094

REICHHELD, J. P., KHAFIF, M., RIONDET, C., DROUX, M., BONNARD, G. & MEYER, Y. (**2007**). Inactivation of thioredoxin reductases reveals a complex interplay between thioredoxin and glutathione pathways in Arabidopsis development. *Plant Cell* 19, 1851-1865, doi:10.1105/tpc.107.050849

RIEMER, J., BULLEID, N. & HERRMANN, J. M. (**2009**). Disulfide formation in the ER and mitochondria: Two solutions to a common process. *Science* 324, 1284-1287, doi:10.1126/science.1170653

ROMA, L. P., DUPREZ, J., TAKAHASHI, H. K., GILON, P., WIEDERKEHR, A. & JONAS, J. C. (**2012**). Dynamic measurements of mitochondrial hydrogen peroxide concentration and glutathione redox state in rat pancreatic beta-cells using ratiometric fluorescent proteins: confounding effects of pH with HyPer but not roGFP1. *Biochemical Journal* 441, 971-978, doi:10.1042/BJ20111770

ROTTENSTEINER, H. & THEODOULOU, F. L. (**2006**). The ins and outs of peroxisomes: Co-ordination of membrane transport and peroxisomal metabolism. *Biochimica Et Biophysica Acta-Molecular Cell Research* 1763, 1527-1540, doi:10.1016/j.bbamcr.2006.08.012

ROUHIER, N., VILLAREJO, A., SRIVASTAVA, M., GELHAYE, E., KEECH, O., DROUX, M., FINKEMEIER, I., SAMUELSSON, G., DIETZ, K. J., JACQUOT, J. P. & WINGSLE, G. (**2005**). Identification of plant glutaredoxin targets. *Antioxidants & Redox Signaling* 7, 919-929, doi:10.1089/ars.2005.7.919

SALLON, S., SOLOWEY, E., COHEN, Y., KORCHINSKY, R., EGLI, M., WOODHATCH, I., SIMCHONI, O. & KISLEV, M. (**2008**). Germination, genetics, and growth of an ancient date seed. *Science* 320, 1464-1464, doi:10.1126/science.1153600

SATTLER, S. E., GILLILAND, L. U., MAGALLANES-LUNDBACK, M., POLLARD, M. & DELLAPENNA, D. (**2004**). Vitamin E is essential for seed longevity, and for preventing lipid peroxidation during germination. *Plant Cell* 16, 1419-1432, doi:10.1105/tpc.021360

SCHIKOWSKY, C., SENKLER, J. & BRAUN, H. P. (**2017**). SDH6 and SDH7 contribute to anchoring succinate dehydrogenase to the inner mitochondrial membrane in *Arabidopsis thaliana*. *Plant Physiology* 173, 1094-1108, doi:10.1104/pp.16.01675

SCHMIDTMANN, E., KÖNIG, A. C., ORWAT, A., LEISTER, D., HARTL, M. & FINKEMEIER, I. (**2014**). Redox regulation of Arabidopsis mitochondrial citrate synthase. *Molecular Plant* 7, 156-169, doi:10.1093/mp/sst144

SCHOPFER, P., PLACHY, C. & FRAHRY, G. (**2001**). Release of reactive oxygen intermediates (superoxide radicals, hydrogen peroxide, and hydroxyl radicals) and peroxidase in germinating radish seeds controlled by light, gibberellin, and abscisic acid. *Plant Physiology* 125, 1591-1602, doi:10.1104/pp.125.4.1591

SCHWARZLÄNDER, M., FRICKER, M. D., MÜLLER, C., MARTY, L., BRACH, T., NOVAK, J., SWEETLOVE, L. J., HELL, R. & MEYER, A. J. (**2008**). Confocal imaging of glutathione redox potential in living plant cells. *Journal of Microscopy* 231, 299-316, doi:10.1111/j.1365-2818.2008.02030.x

SCHWARZLÄNDER, M., LOGAN, D. C., FRICKER, M. D. & SWEETLOVE, L. J. (**2011**). The circularly permuted yellow fluorescent protein cpYFP that has been used as a superoxide probe is highly responsive to pH but not superoxide in mitochondria: implications for the existence of superoxide 'flashes'. *Biochemical Journal* 437, 381-387, doi:10.1042/Bj20110883

SCHWARZLÄNDER, M., WAGNER, S., ERMAKOVA, Y. G., BELOUSOV, V. V., RADI, R., BECKMAN, J. S., BUETTNER, G. R., DEMAUREX, N., DUCHEN, M. R., FORMAN, H. J., FRICKER, M. D., GEMS, D., HALESTRAP, A. P., HALLIWELL, B., JAKOB, U., JOHNSTONN, I. G., JONES, N. S., LOGAN, D. C., MORGAN, B., MÜLLER, F. L., NICHOLLS, D. G., REMINGTON, S. J., SCHUMACKER, P. T., WINTERBOURN, C. C., SWEETLOVE, L. J., MEYER, A. J., DICK, T. P. & MURPHY, M. P. (**2014**). The 'mitoflash' probe cpYFP does not respond to superoxide. *Nature* 514, E12-E14, doi:10.1038/nature13858

SCHWARZLÄNDER, M., DICK, T. P., MEYER, A. J. & MORGAN, B. (**2016**). Dissecting redox biology using fluorescent protein sensors. *Antioxidants & Redox Signaling* 24, 680-712, doi:10.1089/ars.2015.6266

SECHET, J., ROUX, C., PLESSIS, A., EFFROY, D., FREY, A., PERREAU, F., BINIEK, C., KRIEGER-LISZKAY, A., MACHEREL, D., NORTH, H. M., MIREAU, H. & MARION-POLL, A. (**2015**). The ABA-deficiency suppressor locus HAS2 encodes the PPR protein LOI1/MEF11 involved in mitochondrial RNA editing. *Molecular Plant* 8, 644-656, doi:10.1016/j.molp.2014.12.005

SENKLER, J., SENKLER, M., EUBEL, H., HILDEBRANDT, T., LENGWENUS, C., SCHERTL, P., SCHWARZLÄNDER, M., WAGNER, S., WITTIG, I. & BRAUN, H. P. (**2017**). The mitochondrial complexome of *Arabidopsis thaliana*. *Plant Journal* 89, 1079-1092, doi:10.1111/tpj.13448

SHEWRY, P. R., NAPIER, J. A. & TATHAM, A. S. (**1995**). Seed storage proteins - structures and biosynthesis. *Plant Cell* 7, 945-956, doi:10.1105/Tpc.7.7.945

SONDHEIMER, E., TZOU, D. S. & GALSON, E. C. (**1968**). Abscisic acid levels and seed dormancy. *Plant Physiology* 43, 1443-+, doi:10.1104/Pp.43.9.1443

STRÖHER, E., GRASSL, J., CARRIE, C., FENSKE, R., WHELAN, J. & MILLAR, A. H. (**2016**). Glutaredoxin S15 is involved in Fe-S cluster transfer in mitochondria influencing lipoic acid-dependent enzymes, plant growth, and arsenic tolerance in Arabidopsis. *Plant Physiology* 170, 1284-1299, doi:10.1104/pp.15.01308

SWEETLOVE, L. J., TAYLOR, N. L. & LEAVER, C. J. (**2007**). Isolation of intact, functional mitochondria from the model plant *Arabidopsis thaliana*. *Methods in Molecular Biology* 372, 125-136, doi:10.1007/978-1-59745-365-3_9

SZABADOS, L. & SAVOURE, A. (**2010**). Proline: a multifunctional amino acid. *Trends in Plant Science* 15, 89-97, doi:10.1016/j.tplants.2009.11.009

TAO, R., ZHAO, Y., CHU, H., WANG, A., ZHU, J., CHEN, X., ZOU, Y., SHI, M., LIU, R., SU, N., DU, J., ZHOU, H. M., ZHU, L., QIAN, X., LIU, H., LOSCALZO, J. & YANG, Y. (**2017**). Genetically encoded fluorescent sensors reveal dynamic regulation of NADPH metabolism. *Nature Methods*, doi:10.1038/nmeth.4306

THOMPSON, A., SCHÄFER, J., KUHN, K., KIENLE, S., SCHWARZ, J., SCHMIDT, G., NEUMANN, T., JOHNSTONE, R., MOHAMMED, A. K. & HAMON, C. (**2003**). Tandem mass tags: a novel quantification strategy for comparative analysis of complex protein mixtures by MS/MS. *Analytical Chemistry* 75, 1895-1904, doi:10.1021/ac0262560

TOMMASI, F., PACIOLLA, C., DE PINTO, M. C. & DE GARA, L. (**2001**). A comparative study of glutathione and ascorbate metabolism during germination of *Pinus pinea* L. seeds. *Journal of Experimental Botany* 52, 1647-1654, doi:10.1093/jxb/52.361.1647

TORRES, M., DE PAULA, M., PEREZ-OTAOLA, M., DARDER, M., FRUTOS, G. & MARTINEZ-HONDUVILLA, C. J. (**1997**). Ageing-induced changes in glutathione system of sunflower seeds. *Physiologia Plantarum* 101, 807-814, doi:10.1111/j.1399-3054.1997.tb01067.x

TRAVERSO, J. A., MICALELLA, C., MARTINEZ, A., BROWN, S. C., SATIAT-JEUNEMAITRE, B., MEINNEL, T. & GIGLIONE, C. (**2013**). Roles of N-terminal fatty acid acylations in membrane compartment partitioning: Arabidopsis h-type thioredoxins as a case study. *Plant Cell* 25, 1056-1077, doi:10.1105/tpc.112.106849

TRONCONI, M. A., MAURINO, V. G., ANDREO, C. S. & DRINCOVICH, M. F. (**2010**). Three different and tissue-specific NAD-malic enzymes generated by alternative subunit association in *Arabidopsis thaliana*. *Journal of Biological Chemistry* 285, 11870-11879, doi:10.1074/jbc.M109.097477

VANLERBERGHE, G. C., DAY, D. A., WISKICH, J. T., VANLERBERGHE, A. E. & MCINTOSH, L. (**1995**). Alternative oxidase activity in tobacco leaf mitochondria - dependence on tricarboxylic-acid cycle-mediated redox regulation and pyruvate activation. *Plant Physiology* 109, 353-361, doi:10.1104/pp.109.2.353

VERBRUGGEN, N. & HERMANS, C. (**2008**). Proline accumulation in plants: a review. *Amino Acids* 35, 753-759, doi:10.1007/s00726-008-0061-6

VERDOUCQ, L., VIGNOLS, F., JACQUOT, J. P., CHARTIER, Y. & MEYER, Y. (**1999**). *In vivo* characterisation of a thioredoxin h target protein defines a new peroxiredoxin family. *Journal of Biological Chemistry* 274, 19714-19722, doi:10.1074/jbc.274.28.19714

WAGNER, S., NIETZEL, T., ALLER, I., COSTA, A., FRICKER, M. D., MEYER, A. J. & SCHWARZLÄNDER, M. (**2015**). Analysis of plant mitochondrial function using fluorescent protein sensors. *Methods in Molecular Biology* 1305, 241-252, doi:10.1007/978-1-4939-2639-8_17

WALTERS, C. (**1998**). Understanding the mechanisms and kinetics of seed aging. *Seed Science Research* 8, 223-244, doi:10.1017/S096025850000413X

WASZCZAK, C., AKTER, S., EECKHOUT, D., PERSIAU, G., WAHNI, K., BODRA, N., VAN MOLLE, I., DE SMET, B., VERTOMMEN, D., GEVAERT, K., DE JAEGER, G., VAN MONTAGU, M., MESSENS, J. & VAN BREUSEGEM, F. (**2014**). Sulfenome mining in *Arabidopsis thaliana*. *Proceedings of the National Academy of Sciences of the United States of America* 111, 11545-11550, doi:10.1073/pnas.1411607111

WEDEL, N., SOLL, J. & PAAP, B. K. (**1997**). CP12 provides a new mode of light regulation of Calvin cycle activity in higher plants. *Proceedings of the National Academy of Sciences of the United States of America* 94, 10479-10484, doi:10.1073/pnas.94.19.10479

WEERAPANA, E., WANG, C., SIMON, G. M., RICHTER, F., KHARE, S., DILLON, M. B., BACHOVCHIN, D. A., MOWEN, K., BAKER, D. & CRAVATT, B. F. (**2010**). Quantitative reactivity profiling predicts functional cysteines in proteomes. *Nature* 468, 790-795, doi:10.1038/nature09472

WEITBRECHT, K., MÜLLER, K. & LEUBNER-METZGER, G. (**2011**). First off the mark: early seed germination. *Journal of Experimental Botany* 62, 3289-3309, doi:10.1093/jxb/err030

WELLER, J., KIZINA, K. M., CAN, K., BAO, G. & MÜLLER, M. (**2014**). Response properties of the genetically encoded optical H_2O_2 sensor HyPer. *Free Radical Biology and Medicine* 76, 227-241, doi:10.1016/j.freeradbiomed.2014.07.045

WILL, Y., HYNES, J., OGURTSOV, V. I. & PAPKOVSKY, D. B. (**2006**). Analysis of mitochondrial function using phosphorescent oxygen-sensitive probes. *Nature Protocols* 1, 2563-2572, doi:10.1038/nprot.2006.351

WINGER, A. M., TAYLOR, N. L., HEAZLEWOOD, J. L., DAY, D. A. & MILLAR, A. H. (**2007**). Identification of intra- and intermolecular disulfide bonding in the plant mitochondrial proteome by diagonal gel electrophoresis. *Proteomics* 7, 4158-4170, doi:10.1002/pmic.200700209

WOLOSIUK, R. A. & BUCHANAN, B. B. (**1977**). Thioredoxin and glutathione regulate photosynthesis in chloroplasts. *Nature* 266, 565-567, doi:10.1038/266565a0

WONG, J. H., CAI, N., TANAKA, C. K., VENSEL, W. H., HURKMAN, W. J. & BUCHANAN, B. B. (**2004**). Thioredoxin reduction alters the solubility of proteins of wheat starchy endosperm: An early event in cereal germination. *Plant and Cell Physiology* 45, 407-415, doi:10.1093/Pcp/Pch044

WOO, H. A., JEONG, W. J., CHANG, T. S., PARK, K. J., PARK, S. J., YANG, J. S. & RHEE, S. G. (**2005**). Reduction of cysteine sulfinic acid by sulfiredoxin is specific to 2-Cys peroxiredoxins. *Journal of Biological Chemistry* 280, 3125-3128, doi:10.1074/jbc.C400496200

WOODSTOCK, L. W. & GRABE, D. F. (**1967**). Relationships between seed respiration during imbibition and subsequent seedling growth in *Zea mays* L. *Plant Physiology* 42, 1071, doi:10.1104/Pp.42.8.1071

YAMAZAKI, D., MOTOHASHI, K., KASAMA, T., HARA, Y. & HISABORI, T. (**2004**). Target proteins of the cytosolic thioredoxins in *Arabidopsis thaliana*. *Plant and Cell Physiology* 45, 18-27, doi:10.1093/Pcp/Pch019

YANG, J., CARROLL, K. S. & LIEBLER, D. C. (**2016**). The expanding landscape of the thiol redox proteome. *Molecular & Cellular Proteomics* 15, 1-11, doi:10.1074/mcp.O115.056051

YANO, H., WONG, J. H., CHO, M. J. & BUCHANAN, B. B. (**2001**). Redox changes accompanying the degradation of seed storage proteins in germinating rice. *Plant and Cell Physiology* 42, 879-883, doi:10.1093/Pcp/Pce119

YOSHIBA, Y., KIYOSUE, T., NAKASHIM, K., YAMAGUCHI-SHINOZAKI, K. & SHINOZAKJ, K. (**1997**). Regulation of levels of proline as an osmolyte in plants under water stress. *Plant Cell Physiology* 38, 1095-1102

YOSHIDA, K., NOGUCHI, K., MOTOHASHI, K. & HISABORI, T. (**2013**). Systematic exploration of thioredoxin target proteins in plant mitochondria. *Plant and Cell Physiology* 54, 875-892, doi:10.1093/pcp/pct037

YOSHIDA, K. & HISABORI, T. (**2014**). Mitochondrial isocitrate dehydrogenase is inactivated upon oxidation and reactivated by thioredoxin-dependent reduction in Arabidopsis. *Frontiers in Environmental Science*, doi:10.3389/fenvs.2014.00038

YOSHIDA, K. & HISABORI, T. (**2016**). Adenine nucleotide-dependent and redox-independent control of mitochondrial malate dehydrogenase activity in *Arabidopsis thaliana*. *Biochimica Et Biophysica Acta-Bioenergetics* 1857, 810-818, doi:10.1016/j.bbabio.2016.03.001

ZHANG, Y., BEARD, K. F. M., SWART, C., BERGMANN, S., KRAHNERT, I., NIKOLOSKI, Z., GRAF, A., RATCLIFFE, R. G., SWEETLOVE, L. J., FERNIE, A. R. & OBATA, T. (**2017**). Protein-protein interactions and metabolite channelling in the plant tricarboxylic acid cycle. *Nature Communications* 8, 15212, doi:10.1038/ncomms15212

FIGURES & TABLES

Figure 1 Restart of metabolism from quiescence in response to imbibition in orthodox seeds.

Figure 2 Oxygen-dependency of wheat seeds during germination.

Figure 3 Thiol redox modifications of proteins.

Figure 4 *In vitro* identification of targets of the cellular redox machinery.

Figure 5 Global analysis of the redox state of individual thiol peptides by differential thiol labelling strategy and iodoacetyl tandem mass tags.

Figure 6 Molecular mechanism of hydrogen peroxide sensing by the genetically encoded probe roGFP2-Orp1.

Figure 7 Oxygen consumption of Arabidopsis seeds in response to imbibition.

Figure 8 Platereader-based detection of fluorescent biosensors in seeds.

Figure 9 Emission spectra of Arabidopsis seeds expressing cytosolic ATeam.

Figure 10 Cytosolic ATeam response in Arabidopsis seeds at imbibition.

Figure 11 Total adenosine pools in Arabidopsis seed extracts in response to imbibition.

Figure 12 Emission spectra of Arabidopsis seeds expressing Peredox-mCherry in the cytosol.

Figure 13 Nicotinamide adenine dinucleotides in Arabidopsis seeds in response to imbibition.

Figure 14 Organic acid content in seeds in response to imbibition.

Figure 15 Excitation spectra of Arabidopsis seeds expressing roGFP2-based fluorescent biosensors in the cytosol and the mitochondrial matrix.

Figure 16 Glutathione redox state estimated with roGFP2-based fluorescent biosensors in Arabidopsis seeds in response to imbibition.

Figure 17 Representative confocal image of Arabidopsis seeds expressing roGFP2-Grx1 in the mitochondrial matrix.

Figure 18 Mitochondrial matrix roGFP2-Grx1 measurement in isolated embryos of imbibed seeds.

Figure 19 Total glutathione content of Arabidopsis seeds.

Figure 20 Amino acid concentration in dry and imbibed Arabidopsis seeds.

Figure 21 Germination efficiency of Arabidopsis seeds with impaired cytosolic and mitochondrial redox systems.

Figure 22 Stages of Arabidopsis seed germination.

Figure 23 Germination rates of artificially aged Arabidopsis seeds impaired in components of the thiol redox machinery.

Figure 24 Model for restarting the matrix thiol redox machinery in isolated mitochondria through substrate feeding.

Figure 25 Glutathione redox dynamics in the mitochondrial matrix in response to substrate feeding.

Figure 26 Abundance profiles of the redox states of Cys-peptides in quiescent and respiring isolated mitochondria.

Figure 27 Individual replicates of the iodoTMT-based quantification of the redox states of isolated mitochondria supplemented with citrate and their corresponding quiescent controls.

Figure 28 Individual replicates of the iodoTMT-based quantification of the redox states of isolated mitochondria supplemented with 2OG and their corresponding quiescent controls.

Figure 29 Individual replicates of the iodoTMT-based quantification of the redox states of isolated mitochondria supplemented with succinate and their corresponding quiescent controls.

Figure 30 Annotated subcellular localisation of Cys-peptides and proteins identified in isolated mitochondria and redox-shifted by citrate addition.

Figure 31 Schematic topology of identified Cys-peptides of mitochondrial Complex I and of other complexes of the respiratory chain.

Figure 32 Schematic overview of identified Cys-peptides of TCA cycle associated proteins.

Figure 33 Overview of identified Cys-peptides of aminotransferases and their catalysed reactions.

Figure 34 Overview of identified Cys-peptides of amino acid metabolism associated proteins.

Figure 35 Oxygen consumption of imbibed Arabidopsis seeds from mutants of the redox machinery.

Figure 36 Adenosine pools of Arabidopsis seeds with impaired redox machinery.

Figure 37 NADH concentration in seeds of Arabidopsis redox mutants.

Figure 38 TCA cycle intermediates and associated organic acids in seeds of Arabidopsis redox mutants.

Figure 39 Amino acid pools of Arabidopsis seeds with impaired redox machinery.

Figure 40 Global peptide redox state distributions of mitochondria from *ntr a/b* and *trx-o1* mutants.

Figure 41 Individual replicates of the iodoTMT-based quantification of the redox states of isolated mitochondria of the *ntr a/b* mutant supplemented with citrate and their corresponding quiescent controls.

Figure 42 Individual replicates of the iodoTMT-based quantification of the redox states of isolated mitochondria of the *trx-o1* mutant supplemented with citrate and their corresponding quiescent controls.

Figure 43 TMT reporter intensities of the THIOREDOXIN-o1- and NADP-dependent THIOREDOXIN REDUCTASE a/b-derived Cys-peptides identified in mitochondria of wildtype, *ntr a/b* and *trx-o1* mutant backgrounds.

Figure 44 Differences in peptide redox states of mitochondria from *ntr a/b* and *trx-o1* mutants compared with wildtype mitochondria.

Figure 45 Significant redox-switched Cys-peptides in mitochondria of the *ntr a/b* and *trx-o1* mutants in different metabolic states.

Figure 46 Mitochondrial glutathione redox state in *gr2* mutants.

Figure 47 Global distribution of Cys-peptide redox states of mitochondria from *gr2* mutants.

Figure 48 TMT reporter intensities of the GLUTATHIONE REDUCTASE 2-derived Cys-peptides identified in wildtype mitochondria and *gr2*-mutant background.

Figure 49 Differences in redox state of individual Cys-peptides of mitochondria from *gr2* mutants.

Figure 50 Heterologous expression of the hydrogen peroxide sensor roGFP2-Orp1.

Figure 51 Excitation and emission spectra of purified roGFP2-Orp1 protein *in vitro*.

Figure 52 pH dependence of the 400/482 nm excitation ratio of roGFP2-Orp1 *in vitro*.

Figure 53 Hydrogen peroxide responses of pre-reduced roGFP2-Orp1 protein *in vitro*.

Figure 54 Reduction of roGFP2-Orp1 protein extracts by reconstituted TRX and GSH/GRX machineries *in vitro*.

Figure 55 *35S*:roGFP2-Orp1 in epidermis cells of cotyledons of five-day-old Arabidopsis seedlings.

Figure 56 *35S*:TP-β-subunit-ATP-Synthase-roGFP2-Orp1 in root cells of five-day-old Arabidopsis seedlings.

Figure 57 *In vivo* calibration of cytosolic and mitochondrial roGFP2-Orp1 in root tips of five-day-old Arabidopsis seedlings.

Figure 58 The response of mitochondrial roGFP2-Orp1 to menadione-mediated hydrogen peroxide production.

Figure 59 Steady-state of roGFP2-Orp1 in redox mutants.

Figure 60 *In vivo* response of roGFP2-Orp1 to seed imbibition.

Figure 61 Model for the rapid phosphorylation of adenosines in seeds in response to imbibition.

Figure 62 Working model for kick-starting the mitochondrial redox control in Arabidopsis seeds at imbibition.

Figure 63 Model of the relationship between phenotype and redundancy of the mitochondrial thiol redox systems in Arabidopsis.

Tab. 1 Statistics for germination assays of aged Arabidopsis seeds.

Tab. 2 The 50 most strongly redox-shifted peptides at restarting the thiol redox machinery of the mitochondrial matrix by citrate addition.

Tab. 3 Cys-peptides in isolated mitochondria of the *ntr a/b* mutant with significantly different redox states.

Tab. 4 Cys-peptides in isolated mitochondria of the *trx-o1* mutant with significantly different redox states.

Tab. 5 Cys-peptides in quiescent mitochondria of the *gr2* mutant with significantly more reduced redox states.

Tab. 6 Cys-peptides in quiescent mitochondria of the *gr2* mutant with significantly more oxidised redox states.

Tab. 7 *Arabidopsis thaliana* T-DNA insertion lines.

Tab. 8 Buffers and gradients for the isolation of Arabidopsis mitochondria.

Tab. 9 Representative iodoTMT labelling scheme.

Tab. 10 Amino acid sequence of matrix located roGFP2-Grx1.

Tab. 11 Primers used for cloning of cyt-roGFP2-Orp1 and mt-roGFP2-Orp1.

Tab. 12 Plasmids used for the heterologous expression of proteins in *E. coli*.

Tab. 13 Plasmids used for GATEWAY®-cloning of the roGFP2-Orp1 construct.

Tab. 14 Plasmids used for the stable transformation of Arabidopsis plants.

ABBREVIATIONS

δ	dynamic range
2OG	2-oxoglutarate (α-ketoglutaric acid)
AA	amino acid
A.U.	arbitrary unit
ABC	ammonium bicarbonate
ABA	abscisic acid
ACO	aconitase
ADP	adenosine diphosphate
AK	adenylate kinase
AMP	adenosine monophosphate
ANOVA	analysis of variance
AOX	alternative oxidase
Asn	asparagine
ATP	adenosine triphosphate
BIM	basic mitochondrial incubation medium
BSA	bovine serum albumin
BSO	buthionine sulphoximine
C18	octadecyl carbon chain bonded silica
$Carb^R$	resistance against carbenicillin and ampicillin
CAT	catalase
CFP	cyan-fluorescent-protein
CLSM	confocal laser scanning microscopy
CoA	coenzyme a
Col-0	*Arabidopsis thaliana* ecotype *Columbia 0* (wildtype)
cpYFP	circular permutated yellow fluorescent protein
CS	citrate synthase
Cys	cysteine
Cyt *c*	cytochrome *c*
DCF	dichlorofluorescein
DIGE	differential gel electrophoresis
DMSO	dimethyl sulfoxide
DPS	4,4′-dipyridyl disulfide (Aldrithiol™-4)
DTT	dithiothreitol
DYn-2	4-(pent-4-yn-1-yl) cyclohexane-1,3-dione
EDTA	ethylenediaminetetraacetic acid
E_{GSH}	glutathione redox potential
Em	emission wavelength
ER	endoplasmic reticulum
ETC	electron transport chain
ETF / ETFQO	electron transfer flavoprotein-ubiquinone oxidoreductase
Ex	excitation wavelength
FDR	false discovery rate
FLT	fluorescence lifetime
FRET	Förster resonance energy transfer
FUM	fumarase

g	multiples of the earth`s gravitational acceleration
GA	gibberellic acid
GC-MS	gas chromatography-mass spectrometry
Glu	glutamic acid
GR	glutathione-reductase
Grx	glutaredoxin
GSH	glutathione (reduced)
GSSG	glutathione disulfide (oxidised)
HCD	higher-energy collisional dissociation
HEPES	4-(2-hydroxyethyl)-1-piperazineethanesulfonic acid
His	histidine
HPLC	high-performance liquid chromatography
HSP	heat shock protein
ICAT	isotope-coded affinity tag
I(C)DH	isocitrate dehydrogenase
IPTG	isopropyl β-D-1-thiogalactopyranoside
iodoTMT	iodoacetyl tandem mass tag
LB-medium	lysogeny broth - medium
LT	lifetime
mBBr	monobromobimane
MDH	malate dehydrogenase
ME	malic enzyme
MES	2-(N-morpholino)ethanesulfonic acid
MOPS	3-(N-morpholino)propanesulfonic acid
MS (MS^1)	mass spectrometry
MS-medium	Murashige-Skoog - medium
MS/MS (MS^2)	tandem mass spectrometry
NAD^+	nicotinamide adenine dinucleotide (oxidised)
NADH	nicotinamide adenine dinucleotide (reduced)
$NADP^+$	nicotinamide adenine dinucleotide phosphate (oxidised)
NADPH	nicotinamide adenine dinucleotide phosphate (reduced)
NEM	N-ethylmaleimide
NTR	NADPH-thioredoxin-reductase
OD	optical density
OGDC	oxoglutarate dehydrogenase complex
Orp1	oxidant receptor peroxidase-1
PCR	polymerase chain reaction
PEG	polyethylene glycol
PDC	pyruvate dehydrogenase complex
pK_a	acid dissociation constant
PMSF	phenylmethane sulfonyl fluoride
PPP	pentose phosphate pathway
Pro	proline
PRX	peroxiredoxin
PSV	protein storage vacuoles
PTM	posttranslational modifications
PVP-40	polyvinyl-pyrrolidone-40
Q	ubiquinone/ubiquinol
RFU	relative fluorescence unit

Rif^R	resistance against rifampicin
RPM	rounds per minute
roGFP2	redox-sensitive green fluorescent protein 2
ROS	reactive oxygen species
RuBisCO	ribulose bisphosphate carboxylase/oxygenase
SCS	succinyl CoA synthetase
SD	standard deviation
SDH	succinate dehydrogenase
SDS	sodium dodecyl sulfate
STR	sulfurtransferase
Succ	succinate
TP	target peptide
TBS	tris-buffered saline
TCA	trichloracetid acid
TCA cycle	tricarboxylic acid cycle (Krebs cycle)
TCEP	tris(2-carboxyethyl)phosphine
TES-buffer	2-[tris(hydroxymethyl)-methylamino]-ethanesulfonic acid
TFA	trifluoroacetic acid
TIM	translocase of the inner membrane
TMRM	tetramethylrhodamine
Tris	tris(hydroxymethyl)aminomethane
Trx	thioredoxin
Trypsin/P	trypsin cleaving after “K/R” unless followed by “P”
v/v	volume per volume
w/v	weight per volume
YAP 1	yeast activator protein 1-like transcription factor

PUBLICATIONS

During the doctoral studies following publications were published (or submitted for publication):

SCUFFI D., **NIETZEL T.**, DI FINO L., MEYER A. J., LAMATTINA L., SCHWARZLÄNDER M., LAXALT A. M. & GARCÍA-MATA, C. (**2017)**. H_2S increases NADPH oxidase-dependent H_2O_2 and PLD-derived PA in guard cell signalling. *Submitted to Plant Physiology*.

DE COL V., FUCHS P., **NIETZEL T.**, ELSÄSSER M., CHIA P. V., CANDEO A., SEELIGER I., FRICKER M. D., GREFEN C., MØLLER I. M., BASSI M., LEONG L. B., ZANCANI M., MEYER A. J., COSTA A., WAGNER S. & SCHWARZLÄNDER M. (**2017)**. ATP sensing in living plant cells reveals tissue gradients and stress dynamics of energy physiology. *Submitted to eLife.*

NIETZEL T., MOSTERTZ J., HOCHGRÄFE F. & SCHWARZLÄNDER M. (**2016)**. Redox regulation of mitochondrial proteins and proteomes by cysteine thiol switches. *Mitochondrion.*
doi: 10.1016/j.mito.2016.07.010

WAGNER S., BEHERA S., DE BORTOLI S., LOGAN D. C., FUCHS P., CARRARETTO L., TEARDO E., CENDRON L., **NIETZEL T.**, FÜßL M., DOCCULA F. G., NAVAZIO L., FRICKER M. D., VAN AKEN O., FINKEMEIER I., MEYER A. J., SZABÒ I., COSTA A. & SCHWARZLÄNDER M. (**2015)**. The EF-Hand Ca^{2+} Binding Protein MICU Choreographs Mitochondrial Ca^{2+} Dynamics in Arabidopsis. *The Plant Cell*.
doi: 10.1105/tpc.15.00509

MOSELER A., ALLER I., WAGNER S., **NIETZEL T.**, PRZYBYLA-TOSCANO J., MÜHLENHOFF U., LILL R., BERNDT C., ROUHIER N., SCHWARZLÄNDER M. & MEYER A. J. (**2015)**. The mitochondrial monothiol glutaredoxin S15 is essential for iron-sulfur protein maturation in *Arabidopsis thaliana*. *Proceedings of the National Academy of Sciences.*
doi: 10.1073/pnas.1510835112

WAGNER S., **NIETZEL T.**, ALLER I., COSTA A., FRICKER M. D., MEYER A. J. & SCHWARZLÄNDER M. (**2015)**. Analysis of Plant Mitochondrial Function Using Fluorescent Protein Sensors. *Methods in Molecular Biology.*
doi: 10.1007/978-1-4939-2639-8_17

GENERAL STATEMENT

Hereby I declare that I am the sole author of this submitted dissertation.
I have not made use of any sources apart from those referred to. All parts of the text taken over verbatim or analogously from published or not published sources are indicated as such. This thesis has not been submitted in the same or similar form, or in extracts within the context of another examination.

BONN | MONDAY, 18 SEPTEMBER 2017

THOMAS NIETZEL

ACKNOWLEDGEMENT

Mein größter Dank gilt Markus Schwarzländer, nicht nur für die Überlassung dieses spannenden Themas, sondern insbesondere auch dafür, dass er ein kritischer Betreuer und konstruktiver Ideengeber war, und mit seiner enthusiastischen Begeisterung für die Wissenschaft eine einmalige Arbeitsgruppe und Arbeitsatmosphäre geschaffen hat. Ich möchte mich daher auch ausdrücklich bei Stephan Wagner, Philippe Fuchs und Marlene Elsässer bedanken, die hierzu maßgeblich beigetragen haben und mich tatkräftig unterstützten. Die Arbeit mit Euch allen zusammen war immer inspirierend, interessant und hat einfach Spaß gemacht. Es ist nach so langer Zeit schön sagen zu können, dass man die Entscheidung zur Promotion in genau dieser Arbeitsgruppe nicht bereut und genauso wieder treffen würde.

Des Weiteren gilt mein Dank auch insbesondere Andreas Meyer - für so manch` guten Rat und die ständige Bereitschaft zur konstruktiven Diskussion, sowie für die Ermöglichung der Arbeit überhaupt, sei es durch die Finanzierung in meinen ersten Monaten oder die uneingeschränkte Kooperation beider Arbeitsgruppen. Vielen Dank daher auch an alle Mitarbeiter der Arbeitsgruppe, wie z.B. Anna Moseler, aber auch an alle anderen, die zu einer tollen Atmosphäre im Labor beigetragen haben. Dazu zähle ich auch die Mitglieder der AG Hochholdinger – auch ihnen gilt mein herzlichster Dank.

Mein Dank gilt auch besonders Falko Hochgräfe, der mit seiner technischen Expertise im Bereich der Massenspektrometrie, aber vor allem auch mit seiner uneingeschränkten Hilfsbereitschaft meine Arbeit unheimlich bereichert hat.

Ich freue mich auch, dass meine Familie mich immer maßgeblich unterstützt hat – nicht nur in finanzieller Hinsicht während meines Studiums in Hannover. Vielen Dank! Ich bin froh, dass ich während der ganzen langen Zeit von so tollen Menschen begleitet worden bin. Zusätzlich zu meiner Familie zähle ich dazu natürlich noch insbesondere Rosa, die Familie *in spe* oder die (ehemals) Hannoveraner. Vielen Dank Euch allen!